

AD 742696

FOREIGN TECHNOLOGY DIVISION



MONOPULSE RADAR

by

A. I. Leonov and K. I. Fomichev



D D C
RECEIVED
6 JUN 1972
RECEIVED
D

Approved for public release;
Distribution unlimited.

Reproduced by
**NATIONAL TECHNICAL
INFORMATION SERVICE**
Springfield, Va. 22151

UNCLASSIFIED

Security Classification

DOCUMENT CONTROL DATA - R & D

(Security classification of title, body of abstract and indexing annotation must be entered when the overall report is classified)

1. ORIGINATING ACTIVITY (Compara. to author) Foreign Technology Division Air Force Systems Command U. S. Air Force		28. REPORT SECURITY CLASSIFICATION UNCLASSIFIED	
2. REPORT TITLE MONOPULSE RADAR		29. GROUP	
3. AUTHOR(S) (First name, middle initial, last name) Leonov, A. I. and Fomichev, K. I.			
4. REPORT DATE 1970		76. TOTAL NO. OF PAGES 414	75. NO. OF REFS 134
5. CONTRACT OR GRANT NO. 6. PROJECT NO. 60501		29. ORIGINATOR'S REPORT NUMBER(S) FTD-MT-24-982-71	
7. OTHER REPORT NO(S) (Any other numbers that may be assigned this report)			
10. DISTRIBUTION STATEMENT Approved for public release; distribution unlimited.			
11. SUPPLEMENTARY NOTES		12. SPONSORING MILITARY ACTIVITY Foreign Technology Division Wright-Patterson AFB, Ohio	
13. ABSTRACT The book deals with certain problems of monopulse radar. Analyzed are principles of design and basic functional elements of monopulse direction finding systems, problems of accuracy and resolution. The book was written for engineering technical personnel and senior college students specializing in the field of radar engineering. [AM1002419]			

UNCLASSIFIED

Security Classification

KEY WORDS	LINK A		LINK B		LINK C	
	ROLE	WT	ROLE	WT	ROLE	WT
Monograph						
Radar Engineering						
Radar Design Parameter						
Monopulse Radar						
Direction Finding Equipment						
Radar Resolution						
Radar Accuracy						
Radar Antenna						
Angle Measuring Instrument						
Radar Sensitivity						
Mathematic Model						

UNCLASSIFIED

Security Classification

EDITED MACHINE TRANSLATION

MONOPULSE RADAR

By: A. I. Leonov and K. I. Fomichëv

English pages: 414

Source: Monoimpul'snaya Radiolokatsiya,
Izd Vo Sovetskoye Radio, Moscow,
1970, pp. 1-392.

This document is a Systran machine aided
translation, post-edited for technical
accuracy by: L. Heenan

Approved for public release;
distribution unlimited.

UR/0000-70-000-000

THIS TRANSLATION IS A RENDITION OF THE ORIGINAL FOREIGN TEXT WITHOUT ANY ANALYTICAL OR EDITORIAL COMMENT. STATEMENTS OR THEORIES ADVOCATED OR IMPLIED ARE THOSE OF THE SOURCE AND DO NOT NECESSARILY REFLECT THE POSITION OR OPINION OF THE FOREIGN TECHNOLOGY DIVISION.

PREPARED BY:

TRANSLATION DIVISION
FOREIGN TECHNOLOGY DIVISION
WP-APB, OHIO.

TABLE OF CONTENTS

U. S. Board on Geographic Names Transliteration System	viii
Designations of the Trigonometric Functions	vii
Introduction	2
Chapter 1. The Principle and Methods of Monopulse Radar	4
§ 1.1. Principle of monopulse direction finding	4
§ 1.2. Structural diagram of a monopulse radar system	9
§ 1.3. Monopulse radar systems of automatic target tracking	18
1.3.1. Amplitude-amplitude monopulse system	18
1.3.2. Phase-phase monopulse system	20
1.3.3. Amplitude sum-difference monopulse system	23
1.3.4. Phase sum-difference monopulse system	25
§ 1.4. Monopulse radar scanning systems	27
1.4.1. Amplitude-amplitude monopulse system	27
1.4.2. Amplitude sum-difference monopulse system	29
§ 1.5. Design principles for monopulse systems of direction finding in two planes	31
§ 1.6. Design principles of monopulse systems operating in continuous and quasi-continuous radiation modes	43
Chapter 2. Monopulse Radar System Antennas	46
§ 2.1. Relationship between the radiation pattern of the antenna and the current distribution on its surface	46
§ 2.2. Parabolic antennas	52
§ 2.3. Parabolic antennas with a primary radiator	55
§ 2.4. Lens antennas	61

§ 2.5.	Crosspolarization radiation of mirror antennas	66
§ 2.6.	Phased antenna arrays	73
§ 2.7.	Antenna feeds of monopulse radars	77
2.7.1.	A four-horn irradiator operating on several types of waves	80
2.7.2.	A twelve-horn irradiator	81
§ 2.8.	Selection of maximum displacement angle for a radiation pattern and the distance between phase centers	86
§ 2.9.	Waveguide devices for sum-difference signal processing	90
Chapter 3.	Basic Functional Elements of Angular Discriminators	93
§ 3.1.	Logarithmic amplifier	93
3.1.1.	Logarithmic amplifiers with shunting of anode loads by nonlinear elements	97
3.1.2.	Logarithmic amplifiers with summation of stage output voltages	107
§ 3.2.	Phase detector	113
§ 3.3.	System of automatic amplification control	120
Chapter 4.	Resolution and Direction Finding Sensitivity of Monopulse Radars with Respect to Angular Coordinates	130
§ 4.1.	The concept of angular coordinate resolution	130
§ 4.2.	Angular resolution of monopulse radars	136
4.2.1.	An amplitude sum-difference monopulse system of direction finding in one plane	136
4.2.2.	A phase sum-difference monopulse system of direction finding in one plane	142
§ 4.3.	Direction finding sensitivity of monopulse radars	152

§ 4.4.	Methods of improving angular resolution in monopulse radars	155
4.4.1.	Methods for increasing resolution, based on angle gating	156
4.4.2.	A method of increasing resolution, based on functional processing of signals	165
Chapter 5.	Accuracy Problems in Angular Measurement by the Monopulse Method	171
§ 5.1.	The effect of radio wave propagation conditions on direction finding accuracy	171
5.1.1.	The effect of the earth on direction finding accuracy	172
5.1.2.	The effect of refraction and diffraction on direction finding accuracy	175
§ 5.2.	The effect of amplitude and angular fluctuations in reflected signals on direction finding accuracy	177
5.2.1.	The effect of amplitude fluctuations on direction finding accuracy	177
5.2.2.	The effect of angular fluctuations in reflected signals on direction finding accuracy	179
5.2.3.	Errors and the direction finding of targets of complex form	188
5.2.4.	Measurement methodology and target noise analysis	192
§ 5.3.	The effect of internal receiver noises on direction finding accuracy	196
§ 5.4.	Errors caused by receiver noises in monopulse radars with phased antenna array	206
§ 5.5.	Sum error in direction finding caused by the effect of target and receiver noises	211
§ 5.6.	Effect of automatic gain control on direction finding accuracy	213

§ 5.7.	The effect of the depolarization of reflected signals on direction finding accuracy	222
5.7.1.	Reasons for the depolarization of reflected signals	223
5.7.2.	The character of the effect of reflected signal depolarization on direction finding accuracy	225
5.7.3.	Methods of lessening the effect of antenna crosspolarization on direction finding accuracy	235
Chapter 6.	The Effect of Imperfections in Elements of the Receiving Circuit on the Accuracy of Measuring Angular Coordinates by the Monopulse Method	237
§ 6.1.	Main sources of equipment errors	237
§ 6.2.	The effect of imperfect formation of antenna radiation patterns of monopulse systems on direction finding accuracy	238
6.2.1.	The effect of errors in field distribution along the aperture of an antenna array on direction finding accuracy	239
§ 6.3.	The effect of nonidentity of amplitude-phase characteristics for receiving channels of monopulse systems on direction finding accuracy	250
6.3.1.	The effect of nonidentity of amplitude-phase characteristics in an amplitude-amplitude monopulse system on direction finding accuracy	251
6.3.2.	The effect of nonidentity of amplitude-phase characteristics for receiving channels of an amplitude sum-difference monopulse system on direction finding accuracy	255
6.3.3.	The effect of nonidentity in amplitude phase characteristics of receiving channels for a phase-phase monopulse system on direction finding accuracy	269

6.3.4.	The effect of nonidentity of amplitude phase characteristics for receiving channels of a phase sum-difference monopulse system on direction finding accuracy	270
§ 6.4.	Supplementary requirements for identity of amplitude-phase characteristics of receiving channels during the use of wide-band, continuous and quasicontinuous signals	275
6.4.1.	Direction finding on signals with frequency modulation	275
6.4.2.	Direction finding on continuous and quasi-continuous signals with speed selection	278
6.4.3.	Direction finding during the use of pulsed signal compression	279
§ 6.5.	Design methods of decreasing direction finding equipment error	281
6.5.1.	A method of joining receiving channels on high frequency	281
6.5.2.	A method of joining intermediate-frequency receiving channels	283
6.5.3.	A method of joining i-f receiving channels with the use of phase shifts and time delay of signals	286
6.5.4.	A method of receiving channel interconnection with the use of low-frequency modulation in one of the channels	289
6.5.5.	A method of joining receiving channels with the use of signal spacing based on frequency	291
6.5.6.	A method of joining receiving channels with the use of switching	297
Chapter 7.	Interference Immunity of Monopulse Radars	303
§ 7.1.	Methods of creating radar interference	304
7.1.1.	Active camouflaging interference	304
7.1.2.	Passive camouflaging noises	307

7.1.3.	Active misinforming noises	309
7.1.4.	Passive misinforming noises	311
7.1.5.	Noises from atomic explosions	312
§ 7.2.	Noises by monopulse radar systems	314
7.2.1.	Noises of a monopulse radar on receiving channel switching frequency	317
7.2.2.	Coherent noises created from two points in space	321
7.2.3.	Flickering noises created from two points in space	330
7.2.4.	Noises with frequency wobble created from two or more points	335
7.2.5.	Noises on crosspolarization	337
§ 7.3.	Methods of protecting monopulse radars from certain types of radio noises	338
7.3.1.	Methods of protection from flickering noises created from two or more points in space	339
7.3.2.	Protection from noises on cross-polarization	340
Chapter 8.	The Use of Modeling in a Study of Coordinate Determination Errors for Monopulse Radars	342
§ 8.1.	Common problems and trends in simulation	342
§ 8.2.	A model of an amplitude sum-difference monopulse tracking radar	343
§ 8.3.	Overall block diagram of a model of a scanning monopulse radar with frequency-modulated signals and amplitude direction finding	357
8.3.1.	Representation of signal and noise	358
8.3.2.	Modeling the processing of a signal in the receiving channel	367

§ 8.4.	Models of amplitude-amplitude and amplitude sum-difference scanning radars	377
Chapter 9.	Areas of Application at Certain Characteristics of Foreign Monopulse Radars	383
§ 9.1.	Radars for tracking both ballistic and space targets	383
§ 9.2.	Radars systems for remote tracking and communication with satellites and space ships	388
§ 9.3.	Radars of the antimissile defense system	397
§ 9.4.	Radars for guiding antiaircraft rockets	403
§ 9.5.	A radar for detecting ground targets on the local background	406

U. S. BOARD ON GEOGRAPHIC NAMES TRANSLITERATION SYSTEM

Block	Italic	Transliteration	Block	Italic	Transliteration
А а	<i>А а</i>	A, a	Р р	<i>Р р</i>	R, r
Б б	<i>Б б</i>	B, b	С с	<i>С с</i>	S, s
В в	<i>В в</i>	V, v	Т т	<i>Т т</i>	T, t
Г г	<i>Г г</i>	G, g	У у	<i>У у</i>	U, u
Д д	<i>Д д</i>	D, d	Ф ф	<i>Ф ф</i>	F, f
Е е	<i>Е е</i>	Ye, ye; E, e*	Х х	<i>Х х</i>	Kh, kh
Ж ж	<i>Ж ж</i>	Zh, zh	Ц ц	<i>Ц ц</i>	Ts, ts
З з	<i>З з</i>	Z, z	Ч ч	<i>Ч ч</i>	Ch, ch
И и	<i>И и</i>	I, i	Ш ш	<i>Ш ш</i>	Sh, sh
Й я	<i>Й я</i>	Y, y	Щ щ	<i>Щ щ</i>	Shch, shch
К к	<i>К к</i>	K, k	Ъ ъ	<i>Ъ ъ</i>	"
Л л	<i>Л л</i>	L, l	Ы ы	<i>Ы ы</i>	Y, y
М м	<i>М м</i>	M, m	Ь ь	<i>Ь ь</i>	'
Н н	<i>Н н</i>	N, n	Э э	<i>Э э</i>	E, e
О о	<i>О о</i>	O, o	Ю ю	<i>Ю ю</i>	Yu, yu
П п	<i>П п</i>	P, p	Я я	<i>Я я</i>	Ya, ya

* ye initially, after vowels, and after ъ, ь; e elsewhere.
 When written as ѐ in Russian, transliterate as yѐ or ѐ.
 The use of diacritical marks is preferred, but such marks
 may be omitted when expediency dictates.

FOLLOWING ARE THE CORRESPONDING RUSSIAN AND ENGLISH
DESIGNATIONS OF THE TRIGONOMETRIC FUNCTIONS

Russian	English
sin	sin
cos	cos
tg	tan
ctg	cot
sec	sec
cosec	csc
sh	sinh
ch	cosh
th	tanh
cth	coth
sch	sech
csch	csch
arc sin	\sin^{-1}
arc cos	\cos^{-1}
arc tg	\tan^{-1}
arc ctg	\cot^{-1}
arc sec	\sec^{-1}
arc cosec	\csc^{-1}
arc sh	\sinh^{-1}
arc ch	\cosh^{-1}
arc th	\tanh^{-1}
arc cth	\coth^{-1}
arc sch	sech^{-1}
arc csch	csch^{-1}

rot	curl
lg	log

This book is concerned with problems of monopulse radar. In it are examined the design principles and the fundamental functional units of monopulse systems of direction finding; questions of accuracy and resolution are analyzed. Theoretical questions of the simulation of monopulse systems with the aid of electronic computers are discussed; an analysis is made of interference shielding of monopulse position finders in the presence of various forms of interference. Fields of application are described and the fundamental tactical-technical characteristics are given for some foreign monopulse radars.

This book is designed for engineers, technicians, and students of advanced courses at higher educational institutions which specialize in the field of radar technology.

This book contains 10 tables, 166 figures and 134 references.

INTRODUCTION

Because of the substantial increase in the speed of aircraft, the development of rocket and extraterrestrial technology, and also the improvement of jamming facilities, accuracy requirements have become stricter, also the definition of angular coordinates, the rate of data processing, and the requirements for interference shielding of radars. These requirements, to a certain extent, have been satisfied by monopulse radar systems which, in the last decade, have been widely distributed abroad.

Initially, monopulse radar systems implied pulsed radars which accomplished multichannel reception and were able, in principle, to measure angular coordinates according to one pulse reflected from the target. Subsequently, this concept was expanded and encompassed, in addition to pulsed radar, radars with continuous and quasi-continuous modes of emission. Sometimes systems with instantaneous comparison of signals are called monopulse systems.

Because of the intense development of monopulse radars, much data concerning the individual problem of monopulse radar have been published. This information is found mainly in articles and advertisements, as well as various periodicals and patents. As of yet there have been no books covering the subject of monopulse radar thoroughly. Monographs by D. R. Rhodes [41] and E. F. Sviridov [45], dedicated to the general theory and the comparative effectiveness of several types of monopulse systems, do not cover the entire range of questions which are of interest to persons specializing in the field of radar and jamming. Hellgren's work [55] does not touch upon a number of problems of practical importance in monopulse radar.

In this book we have attempted, as much as possible, to correct this deficiency in literature and have arranged the chief problems of monopulse radar in a systematized form, making this available to a wide circle of specialists in the field of radar.

We have used in this book open material from the foreign and domestic press, as well as information from studies carried out by the authors. Chapters 1 (except for § 1.5, 1.6), 2 (except for § 2.5), 3.9 and § 5.4, 6.2.1 were written by A. I. Leonov. Chapter 8 was written by A. I. Leonov with the aid of V. N. Vasenev and F. V. Nagulinko. Chapters 4, 5 (except for § 5.4), 6 (except for § 6.2.1), 7 and § 1.5, 1.6, and 2.5 were written by K. I. Fomichev.

The authors express their sincere appreciation to S. I. Krasnogorov and E. F. Sviridov for their valuable remarks during the review of the manuscript. Particular thanks are expressed to E. F. Sviridov for his aid and helpful criticism in preparing the book for print.

CHAPTER I

THE PRINCIPLE AND METHODS OF MONOPULSE RADAR

§ 1.1. PRINCIPLE OF MONOPULSE DIRECTION FINDING

Determining the direction to a target is one of the basic tasks of a radar.

Until recently, the most widely used methods of determining, accurately and automatically, the direction to a source of signals were methods of conical, linear (planar) scanning and sequential switching of radiation patterns, which were performed by single-channel direction finders. Based on these methods, the direction to a source was determined by a comparison of signals received sequentially by antennas with various radiation patterns. Characteristic of these methods is also the fact that angular information about the target is shaped in the form of amplitude modulation of signals received. The modulation index determines the value of error in direction finding, while the phase is the direction of antenna axis mismatch with respect to the direction to the target being worked.

Since the modulation method of angular error signal shaping requires the reception of sequentially reflected pulses, it is sensitive to amplitude fluctuation in the signals received, generated by random variations in the effective scattering cross section of the target. This is one of the most substantial deficiencies of single-channel methods of direction finding, using conical and linear scanning of a beam or the sequential switching of radiation patterns.

Recently achieving wide use has been the monopulse method of direction finding, with which the reflected pulse gives complete information on the angular position of the target. This explains the origin of the term "monopulse" (one-pulse) direction finding. Since in monopulse systems direction finding is accomplished with one pulse, the amplitude fluctuations of the reflected signal do not have a noticeable effect on the measurement accuracy of angular coordinates.

Multichannel reception can be used for monopulse direction finding. Therefore, the principle of monopulse direction finding lies in the reception of signals reflected from a target simultaneously along several independent receiving channels with the subsequent comparison of their parameters. Usually, two independent receiving channels are provided for each coordinate plane; two channels for azimuth and two channels for elevation.

Originally the monopulse method was developed for precise automatic target tracking. Today the monopulse method is also used for monopulse surveillance radar systems. Under surveillance we include monopulse systems which determine the angular coordinates of all targets found within the radiation pattern and which can be resolved with respect to range, for each position of the beam in space. As a rule, electric beam control is used in monopulse surveillance systems, and they are coupled with electronic computers which perform programmed control of the beam position in space in accordance with a selected surveillance method, determine the coordinates of all targets located in the beam, and plot their trajectories.

There are two basic methods of monopulse direction finding, depending upon the character of the extraction of the target's angular information from the signals received: the amplitude method and the phase method.

In monopulse systems with amplitude direction finding, in order to determine the angular coordinate in one plane, two intersecting antenna radiation patterns are formed, spaced at an angle of

$\pm\theta_0$ from the equisignal direction (Fig. 1.1). Figure 1.1 shows the radiation patterns in the elevation plane. When the circuit deviates by angle θ from the equisignal direction (RSN) and the target is found at point A, the signal received along the lower pattern is greater than the signal received along the upper pattern. The difference in amplitudes of the signals received indicates the amount of target deviation from equisignal direction. The sign of this difference characterizes the direction of the displacement of equisignal direction relative to the target. When equisignal direction coincides with the target, the amplitudes of reflected signals received along both patterns are equal, and their difference reverts to zero. Target azimuth is determined similarly with the aid of the azimuth channel of the receiver and the second pair of radiation patterns in the azimuth plane.

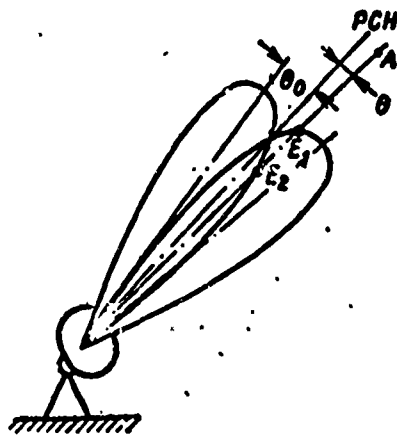


Fig. 1.1. Determining angular coordinates in monopulse systems with amplitude direction finding.

In monopulse systems with phase direction finding, the direction to target in one coordinate plane is determined by a comparison of phases of signals received by two antennas. In the remote zone each antenna irradiates the same volume of space, as a result of which reflected signals originating from a point target are virtually identical in amplitude but differ in phase. Figure 1.2 shows two antennas a distance of l from each other.

The line of sight of the target forms angle θ with the axis perpendicular to the line connecting both antennas, i.e., equisignal direction. The distance between antenna 1 and the target is

$$R_1 = R + \frac{l}{2} \sin \theta,$$

and the distance between antenna 2 and the target is

$$R_2 = R - \frac{l}{2} \sin \theta.$$

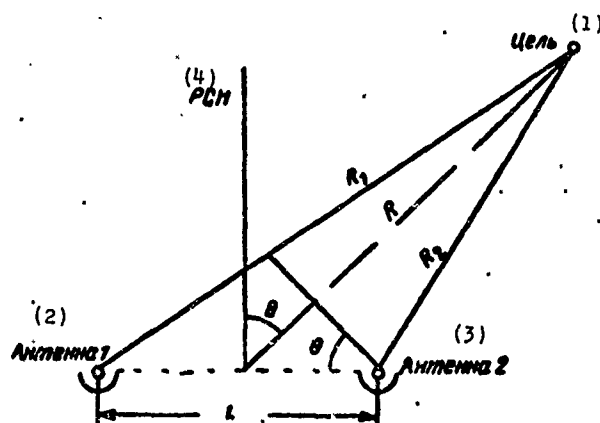


Fig. 1.2. Determining angular coordinates and monopulse systems with phase direction finding.

KEY: (1) Target; (2) Antenna 1; (3) Antenna 2; (4) ESD.

The difference in distances from target to antennas

$$\Delta R = R_1 - R_2 = l \sin \theta$$

gives a phase difference of

$$\Delta \varphi = \frac{2\pi}{\lambda} \Delta R = \frac{2\pi l}{\lambda} \sin \theta, \quad (1.1)$$

where λ is wavelength.

This makes it possible to determine the angle of approach θ with respect to the measured quantity of phase shifts of signals reflected from the target and received on two spaced antennas.

Expression (1.1) shows that the phase shift of signals $\Delta\phi$ reverts to zero not only with $\theta = 0$, but also with other displacement angles corresponding to condition

$$\theta = \arcsin \frac{2n\pi}{k_1 l},$$

where $n = 1, 2, \dots$,

$$k_1 = \frac{2\pi}{\lambda}.$$

Due to this, the direction finding characteristic is sign-alternating and has, along with a main direction, many erroneous equisignal directions. This is the reason for the ambiguity of measurements by the phase method. However, the ambiguity is not a very serious disadvantage if the erroneous equisignal directions fall within the main lobe of the radiation pattern. For this, it is necessary that the distance between centers of receiving antennas not exceed the diameter of each of them. Such a system can be made, for example, in the form of two antennas arranged in a row.

In addition to the main methods, there is also an amplitude-phase method (or complex) [11, 41, 45], which is a combination of the basic methods.

As a source of angular information in the methods listed, we use amplitude, phase, and amplitude-phase ratios of signals received by independent channels. Different methods of extracting angular information, in turn, generate certain differences in processing signals received and, consequently, in the structure of a monopulse system on the whole. Let us examine a structural diagram of a monopulse radar system in a general form.

§ 1.2. STRUCTURAL DIAGRAM OF A MONOPULSE RADAR SYSTEM

As mentioned above, in monopulse systems, the information concerning the angular position of a target is obtained by comparing pairs of received signals. With such a comparison the voltage at output of the monopulse angular measuring system does not depend upon the absolute value of the amplitudes of received signals, but is determined only by the signal arrival angle. The direction finding characteristic of a monopulse system must indicate the value and sign of the arrival angle of the received signal, i.e., must be an uneven actual function of the signal arrival angle. The initial data concerning the arrival angle, contained in the signal pair, are formed upon reception by the monopulse antenna, which is called the angle-data transmitter.

In accordance with these assumptions, the signals received must be handled so that there can be obtained a function, a substantial part of which would satisfy requirements imposed on direction finding characteristics (independence of signal intensity and oddness relative to equisignal direction).

Let us examine analytically the possible solutions to the problem posed [41, 45]. The field strength at the point of reception in complex form can be written as a function of time t :

$$\dot{E}(t) = E_m \exp i(\omega t - \phi_0) \quad 0 < t < T, \quad (1.2)$$

where E_m is amplitude;
 ω is frequency;
 ϕ_0 is initial phase of field.

The radiation patterns of the antenna system, which are complex functions of the angle, are expressed by relationships

$$\begin{aligned} \dot{j}_1(\theta) &= F_1(\theta) \exp i\varphi_1(\theta), \\ \dot{j}_2(\theta) &= F_2(\theta) \exp i\varphi_2(\theta), \end{aligned} \quad (1.3)$$

where $F_1(\theta)$ and $F_2(\theta)$ are amplitude radiation patterns;
 $\phi_1(\theta)$ and $\phi_2(\theta)$ are phase radiation patterns.

Phase radiation patterns will be assumed mirror reflections of each other relative to equisignal direction, while amplitude radiation patterns are identical and their maxima displaced by angle $\pm\theta_0$ relative to equisignal direction, i.e.,

$$\left. \begin{aligned} \varphi_1(\theta) &= \frac{1}{2} \varphi(\theta), \quad \varphi_2(\theta) = -\frac{1}{2} \varphi(\theta), \\ F_1(\theta) &= F(\theta_0 - \theta), \quad F_2(\theta) = F(\theta_0 + \theta), \end{aligned} \right\} \quad (1.4)$$

where $\phi(\theta)$ is the difference-phase radiation pattern of the antenna system.

Reflected signals which are received by the spaced antennas can be written as:

$$\left. \begin{aligned} \dot{E}_1(t, \theta) &= \dot{E}(t) \dot{f}_1(\theta), \\ \dot{E}_2(t, \theta) &= \dot{E}(t) \dot{f}_2(\theta). \end{aligned} \right\} \quad (1.5)$$

Then the ratio of the two received signals can be written as

$$r_m(\theta) = \frac{\dot{E}_1(t, \theta)}{\dot{E}_2(t, \theta)} = \frac{\dot{f}_1(\theta)}{\dot{f}_2(\theta)} = \frac{F_1(\theta) \exp i\varphi_1(\theta)}{F_2(\theta) \exp i\varphi_2(\theta)} \quad (1.6)$$

The ratio, which subsequently will be called multiplicative, under certain conditions, can be the basic ratio for forming a direction finding characteristic.

In order to form a direction finding characteristic, we can also use the ratio of the difference signal to total signal

$$r_n(\theta) = \frac{\dot{E}_1(t, \theta) - \dot{E}_2(t, \theta)}{\dot{E}_1(t, \theta) + \dot{E}_2(t, \theta)} = \frac{\dot{f}_1(\theta) - \dot{f}_2(\theta)}{\dot{f}_1(\theta) + \dot{f}_2(\theta)} \quad (1.7)$$

which is usually called the additive ratio of received signals. The relationship between multiplicative and additive signal ratios is established with the aid of the following expressions:

$$\left. \begin{aligned} r_a(\theta) &= \frac{r_m(\theta) - 1}{r_m(\theta) + 1} \\ r_m(\theta) &= \frac{1 + r_a(\theta)}{1 - r_a(\theta)} \end{aligned} \right\} \quad (1.8)$$

In addition to multiplicative and additive ratios, we can form other ratios which satisfy requirements imposed on the direction finding characteristics of a monopulse system. When we multiply multiplicative and additive ratios by a complex constant

$$\dot{a} = a_0 \exp i\psi_0$$

we obtain linearly transformed ratios [45]:

$$\left. \begin{aligned} \dot{r}_m(\theta) &= \dot{a} r_m(\theta) \\ \dot{r}_a(\theta) &= \dot{a} r_a(\theta) \end{aligned} \right\} \quad (1.9)$$

Devices which form the sum and difference of received signals or perform the operation of multiplying received signals by coefficient \dot{a} are called converters since in them, generally, we can convert information from amplitude ratios to phase ratios and back. These conversions are accomplished usually at high frequencies with the use of passive elements because of their relative simplicity and stability of characteristics.

The operation of calculating the ratio of two signals, converted or unconverted, cannot be done without their preliminary amplification. The device containing active elements, including amplifiers and comparison circuit, which distinguishes multiplicative and additive ratios and forms the direction finding characteristic, is called the angular discriminator.

With amplitude direction finding, angular information is contained in amplitude diagrams $F_1(\theta)$ and $F_2(\theta)$. In this case, with identical phase diagrams, multiplicative and additive ratios are expressed only through amplitude radiation patterns

$$\left. \begin{aligned} r_m(\theta) &= \frac{F_1(\theta)}{F_2(\theta)} = \rho(\theta), \\ r_a(\theta) &= \frac{F_1(\theta) - F_2(\theta)}{F_1(\theta) + F_2(\theta)} = \frac{\rho(\theta) - 1}{\rho(\theta) + 1}. \end{aligned} \right\} \quad (1.10)$$

With phase direction finding, when the amplitude patterns are identical, angular information is contained in the phase difference

$$\varphi(\theta) = \varphi_1(\theta) - \varphi_2(\theta). \quad (1.11)$$

Multiplicative and additive ratios are expressed only through phase pattern

$$\left. \begin{aligned} r_m(\theta) &= \frac{\exp i \varphi_1(\theta)}{\exp i \varphi_2(\theta)} = \exp i \varphi(\theta), \\ r_a(\theta) &= \frac{\exp i \varphi_1(\theta) - \exp i \varphi_2(\theta)}{\exp i \varphi_1(\theta) + \exp i \varphi_2(\theta)} = i \operatorname{tg} \frac{\varphi(\theta)}{2}. \end{aligned} \right\} \quad (1.12)$$

Amplitude ratio $\rho(\theta)$ and phase difference $\varphi(\theta)$ will be called multiplicative functions of the angle, while the ratios $(\rho(\theta)-1)/(\rho(\theta)+1)$ and $\operatorname{tg}(\varphi(\theta))/2$ are the additive functions of the angle.

An angular discriminator in which in order to form the direction finding characteristic the multiplicative function of the angle is used, reacting only to amplitude ratios of received signals, is called an amplitude discriminator, while one reacting only to phase ratios is called phase discriminator. An angular discriminator which reacts both to amplitude and phase signal ratios and in which, in order to form the direction finding characteristic, the additive function of the angle is used is called a sum-difference discriminator.

Thus, only three different methods of angular measurement are possible (three types of angular discriminators): amplitude, phase, and sum-difference. Each of them can be used either with amplitude or phase or complex direction finding. Since each of the types of direction finding can be used in combination with any of the angular discriminators, nine basic classes are possible for monopulse systems; their classification is presented in Table 1.1 [45].

Based on the classification taken, the first word in the name of a monopulse system will describe the type of direction finding and the second the type of angular discriminator. Thus, for example, a monopulse system with amplitude angular discriminator and amplitude direction finding will be called an amplitude-amplitude system, whereas with phase direction finding it will be called a phase-amplitude system. A monopulse system with a phase angular discriminator and amplitude direction finding will be called an amplitude-phase system, and with phase direction finding a phase-phase system. A monopulse system with a sum-difference angular discriminator, depending upon the type of direction finding, will be called an amplitude sum-difference system, a phase sum-difference system, or a complex sum-difference system.

Table 1.1.

(1) Метод измерения (тип углового дискриминатора)	(2) Основные классы моноимпульсных радиолокационных систем для трех видов пеленгации		
	(3) амплитудной (А)	(4) фазовой (Ф)	(5) комплексной (К)
(6) Амплитудный (А)	(9) АА	(10) ФА	(11) КА
(7) Фазовый (Ф)	(12) АФ	(13) ФФ	(14) КФ
(8) Суммарно-разностный (СР)	(15) АСР	(16) ФСР	(17) КСР

KEY: (1) Measurement method (type of angular discriminator); (2) Main classes of monopulse radar systems for three types of direction finding; (3) amplitude (A); (4) phase (F); (5) complex (K); (6) Amplitude (A); (7) Phase (F); (8) Sum-difference (SR); (9) AA; (10) FA; (11) KA; (12) AF; (13) FF; (14) KF; (15) ASR; (16) FSR; (17) KSR.

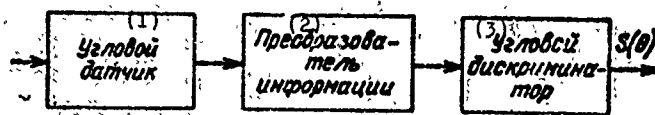


Fig. 1.3. Block diagram of a monopulse system.

KEY: (1) Angle-data transmitter; (2) Information converter; (3) Angular discriminator.

Of the nine possible classes of monopulse system, indicated in Table 1.1, four systems are the most widely used: amplitude-amplitude (AA), phase-phase (FF), amplitude sum-difference (ASR), and phase sum-difference (FSR). These monopulse systems will be examined later.

Based on the sequence of operations performed by the monopulse system, its structural diagram must contain the following basic elements (Fig. 1.3):

- an angle-data transmitter which forms signals in whose parameter ratios is contained information concerning the angular position of the target;
- an information converter which converts the signals' parameter ratios;
- an angular discriminator which distinguishes the actual function of the signal's parameter ratio uniquely connected with the arrival angle.

The angle-data transmitter is the antenna of the monopulse system and the most important element. It possesses certain peculiarities which will be examined in detail in Chapter 2.

As a converter in monopulse systems is used, a $\pi/2$ phase switcher which performs the operation of multiplication by ± 1 , and a sum-difference converter, for which an annular waveguide bridge or double waveguide T-joint is used. (The sum-difference converter is also discussed in Chapter 2.)

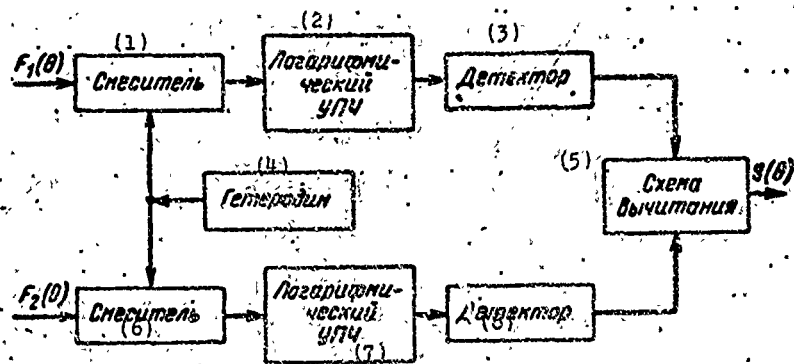


Fig. 1.4. Block diagram of an amplitude angular discriminator.
 KEY: (1) Mixer; (2) Logarithmic i-f amplifier; (3) Detector; (4) Heterodyne; (5) Differential amplifier; (6) Mixer; (7) Logarithmic i-f amplifier; (8) Detector.

Diagrams of each of the three types of angular discriminators are presented in Figs. 1.4-1.6. In each diagram there is one heterodyne for forming intermediate frequency in both receiving channels, which makes it possible to preserve symmetry of the two channels and maintain phase coherence between them. The ratio of received signals $r_m(\theta)$ or $r_a(\theta)$, which characterizes the direction of arrival, is formed because of the normalizing property of amplifiers used in these diagrams.

In the amplitude angular discriminator presented in Fig. 1.4, the ratio $r_m(\theta)$ is obtained by subtracting the values of the amplitude logarithms of the two signals, which is equivalent to forming the logarithm of the ratio. Since the values of the amplitude logarithms of the two signals are subtracted, the output voltage does not depend upon the absolute level of signals received. The expression $\ln r_m(\theta)$ becomes equal to zero in the equisignal direction [$r_m(\theta) = 1$] and has uneven symmetry relative to this direction, i.e., it can be used to obtain the direction finding characteristic

$$S(\theta) = \operatorname{Re} \ln r_m(\theta) = \ln |u_1(t, \theta)| - \ln |u_2(t, \theta)|, \quad (1.13)$$

where $|u_1(t, \theta)|$ and $|u_2(t, \theta)|$ are signal amplitudes at output of receiving-amplifying channels as a function of time and angular error in direction finding.

Phase difference between signals at amplifier input does not affect the ratio $r_m(\theta)$ since signals are detected before the amplitude logarithms of these signals are subtracted.

In the phase angular discriminator with normalization, it is necessary to eliminate amplitude modulation. For this either amplifiers with limitation (Fig. 1.5a) are used, at whose output the amplitudes do not depend upon the amplitudes of the signals received, or independent automatic regulation of amplification in both channels is used (Fig. 1.5b). To form the direction finding characteristic we can use function $r_m(\theta)$, determined by equality (1.12), since its effective part

$$S(\theta) = \operatorname{Re}[-i \exp i \varphi(\theta)] = \sin \varphi(\theta) \quad (1.14)$$

does not take into account the amplitude ratios.

In a sum-difference angular discriminator the ratio $r_a(\theta)$ is ensured by the automatic adjustment of amplification in both channels in order to form the voltages of which the total signal is used (Fig. 1.6). As a result, there is a normalization of the amplitudes of the sum and difference signals with respect to the amplitude of the sum signal.

In order to obtain the direction finding characteristic, the additive function of the angle is used; then with identical receiving channels, in the case of amplitude direction finding,

$$S(\theta) = \operatorname{Re} \frac{j_1(\theta) - j_2(\theta)}{j_1(\theta) + j_2(\theta)} = \frac{F_1(\theta) - F_2(\theta)}{F_1(\theta) + F_2(\theta)}, \quad (1.15)$$

and in the case of phase direction finding,

$$S(\theta) = \operatorname{Re} \frac{e^{i\varphi(\theta)} - e^{-i\varphi(\theta)}}{e^{i\varphi(\theta)} + e^{-i\varphi(\theta)}} = \operatorname{tg} \frac{\varphi(\theta)}{2}. \quad (1.16)$$

After examining the structural diagram of a monopulse system, we proceed to a more detailed description of the most frequently used monopulse radar system.

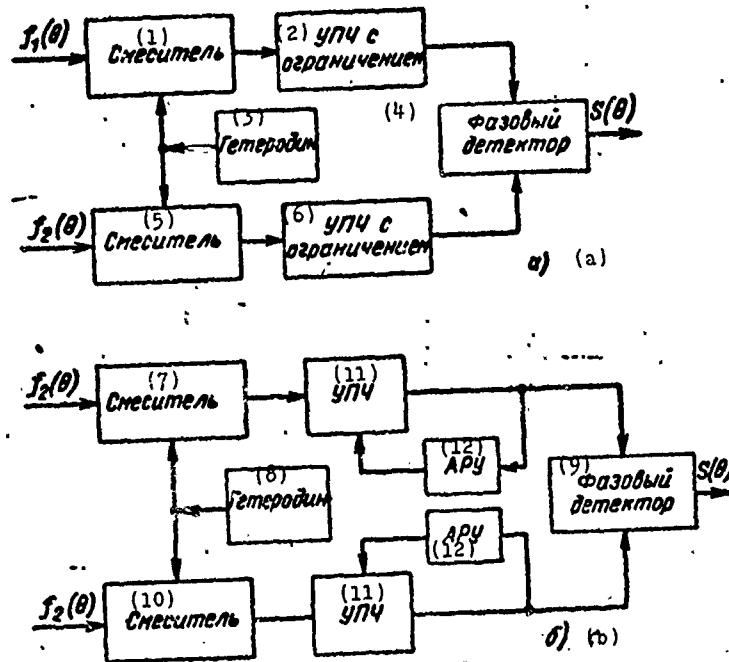


Fig. 1.5. Block diagram of a phase angular discriminator with different methods of normalization, limiting (a) and AGC (b).

KEY: (1) Mixer; (2) I-f amplifier with limiting; (3) Heterodyne; (4) Phase detector; (5) Mixer; (6) I-f amplifier with limiting; (7) Mixer; (8) Heterodyne; (9) Phase detector; (10) Mixer; (11) I-f amplifier; (12) AGC.

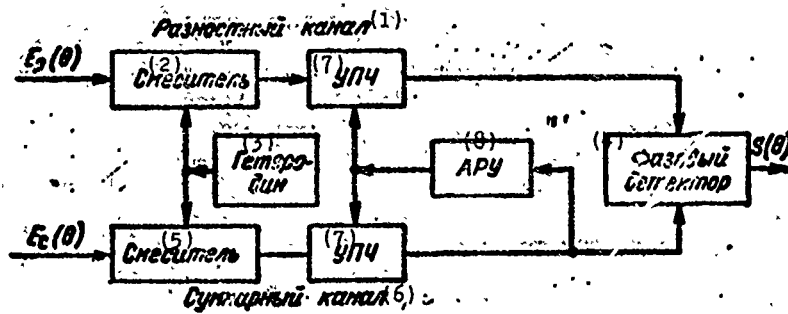


Fig. 1.6. Block diagram of sum-difference angular discriminator.
 KEY: (1) Difference channel; (2) Mixer; (3) Heterodyne; (4) Phase Detector; (5) Mixer; (6) Sum channel; (7) I-f amplifier; (8) AGC.

§ 1.3. MONOPULSE RADAR SYSTEMS OF AUTOMATIC TARGET TRACKING

1.3.1. Amplitude-amplitude monopulse system. As discussed in § 1.1, in monopulse systems with amplitude direction finding, the reception of signals reflected from the target is carried out with the aid of the antenna system forming in each coordinate plane two beams deflected from the equisignal direction by angle $\pm\theta_0$ (Fig. 1.1).

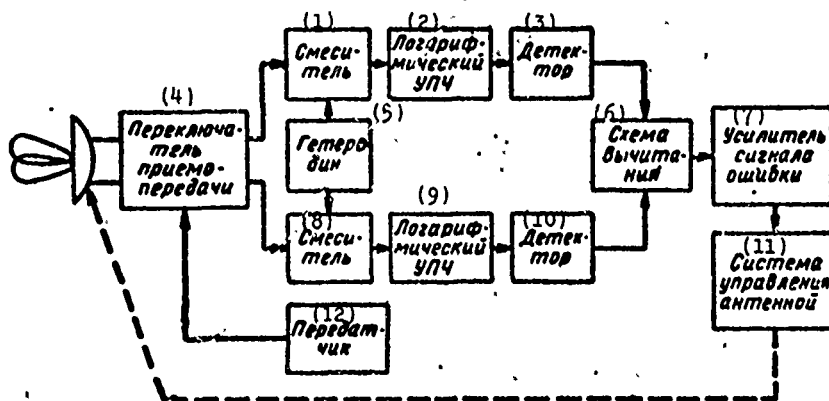


Fig. 1.7. Block diagram of amplitude-amplitude monopulse system of target tracking in one plane.
 KEY: (1) Mixer; (2) Logarithmic i-f amplifier; (3) Detector; (4) Send-receive switch; (5) Heterodyne; (6) Differential amplifier; (7) Error signal amplifier; (8) Mixer; (9) Logarithmic i-f amplifier; (10) Detector; (11) Antenna control system; (12) Transmitter.

The unbalance with respect to signal amplitude in the independent receiving channel is more directly related with tracking error the greater this error is. In the absence of mismatch, signals received by independent channels are equal in amplitude. In accordance with this, direction finding of targets is achieved by turning the antenna system up to the moment of amplitude equality for signals received.

Figure 1.7 presents a simplified block diagram of an amplitude-amplitude monopulse system for target direction finding in one plane, in which normalization is accomplished with the aid of logarithmic i-f amplifier.

If into the input of the antenna signal $\dot{E}(t) = E_m e^{i\omega t}$ enters, reflected from the target, when the target deviates from equisignal direction by angle θ , at antenna output of the first and second channels the signals received will be determined by expression

$$\begin{aligned}\dot{E}_1(t, \theta) &= E_m F_1(\theta) \exp i\omega t = E_m F(\theta_0 - \theta) \exp i\omega t, \\ \dot{E}_2(t, \theta) &= E_m F_2(\theta) \exp i\omega t = E_m F(\theta_0 + \theta) \exp i\omega t.\end{aligned}\tag{1.17}$$

After frequency conversion, amplification on intermediate frequency, and linear detection, signals at the input of the differential amplifier are equal to

$$\begin{aligned}u_1(\theta) &= \ln \kappa_1 E_m F(\theta_0 - \theta), \\ u_2(\theta) &= \ln \kappa_2 E_m F(\theta_0 + \theta),\end{aligned}\tag{1.18}$$

where κ_1 and κ_2 are signal transmission coefficients in the channels.

At the output of the differential amplifier we obtain

$$S(\theta) = \ln \frac{\kappa_1 F(\theta_0 - \theta)}{\kappa_2 F(\theta_0 + \theta)}.\tag{1.19}$$

Error signal from output of the differential amplifier is fed to the amplifier and then to the antenna control system.

From equality (1.19) it is apparent that the direction finding characteristic in such a monopulse system depends upon the radiation patterns, the properties and identical nature of the logarithmic amplifiers. Therefore, instability and nonidentity of amplitude characteristics of the logarithmic amplifiers lead to a distortion in the direction finding characteristic and, consequently, error in determining direction to target.

With identical receiving channels ($k_1 = k_2 = k$) and small angular errors, expression (1.19) can be written in the following form:

$$S(\theta) = \ln \frac{F(\theta_0 - \theta)}{F(\theta_0 + \theta)} = \ln \frac{F(\theta_0)(1 - \mu\theta)}{F(\theta_0)(1 + \mu\theta)} = \ln \frac{1 - \mu\theta}{1 + \mu\theta} \approx$$

$$\approx 2 \left[\mu\theta + \frac{\mu^2\theta^2}{2} + \frac{\mu^2\theta^2}{2} + \dots \right] \approx 2\mu\theta, \quad (1.20)$$

where $F(\theta_0)$ is the amplification factor of the antenna in the equi-signal direction;

μ is the steepness of the working section of the antenna radiation pattern.

The need to maintain high identity in amplitude characteristics of the amplifier is the main disadvantage of the system with an amplitude angular discriminator.

1.3.2. Phase-phase monopulse system. A simplified block diagram of a phase-phase monopulse system which ensures direction finding in one plane is presented in Fig. 1.8. In this system signal reception is performed by an antenna system which forms, in each coordinate plane, two beams oriented in parallel.

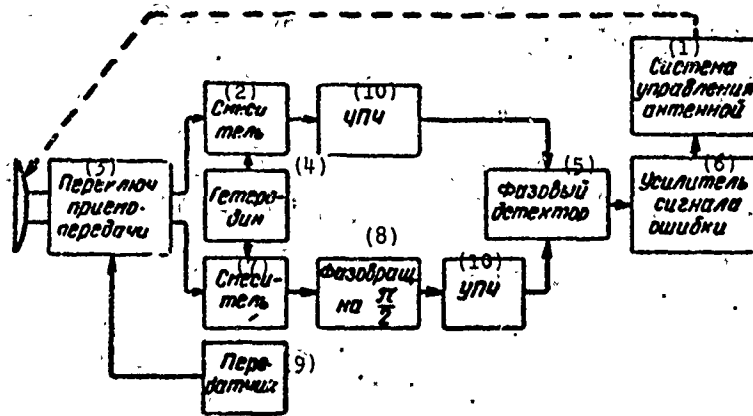


Fig. 1.8. Block diagram of phase-phase monopulse system for tracking a target in one plane.

KEY: (1) Antenna control system; (2) Mixer; (3) Send-receive switch; (4) Heterodyne; (5) Phase detector; (6) Error signal amplifier; (7) Mixer; (8) Phase converter; (9) Transmitter; (10) I-f amplifier.

Signals received by antennas with identical radiation patterns are written in the form

$$\left. \begin{aligned} \dot{E}_1(t, \theta) &= E_m F(\theta) \exp i \left(\omega t + \frac{\Delta \varphi}{2} \right), \\ \dot{E}_2(t, \theta) &= E_m F(\theta) \exp i \left(\omega t + \gamma_\phi - \frac{\Delta \varphi}{2} \right). \end{aligned} \right\} \quad (1.21)$$

where $\Delta \phi$ is phase shift because of difference in the paths of signal approach from target to antennas, determined by equality (1.1); $\gamma_\phi = \pi/2$ is initial phase shift necessary to ensure that output signal equals zero when equisignal direction coincides with direction to target ($\theta = 0$).

Signals at i-f amplifier outputs are equal, respectively, to

$$\left. \begin{aligned} \dot{i}_1(t, \theta) &= \kappa_1 E_m F(\theta) \exp i \left(\omega_{np} t + \frac{\Delta \varphi}{2} \right), \\ \dot{i}_2(t, \theta) &= \kappa_2 E_m F(\theta) \exp i \left(\omega_{np} t + \frac{\pi}{2} - \frac{\Delta \varphi}{2} \right). \end{aligned} \right\} \quad (1.22)$$

When limiting is used for standardization, signals at input of the phase detector can be represented in the form of the following expression

$$\left. \begin{aligned} \dot{u}'_1(t, \theta) &= U_{\text{огр}} \exp i \left(\omega_{\text{нп}} t + \frac{\Delta \varphi}{2} \right), \\ \dot{u}'_2(t, \theta) &= U_{\text{огр}} \exp i \left(\omega_{\text{нп}} t + \frac{\pi}{2} - \frac{\Delta \varphi}{2} \right). \end{aligned} \right\} \quad (1.23)$$

where $U_{\text{огр}}$ is the threshold of amplitude limitation.

If the amplitude detector and the phase detector are operating in the square-law detection mode, i.e., the phase detector performs the multiplication and averaging of input signals, the signal at output of the phase detector can be written in the form

$$S(\theta) = \kappa_{\phi \lambda} \text{Re} [\dot{u}'_1(t, \theta) \dot{u}'_2(t, \theta)], \quad (1.24)$$

where $\kappa_{\phi \lambda}$ is the transmission factor of the phase detector.

Consequently,

$$S(\theta) = \kappa_{\phi \lambda} U_{\text{огр}}^2 \sin \Delta \varphi. \quad (1.25)$$

Substituting in place of $\Delta \varphi$ its value from (1.1), we obtain

$$S(\theta) = \kappa_{\phi \lambda} U_{\text{огр}}^2 \sin \left(\frac{2\pi l}{\lambda} \sin \theta \right). \quad (1.26)$$

The error signal from the phase detector is fed to the error signal amplifier and then to the antenna control system, which turns the antenna to the necessary angle.

The main disadvantage of systems with a phase angular discriminator, as will be shown in Chapter 6 in detail, is the considerable dependence of direction finding accuracy on the identity of the phase characteristics of the receiving channel and their stability.

1.3.3. Amplitude sum-difference monopulse system: A monopulse system with a sum-difference angular discriminator has less strenuous requirements on the identity of the characteristics of the receiving channels and, therefore, is more widely used in contemporary radar stations. In such systems the signals received from the target move from antenna output to the sum-difference converter (waveguide bridge) where they are added and subtracted. From the outputs of the waveguide bridge the sum and difference high-frequency signals are fed to the sum and difference receiving channels where they are converted to signals of intermediate frequency and amplified to the necessary value. The amplitude of the difference signals determines the amount of angular error, while the phase difference between the sum and difference signals determines the sign of the angular error, i.e., direction of target deviation from equisignal direction.

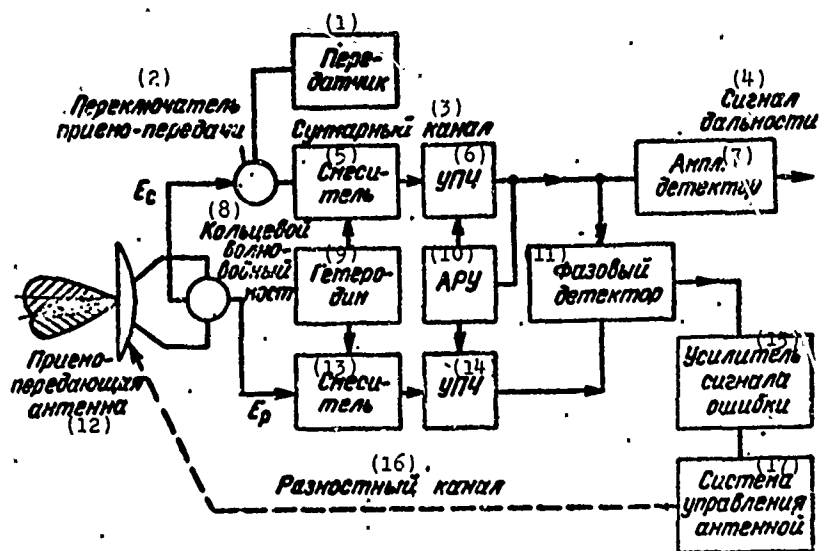


Fig. 1.9. Block diagram of an amplitude sum-difference monopulse system of target tracking for direction finding in one plane.

KEY: (1) Transmitter; (2) Send-receive switch; (3) Sum channel; (4) Range signal; (5) Mixer; (6) I-f amplifier; (7) Amplitude detector; (8) Snnular waveguide bridge; (9) Heterodyne; (10) AGC; (11) Phase detector; (12) Send-receive antenna; (13) Mixer; (14) I-f amplifier; (15) Error signal amplifier; (16) Difference channel; (17) Antenna control system.

A block diagram of an amplitude sum-difference monopulse system for direction finding in one plane is presented in Fig. 1.9. Signals at antenna output of the first and second channels with small target deviations from equisignal direction are determined by expression

$$\left. \begin{aligned} \dot{E}_1(t, \theta) &= E_m F_1(\theta) \exp i \omega t = E_m F(\theta_0 - \theta) \exp i \omega t = \\ &= E_m F(\theta_0) (1 + \mu \theta) \exp i \omega t, \\ \dot{E}_2(t, \theta) &= E_m F_2(\theta) \exp i \omega t = E_m F(\theta_0 + \theta) \exp i \omega t = \\ &= E_m F(\theta_0) (1 - \mu \theta) \exp i \omega t. \end{aligned} \right\} \quad (1.27)$$

The sum and difference signals at output of the waveguide bridge, taking into account the power balance, assume the form

$$\left. \begin{aligned} \dot{E}_c(t, \theta) &= \frac{1}{\sqrt{2}} [\dot{E}_1(t, \theta) + \dot{E}_2(t, \theta)] = \\ &= \sqrt{2} E_m F(\theta_0) \exp i \omega t, \\ \dot{E}_p(t, \theta) &= \frac{1}{\sqrt{2}} [\dot{E}_1(t, \theta) - \dot{E}_2(t, \theta)] = \\ &= \sqrt{2} E_m F(\theta_0) \mu \theta \exp i \omega t. \end{aligned} \right\} \quad (1.28)$$

The dependence of the error signal on amplitude of received signals is eliminated by the AGC system.

After frequency conversion and amplification, taking into account the work of the AGC system, at input of the phase detector the sum and difference signals can be represented by expression

$$\left. \begin{aligned} \dot{u}_c(t, \theta) &= \exp i(\omega_{np} t + \varphi_1), \\ \dot{u}_p(t, \theta) &= \frac{\kappa_2}{\kappa_1} \mu \theta \exp i(\omega_{np} t + \varphi_2), \end{aligned} \right\} \quad (1.29)$$

where ϕ_1 and ϕ_2 are the phase shifts in the channels.

At phase detector output we obtain

$$S(\theta) = \kappa_{\phi \Delta} \frac{\kappa_2}{\kappa_1} \mu \theta \cos(\varphi_1 - \varphi_2). \quad (1.30)$$

The sum and difference radiation patterns of an amplitude sum-difference monopulse system, with the conditional designation of phase ratios by the signs "+" and "-" are illustrated in Fig. 1.10. From the figure it is apparent that the phase of the difference signal at antenna output changes as a function of the direction of target deviation relative to equisignal direction and can either coincide with the phase of the sum signal or be in opposite phase to it. In the absence of disagreement, when direction to target coincides with equisignal direction of the antenna system, the signals reflected from the target at the input of the receiving channels have equal amplitude. Due to this, the difference signal is zero.

The difference signal is used directly in controlling the position of the antenna system in the process of direction finding or in the process of automatic target tracking.

The sum signal forming upon reception is used not only as the reference signal but also for target detection as well as measurement of range to target and its velocity.

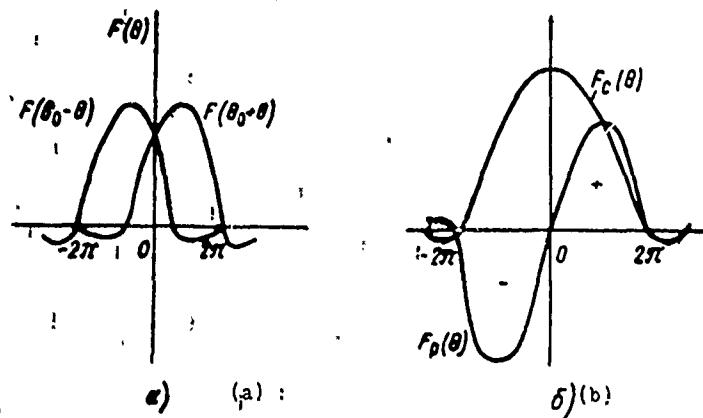


Fig. 1.10. Radiation pattern of an amplitude sum-difference monopulse system with direction finding in one plane: a) partial patterns; b) sum and difference patterns.

1.3.4. Phase sum-difference monopulse system. Let us examine the processing of signals in a phase sum-difference monopulse system (Fig. 1.11). In analogy with the phase-phase system examined in 1.3.2 the signals at antenna output, in the given case, can be written in the form

$$\left. \begin{aligned} \dot{E}_1(t, \theta) &= E_m F(\theta) \exp i \left(\omega t + \frac{\Delta\varphi}{2} \right), \\ \dot{E}_2(t, \theta) &= E_m F(\theta) \exp i \left(\omega t - \frac{\Delta\varphi}{2} \right). \end{aligned} \right\} \quad (1.31)$$

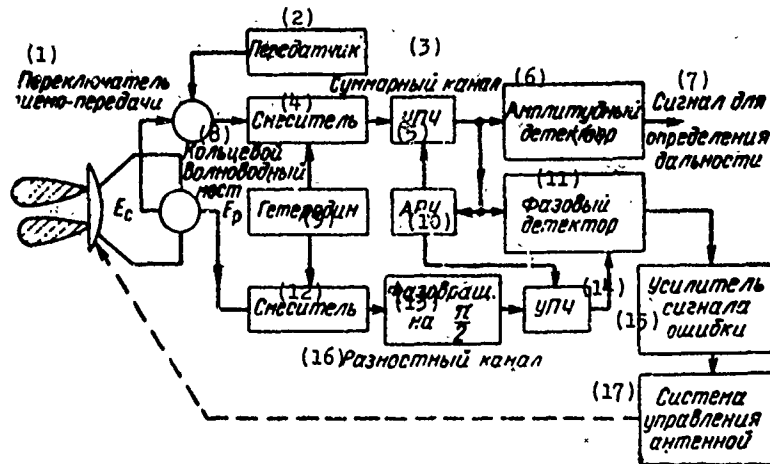


Fig. 1.11. Block diagram of a phase sum-difference monopulse system of target tracking in one plane.

КЭУ: (1) Send-receive switch; (2) Transmitter; (3) Sum channel; (4) Mixer; (5) I-f amplifier; (6) Amplitude detector; (7) Signal for determining range; (8) Annular waveguide bridge; (9) Heterodyne; (10) AGC; (11) Phase detector; (12) Mixer; (13) Phase switcher; (14) I-f amplifier; (15) Error signal amplifier; (16) Difference channel; (17) Antenna control system.

At output of the waveguide bridge we obtain the sum and difference signals in the form

$$\left. \begin{aligned} \dot{E}_c(t, \theta) &= \frac{1}{\sqrt{2}} E_m F(\theta) \left[\exp i \left(\omega t + \frac{\Delta\varphi}{2} \right) + \right. \\ &\quad \left. + \exp i \left(\omega t - \frac{\Delta\varphi}{2} \right) \right], \\ \dot{E}_p(t, \theta) &= \frac{1}{\sqrt{2}} E_m F(\theta) \left[\exp i \left(\omega t + \frac{\Delta\varphi}{2} \right) - \right. \\ &\quad \left. - \exp i \left(\omega t - \frac{\Delta\varphi}{2} \right) \right]. \end{aligned} \right\}$$

(1.32)

At output of the phase detector after frequency conversion and amplification, taking into account the work of the AGC and the additional phase shift in the difference channel by $\pi/2$, we can write

$$S(\theta) = \frac{\operatorname{Re} \dot{u}_c(t, \theta) \dot{u}_p^*(t, \theta)}{\dot{u}_c(t, \theta) \dot{u}_c^*(t, \theta)}, \quad (1.33)$$

where \dot{u}_c^* and \dot{u}_p^* are the complex conjugate values of signals at output of the sum and difference channels.

Taking into account (1.32), expression (1.33) assumes the form

$$S(\theta) = \frac{\kappa_2}{\kappa_1} \kappa_{\phi n} \frac{\sin \Delta\varphi}{1 + \cos \Delta\varphi} = \frac{\kappa_2}{\kappa_1} \kappa_{\phi n} \operatorname{tg} \frac{\Delta\varphi}{2}. \quad (1.34)$$

After substituting values of $\Delta\varphi$ from (1.1), we obtain

$$S(\theta) = \frac{\kappa_2}{\kappa_1} \kappa_{\phi n} \operatorname{tg} \left(\frac{\pi l}{\lambda} \sin \theta \right). \quad (1.35)$$

Error signal from output of the phase detector is fed to the antenna control system.

§ 1.4. MONOPULSE RADAR SCANNING SYSTEMS

In § 1.1 we mentioned that systems which determine the coordinates of all targets located within the antenna pattern and resolvable with respect to range for each position of the beam in space are called monopulse scanning systems. Let us examine these systems using the example of systems with amplitude direction finding.

1.4.1. Amplitude-amplitude monopulse system. As mentioned above, an amplitude angular discriminator with logarithmic amplifiers has a considerable disadvantage in the need to maintain high identity and stability of the amplifiers' amplitude characteristics. This disadvantage makes its practical application difficult in amplitude-amplitude monopulse systems.

We shall examine another structural diagram of such a system, which makes it possible to eliminate the use of logarithmic amplifiers. In the system whose block diagram is presented in Fig. 1.12 no logarithmic amplifiers are used and standardization is accomplished according to the sum signal formed at video frequency.

Let us describe the forming of the direction finding characteristic in an amplitude-amplitude monopulse scanning system with standardization according to the sum signal formed at video frequency.

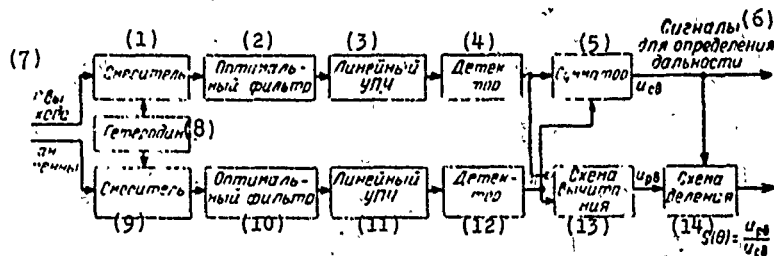


Fig. 1.12. Block diagram of amplitude-amplitude monopulse scanning system for determining coordinates in one plane.

KEY: (1) Heterodyne; (2) Optimal filter; (3) Linear 1-f amplifier; (4) Detector; (5) Summator; (6) Signal for range determination; (7) From antenna output; (8) Heterodyne; (9) Mixer; (10) Optimal filter; (11) Linear 1-f amplifier; (12) Detector; (13) Differential amplifier; (14) Divider circuit.

When the target deviates from equisignal direction by angle θ , the signal at antenna output will be determined by formula (1.27). At detector output the expression for signals assumes the form

$$\left. \begin{aligned} u_1(\theta) &= \kappa_1 E_m F(\theta_0) (1 + \mu\theta), \\ u_2(\theta) &= \kappa_2 E_m F(\theta_0) (1 - \mu\theta). \end{aligned} \right\} \quad (1.36)$$

With identical receiving channels ($\kappa_1 = \kappa_2 = \kappa$) at the output of the summing device we write

$$u_{cв} = u_1(\theta) + u_2(\theta) = 2\kappa E_m F(\theta), \quad (1.37)$$

and at the output of the differential amplifier

$$u_{p u} = u_1(\theta) - u_2(\theta) = 2\kappa E_m F(\theta_0) \mu \theta. \quad (1.38)$$

Then at output of the divider circuit we obtain

$$S(\theta) = \frac{u_{p u}}{u_{c u}} = \frac{2\kappa E_m F(\theta_0) \mu \theta}{2\kappa E_m F(\theta_0)} = \mu \theta. \quad (1.39)$$

A comparison of equalities (1.20) and (1.39) shows that they coincide with accuracy up to the constant coefficient, i.e., and in the system with standardization according to the sum signal, at output there is received a signal proportional to the angular error in direction finding and, therefore, it can be used as angular information in determining angular coordinates of targets.

In practice, when building amplitude-amplitude monopulse radar scanning systems with standardization according to the sum signal, which must have a dynamic range of 80-100 dB, linear i-f amplifiers cannot be used. In these cases, it is necessary to use logarithmic i-f amplifiers in which, in order to eliminate the need for maintaining high identity of logarithmic amplitude characteristics of amplifiers in various channels, it is necessary to perform standardization with the aid of a periodic sequence of monitoring signals and then construct the processing circuit as shown in Fig. 1.12.

1.4.2. Amplitude sum-difference monopulse system. A block diagram of an amplitude sum-difference monopulse scanning system is presented in Fig. 1.13. By comparing this block diagram and the one presented in Fig. 1.9, it is apparent that in both systems standardization is performed according to the sum signal. However, in the scanning system standardization is performed not at intermediate frequency with the aid of AGC, but at video frequency by dividing the signal from phase detector output by the sum signal. This is explained by the impossibility of using an AGC system in monopulse

scanning systems because in these systems it is necessary to determine the coordinates of all targets located in the beam and resolvable with respect to range. An AGC system has a certain time lag and cannot operate with several closely located targets.

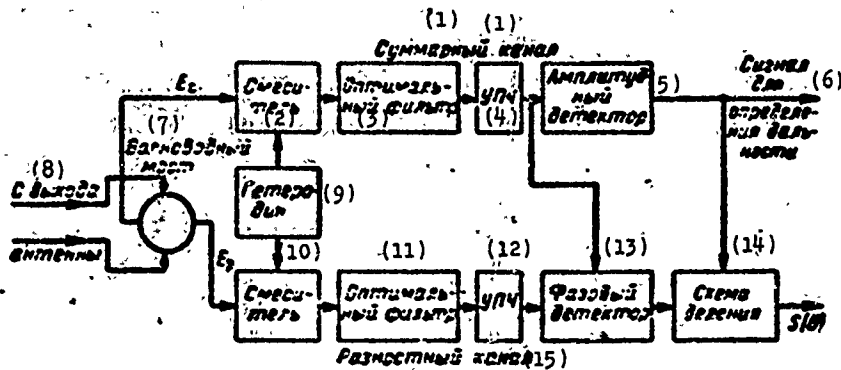


Fig. 1.13. Block diagram of an amplitude sum-difference monopulse scanning system for determining coordinates in one plane.

KEY: (1) Sum channel; (2) Mixer; (3) Optimal filter; (4) I-f amplifier; (5) Amplitude detector; (6) Signal for determining range; (7) Waveguide bridge; (8) From antenna output; (9) Heterodyne; (10) Mixer; (11) Optimal filter; (12) I-f amplifier; (13) Phase detector; (14) Divider circuit; (15) Difference channel.

Let us examine the formation of the direction finding characteristic in an amplitude sum-difference scanning system. The sum and difference channels at the output of the waveguide bridge are determined by formula (1.28).

At phase detector input they can be written, respectively, as

$$\left. \begin{aligned} \dot{u}_c(t, \theta) &= \sqrt{2} \kappa_1 E_m F(\theta_0) \exp i(\omega_{np} t + \varphi_1), \\ \dot{u}_p(t, \theta) &= \sqrt{2} \kappa_2 E_m F(\theta_0) \mu \theta \exp i(\omega_{np} t + \varphi_2). \end{aligned} \right\} \quad (1.40)$$

The sum signal at amplitude detector output, considering its transmission factor equal to one, will be

$$u_c = \sqrt{2} \kappa_1 E_m F(\theta_0), \quad (1.41)$$

and voltage at output of the quadratic phase detector will be

$$u_{\phi R} = 2\kappa_{\phi R} \kappa_1 \kappa_2 [E_m F(\theta_0)]^2 \mu \theta \cos(\varphi_1 - \varphi_2). \quad (1.42)$$

When using a quadratic phase detector in the block diagram presented in Fig. 1.13, it is necessary to provide a device which will square the sum signal at amplitude detector output. Then at divider circuit output we obtain

$$S(\theta) = \frac{u_{\phi 2}}{u_c^2} = \kappa_{\phi 2} \frac{\kappa_2}{\kappa_1} \mu^2 \cos(\varphi_1 - \varphi_2). \quad (1.43)$$

A comparison of formulas (1.43) and (1.30) shows that they agree i.e., standardization according to sum signal at video frequency gives the same effect as standardization at intermediate frequency with the aid of AGC.

The creation of a monopulse sum-difference scanning system which has high resolution with respect to range (on the order of 10-30 m) can prove to be impossible because of the technical difficulty involved in making a phase detector which will operate with pulse width near 0.1 μ s. In this case, we must turn to the development of amplitude-amplitude monopulse scanning systems.

§ 1.5. DESIGN PRINCIPLES FOR MONOPULSE SYSTEMS OF DIRECTION FINDING IN TWO PLANES

The monopulse radar systems examined thus far have been designed for finding targets in one plane. Direction finding systems for two planes are considerably more complex.

Monopulse systems for target finding in two planes with amplitude and phase angular discriminators can be made by a simple combination of two monopulse systems, one of which is designed to operate in the azimuth plane and the second in the elevation plane. From the block diagram of the amplitude-amplitude system for direction finding in two planes, presented in Fig. 1.14, it is apparent that such a design requires the use of an antenna with four radiation patterns and four amplification channels. However, in systems with the above indicated angular discriminators, in two-plane direction finding there can be one amplification channel for both azimuth and elevation

planes. This simplifies antenna design and the direction finding system as a whole.

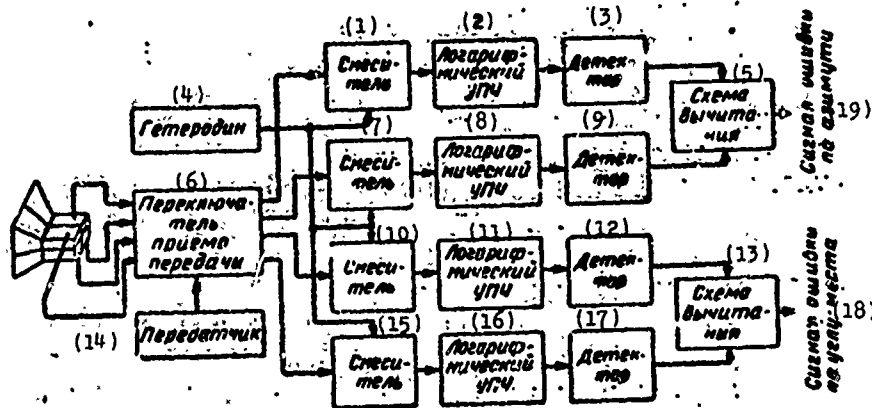


Fig. 1.14. Block diagram of amplitude-amplitude monopulse system for direction finding in two planes.

KEY: (1) Mixer; (2) Logarithmic i-f amplifier; (3) Detector; (4) Heterodyne; (5) Differential amplifier; (6) Send-receive switch; (7) Mixer; (8) Logarithmic i-f amplifier; (9) Detector; (10) Mixer; (11); Logarithmic i-f amplifier; (12) Detector; (13) Differential amplifier; (14) Transmitter; (15) Mixer; (16) Logarithmic i-f amplifier; (17) Detector; (18) Elevation error signal; (19) Azimuth error signal.

As an example, a simplified block diagram of one of the first phase-phase monopulse radar system is presented in Fig. 1.15 [41]. The antenna system of this radar consists of four rigidly connected parabolic reflectors with feeds. One of the antennas is the transmitting antenna and the others are receiving antennas; one of the latter is a common antenna for azimuth and elevation channels.

The main disadvantage of this system lies in the ineffective use of antenna aperture since part of the antenna is used only for direction finding with respect to azimuth, part for direction finding with respect to elevation, and part for emission. With four receiving radiation patterns this disadvantage is eliminated since for reception and transmission the entire antenna aperture can be used.

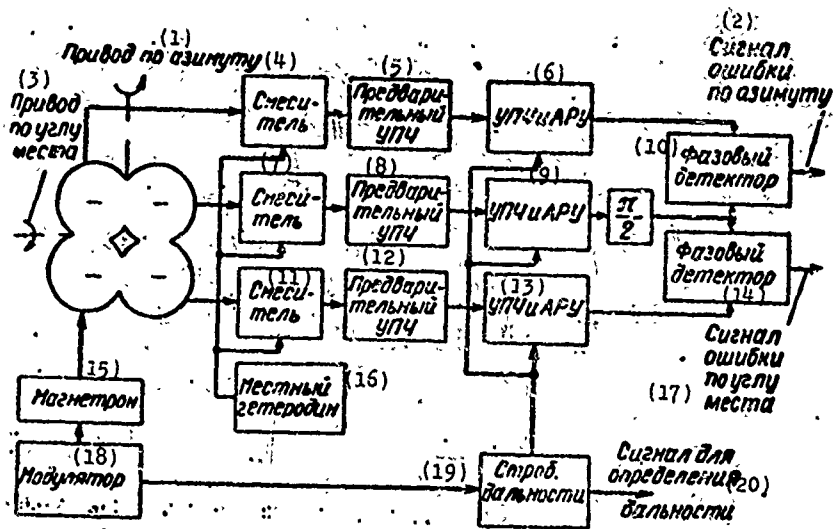


Fig. 1.15. Block diagram of a phase-phase monopulse system for direction finding in two planes.
 KEY: (1) Azimuth drive; (2) Azimuth error signal; (3) Elevation drive; (4) Mixer; (5) Preliminary i-f amplifier; (6) I-f amplifier and AGC; (7) Mixer; (8) Preliminary i-f amplifier; (9) I-f amplifier and AGC; (10) Phase detector; (11) Mixer; (12) Preliminary i-f amplifier; (13) I-f amplifier and AGC; (14) Phase detector; (15) Magnetron; (16) Local heterodyne; (17) Elevation error signal; (18) Modulator; (19) Range gate; (20) Signal for determining range.

In monopulse systems for direction finding in two planes with a sum-difference discriminator, unlike systems of direction finding in one plane, an antenna with four radiation patterns (instead of two) and three or four waveguide bridges (instead of one) is used; there is also added one difference receiving channel and a number of other elements. Figure 1.16 shows an amplitude sum-difference system with direction finding in two planes, using four waveguide bridges; signal processing in such a system is shown in Figure 1.17. The method of signal processing using three waveguide bridges is illustrated in Fig. 1.18.

In a monopulse system with four waveguide bridges the sum signal is formed by paired preliminary summation of signals 1 and 2, 3 and 4 on the first two bridges and then a final summation on the third and fourth bridges. The high-frequency power of the transmitter, with the aid of these bridges, is distributed equally and in phase

between all four radiators, ensuring the formation of a sum radiation pattern in space. The difference signal of elevation is obtained by subtracting from the sum of the signals of radiators 1 and 2, the sums of signals of radiators 3 and 4.

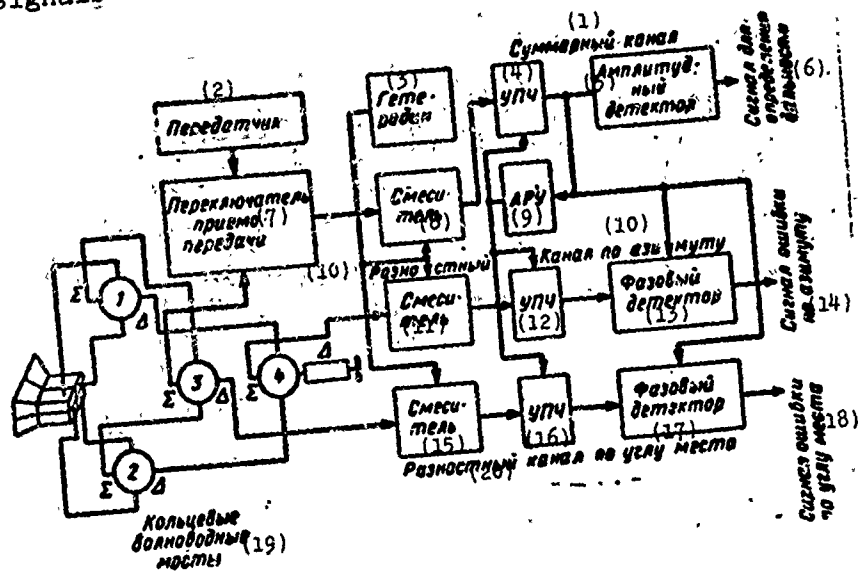


Fig. 1.16. Block diagram of an amplitude sum-difference monopulse system for direction finding in two planes. Σ - sum output of bridge; Δ - difference output of bridge.
 KEY: (1) Sum channel; (2) Transmitter; (3) Heterodyne; (4) I-f amplifier; (5) Amplitude detector; (6) Signals for determining range; (7) Send-receive switch; (8) Mixer; (9) AGC; (10) Difference channel for azimuth; (11) Mixer; (12) I-f amplifier; (13) Phase detector; (14) Azimuth error signal; (15) Mixer; (16) I-f amplifier; (17) Phase detector; (18) Elevation error signal; (19) Annular waveguide bridges; (20) Difference channels for elevation.

In order to obtain a difference signal for azimuth in the fourth bridge, the sum of the signals of radiators 2 and 4 is subtracted from the sum of the signals of radiators 1 and 3.

Analytically, these signals can be represented in the form of the following expressions:

- sum signal (at output of the sum branch of the third bridge)

$$E_c(t, \theta) = \frac{1}{2} E(t) [F_1(\theta) + F_2(\theta) + F_3(\theta) + F_4(\theta)], \quad (1.44)$$

- difference signal for elevation (at output of the difference branch of the third bridge)

$$E_{\text{раз}}(t, \theta) = \frac{1}{2} E(t) \{ [F_1(\theta) + F_2(\theta)] - [F_3(\theta) + F_4(\theta)] \}. \quad (1.45)$$

- difference signal for azimuth (at output of the sum branch of the fourth bridge)

$$E_{\text{раз}}(t, \theta) = \frac{1}{2} E(t) \{ [F_1(\theta) + F_2(\theta)] - [F_3(\theta) + F_4(\theta)] \}. \quad (1.46)$$

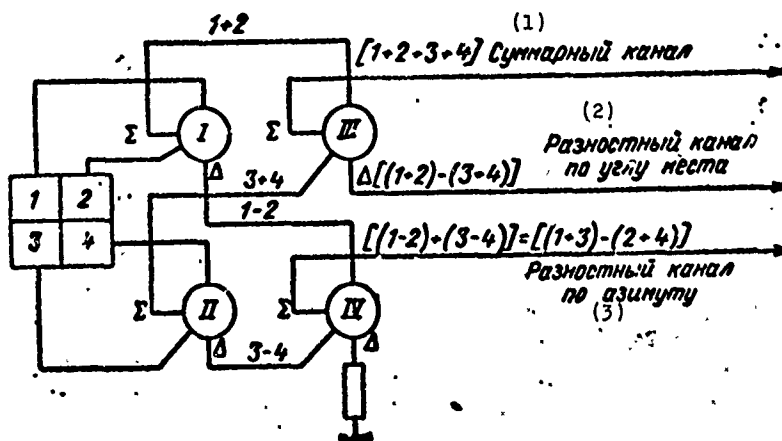


Fig. 1.17. Diagram for forming sum and difference signals with the use of four waveguide bridges. Σ - sum output of bridge; Δ - difference output of bridge.

KEY: (1) Sum channel; (2) Difference channel for elevation; (3) Difference channel for azimuth.

The output of the difference branch of the fourth bridge is usually not used and terminates in the dummy.

With the use in a monopulse system of three waveguide bridges the sum signal is formed by the preliminary paired summation of signals 2 and 3, 1 and 2 on two bridges, and then by the final summation in the third bridge. The difference branch of the third bridge is not used and terminates in the dummy. The difference signal

in one plane is formed by the difference of signals 1 and 2 and in the other plane by the difference of signals 2 and 3.

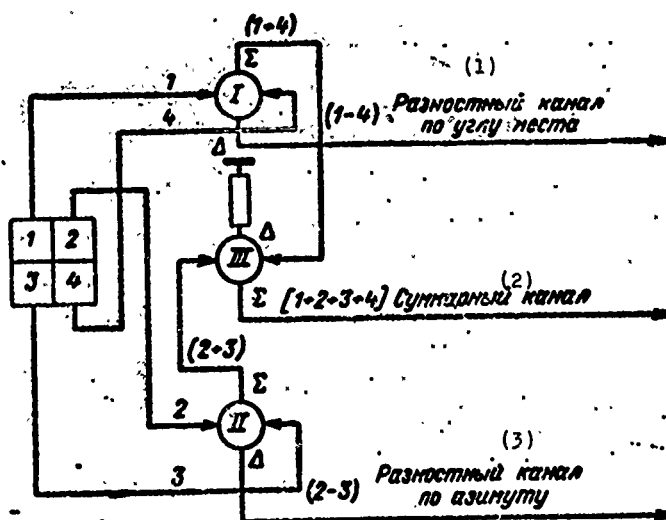


Fig. 1.18. Diagram for forming sum and difference signals with the use of three waveguide bridges. Σ - sum output of bridge; Δ - difference output of bridge. KEY: (1) Difference channel for elevation; (2) Sum channel; (3) Difference channel for azimuth.

With the application of three waveguide bridges the sum signal is determined by equality (1.44) and the difference signal is equal to

$$E_{\text{разн}} = \frac{1}{\sqrt{2}} E(t) [F_1(\theta) - F_4(\theta)], \quad (1.47)$$

$$E_{\text{разн}} = \frac{1}{\sqrt{2}} E(t) [F_2(\theta) - F_3(\theta)]. \quad (1.48)$$

Amplitude and phase sum-difference monopulse systems are identical in method of processing angular information; however, they have principal differences in the formation of the antenna pattern. Angular target information in an amplitude system is contained in the ratio of signal amplitudes, and in a phase system in the phase shift caused by the difference in signal paths from target to antennas of the corresponding direction finding channels.

Combined monopulse direction finding systems have certain advantages in design. They are based on a formation of antenna

radiation pattern which ensures the obtaining of independent target information simultaneously with amplitude and phase relationships of signals received. In this case, it can be avoided with direction finding in two planes only by two interconnected channels with one waveguide bridge at their input (Fig. 1.19).

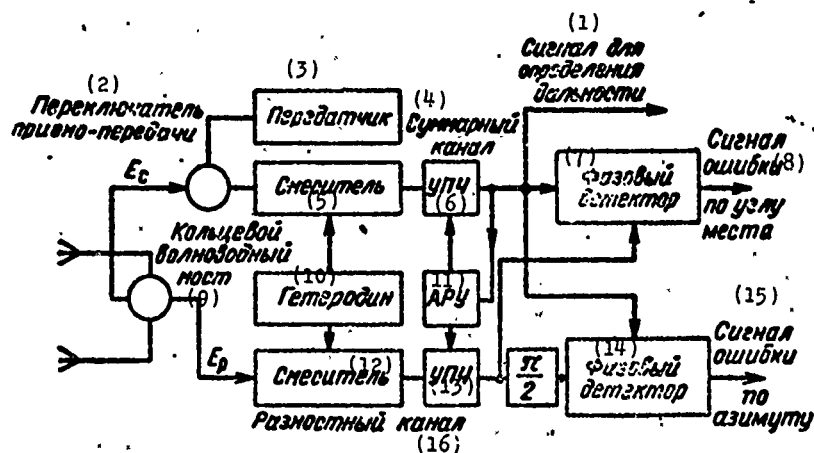


Fig. 1.19. Block diagram of a combined monopulse system for direction finding in two planes.
 KEY: (1) Signal for determining range; (2) Send-receive switch; (3) Transmitter; (4) Sum channel; (5) Mixer; (6) I-f amplifier; (7) Phase detector; (8) Elevation error signal; (9) Annular waveguide bridge; (10) Heterodyne; (11) AGC; (12) Mixer; (13) I-f amplifier; (14) Phase detector; (15) Azimuth error signal; (16) Difference channel.

The principle of forming angular errors based on two coordinates is illustrated at the same time by the vector pattern (Fig. 1.20). Designations \vec{U}_1 and \vec{U}_2 correspond to signals in the vector concept for the first and second channels. Signals differ in amplitude and phase.

Difference signal $\vec{U}_2 - \vec{U}_1$, as seen in the figure, can be represented in the form of two independent components, one of which is found in quadrature with the sum signal, which is characteristic for a phase direction finding system, and the other component is in phase or in opposite phase with the sum signal, which is characteristic for an amplitude direction finding system. The first component, as will be shown below, can be used as an azimuth error signal and the second as an elevation error signal.

The two beams formed by the antenna in the vertical plane are deflected from each other by angle $2\theta_0$, and in the horizontal plane are parallel to each other and separated by a distance l , which ensures target finding in the vertical plane by the amplitude method and in the horizontal plane by the phase method.

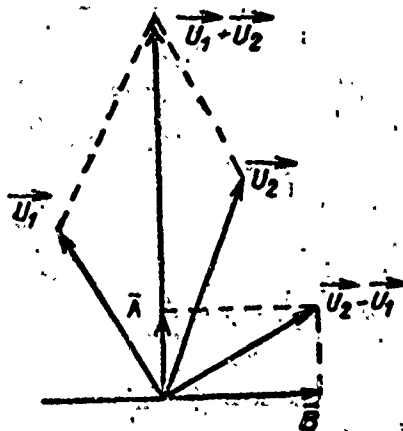


Fig. 1.20. Vector diagram illustrating the principle of a combined direction finding system: A - is the in-phase component of the difference signal (elevation error); B is the quadrature-phase component of the difference signal (azimuth error).

In order to form beams which are parallel in the azimuth plane, linear feeds of the antenna are tilted and irradiate the left and right halves of the parabolic cylinder. In order to slant the beams relative to each other in the vertical plane, the feeds are located on different sides from the focal plane (one above and the other below) (Fig. 1.21).

To extract angular information with respect to each coordinate, at output of receiving channels there are two phase detectors, one of which forms the elevation error and the other the azimuth error signal. The difference signal is fed to the azimuth phase detector with a phase shift of 90° relative to the sum signal, which is the reference signal. The other elements of a combined amplitude-phase

system are similar to the elements of the amplitude and phase systems discussed above.

Let us examine the formation of the direction finding characteristic in a combined amplitude-phase monopulse system. Let the object of the direction finding be displaced from equisignal direction in azimuth by angle θ_{az} and in elevation by angle θ_{ym} . Then the signals at antenna output will differ in phase in accordance with the azimuthal displacement of the angle and in amplitude in accordance with its elevation displacement and can be represented in the form of the following expressions:

$$\left. \begin{aligned} \dot{E}_1(t, \theta) &= E_m F(\theta_{az}) F(\theta_0 - \theta_{ym}) \exp i \left(\omega t + \frac{\Delta \varphi_{az}}{2} \right), \\ \dot{E}_2(t, \theta) &= E_m F(\theta_{az}) F(\theta_0 + \theta_{ym}) \exp i \left(\omega t - \frac{\Delta \varphi_{az}}{2} \right). \end{aligned} \right\} \quad (1.49)$$

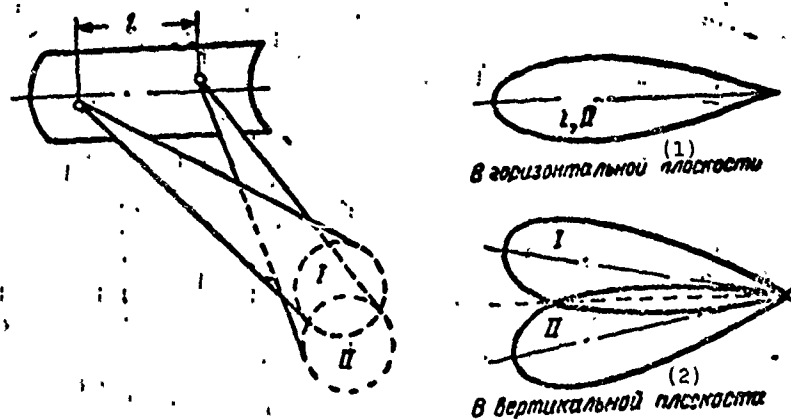


Fig. 1.21. The principle of forming radiation patterns and combined monopulse systems.

KEY: (1) In the horizontal plane; (2) In the vertical plane.

At output of the waveguide bridge the sum and difference signals, with an accuracy up to the constant coefficient, can be written in the form

$$\left. \begin{aligned}
 \dot{E}_c(t, \theta) &= E_x \left[F(\theta_0 - \theta_{ym}) \exp i \left(\omega t + \frac{\Delta \varphi_{as}}{2} \right) + \right. \\
 &\quad \left. + F(\theta_0 + \theta_{ym}) \exp i \left(\omega t - \frac{\Delta \varphi_{as}}{2} \right) \right], \\
 E_p(t, \theta) &= E_x \left[F(\theta_0 - \theta_{ym}) \exp i \left(\omega t + \frac{\Delta \varphi_{as}}{2} \right) - \right. \\
 &\quad \left. - F(\theta_0 + \theta_{ym}) \exp i \left(\omega t - \frac{\Delta \varphi_{as}}{2} \right) \right],
 \end{aligned} \right\} \quad (1.50)$$

where

$$E_x = \frac{1}{\sqrt{2}} E_m F(\theta_{as}).$$

After frequency conversion and amplification in the I-f amplifier, without taking into account phase shifts and signal standardization, we obtain

$$\left. \begin{aligned}
 \dot{u}_c(t, \theta) &= E_x \kappa_c \left[F(\theta_0 - \theta_{ym}) \exp i \left(\omega_{np} t + \frac{\Delta \varphi_{as}}{2} \right) + \right. \\
 &\quad \left. + F(\theta_0 + \theta_{ym}) \exp i \left(\omega_{np} t - \frac{\Delta \varphi_{as}}{2} \right) \right], \\
 \dot{u}_p(t, \theta) &= E_x \kappa_p \left[F(\theta_0 - \theta_{ym}) \exp i \left(\omega_{np} t + \frac{\Delta \varphi_{as}}{2} \right) - \right. \\
 &\quad \left. - F(\theta_0 + \theta_{ym}) \exp i \left(\omega_{np} t - \frac{\Delta \varphi_{as}}{2} \right) \right].
 \end{aligned} \right\} \quad (1.51)$$

At output of the quadratic phase detector, taking into account signal standardization in the receiving device, the error signal is determined by expression

$$S(\theta) = \kappa_{\phi \pi} \frac{\operatorname{Re} \dot{u}_c(t, \theta) \dot{u}_p^*(t, \theta)}{\dot{u}_c(t, \theta) \dot{u}_c^*(t, \theta)}. \quad (1.52)$$

In accordance with this, at output of the elevation channel phase detector, after elementary conversion the error signal will have the form

$$S(\theta_{y\mu}) = \kappa_{\phi\pi} \frac{\kappa_p}{\kappa_c} \times \frac{F^2(\theta_0 - \theta_{y\mu}) - F^2(\theta_0 + \theta_{y\mu})}{F^2(\theta_0 - \theta_{y\mu}) + F^2(\theta_0 + \theta_{y\mu}) + 2F(\theta_0 - \theta_{y\mu})F(\theta_0 + \theta_{y\mu}) \cos \Delta\varphi_{as}} \quad (1.53)$$

In the presence of small angular errors, when a linear approximation of the radiation pattern is valid,

$$F(\theta_0 \pm \theta_{y\mu}) = F(\theta_0) (1 \pm \mu\theta_{y\mu}) \quad (1.54)$$

$$F^2(\theta_0 \pm \theta_{y\mu}) \approx F^2(\theta_0) (1 \pm 2\mu\theta_{y\mu}) \quad (1.55)$$

Then expression (1.53), when the transmission factors of the receiving channel are equal, can be changed to the form

$$S(\theta_{y\mu}) = \kappa_{\phi\pi} \frac{\mu\theta}{\cos^2 \frac{\Delta\varphi_{as}}{2}} \quad (1.56)$$

In the absence of disagreement in the azimuth plane ($\Delta\phi_{az} = 0$) we obtain

$$S(\theta_{y\mu}) = \kappa_{\phi\pi} \mu\theta \quad (1.57)$$

i.e., expression (1.57) is similar to expression (1.30), deduced for an amplitude sum-difference monopulse system under the condition that the amplitude-phase characteristics of the receiving channels were identical.

At output of the azimuth channel phase detector, taking into account the additional phase shift of the difference signal by $\pi/2$, when $\kappa_c = \kappa_p$, we obtain

$$\begin{aligned}
S(\theta_{as}) &= K_{\phi} \kappa \frac{\operatorname{Re} \dot{u}_c(t, \theta) \dot{u}_p^*(t, \theta) \exp i \frac{\pi}{2}}{\dot{u}_c(t, \theta) \dot{u}_c^*(t, \theta)} = \\
&= K_{\phi} \kappa \frac{2F(\theta_0 - \theta_{ym}) F(\theta_0 + \theta_{ym}) \sin \Delta \varphi_{as}}{F^2(\theta_0 - \theta_{ym}) + F^2(\theta_0 + \theta_{ym}) + 2F(\theta_0 - \theta_{ym}) F(\theta_0 + \theta_{ym}) \cos \Delta \varphi_{as}} \approx \\
&\approx K_{\phi} \kappa \frac{\sin \Delta \varphi_{as}}{1 + \cos \Delta \varphi_{as}} = K_{\phi} \kappa \operatorname{tg} \frac{\Delta \varphi_{as}}{2}.
\end{aligned} \tag{1.58}$$

Expression (1.58) agrees with expression (1.34), obtained for a phase sum-difference monopulse system. The error signals obtained are used for turning the antenna system or for indicating the value and direction of antenna mismatch by the usual method.

Thus, a combined amplitude-phase system ensures the obtaining of an error signal in both direction finding planes in the presence of only two channels. In this lies the advantage of such systems over purely amplitude or purely phase sum-difference monopulse systems, since with direction finding in two planes they normally require four radiation patterns, four hybrid bridges, and three i-f channels. However, we must keep in mind that the radiation pattern of a combined amplitude-phase system has considerable lobe properties and the amplification of the sum radiation pattern and direction finding sensitivity are approximately 3 dB below optimal. Therefore, we must choose a combined amplitude phase system on the basis of thorough calculations taking into account all the advantages and disadvantages of these systems. We should also consider that combined systems have the potential of increasing resolution with respect to angular coordinates. This is due to the fact that when using them, only two channels and two antenna feeds are necessary. The use in such systems of four or more independent feeds furnishes extra information which can be used to compare an additional number of equations which determine target positions in space and to ensure the resolution of targets located at the same range within the range beam. This will be discussed in greater detail in Chapter 4.

Since combined systems have certain structural advantages, they have found wide application in airborne radar technology where the weight and size of the equipment is of prime importance.

One of the first monopulse radars operating by the combined method is the AN/APG-25 experimental aircraft radar in the 3-cm range, designed as part of the fire control system in the tail of a US Navy patrol aircraft [94].

Along with combined systems of the sum-difference type we can use combined systems with postdetector signal processing, similar to simple amplitude and phase monopulse systems.

§ 1.6. DESIGN PRINCIPLES OF MONOPULSE SYSTEMS OPERATING IN CONTINUOUS AND QUASICONTINUOUS RADIATION MODES

Characteristic for monopulse systems operating in continuous and quasicontinuous radiation modes is the use of target selection with respect to speed, which makes a certain impression on their design scheme. Figure 1.22 presents a typical block diagram of the receiver of such a monopulse system.

Each of the receiver channels, in principle, is like the 1-channel angle-measuring devices used in a radar with continuous radiation. After frequency conversion and amplification, i-f signals are fed to the mixers (4) and (5), the heterodyne voltage for which is the reference signal of the transmitter on intermediate frequency. The Doppler-frequency signals forming at mixer output are then amplified in Doppler-frequency amplifiers (D-f Ampl.) and selected with respect to frequency.

For the selection of signals based on Doppler frequencies, which corresponds to the selection of targets based on speed, in the receiver are provided mixers (6) and (7) at whose output narrow-band Doppler filters F-1 and F-2 are installed, whose passband width is selected in accordance with requirements for target

resolution based on speed. Frequency conversion is accomplished with the aid of signals from the tracking heterodyne, controlled by signals of the frequency discriminator.

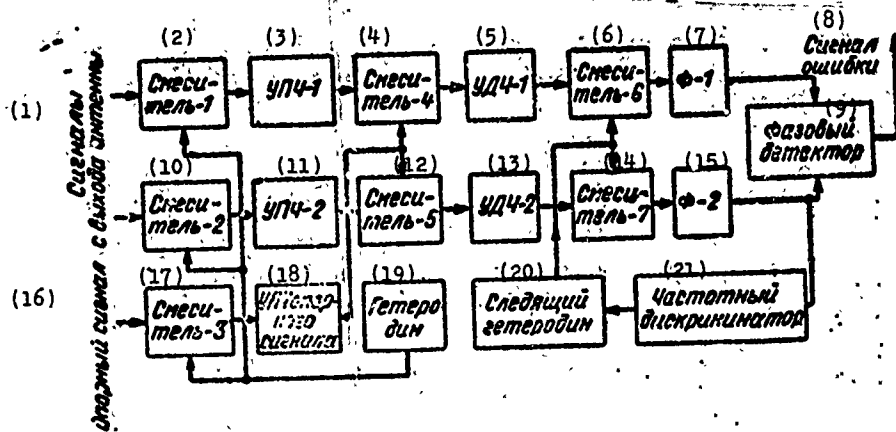


Fig. 1.22. Block diagram of a receiver of a monopulse system with selection based on speed.

KEY: (1) Signal from antenna output; (2) Mixer -1; (3) I-f amplifier -1; (4) Mixer -4; (5) Doppler frequency amplifier -1; (6) Mixer -6; (7) F-1; (8) Error signal; (9) Phase detector; (10) Mixer -2; (11) I-f amplifier -2; (12) Mixer -5; (13) Doppler frequency amplifier -2; (14) Mixer -7; (15) F-2; (16) Reference signal; (17) Mixer -3; (18) I-f amplifier of reference signal; (19) Heterodyne; (20) Tracking heterodyne; (21) Frequency discriminator.

Signals from outputs of the Doppler filters, containing information concerning the direction to a chosen target, are fed to the phase detector where the error signal is formed which is used in a direction finding system on the usual order.

Direction finding systems with selection based on speed are rather narrow-band. This imposes additional requirements on the receiving channels with respect to the identity of their amplitude-phase characteristics. Nonidentity of channels, particularly of Doppler filters, will cause target finding error. Since the narrow-band filters have great steepness of phase-frequency characteristics, while target speed and Doppler frequency connected with it, i. the

tracking process based on speed, varies within considerable limits, even a slight nonidentity of phase-frequency characteristics of the Doppler filters will cause a large parasitic signal phase shift entering the phase detector and bring about considerable error in direction finding.

The quasicontinuous mode of radiation, which characterizes the emission of pulses with a low duty cycle, also makes it possible to select targets based on speed. Therefore, the design of the receiver of a monopulse quasicontinuous radar is similar to that discussed above. The only difference lies in the fact that when using a quasicontinuous mode of radiation, there is introduced into the receiver a gating of the i-f range amplifiers. Requirements for identity of receiving channels remain the same as they are with a continuous signal.

CHAPTER 2

MONOPULSE RADAR SYSTEM ANTENNAS

§ 2.1. RELATIONSHIP BETWEEN THE RADIATION PATTERN OF THE ANTENNA AND THE CURRENT DISTRIBUTION ON ITS SURFACE

The antenna is the main element of a monopulse radar. It connects the radiating source and the angular discriminator. The main characteristics of monopulse radars depend considerably upon the design of the antenna system.

The shape of the radiation pattern in a monopulse radar has a considerable effect on the direction finding characteristic. In order to obtain a predetermined shape of radiation pattern and, consequently, a predetermined direction finding characteristic, we must select the proper current distribution on the antenna surface or the field distribution in the aperture.

To derive the relationship between antenna radiation pattern and current distribution on the antenna surface, we should examine a rectangular antenna (Fig. 2.1), whose width in the direction of the y-axis is d. When $d \gg \lambda$, the expression for the electrical field intensity in the remote zone has the form [44]

$$E\left(\pi \frac{d}{\lambda} \sin \theta\right) = \frac{2}{d} \int_{-\frac{d}{2}}^{\frac{d}{2}} W\left(\frac{2}{d}y\right) \exp i\left(2\pi \frac{y}{\lambda} \sin \theta\right) dy, \quad (2.1)$$

where

$$\Psi\left(\frac{2}{d}y\right) = A\left(\frac{2}{d}y\right) \exp i\psi\left(\frac{2}{d}y\right)$$

is the complex function of current distribution on the antenna surface at distance y from the center of the aperture; $\frac{2}{d}y$ is the generalized coordinate of the antenna aperture; $\pi\frac{d}{\lambda}\sin\theta$ is the generalized approach angle.

After change of the variables

$$u = \pi\frac{d}{\lambda}\sin\theta; \quad v = \frac{2}{d}y \quad (2.2)$$

equation (2.1) can be written in the form

$$E(u) = \int_{-1}^1 \Psi(v) \exp iuv dv, \quad (2.3)$$

where

$$\Psi(v) = A(v) \exp i\psi(v).$$

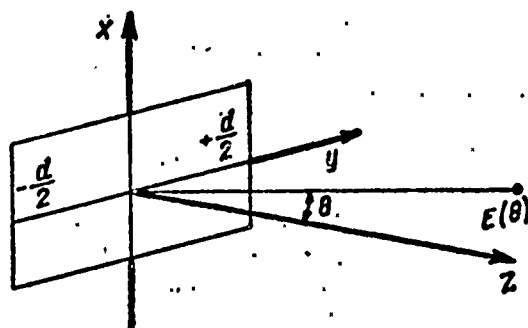


Fig. 2.1. Radiating aperture of antenna.

Equation (2.3) in mathematical respects is similar to the inverse Fourier transform. Consequently, the theory of Fourier transforms can be applied to the calculation of the field intensity pattern if we know the current distribution on the antenna surface.

The Fourier transform of function $f(t)$ is written in the following manner:

$$F(f) = \frac{1}{2\pi} \int_{-\infty}^{\infty} f(t) e^{-i f t} dt. \quad (2.4)$$

and the inverse Fourier transform has the form

$$f(t) = \int_{-\infty}^{\infty} F(f) e^{i f t} df. \quad (2.5)$$

In equation (2.3) the limits of integration can be extended to an interval from $-\infty$ to $+\infty$ since current distribution $\Psi(v)$ is equal to zero for $|v| > 1$. Then the function of current distribution on the antenna surface is a Fourier transform of the field intensity diagram $E(u)$:

$$\Psi(v) = \frac{1}{2\pi} \int_{-\infty}^{\infty} E(u) e^{-i u v} du. \quad (2.6)$$

Thus, based on equation (2.6), we can find current distribution $\Psi(v)$, which ensures the obtaining of a given pattern $E(u)$ and, based on equation (2.3), we can calculate the antenna radiation pattern with different current distributions for the antenna radiation pattern field in its aperture.

For example, for a uniform field distribution in the aperture, when the constant value of field amplitude is A_0 , and phase distribution along the aperture constant, the antenna radiation pattern calculated according to equation (2.3) has the form

$$F(u) = A_0 \int_{-1}^1 e^{i u v} dv = A_0 \frac{\sin u}{u}. \quad (2.7)$$

This radiation pattern in coordinates "u" exists within limits from $-\infty$ to $+\infty$ (Fig. 2.2). However, since the function of field distribution in the aperture must revert to zero beyond the antenna aperture, angle θ , measured from axis Z, cannot be greater than $\pm 90^\circ$ and $-1 \leq \sin \theta \leq 1$.

Then the range of effective approach angle lies within $-\pi \frac{d}{\lambda} \leq u \leq \pi \frac{d}{\lambda}$ and, consequently, only the part of the antenna pattern located in the above mentioned interval corresponds to the physically possible range of approach angles. The portion of the radiation pattern located outside this interval can be defined as "invisible."

In reference [15] it is shown that the powers in the "visible" and "invisible" portions of the radiation pattern are connected, respectively, with the active and reactive powers in the aperture.

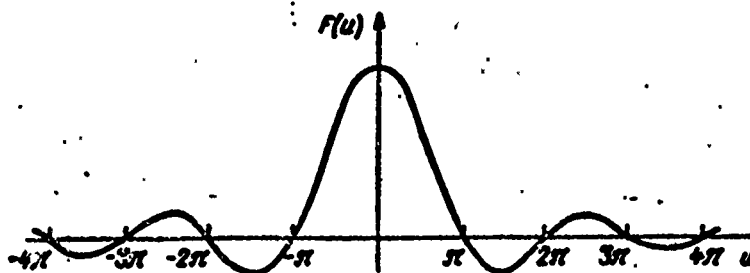


Fig. 2.2. Antenna radiation pattern in the case of uniform field distribution in the aperture.

The presence of an "invisible" part of the antenna radiation pattern represents certain requirements on the multiplicative ratio of signals $r_m(u)$. When using for direction finding either amplitude or phase patterns, it is necessary that $r_m(u)$ be independent of the unused ("invisible") pattern for direction finding [41]. From equation (1.6) it is apparent that the necessary and sufficient condition is the requirement that the usable radiation pattern be an even function with respect to equisignal direction, i.e., for purely amplitude direction finding

$$\varphi_1(u) = \varphi_2(u), \quad (2.8)$$

and for purely phase direction finding

$$F_1(u) = F_2(u). \quad (2.9)$$

The requirements, imposed by equalities (2.8) and (2.9), on the unusable radiation patterns are limited in a certain manner to the form of current distribution on the antenna surface. As indicated in Chapter 1, in monopulse direction finding systems it is usually accomplished by the displacement of two amplitude patterns by a small angle θ_0 relative to equisignal direction or by the displacement of the phase centers of the two patterns. Amplitude patterns at an angle to each other are formed by currents which have a linear phase distribution function. A displacement of the phase centers of the two patterns can be obtained only if the phase distribution function is constant.

In reference [62] it is indicated that with linear current phase distribution the maximum possible antenna amplification is ensured. Therefore, we shall assume that the phase distribution function is linear for amplitude direction finding and constant for phase direction finding. With this assumption, amplitude distribution for amplitude direction finding with linear phase distribution must be a symmetrical function with respect to the center of aperture, while for phase direction finding with constant phase distribution it can be any arbitrary function [41].

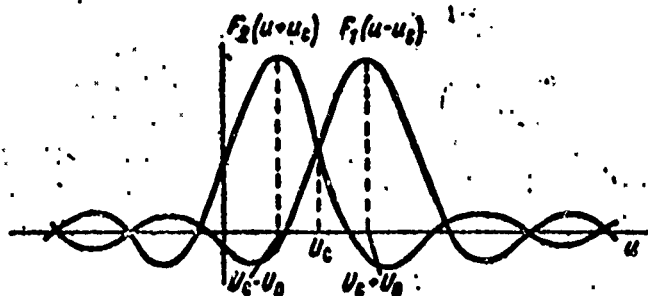


Fig. 2.3. Antenna radiation patterns with displaced equisignal direction.

The introduction not of the approach angle itself θ but of generalized u as an independent variable makes it possible to extend the basic theoretical positions of the monopulse method, in the above

assumption, that equisignal direction is perpendicular to the plane of the antenna aperture, to the case of an arbitrary direction for the equisignal line.

Figure 2.3 presents antenna radiation pattern of a monopulse system for direction finding in one plane. If the initial pattern $F(u)$ is displaced along axis u to a generalized displacement angle of equisignal direction $u_{\text{сдв}}$, connected with the physical displacement angle $\theta_{\text{сдв}}$ by equation

$$u_{\text{сдв}} = \frac{\pi d}{\lambda} \sin \theta_{\text{сдв}} \quad (2.10)$$

the displaced complex radiation pattern, in accordance with equation (2.3), is written in the form

$$f_1(u - u_{\text{сдв}}) = \int_{-1}^1 A(v) \exp \{i [\psi(v) - (u - u_{\text{сдв}}) v]\} dv \quad (2.11)$$

The displacement of the radiation pattern is achieved physically by a linear shift of the initial distribution in the aperture by quantity $u_{\text{сдв}} v$. If the initial pattern was displaced with respect to equisignal direction by angle

$$u_0 = \frac{\pi d}{\lambda} \sin \theta_0 \quad (2.12)$$

the displaced pattern also will be shifted with respect to the displaced equisignal direction $u_{\text{сдв}}$ by angle u_0 .

The multiplicative ratio of signals received with displaced equisignal direction will be determined by expression

$$r_m(u) = \frac{f_1(u - u_{\text{сдв}})}{f_2(u + u_{\text{сдв}})} \quad (2.13)$$

which, when $u_{\text{CDB}} = 0$, reduces to the usual determination in accordance with (1.6).

Thus, radiation patterns and monopulse ratios are preserved without distortion in the presence of arbitrary displacement of equisignal direction, when they are expressed in terms of a generalized coordinate of the radiation pattern.

§ 2.2 PARABOLIC ANTENNAS

A diagram of a parabolic antenna, which consists of a metal mirror in the form of a paraboloid of rotation and a feed, is presented in Fig. 2.4.

The main properties of the parabolic mirror are the following:

- 1) diverging beams, proceeding from a source installed in the focus of the mirror, after reflection from its surface become parallel;
- 2) the distance crossed by any beam from focus to mirror and after reflection from a plane perpendicular to the axis of the paraboloid does not depend upon the angle at which the beam left the focus. Because of this, a plane wave front with a uniform phase is formed.

A paraboloid which has an aperture angle of $2\alpha_0 > \pi$ is called a short-focus, and a paraboloid which has $2\alpha_0 < \pi$ a long-focus. For a short-focus paraboloid the ratio of focal distance to mirror diameter is $f_{\text{n}}/d_{\text{n}} < 0.25$, and for a long-focus paraboloid it is $f_{\text{n}}/d_{\text{n}} > 0.25$. Parabolic antennas for monopulse radar stations usually have $f_{\text{n}}/d_{\text{n}}$ ratios lying within 0.5-1, which makes it possible to intersperse the radiation patterns at the prescribed level.

The most widely used type of feed for parabolic monopulse antennas is the waveguide horn which can be installed by one of the methods indicated in Fig. 2.5. In both cases, the waveguide feeding the horn passes through the reflector, which leads to a shading of the aperture and the appearance of a reverse reaction

on the feed because of the energy reflected from the mirror. The feed, the waveguide, and the attachment element shade the aperture of the mirror and changes the effective radiation pattern, while the energy reflected from the mirror, falling on the feed and being propagated in the reverse direction along the waveguide, causes a mismatch in total resistance and worsens the transmission characteristic.

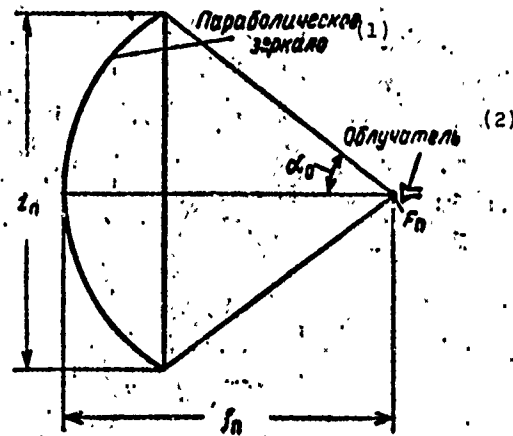


Fig. 2.4. Diagram of a parabolic antenna: d_n - diameter of parabolic mirror; f_n - focal distance; F_n - focus of mirror; $2\alpha_0$ - angle of aperture.
KEY: (1) Parabolic mirror; (2) Feed.

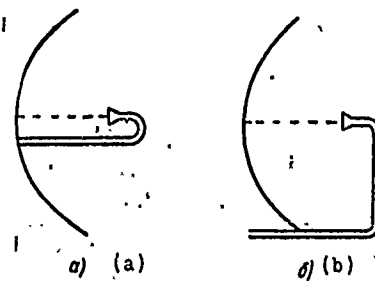


Fig. 2.5. Methods of attaching feeds to parabolic antennas.

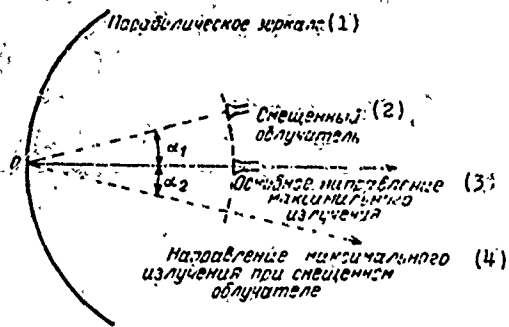


Fig. 2.6. Change in direction of maximum radiation with displacement of feed.

KEY: (1) Parabolic mirror; (2) Displaced feed; (3) Main direction of maximum radiation; (4) Direction of maximum radiation with displaced feed.

If the feed is displaced from the focus of the parabolic antenna by angle α_1 along a circumference with a center located at the apex of the paraboloid, the direction of maximum radiation is deflected from the axis of the mirror by angle α_2 , somewhat less than angle α_1 (Fig. 2.6). The direction of maximum radiation is turned to the direction opposite the displacement of feed.

In monopulse systems with amplitude direction finding, a pair of feeds displaced symmetrically from the focus gives symmetrically overlapping amplitude radiation patterns for direction finding in one plane (see Fig. 1.1).

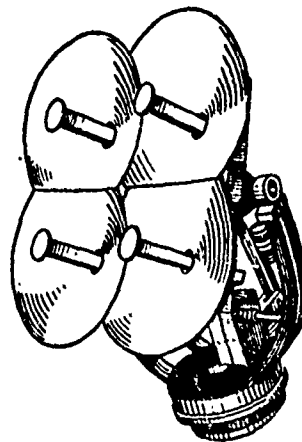
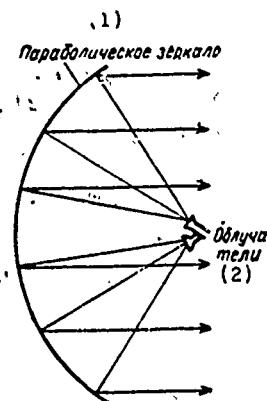


Fig. 2.7. Antenna of a monopulse system with phase direction finding.

Fig. 2.8. Parabolic mirror with slanted feeds.
 KEY: (1) Parabolic mirror;
 (2) Feeds.



In monopulse systems with phase direction finding, the antenna system for direction finding in one plane consists of two separate parabolic antennas spaced at a distance (base line) l (see Fig. 1.2), with the feed located in the focus. One of the antennas or both of the antennas can be used for transmitting. An example of such an antenna is the antenna (Fig. 2.7), used in the first monopulse system, developed by General Electric [41]. In design the antenna consists of four 16-inch parabolic mirrors, cut off and welded together with separate feeds located in the corresponding focus. For reception, three antennas were used, and since for elevation and azimuth direction finding two reflectors each are used, one is common for both planes. The use of a separate transmitting antenna eliminates the necessity for switching the antenna system to transmission and to reception.

The development of monopulse systems with phase direction finding led to the creation of single-mirror antennas with a four-horn feed located in the focus of the mirror; however, each horn is slanted with respect to its axis (Fig. 2.8). In this case, in each plane two parallel beams are formed.

§ 2.3. PARABOLIC ANTENNAS WITH A PRIMARY RADIATOR

Parabolic antennas with a primary radiator (Cassegrain) have found wide application in monopulse systems because of a number of

advantages which will be discussed below. In such antennas, (Fig. 2.9) the feed is located at the apex of the parabolic mirror, and a hyperbolic primary radiator is located between the apex and the focus of the parabola. One of the two foci of the hyperbola is the actual focus of the antenna system F_p and is located in the center of the feed; the other is the imaginary F'_p and is located in the focus of the parabola. Points F'_p and F_p are conjugate foci of the hyperbolic primary radiator. Waves from the reflector and primary radiator are reflected according to laws of geometric optics (Fig. 2.9b) and after reflection, the beams proceed in parallel and the wave front is flat.

Parameters of a parabolic antenna with a primary radiator, indicated in Fig. 2.9a, are connected by the following equations [56]:

$$\operatorname{tg} \frac{\alpha_0}{2} = \frac{d_n}{4f_p}, \quad (2.14)$$

$$\frac{1}{\operatorname{tg} \alpha_0} + \frac{1}{\operatorname{tg} \alpha_p} = 2 \frac{f_p}{d_n}, \quad (2.15)$$

$$\frac{\sin \left(\frac{\alpha_0 - \alpha_p}{2} \right)}{\sin \left(\frac{\alpha_0 + \alpha_p}{2} \right)} = 2 \frac{f_p}{d_n}. \quad (2.16)$$

Usually parameters d_n , f_p and α_p are determined based on the necessary dimensions and characteristics of the antenna system, and according to them α_0 , d_n and f_0 are calculated.

If we consider the primary radiator a hyperbolic mirror creating a mirror image of the feed at F'_p , located in the focus of the parabola, an antenna with a primary radiator can be considered an ordinary single-mirror parabolic antenna but with another feed (Fig. 2.10). Then the solid angle $2\alpha_p$, formed by the primary radiator at point F_p , will differ from solid angle $2\alpha_0$. The imaginary feed has a effective aperture smaller, while the radiation pattern is wider, than actual, i.e., amplification occurs because of the use of a hyperbolic primary radiator and is equal to

$$k_r = \frac{e_r + 1}{e_r - 1} \quad (2.17)$$

where

$$e_r = \frac{\sin\left(\frac{\alpha_o + \alpha_p}{2}\right)}{\sin\left(\frac{\alpha_o - \alpha_p}{2}\right)}$$

is the eccentricity of the hyperbolic primary radiator.

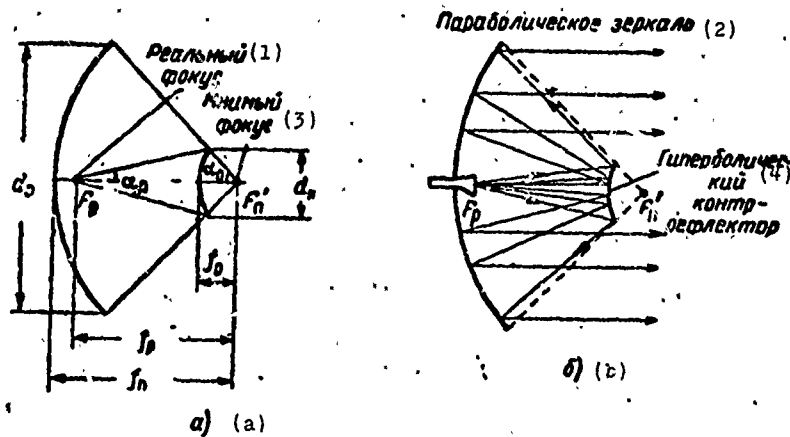


Fig. 2.9. Diagram of parabolic antenna with primary radiator:
 a) geometry of antenna; b) principle of antenna action.
 KEY: (1) Actual focus; (2) Parabolic mirror; (3) Imaginary focus;
 (4) Hyperbolic primary radiator.

Amplification is also equal to the ratio of the difference between the distances from primary reflector to real and imaginary foci to the distance from primary reflector to imaginary focus

$$k_r = \frac{f_p - f_o}{f_o} \quad (2.18)$$

However, on the other hand, the use of a primary reflector in such an antenna system leads to the shading of the aperture, which causes a dip in the amplitude field distribution, as a result of which amplification decreases and the level of the side lobes increases.

In order to reduce shading, we can reduce the dimensions of the primary reflector, simultaneously increasing the directivity of the feed or bringing it nearer the primary reflector. However, the shading of the aperture can be caused by the feed itself and can be greater than the shading caused by the primary reflector. Therefore, when selecting the dimensions of a primary reflector, we must find a compromise solution. Shading is minimal when the size of the feed and the distance are selected so that shadings caused by the primary reflector and the feed are approximately the same. In reference [56] the chief condition for minimal shading is obtained (Fig. 2.10):

$$\frac{f_p}{f_n} \approx \frac{k_f d_f^2}{2F_p \lambda} \approx \frac{d_f}{d_n} \quad (2.19)$$

where d_f is the diameter of the feed aperture; k_f is the ratio of effective and geometric diameters of the aperture of the feed.

The approximate equality (2.19) is obtained on the assumption angle α_p and α_f are small and the primary reflector is located considerably nearer the imaginary focus than it is to the feed.

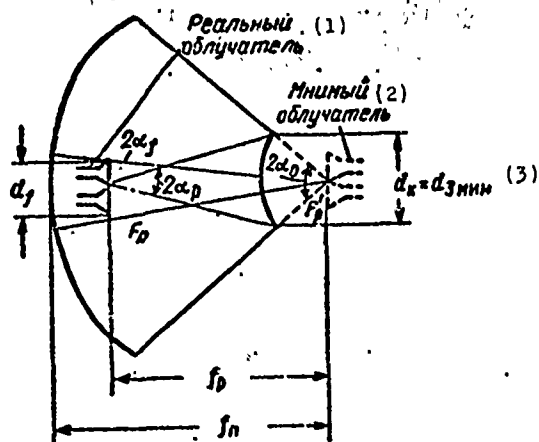


Fig. 2.10. Minimum shading of primary radiator.
KEY: (1) Actual feed; (2) Imaginary feed; (3) $d_k = d_3 \text{ min}$.

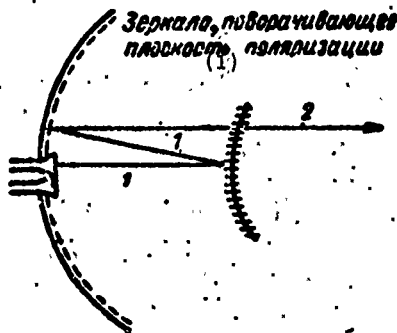


Fig. 2.11. Antenna with turning of polarization plane to eliminate shading of the primary radiator. 1 - horizontal polarization; 2 - vertical polarization.
KEY: (1) Mirror which turns polarization plane.

The minimal diameter of shading is approximately [56]

$$d_{3 \text{ мин}} = \sqrt{\frac{2}{k_f} f \lambda}. \quad (2.20)$$

The relationships examined above for minimal shading are valid for operation at any polarization. However, in case of operation with only linear polarization, we can reduce shading by using methods for turning polarization. In this case, the primary radiator (Fig. 2.11) is a horizontal grid which reflects a horizontally polarized wave and transmits vertically polarized waves. Near the surface of the main mirror is located a device which changes, during reflection, the polarization of a wave from horizontal to vertical; the wave then passes without hinderance through the primary radiator with very small reflections, causing virtually no shading.

Since feeds can be made with small dimensions, the shading they cause will be small and comparable with the shading in an ordinary parabolic mirror. Consequently, in antenna systems with deflection of polarization plane, it is expedient to use a large primary radiator and a small feed.

The formation of two radiation patterns for direction finding in one plane in monopulse systems using parabolic antennas with a primary radiator is carried out by the same methods as in monopulse systems with ordinary parabolic antennas.

The most important advantage of a parabolic antenna with a primary radiator when using it in a monopulse system is the possibility of placing the feed behind the mirror, which makes it possible to reduce the length of the feeder line which supplies the feed and, consequently, to reduce error in angular coordinate measurement because of the appearance of phase difference between segments of feeder lines. In addition, in this case, it is possible to use in the receiving device, low-noise amplifiers (quantum-mechanical or parametric) since they can be placed directly beside the feeds. In ordinary parabolic antennas, losses in the feeder line connecting the feed with the low-noise amplifier located behind the mirror cause significant reduction in sensitivity of the receiving device, while the location of the low-noise amplifier near the focus of the paraboloid leads to an increase in aperture shading.

Another important advantage of an antenna with a primary radiator is the possibility of obtaining an equivalent focal distance exceeding the actual axial dimension of the antenna, i.e., the possibility of obtaining from a parabolic surface with a low f_n/d_n ratio the same effect as in the case of using a parabolic surface with a high f_n/d_n ratio. When locating the feeds at the apex of the parabolic reflector or between the reflector and the primary radiator, the effective f_n/d_n ratio can exceed the f_n/d_n ratio for ordinary parabolic antennas by no more than a factor of two. Thus, the total length of an antenna with primary radiator can be cut in half as compared with an ordinary parabolic antenna.

A third advantage of this antenna is the possibility of swinging the beam by moving the primary radiator.

§ 2.4. LENS ANTENNAS

Lens antennas are also used in monopulse radar stations.

The principle of action of a lens antenna is based on the laws of beam refraction at the interface of two media. From optics we know that if the beam falls on a flat interface of two media with dielectric constants ϵ_1 and ϵ_2 , respectively, the angle of refraction can be found from relationship

$$\sin \beta_1 = \frac{n_1}{n_2} \sin \beta_2, \quad (2.21)$$

where β_2 is the angle of incidence; n_1 and n_2 are the refractive indices of the media.

The refractive indices of a medium is the ratio of the propagation velocity of electromagnetic waves in free space to their propagation velocity in a given medium. It is equal to the square root of the dielectric constant of this medium:

$$n_1 = \sqrt{\epsilon_1}; \quad n_2 = \sqrt{\epsilon_2}.$$

Thus,

$$\sin \beta_1 = \sqrt{\frac{\epsilon_1}{\epsilon_2}} \sin \beta_2. \quad (2.22)$$

Using this property of beams, we can explain the physical essence of the action of a dielectric lens (Fig. 2.12) in the following manner. The source F_n , radiating a beam of diverging rays, is located in air ($n_1 = 1$). In the dielectric lens the propagation velocity of the wave front is less than in air and, therefore, the path followed by the wave will be longer in the center of the lens and shorter on its edges. Correspondingly, the wave front in the central part of the lens is propagated more slowly than the wave front on its edges. Consequently, as the wave front moves in the direction

away from the feed toward the unilluminated surface of the lens, its gradual rectification occurs. With the proper selection of lens profile, a flat wave front is obtained on its unilluminated surface. Ordinary dielectric lenses, since they are expensive and heavy, have not found wide application in monopulse radars. Laminated metal lenses and Luneberg lenses have been most widely used in actual practice.

A laminated metal lens (Fig. 2.13a) consists of plates parallel to the vector of the electrical field and spaced at a distance of l_n from each other ($\lambda/2 < l_n \leq \lambda$). The space between the plates acts as a waveguide in which the phase velocity is higher than in air; therefore, the refractive index is less than one and is calculated according to formula

$$n_2 = \sqrt{1 - \frac{\lambda^2}{4l_n^2}} \quad (2.23)$$

With the proper selection of lens shape, all beams passing from point F_n reach the aperture at the same time and the field in the aperture will be cophased.

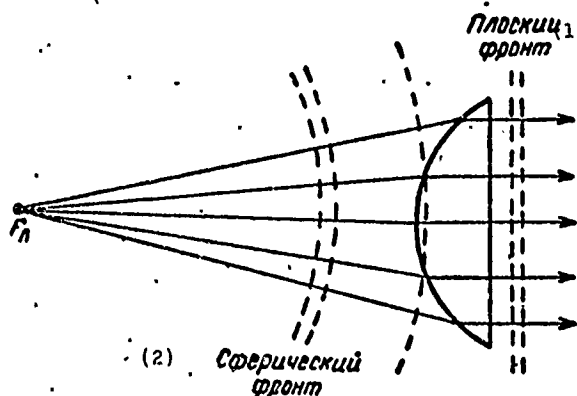


Fig. 2.12. Dielectric lens
KEY: (1) Flat front; (2) Spherical front.

The less distance between plates the less the refractive index and the thinner the lens. But even when the refractive index is on

the order of 0.5 ($l_n = 0.56\lambda$), the thickness of the laminated metal lens is still considerable. In order to reduce the thickness, staggered laminated metal lenses are used (Fig. 2.13b). In a staggered lens at points where the phase advance reaches 360° , lens thickness is decreased by jumps, i.e., when the length of the plate reaches the value $l_n = \lambda/1-n$, plate thickness is reduced to the value it has in the center of the lens. The 360° phase change at various points of the aperture has no effect on phase distribution of the field in the aperture.

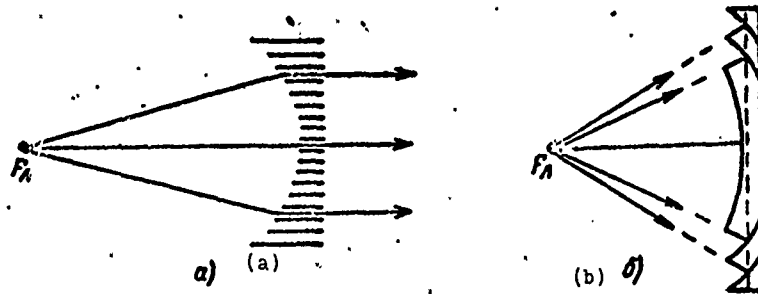


Fig. 2.13. Laminated metal lenses: a) waveguide; b) staggered.

The disadvantages of the staggered lenses are the energy losses and the increase in the level of side lobes caused by the shading from the staggering and the increase in lens sensitivity to frequency change.

The formation of two radiation patterns for direction finding in one plane in lens antennas is carried out by the same methods as in parabolic antennas.

The Luneberg lens (Fig. 2.14) is made in the form of a sphere and has a varying refractive index. Thanks to the spherical symmetry of the lens, its focusing ability does not depend upon the direction of wave approach. The main properties of a Luneberg lens include the fact that the plane wave falling on it is focused at a point lying on the opposite side of the surface and, consequently, the wave from the point source O_n , located on the surface of the lens, during passage through it, is transformed into a plane wave (Fig. 2.14).

The refraction index in the Luneberg lens is changed in the following manner:

$$n_r = \sqrt{2 - \frac{r_n^2}{r^2}}, \quad (2.24)$$

where r_n is the radius of the Luneberg lens;

r is the distance from the center of the lens to a point where the refraction index is calculated.

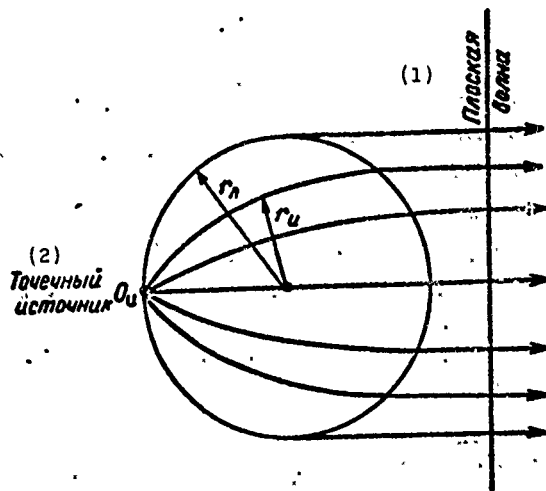


Fig. 2.14. Spherical Luneberg lens.
KEY: (1) Plane wave; (2) Point source.

As is apparent from formula (2.24), in the center of the lens the refraction index has the highest value and is equal to $\sqrt{2}$; on the surface of the lens it is equal to one.

Since ground and airborne radar sets usually ensure scanning and tracking of targets only in the upper hemisphere, a Luneberg lens in the form of a hemisphere is used (Fig. 2.15), in the base of which a flat reflecting surface is installed which provides a mirror reflection of the feed from point O_n to point O'_n .

In the Luneberg lens, shifting the source along its surface causes a corresponding displacement of the beam in the opposite

direction. Swinging the beam can be accomplished by two methods: either by moving a single feed along the surface of the lens or with the aid of a large number of feeds located on its surface, and switching the transmitter or receiver from one feed to another. In order to form several beams, several feeds located in a corresponding manner on the lens surface are necessary.

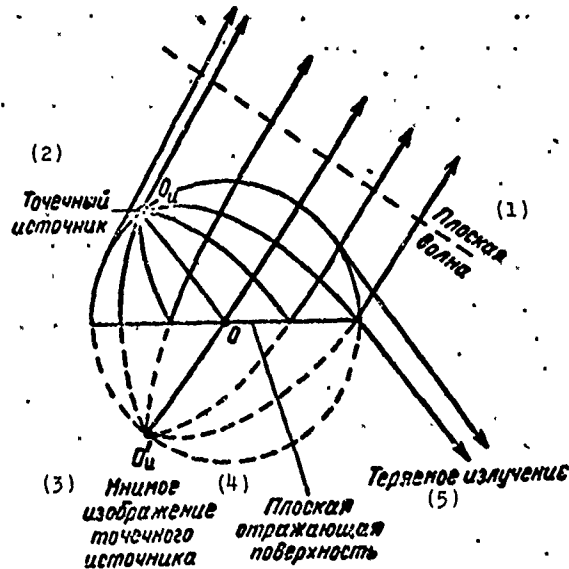


Fig. 2.15. Luneberg hemispherical lens.

KEY: (1) Plane wave; (2) Point source; (3) Virtual image of point source; (4) Plane reflecting surface; (5) Lost radiation.

A Luneberg lens can be used in antennas which have to provide rapid scanning of a beam within a large angle and also when the antenna is installed on an unstable object, for example, an aircraft. In the latter case, beam stabilization during the motion of the vehicle can be achieved by changing the position of the feed. A lens antenna possesses a number of advantages when compared with a mirror antenna. One of the main advantages is the absence of aperture shading since the feed and the waveguide are not in the radiation field; another is the possibility of rapid shift of beam in a large sector. For example, the Luneberg lens can ensure beam displacement

throughout the upper hemisphere. In addition, lens antennas require less rigid mechanical and electrical tolerances and have a short time lag.

Disadvantages of these antennas include their low efficiency ratio due to loss in materials, the considerable volume occupied, and the complexity of preparation.

§ 2.5. CROSSPOLARIZATION RADIATION OF MIRROR ANTENNAS

In mirror antennas because of the geometry of the antenna system and also because of the imperfection of reflecting surfaces and feeds, the displacements of feeds from the focus of the reflector, and diffraction phenomena, depolarization (crosspolarization) occurs, i.e., the radiation of a wave polarized in a different manner than required [1, 16, 62, 63, 100, and 101].

Taking into account the effect of crosspolarization radiation on the directivity factor of the antenna and the accuracy of direction finding, let us examine it with respect to parabolic antennas.

The appearance of crosspolarization radiation caused by the geometry of the antenna system (curvature of reflecting surface) can be studied in the example of a paraboloid excited by a short electrical dipole. In this case, the electrical field in the aperture (Fig. 2.16) is determined by expression [63]

$$\vec{E}_n = \frac{-i\eta_n I_n \exp i k_\lambda (f_n + z_0)}{4\lambda r_n} \left\{ \vec{x} [(1 + \cos \psi_n) - (1 - \cos \psi_n) \cos 2\xi_n] - \vec{y} \sin 2\xi_n (1 - \cos \psi_n) \right\} \quad (2.25)$$

where r_n , ξ_n and ψ_n are the elements of a spherical system of coordinates (Fig. 2.16);

I_n is the value of current on the surface of a mirror;

f_n is the focal distance of the paraboloid;

z_0 is the depth of the paraboloid;

\vec{x}, \vec{y} are the unit vectors of a rectangular system of coordinates;
 $k_\lambda = 2\pi/\lambda$ is the propagation constant;
 η_n is the coefficient determining the level of side lobes.

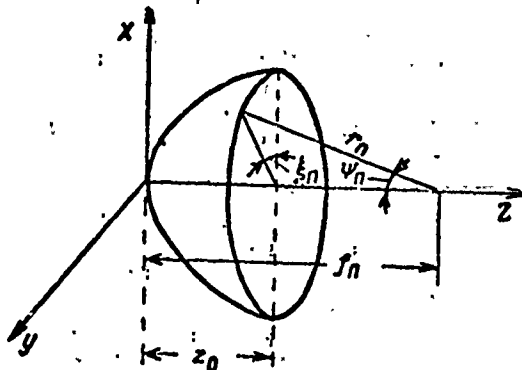


Fig. 2.16. System of coordinates for determining field in paraboloid aperture.

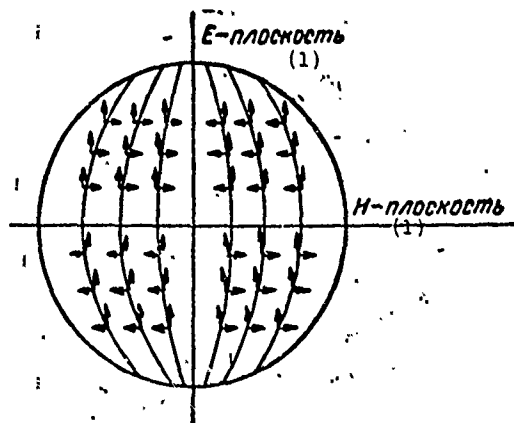


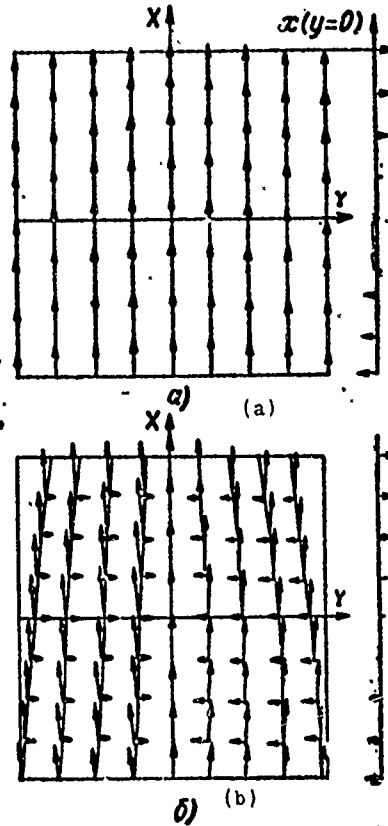
Fig. 2.17. Field intensity distribution in aperture of paraboloid excited by electrical dipole.
 KEY: (1) Plane.

Figure 2.17 presents the typical pattern of the field in the aperture of a paraboloid excited by an electrical dipole located

in the focus parallel to the x-axis. The arrows indicate the components of the vector of field intensity at various points of the aperture. The component orthogonal to the vector of the dipole's electrical field, whose appearance is due to the curvature of the mirror surfaces, is called the crosspolarization component.

From equation (2.25) it is apparent that the level of crosspolarization radiation grows with a decrease in f_{Π} . This is explained by the fact that at low f_{Π}/d_{Π} the curvature of the mirror surface is greater.

Fig. 2.18. Field intensity distribution in the aperture of a paraboloid excited by electrical and magnetic dipoles: a) dipoles in focus; b) dipoles out of focus.



If a magnetic dipole is used as the feed, field distribution in the paraboloid aperture has the same character but the crosspolarization components are opposite in phase to the corresponding crosspolarization components when the paraboloid is excited by an

electrical dipole. Consequently, if the paraboloid feed is a combination of electrical and magnetic dipoles located at right angles to each other, we can, to a certain extent, compensate for the crosspolarization radiation of the antenna caused by the curvature of its surface. A small rectangular horn can serve as such a feed with sufficient accuracy. However, as shown in reference [100], compensation is not complete.

Moving the feed from the focus, which is virtually what occurs in amplitude monopulse systems, causes amplitude asymmetry in current distribution on the paraboloid surface and, as a consequence, an increase in the level of the crosspolarization component in the direction of feed displacement [16]. In this case, compensation of crosspolarization radiation, if such occurred during the irradiation of a mirror by a set of electrical and magnetic dipoles located orthogonally in the focus of the mirror, is impaired. As seen from Fig. 2.18a, with the arrangement of electrical and magnetic dipoles in the focus, the resulting currents flow along lines parallel to the x-axis instead of the global lines as occurs during irradiation by single dipoles. When the feed is removed from the focus (Fig. 2.18b), there is observed a constriction of current lines along the direction toward one of the mirror's edge. From the crosspolarization components which then occur, only those which are located on different sides from the x-axis are in opposite phase. This is the difference from the case of mirror irradiation by a single dipole, when opposite phase occurs for all crosspolarization components located in various quadrants of the paraboloid surface. A similar distribution of field components will also occur in the aperture of the paraboloid.

The radiation pattern of a parabolic mirror when it is excited by a linearly polarized field is characterized by two patterns; a radiation pattern with the main (operating) polarization and a radiation pattern with crosspolarization. When mirror excitation is symmetric, linear polarization occurs only in the direction of the main planes: with deviation from them there occurs a distortion of polarization which generally assumes the form of elliptic polarization,

Figure 2.19 presents a standardized radiation pattern in plane H, calculated for a parabolic mirror with aperture diameter $d_n = 37\lambda$ and $f_n/d_n = 0.25$, irradiated by an electrical dipole [100]. From the figure it is apparent that the radiation pattern with crosspolarization in the direction of the optical axis of the antenna has a deep minimum and two symmetrical maxima. The lobes of the crosspolarization pattern are located at a 45° angle to the main plane and its maxima coincide with the first minimum of the radiation pattern.

A displacement of the feed with respect to the antenna axis is accompanied by a shift in the patterns of crosspolarization components. Figure 2.20 presents the calculated radiation pattern with crosspolarization for three values of feed displacement from the focus of the paraboloid in plane x ($x_c = 6.25\lambda, 15\lambda$ and 19λ) [14]. It is apparent from the figure that when the feed is removed from the focus, there is a deformation of the crosspolarization pattern; its minimum becomes less deep and its maximum more mildly sloping. The level of the crosspolarization radiation and the width of the crosspolarization lobes increase.

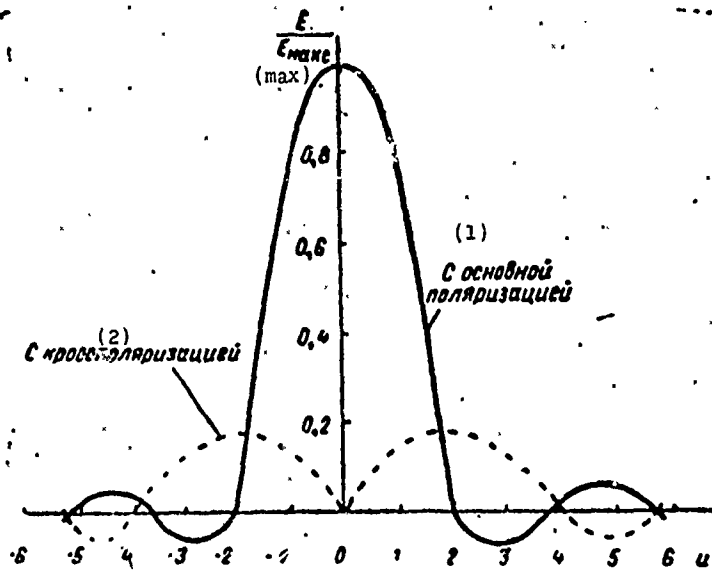


Fig. 2.19. Radiation pattern of a mirror antenna irradiated by an electrical dipole.

KEY: (1) With basic polarization; (2) With crosspolarization.

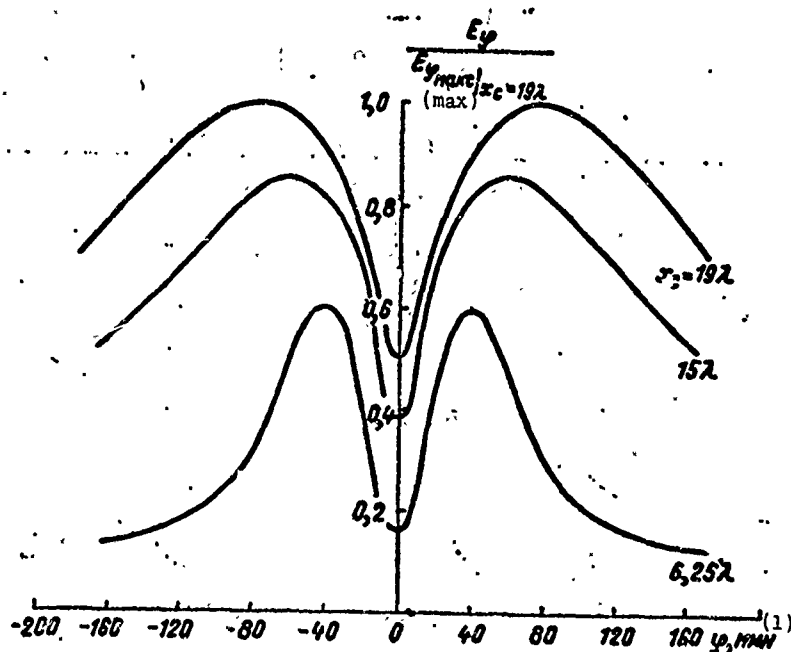


Fig. 2.20. Amplitude radiation patterns in ϕ planes for components $E_{\phi}/E_{\phi \text{ макс}}$ when $x_c = 19\lambda$.
KEY: (1) min.

Crosspolarization radiation is also observed in the case of excitation in a mirror antenna of a wave with circular polarization. As we know, in order to excite a wave with circular polarization, two orthogonally polarized waves with identical amplitudes and phase shift of $\pi/2$ are required. Crosspolarization of an antenna leads to distortion in amplitude and phase ratios for these components of the excitation field. In this case, the presence of circular polarization in the direction of maximum feed radiation does not guarantee circular polarization in the direction of maximum mirror radiation. In many cases, in order to obtain optical circular polarization, it is necessary to resort to feeds with elliptical polarization. However, even in this case, circular polarization can be obtained only in the direction of the mirror's optical axis. In other directions the polarization of the radiation pattern is elliptical and even linear.

In reference [101] there is calculated a radiation pattern with crosspolarization for a square horn excited by two orthogonal oscillations of the type H_{11} occurring in quadrature. Figure 2.21 illustrates an antenna pattern with basic polarization in a diagonal plane and crosspolarization in the main plane. Calculation of the crosspolarization pattern is carried out according to formula

$$E_x = \frac{\sin u}{u} - \left(\frac{\pi}{2}\right)^2 \frac{\cos u}{\left(\frac{\pi}{2}\right)^2 - u^2}$$

As seen from the figure, the maximum level of crosspolarization with respect to the main maximum is -16 dB. Thus, actual antennas of circular polarization also have crosspolarization by which we mean circular polarization of opposite rotation.

Since the receiving channels of monopulse systems have several radiators, the polarization structure of the antenna radiation, described above, fully corresponds to the radiation patterns of each receiving channel of monopulse radars. Hence it follows that the antenna radiation pattern of a monopulse radar has a complex polarization structure and contains components of both basic polarization and crosspolarization. This provides a certain sensitivity to the polarization characteristics of signals received.

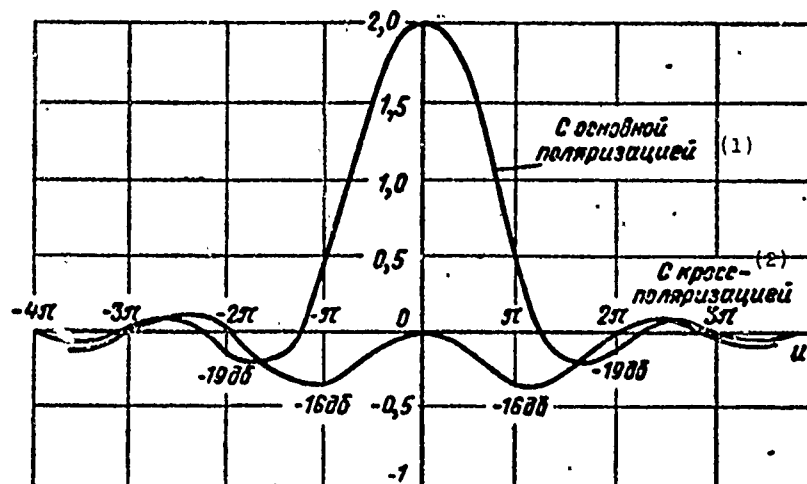


Fig. 2.21. Calculated radiation pattern of a square horn with circular polarization.
KEY: (1) With basic polarization; (2) With crosspolarization.

When the polarization of the signals received coincides with the basic polarization of the receiving antenna, we can disregard the effect of the crosspolarization components and examine the radiation pattern of the receiving antenna in its classical form. However, due to the effect of various causes, the reflected signals fed to receiver input are depolarized, i.e., differ in polarization from the signals radiated in the direction of the target. This complicates the work of a monopulse system and, in many cases, increases its error because of antenna crosspolarization. We shall examine in Chapter 5, in greater detail, the depolarization of reflected signals and its effect on direction finding accuracy.

§ 2.6. PHASED ANTENNA ARRAYS

At the present time, antennas made in the form of phased arrays have found wide application in monopulse systems. A phased antenna array is an antenna system consisting of a large number of radiating elements arranged in a specific manner with respect to each other. When signals entering all elements agree in magnitude and phase, a beam is formed perpendicular to the plane of the antenna array. The beam is shifted by a corresponding change in the phase of signals fed to each element.

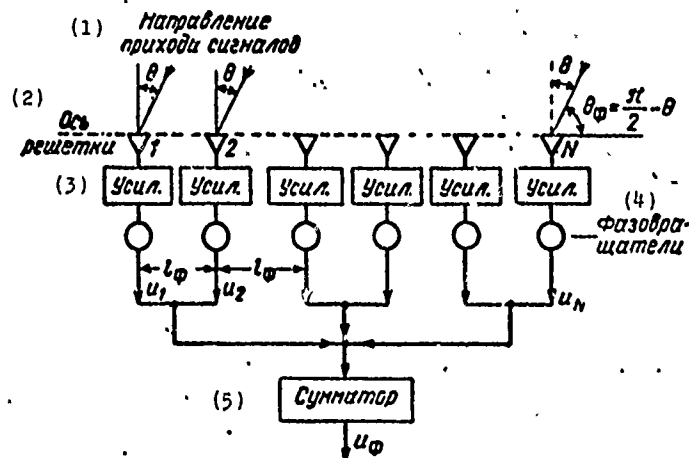


Fig. 2.22. Diagram of a phased array.
KEY: (1) Direction of signal approach; (2) Axis of array; (3) Ampl.; (4) Phase switcher; (5) Summator.

Figure 2.22 presents the diagram of an array consisting of N elements with various distances between them. In the signal reception mode, at summator output total output voltage u_ϕ is formed. We shall assume that the elements of the array are isotropic point sources radiating energy uniformly in all directions. The signal of the first element is considered the reference signal with phase ϕ_ϕ . Phase difference for signals in the adjacent elements is

$$\Delta\varphi_p = \frac{2\pi l_\phi}{\lambda} \sin \theta.$$

Then the radiation pattern with respect to the power of such an array has the form [44]

$$F_\phi(\theta) = \frac{\sin^2\left(N\pi \frac{l_\phi}{\lambda} \sin \theta\right)}{N^2 \sin^2\left(\pi \frac{l_\phi}{\lambda} \sin \theta\right)}. \quad (2.26)$$

Since a reflecting screen is placed behind the antenna array, it is advisable to study radiation only in the forward sector of the antenna when angle θ lies within -90° to $+90^\circ$.

When the beam is displaced in the sector $+90^\circ$, the smallest side lobes are obtained when the distance between elements is half the wavelength, i.e., $l_\phi = \lambda/2$. If, however, $l_\phi > \lambda/2$, then with a sweep of the beam there appear in the radiation pattern diffraction maxima of the highest orders whose amplitude is equal to the amplitude of the main beam. From equation (2.26) it is apparent that they appear when both the numerator and denominator are equal to zero or when $\pi(l_\phi/\lambda) \sin \theta = 0, \pi, 2\pi$, etc. Thus, for example, when $l_\phi = \lambda$, the diffraction maxima appear at $\theta = \pm 90^\circ$, and when $l_\phi = 2\lambda$, they appear at $\theta = \pm 30^\circ$ and $\theta = \pm 90^\circ$.

In practice, the distance between lattice elements l_ϕ is selected based on the condition of obtaining the necessary width of radiation pattern and ensuring the prescribed limits of beam swing. The diffraction maximum can also be suppressed by the nonuniform arrangement of

array elements since the directions in which diffraction maxima are formed for various segments of the array will be different, which leads to a blurring of the diffraction maximum of the array. In addition, the nonuniform arrangement of elements makes it possible to reduce the total number of radiators in the array without a significant change in the width of the radiation pattern.

In an antenna array with a nonuniform arrangement of radiators the closest arrangement of elements is made in the center of the antenna. Moving from center, spacing between elements increases according to a certain rule. Elements are arranged symmetrically with respect to the center of the array.

If we assume $l_\phi = \lambda/2$ in equation (2.26) and replace the sine of θ in the denominator by its argument, the width of the beam with respect to points of half power will be approximately equal to

$$\theta_{0.5} = \frac{101.8}{N}. \quad (2.27)$$

With the use of directed elements, the radiation pattern with respect to power of a linear antenna array is described by the expression

$$F_\phi(\theta) = F_l(\theta) \frac{\sin^2 \left(N\pi \frac{l_\phi}{\lambda} \sin \theta \right)}{N^2 \sin^2 \left(\pi \frac{l_\phi}{\lambda} \sin \theta \right)}, \quad (2.28)$$

where $F_l(\theta)$ is the radiation pattern with respect to power of a particular element of the array.

Equation (2.28) is valid only when the radiation patterns of the array elements are identical. In practice, however, the condition of identity for radiation patterns of separate elements in the array is not fulfilled because of the interaction between elements. Therefore, equation (2.28) is approximate and may be inappropriate in

designing an array. The radiation pattern of an array can be determined accurately by adding the radiation patterns of all elements, taking into account the corresponding amplitudes and phases. The pattern of each element must be removed in the presence of all other elements.

As radiators of an antenna array, various weakly directional antennas are usually used: vibrators, slits, horns, dielectric rods, and spirals.

The radiation pattern of a two-dimensional rectangular flat array can be represented in the form of the product of radiation patterns in two planes containing the main axes of the antenna.

In antenna arrays when the beam is deflected from the direction perpendicular to the antenna plane, the width of the beam increases approximately in inverse proportion to $\cos \theta$.

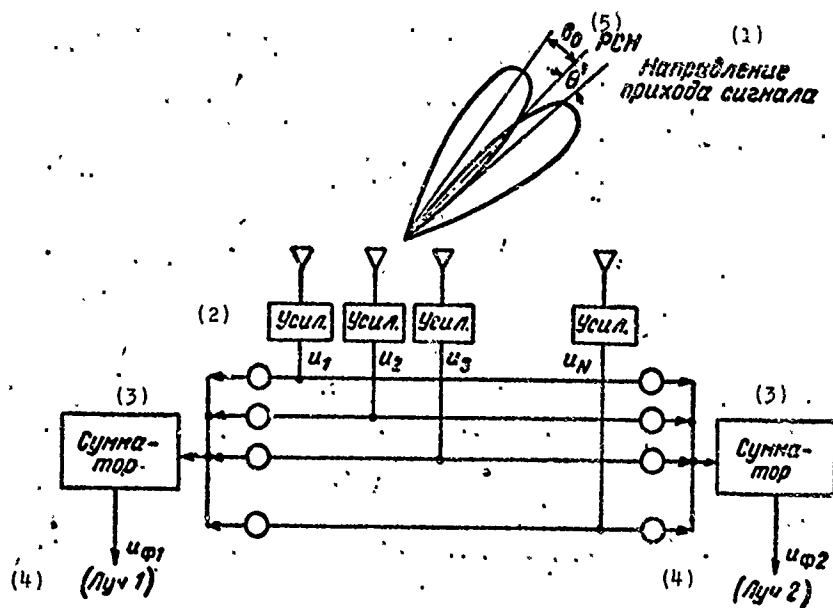


Fig. 2.23. The formation of beams by an antenna array in a monopulse radar with amplitude direction finding.
 KEY: (1) Direction of signal approach; (2) Ampl.; (3) Summator;
 (4) Beam; (5) ESD [equisignal direction].

An array forming a single beam can be transformed into a multi-beam antenna by including additional phase switchers at the output of each element. In order to form each beam, one additional phase switcher is required.

In monopulse systems with amplitude direction finding, the formation of two intersecting radiation patterns is carried out as shown in Fig. 2.23. Signals from amplifier output of each element are fed to two groups of phase switchers forming two beams. From the outputs of the phase switchers signals are fed to the summator.

In monopulse systems with phase direction finding, two radiation patterns are formed by the coherent summation of signals (at high or intermediate frequency with the conservation of phases) separately from each half of the array.

§ 2.7. ANTENNA FEEDS OF MONOPULSE RADARS

In monopulse radars with phase direction finding each of the four feeds usually has its own reflector (Fig. 2.24). In monopulse radar with amplitude direction finding in which an antenna is used which consists of four horns irradiating the reflector (primary radiator) or a lens, greatest propagation is obtained by the irradiator arrangement shown in Fig. 2.25. With this arrangement, for both types of direction finding in systems with four bridges, angular information is extracted by a comparison of paired sums of signals; when comparing the sum of signals (1 + 2) with the sum (3 + 4), elevation is measured, and with a comparison of sum (1 + 3) with sum (2 + 4) azimuth is measured. The horns are excited according to the diagram shown in Fig. 2.26. At each joint, indicated on the diagram by a point, a waveguide bridge is used. The sum signal (Σ) is formed by addition in bridge III of signals 1 and 3, 2 and 4, preliminarily summed in pairs on the first two waveguide bridges. The difference signal (Δ) with respect to azimuth is obtained by subtracting in bridge III from the sum of signals 1 + 3 the sum of signals 2 + 4. The difference signal with respect to elevation is formed by

summation in bridge IV of the difference of signals 1 - 3 and 2 - 4, obtained on the first two bridges. This gives the required result because the system is linear and the associative law is applicable to it $(1 - 3) + (2 - 4) = (1 + 2) - (3 + 4)$.

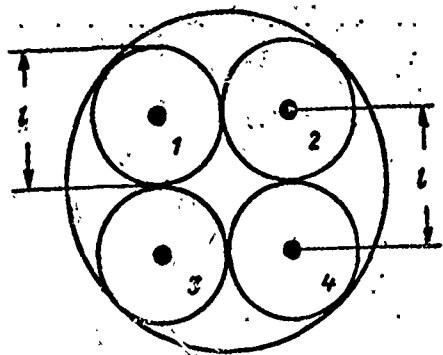


Fig. 2.24. Arrangement of feeds in the antenna system of a monopulse radar with phase direction finding.

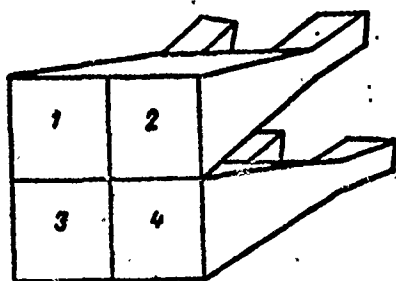


Fig. 2.25. A four-horn irradiator.

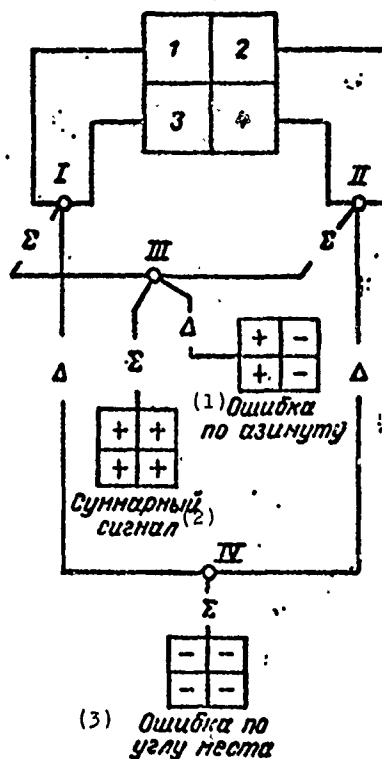


Fig. 2.26. Excitation diagram of a four-horn irradiator.
KEY: (1) Azimuth error; (2) Sum signal; (3) Elevation error.

In order to form the sum radiation pattern, the shaping circuit of the irradiating system excites in phase all four-horns (Fig. 2.27). In order to obtain the most optimal radiation, horn dimensions are selected so that in the formation of the sum beam the antenna has maximum amplification with uniform irradiation of the mirror.

Figure 2.28 illustrates the optimal method of irradiation, eliminating energy loss past the reflector [95]. It is only necessary, to approximately double the appropriate dimensions of the irradiators used for forming the difference patterns. Irradiation limits in essence are established by the surface of the reflector and, as a result, optimal characteristics in both difference patterns can be obtained. In order to get the optimal sum pattern, irradiator dimensions must be original; thus, the dimensions and their written expression must be different for all three patterns (Fig. 2.28), and in order to obtain optimal characteristics for all three patterns, special devices for controlling channels must be developed.

Below we examine four-horn and twelve-horn irradiators, which ensure the independent optimization of both sum and difference channels of a monopulse radar with respect to the amplification of the antenna system and the reduction of the side lobe level.

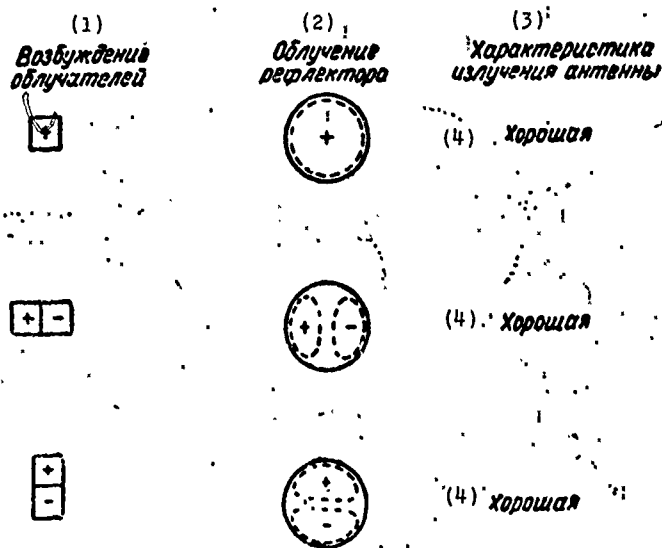


Fig. 2.28. Optimal irradiation in the antenna of a monopulse radar. KEY: (1) Excitation of irradiator; (2) Irradiation of reflector; (3) Characteristic of antenna radiation; (4) Good.

2.7.1. A four-horn irradiator operating on several types of waves. Four horns located in a row (Fig. 2.29) are used in this

irradiator [95]. At the open end of the horns are correcting lenses since in order to operate the antenna it is frequently necessary that the dimensions of the aperture be equal to several wavelengths. In the power circuit eight double waveguide T-joints are used. Four, located behind, excite the inputs of the four-horns; the character of excitation is determined by the channel to which the signal is fed. Each of the remaining four T-joints is connected with one of the four-horns and provides even or uneven excitation in the corresponding horn.

Horns, in their narrow part, have an oscillator of normal types of wave. In the excitation of an even type of wave, field distribution in the aperture of the irradiator is represented by the sum of the first and third types of waves; uneven excitation is generated by the second type of wave. Horns 2 and 3, in excitation on the uneven types of wave, are used to obtain the difference pattern in the elevation plane, and in excitation on the even type, to obtain the sum pattern. When all four horns are excited on an even type of wave, a difference pattern in the azimuth plane is formed; we take the difference between the sum of signals of horns 1 and 2 and the sum of signals of horns 3 and 4.

Figure 2.30 shows the corresponding field distribution along the aperture of an irradiator in the case of forming the sum and difference patterns for azimuth and elevation.

The dashes show the equivalent regions of the irradiator which are excited in the three cited modes of operation. We see from the figure the relationship between these and the regions required for optimal irradiation in accordance with Fig. 2.28.

2.7.2. A twelve-horn irradiator. The external view of a twelve-horn irradiator is presented in Figure 2.31. In order to decrease side lobes, each pyramidal horn consists of four sectioned horns. Thus, in this irradiating system there are 48 sectioned horns in all [119].

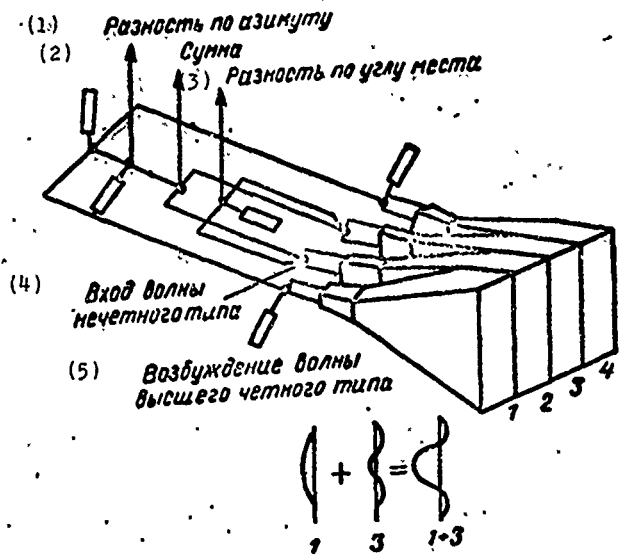


Fig. 2.29. A four-horn irradiator operating on several types of waves.
 KEY: (1) Azimuth difference; (2) Sum; (3) Elevation difference; (4) Input of uneven wave; (5) Excitation of highest even wave.

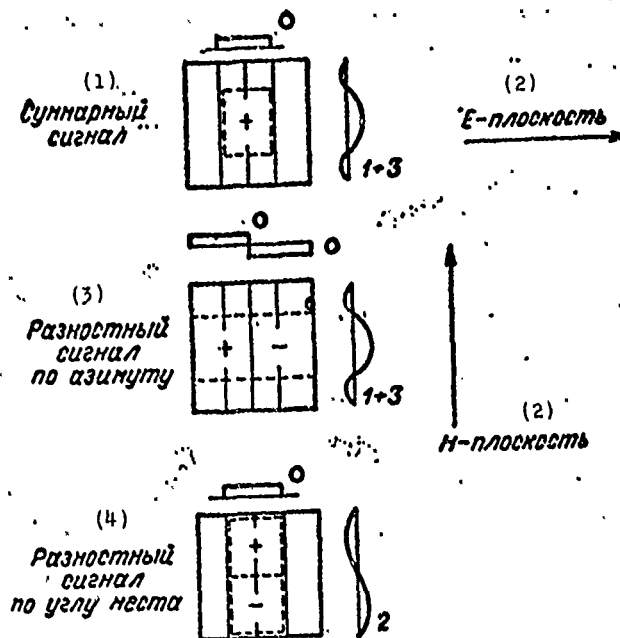
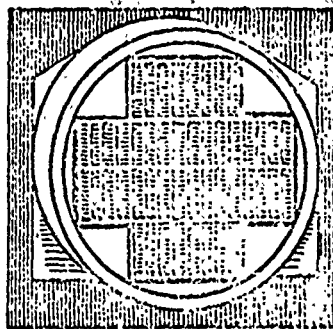


Fig. 2.30. Excitation of a four-horn irradiator operating on the highest types of waves.
 KEY: (1) Sum signal; (2) Plane; (3) Difference signal for azimuth; (4) Difference signal for elevation.

Fig. 2.31. External view of a twelve-horn irradiator.



The basic diagram of such an irradiator is presented in Fig. 2.32. Information which cannot be used for forming radiation patterns at the outputs of the waveguide bridge arms, is fed to the matched load. The sum pattern is formed by exciting the four central horns in the same manner as in the four-horn system. Two other groups of four irradiators each are used for forming difference patterns in the amplitude and elevation planes.

Since the difference patterns, in this case, are formed by a system of irradiators with a larger aperture than in the system with four irradiators, losses to energy overflow are reduced. Therefore, the intensity of irradiation on the edges of the reflector is approximately the same in the case of sum or difference signals.

2.7.3. A one-horn irradiator. An overall view of a one-horn irradiator is shown in Fig. 2.33 [109]. To study the operating principle of this irradiator let us assume that it is used for the reception of linearly polarized waves with polarization directed in parallel to the narrow side of the neck of the irradiator.

When a signal arrives from a point located in plane H (elevation plane), in the neck there are excited waves TE_{10} and TE_{20} whose relative amplitude and phase values characterize the angle of approach. These waves excite a wave of type TE_{10} in the two side arms; the components of the wave in these arms are equal in amplitude but

shifted by 180° in phase. The difference in the signals of the side arms makes it possible to determine the angle which the wave has with the axis in plane H. If, however, a signal arrives from a point located on the axis of the irradiator, then only one wave TE_{10} is excited in the neck, while the wave excited in the two side arms will be equal in amplitude and phase. Consequently, the difference in the signals of the side arms will be equal to zero.

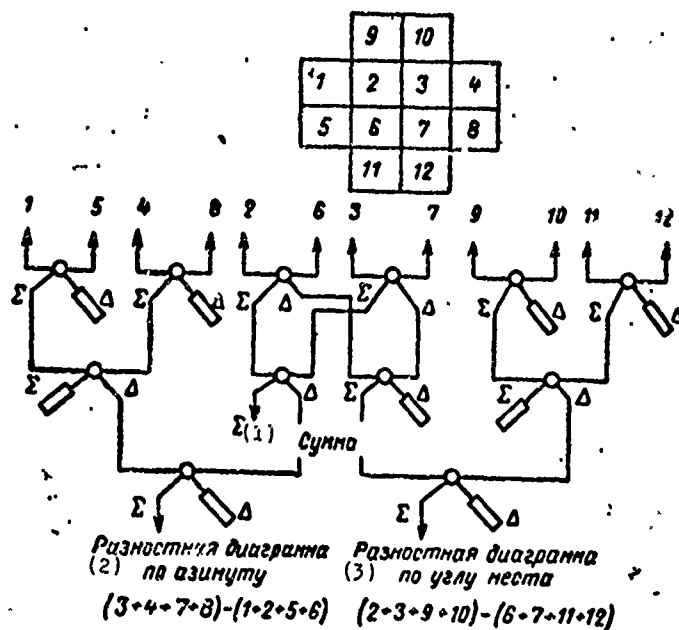


Fig. 2.32. Shaping circuit for sum and difference patterns in a twelve-horn irradiator.
 KEY: (1) Sum; (2) Difference pattern for azimuth; (3) Difference pattern for elevation.

If a signal arrives from a point in plane E (azimuth plane), in the neck of the irradiator waves TE_{10} , TE_{11} , TM_{11} can be excited. These types of waves excite the components of wave TE_{10} in the upper and lower arms, which are equal in amplitude and shifted by 180° in phase. The difference of signals in the upper and lower arms determines the angle of signal approach with respect to the axis in plane E of the antenna. When a signal approaches from a point located on the axis of the irradiator, the difference in the signals of the upper and lower arms will be equal to zero.

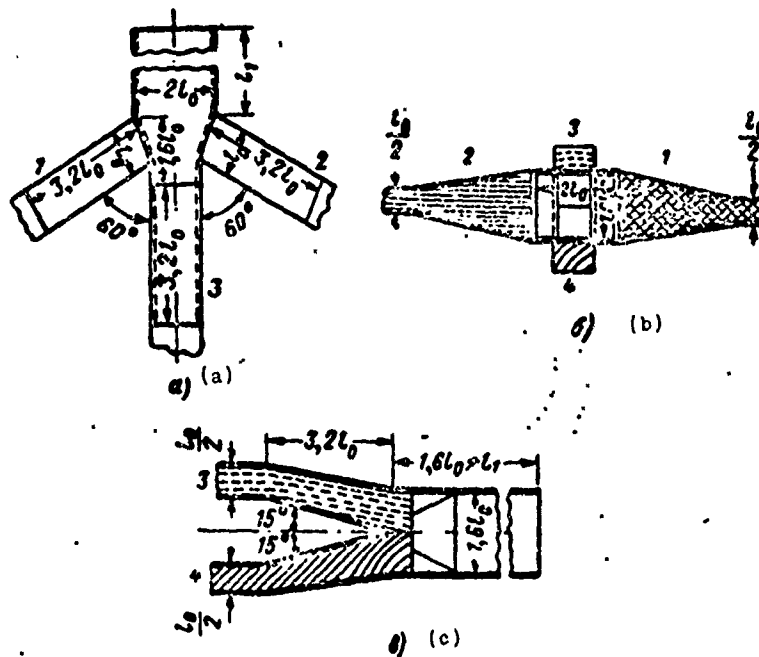


Fig. 2.33. Overall view of a one-horn irradiator: a) top view; b) front view; c) vertical cross-section along the axis of symmetry; 1 - left side arm; 2 - right side arm; 3 - upper arm; 4 - lower arm.

A signal can approach from a point located neither in plane H or in plane E. Then in the neck of the irradiator waves TE_{21} , and TM_{21} are excited. The amount of connection between these waves and the four arms depends upon the signal approach angles with respect to the axes of planes H and E, while the difference of signals in corresponding pairs of arms determines the signal approach angle in the corresponding plane.

In designing irradiators there is an effort to make the neck big enough that waves of types TE_{10} , TE_{20} , TE_{11} , TM_{11} , TM_{12} can be propagated. The dimensions l_0 must be approximately 0.7λ . The dimension l_1 is not critical.

Table 2.1 presents formulas for critical wavelength λ_c of a different type, which can be excited in the neck of the irradiator. All formulas pertain to a rectangular type of waveguide (a_c and b_c are waveguide dimensions).

Table 2.1.

(1) Тип волны	TE ₁₀	TE ₂₀	TE ₁₁ , TM ₁₁	TE ₂₁ , TM ₂₁
λ_c	$2a_c$	a_c	$\frac{2a_c}{\sqrt{1+(a_c/b_c)^2}}$	$\frac{a_c}{\sqrt{1+(a_c/2b_c)^2}}$

KEY: (1) Type of wave.

§ 2.8. SELECTION OF MAXIMUM DISPLACEMENT ANGLE FOR A RADIATION PATTERN AND THE DISTANCE BETWEEN PHASE CENTERS

An important antenna parameter for a monopulse radar is the maximum displacement angle of the radiation pattern relative to equisignal direction during amplitude direction finding and the distance between phase centers of antennas during phase direction finding. These parameters have a considerable effect on the accuracy of direction finding and effective range. In determining optimal value for these quantities, let us examine the example of a monopulse system with a sum-difference angular discriminator.

Direction finding error is inversely proportional to the curvature of the direction finding characteristic μ and the signal-noise ratio q :

$$\sigma_e \approx \frac{1}{\mu q} \quad (2.29)$$

Curvature μ characterizes the direction finding sensitivity and is

$$\mu = \left. \frac{dS(\theta)}{d\theta} \right|_{\theta=0}$$

In an amplitude sum-difference monopulse system, near the equisignal direction the sum radiation pattern is virtually constant

while the difference pattern is linear; therefore,

$$\mu = \frac{d}{d\theta} \left| \frac{F_1(\theta) - F_2(\theta)}{F_1(\theta) + F_2(\theta)} \right|_{\theta=0} = \frac{F'_p(0)}{F_c(0)}. \quad (2.30)$$

The optimal displacement angle ensuring maximum direction findings sensitivity could be found by solving equation

$$\frac{d}{d\theta} \left| \frac{F'_p(0)}{F_c(0)} \right| = 0. \quad (2.31)$$

However, from the values of $F_c(\theta)$, $F'_p(0)$, $(F'_p(0))/(F_c(0))$ and $F_c(0) \cdot F'_p(0)$, presented in Fig. 2.34, as a function of the displacement angle, it is apparent that ratio $F'_p(0)/F_c(0)$ grows monotonically and within the main lobe of the radiation pattern does not have a maximum, i.e., there is no optimal displacement angle ensuring maximum direction finding sensitivity.

The signal/noise ratio q is proportional to the sum pattern $F_c(0)$; therefore, the product

$$\mu q = \kappa_p F'_p(0) \quad (2.32)$$

is determined only by the curvature of the difference radiation pattern times equisignal direction. With the substitution of (2.32) and expression (2.29) we see that direction finding accuracy and the equisignal direction depends on the curvature of the difference pattern.

If as the criterion for determining optimal displacement angle we choose the maximum curvature of the difference pattern, we can obtain the minimum direction finding error. However, the requirement for obtaining maximum curvature of difference pattern is not an advisable criterion since, with such a displacement angle, the radiation patterns intersect at a very low level and the power of the signal received in the sum channel is much less than in the direction

of maximum; this leads to a considerable reduction in target detection range.

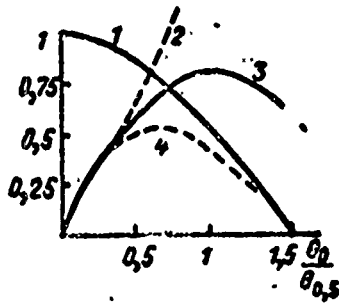


Fig. 2.34. Dependence of relative values on separation angle: 1) $F_c(0)$; 2) $F'_p(0)/F_c(0)$; 3) $F'_p(0)$; 4) $F_c(0)F'_p(0)$.

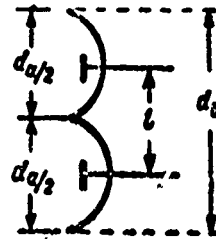


Fig. 2.35. Relationship between separation of irradiators and antenna aperture in a monopulse radar with phase direction finding.

Consequently, as the optimal displacement angle, it is advisable to take the angle corresponding to maximum product of sum pattern and curvature of difference pattern, i.e., to choose the displacement angle as a compromise between a loss in effective range and direction finding accuracy. From the curves presented in Fig. 2.34 it is apparent that the function $F_c(0) \cdot F'_p(0)$ has a maximum at $\theta_0 = 0.65\theta_{0.5}$.

With such a displacement angle two radiation patterns will intersect below their maxima at a level near 3 dB, i.e., on a level of half power. From this it follows that the optimal displacement angle is approximately a half-width of the radiation pattern with respect to the level of half power.

Optimal distance between phase centers of antennas (Fig. 2.35) in a phase sum-difference monopulse system is also found based on the condition of obtaining the maximum product of the sum pattern and the curvature of the difference pattern, i.e., from the solution to equation

$$\frac{d}{dt} |F_c(0) \cdot F'_p(0)| = 0.$$

As seen from Fig. 2.35, the aperture of the antenna system of a monopulse radar with phase direction finding is determined by equality

$$d_\phi = 2(d_a - l),$$

where d_a is the prescribed overall dimensions of the antenna system.

Since the amplitude of the sum signal at receiver input is determined by the product of the pattern times transmission and reception and is proportional to the aperture of the antenna, we can write

$$F_c^2(0) \equiv C_\phi (d_a - l), \quad (2.33)$$

where C_ϕ is the coefficient of proportionality.

The difference pattern is determined by the following expression

$$F_p(\theta) = F_c(0) \operatorname{tg} \frac{\varphi(\theta)}{2}. \quad (2.34)$$

With small angles of deflection, we have a difference in signal phases, received by the two patterns,

$$\varphi(\theta) = 2\pi \frac{l}{\lambda} \theta.$$

Then the curvature of the difference pattern in equisignal direction is determined by formula

$$\left. \frac{dF_p(\theta)}{d\theta} \right|_{\theta=0} = F'_p(0) = \frac{1}{2} F_c(0) \varphi'(0) = \frac{\pi l}{\lambda} F_c(0).$$

Consequently, the product of the sum pattern and the curvature of the difference pattern will be

$$F_c(0) \cdot F_p^i(0) = F_c^2(0) \frac{\pi l}{\lambda} = C_0 \frac{\pi l}{\lambda} (d_a - l).$$

This product is maximum when

$$\frac{d}{dl} \left[C_0 \frac{\pi l}{\lambda} (d_a - l) \right] = 0,$$

i.e.,

$$\frac{C_0 \pi}{\lambda} (d_a - l) - \frac{C_0 \pi}{\lambda} l = 0,$$

hence the optimal distance between phase centers is

$$l = \frac{d_a}{2}. \quad (2.35)$$

Thus, the optimal distance between phase centers is equal to half the length of the antenna aperture.

§ 2.9. WAVEGUIDE DEVICES FOR SUM-DIFFERENCE SIGNAL PROCESSING

In sum-difference monopulse radars the sum and difference signals can be obtained at high frequency with sum-difference bridges: annular (Fig. 2.36) and double waveguide T-joint (Fig. 2.37).

The annular sum-difference bridge has four leadoffs along one semicircle. Distances between leadoffs are $\lambda/4$. In this diagram, the leadoff Σ is sum and the leadoff Δ is difference. Actually, if cophased high-frequency signals are fed to leadoffs 1 and 2, then to leadoff Σ these signals pass along the same paths and, consequently, are added in phase while to leadoff Δ they pass along different paths and are added in opposite phase. The signal in the difference leadoffs will have the phase of that signal whose amplitude is greater.

When the signal in leadoff 1 exceeds the signal in leadoff 2, the phase of the difference signal, determined by the phase of the signal from leadoff 1, is shifted relative to leadoff 1 proportionally to $3\lambda/4$. The sum signal is shifted in phase relative to leadoffs 1 and 2 proportionally to $\lambda/4$. Therefore, difference and sum signals are in opposite phase.

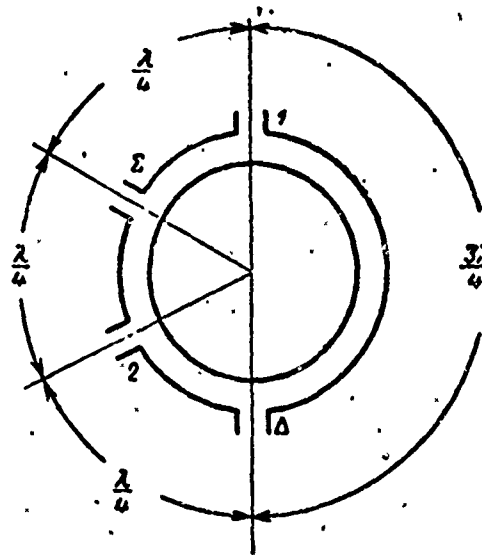


Fig. 2.36. Annular waveguide bridge.

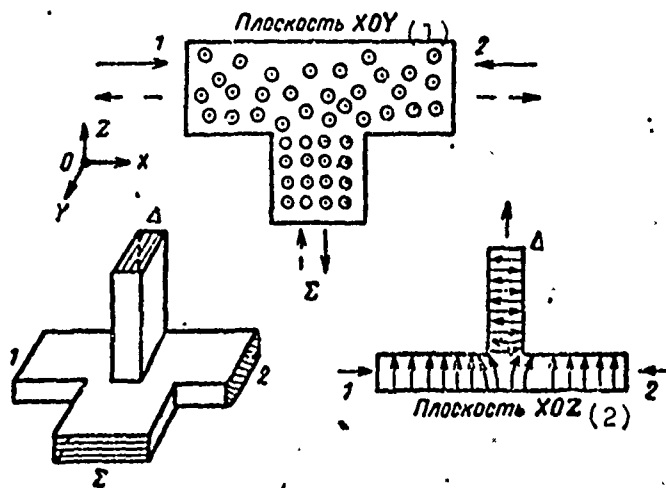


Fig. 2.37. Double waveguide T-joint
KEY: (1) Plane XDY; (2) Plane XOZ.

If the signal in leadoff 1 is less than the signal in leadoff 2, the phase of the difference signal, determined by the phase of the signal from leadoff 2, is shifted relative to leadoff 2 proportionally to $\lambda/4$. The sum signal has the same shift with respect to leadoff 2. In this case, the sum and difference signals are in phase.

In the double waveguide T-joint two cophased signals, proceeding to waveguides 1 and 2, form in leadoff Σ (plane xoy) the sum signal, and in leadoff Δ (plane xoz) the difference signal [18]. Actually, if we assume that the force lines of the electrical field of the waveguide in the horizontal plane are directed from the bottom up, the vectors of the electrical field of signals 1 and 2 proceeding to leadoff Δ have opposite direction.

The signal in the difference leadoff will have the phase of that signal whose amplitude is greater. In the case of the equality of signals 1 and 2, the difference signal will be equal to zero.

Besides these sum-difference bridges, we can also use other types of bridges, for example, slot balance bridges [131].

CHAPTER 3

BASIC FUNCTIONAL ELEMENTS OF ANGULAR DISCRIMINATORS

§ 3.1. LOGARITHMIC AMPLIFIER

A logarithmic amplifier is a nonlinear amplifier which has a logarithmic relationship between the amplitudes of output $U_{\text{ВЫХ}}$ and input $U_{\text{ВХ}}$ voltages.

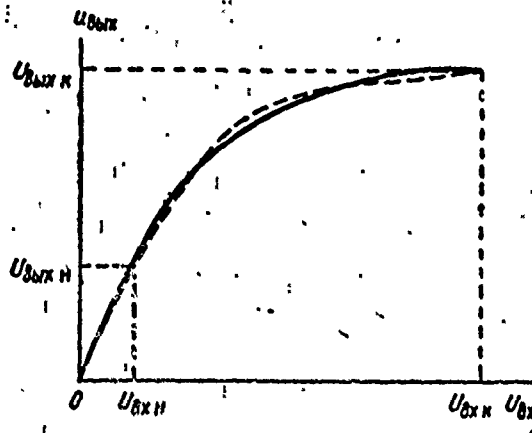


Fig. 3.1. Amplitude characteristic of a logarithmic amplifier. — calculated; - - - experimental.

The amplitude characteristic of a logarithmic amplifier (Fig. 3.1) when operating in linear mode ($U_{\text{ВХ}} \leq U_{\text{ВХ Н}}$) is described by equation

$$U_{\text{ВЫХ}} = K_0 U_{\text{ВХ}}, \quad (3.1)$$

where k_0 is the maximum amplification factor in the linear segment;
 U_{BXH} is the input voltage beginning with which the characteristic becomes logarithmic.

When a logarithmic amplifier operates in the logarithmic mode ($U_{\text{BXH}} < U_{\text{BX}} < U_{\text{BXH}}$), the expression for the logarithmic amplitude characteristic (LAC) will have the form [12]

$$U_{\text{ВЫХ}} = k_0 U_{\text{ВХ}} \left(a_n \ln \frac{U_{\text{ВХ}}}{U_{\text{ВХН}}} + 1 \right), \quad (3.2)$$

where a_n is the coefficient characterizing the slope of the logarithmic characteristic;

$U_{\text{ВХН}}$ is the final input voltage at which the LAC of the amplifier is evaluated.

In addition, a logarithmic amplifier can be characterized by the following basic qualitative indices:

1) $U_{\text{ВЫХН}}$ and $U_{\text{ВЫХН}}$ are the output voltages corresponding to the beginning and end of the amplifier's logarithmic amplitude characteristics;

2) dynamic range with respect to input and output voltages is

$$D_{\text{LX}} = \frac{U_{\text{ВХН}}}{U_{\text{ВХН}}}; \quad D_{\text{LXX}} = \frac{U_{\text{ВЫХН}}}{U_{\text{ВЫХН}}}; \quad (3.3)$$

3) the compression factor of the amplifier voltage is

$$K_{\text{СЖ}} = \frac{D_{\text{ВХ}}}{D_{\text{ВЫХ}}}; \quad (3.4)$$

4) the relative accuracy of reproducing the logarithmic amplitude characteristic of the amplifier, which is the deviation of the experimental characteristic from the calculated characteristic (Fig. 3.1)

$$\delta_{\text{X}} = \frac{U_{\text{ВЫХЭ}} - U_{\text{ВЫХР}}}{U_{\text{ВЫХР}}}, \quad (3.5)$$

where $U_{\text{ВЫХ } \text{Э}}$ is the output voltage throughout the dynamic range with experimental LAC.

$U_{\text{ВЫХ } \text{Р}}$ is the output voltage throughout the dynamic range with calculated LAC.

In § 1.3 we have shown that in a monopulse radar with an amplitude angular discriminator using logarithmic amplifiers, the discrimination of angular information actually occurs as a result of the subtraction of the logarithmic values of two signals, which is equivalent to the formation of a logarithm of the ratio. Actually, voltage at output of the subtracting device (Fig. 1.4), on the assumption that the logarithmic amplifiers are identical, will be

$$u_{\text{В } \text{Y}} = u_{\text{ВЛН } \text{1}} - u_{\text{ВЛН } \text{2}} = K_{\text{В } \text{Y}} K_0 u_{\text{ВХ } \text{2}} a_{\text{Л}} \ln \frac{u_{\text{ВХ } \text{1}}}{u_{\text{ВХ } \text{2}}}, \quad (3.6)$$

where $K_{\text{В } \text{Y}}$ is the transmission factor of the subtracting device.

In accordance with equalities (1.4 and 1.5), we can write

$$\left. \begin{aligned} u_{\text{ВХ } \text{1}} &= E(t) F_1(\theta) = E(t) F(\theta_0 - \theta), \\ u_{\text{ВХ } \text{2}} &= E(t) F_2(\theta) = E(t) F(\theta_0 + \theta). \end{aligned} \right\} \quad (3.7)$$

Then equation (3.6) assumes the form

$$u_{\text{В } \text{Y}} = K_{\text{В } \text{Y}} K_0 U_{\text{ВХ } \text{2}} a_{\text{Л}} \ln \frac{F(\theta_0 - \theta)}{F(\theta_0 + \theta)}. \quad (3.8)$$

Equality (3.8) describes the direction finding characteristic. From it we see that the direction finding characteristic in such a monopulse system depends upon the properties of the logarithmic amplifier and not upon the value of the signal. Therefore, any deviation of the actual amplitude characteristics of amplifiers from a precisely logarithmic characteristic leads to a distortion in the direction finding characteristic and, consequently, to error in determining target direction.

With a given permissible relative error of $\delta_n = \frac{\Delta m_n}{m_n}$ in determining ratio $m_n = \frac{U_{BX1}}{U_{BX2}}$, the values of permissible absolute and relative deviation in the actual amplitude characteristic from a precisely logarithmic characteristic at any of its points are respectively equal to [12]

$$\left. \begin{aligned} |\pm \Delta U_{BX}| &= 0,7\kappa_0 U_{BX} a_n \ln(1 + \delta_n), \\ \delta_{BX} &= \left| \pm \frac{\Delta U_{BX}}{U_{BX}} \right| = \frac{0,7a_n (1 + \delta_n)}{a_n \ln \frac{U_{BX}}{U_{BX}} + 1}. \end{aligned} \right\} (3.9)$$

From equation (3.9) it is apparent that the permissible absolute deviation of the experimental amplitude characteristic from the calculated logarithmic characteristic is higher the greater the maximum amplification factor and input voltage and is constant throughout the logarithmic range of the amplifier, while the permissible relative deviation is a variable quantity and reduces with an increase in the level of comparable voltages. Consequently, logarithmic amplifiers used in monopulse radars must reproduce the logarithmic law of amplification at the end of the logarithmic range with greater accuracy than at its beginning. This accuracy increases with an increase in the dynamic range of the amplifier.

In case of nonidentity of amplitude characteristics for two logarithmic amplifiers (a deviation in the experimental amplitude characteristic of each amplifier from the calculated logarithmic characteristic greater than the permissible value), output voltage of an amplitude angular discriminator does not satisfy requirements imposed on direction finding characteristics of monopulse systems. Therefore, it is necessary to achieve, by special measures, an identity of amplitude characteristics in both amplification channels.

There are several methods for obtaining amplifiers with logarithmic amplitude characteristics. At the present time the most widely used method is the shunting of anode loads in the amplifier by nonlinear elements and the method of adding in sequence the amplifiers' stages output voltages [12].

nonlinear stage begins to work in the logarithmic mode and its input voltage is

$$U_H = U_{\text{ЭХЭ}} \cdot K_1^{n-1}. \quad (3.10)$$

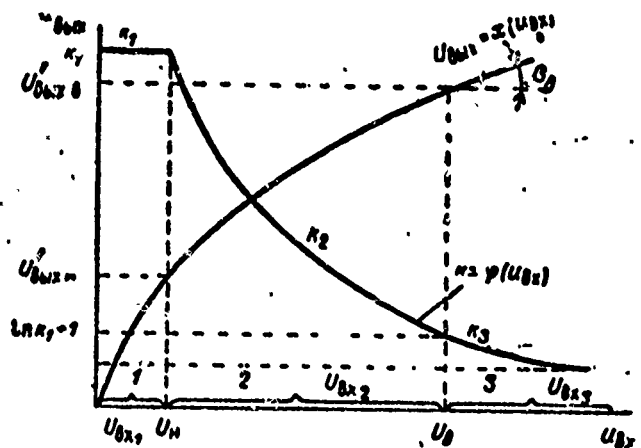


Fig. 3.3. Amplitude characteristic of a nonlinear stage.

With an increase in the input voltage of the last stage to U_B , it works in the logarithmic mode and all the others operate in linear mode. With this the voltage at output of the nonlinear stage is

$$U_{\text{ЭХЭ}} = K_1 U_H \left(a_n \ln \frac{U_{0x2}}{U_H} + 1 \right). \quad (3.11)$$

In the future for the sake of simplicity we shall assume that $a_n = 1$. When the input voltage of the last stage is changed in a range from U_H to U_B , voltage at input of the logarithmic amplifier

changes in the range $\frac{U_H - U_B}{K_1^{n-1}}$, and its amplification factor is

determined by expression

$$K_0(n) = K_1^{n-1} \frac{K_1 U_H}{U_{0x2}(n)} \left(\ln \frac{U_{0x2}(n)}{U_H} + 1 \right), \quad (3.12)$$

where $U_{BX(n)} = U_{BX} \cdot k_1^{n-1} = U_{BX} \cdot 2$ is the voltage at input of the n-th stage;

U_{BX} is the voltage at amplifier input.

The logarithmic amplitude characteristic of the amplifier, in this case, will be described by expression

$$\begin{aligned} U_{BX0(n)} &= U_{BX} \cdot K_0(n) = K_1 U_n \left(\ln \frac{U_{BX(n)}}{U_n} + 1 \right) = \\ &= K_1 U_n \left(\ln \frac{U_{BX} \cdot 2}{U_n} + 1 \right) = K_0 U_{BX} \left(\ln \frac{U_{BX}}{U_n} + 1 \right). \end{aligned} \quad (3.13)$$

When voltage at input of n-th stage becomes equal to u_B the stage begins to operate in quasilinear mode on the third section of the amplitude characteristic. In order to accomplish the successive operation of stages in logarithmic mode, it is necessary that voltage at stage input (n - 1) be equal to

$$U_n = U_{BX} \cdot k_1^{n-2}.$$

In order to satisfy this condition, the maximum amplification factor of a nonlinear stage must be

$$K_1 = \frac{U_B}{U_n} = D_{1x1}. \quad (3.14)$$

The U_B/U_H also determines the logarithmic range of a nonlinear stage.

When voltage at amplifier input changes in the range $\frac{U_H - U_B}{k_1^{n-2}}$ the (n - 1)-th stage operates in logarithmic mode, all stages preceding it operate in linear mode, and the last stage operates in quasilinear mode. The expression for the amplification factor of the amplifier when the (n - 1)-th nonlinear stage is operating in logarithmic mode will have the form

$$\kappa_{3(n-1)} = \kappa_1^{n-2} \frac{\kappa_1 U_{\Sigma}}{U_{\Sigma X(n-1)}} \left(\ln \frac{U_{\Sigma X(n-1)}}{U_{\Sigma}} + 1 \right) \kappa_{3(n)}, \quad (3.15)$$

where $U_{\Sigma X(n-1)} = U_{\Sigma X} k_1^{n-2} = U_{\Sigma X 2}$ is the voltage at input of the $(n-1)$ -th stage;

$\kappa_{3(n)}$ is the amplification factor of the n -th stage.

None of the preceding stages operating in linear modes has any effect on the shape of the amplitude characteristic of the amplifier. The last stage, operating in quasilinear mode, does not introduce distortions into the logarithmic amplitude characteristic of the amplifier if its amplification factor $\kappa_{3(n)}$ is constant and equal to one or is variable and greater than one; however, then the differential amplification factor must be equal to one.

The amplification factor of a nonlinear stage on the boundary of the transition from the second section to the third is equal to

$$\kappa_2 = \frac{\kappa_1 U_{\Sigma}}{U_{\Sigma}} \left(\ln \frac{U_{\Sigma}}{U_{\Sigma}} + 1 \right) = \ln \kappa_1 + 1. \quad (3.16)$$

And since $\kappa_1 > 1$ and $\ln \kappa_1 > 0$, then $\kappa_2 > 1$ and, consequently, at the moment of transition from logarithmic mode to quasilinear, the amplification factor of a nonlinear stage is $\kappa_3 = \kappa_2 > 1$.

The value of the differential amplification factor of a nonlinear stage when it is operating in quasilinear mode is found from the condition of the equality of the first derivatives and ordinates for the point where the second section of the amplitude characteristic of a nonlinear stage changes into the third section:

$$b_2 = \frac{dU_{\Sigma X 2}}{dU_{\Sigma X 2}} = \frac{dU_{\Sigma X 2}}{dU_{\Sigma X 3}}$$

Using equation (3.14), we can write

$$\frac{d \left[\kappa_1 U_H \left(\ln \frac{U_{BX2}}{U_H} + 1 \right) \right]}{dU_{BX2}} =$$

$$= \frac{d \left[\kappa_1 U_H (\ln \kappa_1 + 1) + b_H (U_{BX2} - U_H) \right]}{dU_{BX2}}.$$

Differentiating we obtain

$$\frac{\kappa_1 U_H}{U_H} = b_H.$$

Since at the transition point $U_B = U_H \cdot \kappa_1$ then $b_H = 1$.

Voltage at the output of a nonlinear stage operating in quasi-linear mode can be written in the form

$$U_{BX3} = U'_{BX3} + b_H (U_{BX3} - U_H) = \kappa_1 U_H \left(\ln \kappa_1 + \frac{U_{BX3}}{U_H} \right). \quad (3.17)$$

Then the amplification factor of the nonlinear stage for the third section of amplitude characteristic is

$$\kappa_3 = \frac{\kappa_1 U_H}{U_{BX3}} \left(\ln \kappa_1 + \frac{U_{BX3}}{U_H} \right) = \frac{\kappa_1 U_H \ln \kappa_1}{U_{BX3}} + 1. \quad (3.18)$$

From equality (3.18) it is apparent that κ_3 is a variable quantity and when there is a considerable increase in input voltage, this quantity approaches unity.

Substituting the obtained value of κ_3 into equation (3.15), we obtain

$$\kappa_{0(n-1)} = \kappa_1^{n-2} \frac{\kappa_1 U_H}{U_{BX(n-1)}} \left(\ln \frac{U_{BX(n-1)}}{U_H} + 1 \right) \times$$

$$\times \left(\frac{\kappa_1 U_H \ln \kappa_1}{U_{BX(n)}} + 1 \right).$$

Consequently, voltage at amplifier output will be

$$U_{\text{вых}0(n-1)} = U_{\text{вх}0(n-1)} = \kappa_1 U_{\text{вх}} \ln \kappa_1 + U_{\text{вх}} \kappa_1 \left(\ln \frac{U_{\text{вх}(n-1)}}{U_{\text{вх}}} + 1 \right),$$

and since $U_{\text{вх}(n-1)} = U_{\text{вх}2}$, we can write

$$U_{\text{вых}0(n-1)} = \kappa_1 U_{\text{вх}} \ln \kappa_1 + U_{\text{вх}} \kappa_1 \left(\ln \frac{U_{\text{вх}2}}{U_{\text{вх}}} + 1 \right).$$

With a subsequent increase in the input voltage of the amplifier the $(n-1)$ -th stage begins to operate in quasilinear mode, the $(n-2)$ -th stage enters the logarithmic mode, and the amplification factor of the amplifier and the voltage at its output are respectively equal to

$$\begin{aligned} \kappa_0(n-2) &= \kappa_1^{n-3} \frac{\kappa_1 U_{\text{вх}}}{U_{\text{вх}(n-2)}} \left(\ln \frac{U_{\text{вх}(n-2)}}{U_{\text{вх}}} + 1 \right) \times \\ &\times \left(\frac{\kappa_1 U_{\text{вх}} \ln \kappa_1}{U_{\text{вх}(n-1)}} + 1 \right) \left(\frac{\kappa_1 U_{\text{вх}} \ln \kappa_1}{U_{\text{вх}(n)}} + 1 \right); \\ U_{\text{вых}0(n-2)} &= 2\kappa_1 U_{\text{вх}} \ln \kappa_1 + U_{\text{вх}} \kappa_1 \left(\ln \frac{U_{\text{вх}2}}{U_{\text{вх}}} + 1 \right). \end{aligned}$$

Reasoning in a similar manner, we can obtain an expression for the amplification factor and voltage at input of the logarithmic n -stage amplifier when the first nonlinear stage is working in logarithmic mode:

$$\begin{aligned} \kappa_0(n) &= \frac{\kappa_1 U_{\text{вх}}}{U_{\text{вх}}} \left(\ln \frac{U_{\text{вх}}}{U_{\text{вх}}} + 1 \right) \left(\frac{\kappa_1 U_{\text{вх}} \ln \kappa_1}{U_{\text{вх}2}} + 1 \right) \dots \\ &\dots \left(\frac{\kappa_1 U_{\text{вх}} \ln \kappa_1}{U_{\text{вх}(n-1)}} + 1 \right) \left(\frac{\kappa_1 U_{\text{вх}} \ln \kappa_1}{U_{\text{вх}(n)}} + 1 \right); \end{aligned} \quad (3.19)$$

$$U_{\text{ВМХ}0}(1) = (n-1)\kappa_1 U_n \ln \kappa_1 + \kappa_1 U_n \left(\ln \frac{U_{\text{ВХ}0}}{U_n} + 1 \right) \quad (3.20)$$

Thus, based on the above consideration, we can write a general expression for the amplification factor of a n-stage amplifier and the voltage at its output with the strict alternate operation of nonlinear stages:

$$\begin{aligned} \kappa_0 = & \kappa_1^{n-m} \frac{U_n \kappa_1}{U_{\text{ВХ}}(n-m+1)} \left[\ln \frac{U_{\text{ВХ}}(n-m+1)}{U_n} + 1 \right] \times \\ & \times \prod_{i=2}^{l=m-1} \left(\frac{\kappa_i U_n \ln \kappa_i}{U_{\text{ВХ}}(n-m+i)} + 1 \right), \end{aligned} \quad (3.21)$$

where $(n - m)$ is the number of nonlinear stages operating in linear modes;

$(n - m + 1)$ is the number of the stage operating in logarithmic mode;

$(m - 1)$ is the number of nonlinear stages operating in quasi-linear mode.

Then

$$U_{\text{ВМХ}0} = \kappa_0 U_{\text{ВХ}}. \quad (3.22)$$

Here, after conducting such an analysis, it is easy to express the basic qualitative indices of a n-stage logarithmic amplifier for the general case $a_n \neq 1$ in terms of the indices of the separate stages.

The beginning of the logarithmic amplitude characteristic of the amplifier corresponds to the input voltage at which the last nonlinear stage begins to operate in logarithmic mode,

$$U_{\text{ВМХ}} = \frac{U_n}{\kappa_1^{n-1}}. \quad (3.23)$$

In this case, voltage at amplifier output will be

$$U_{\text{BHX}} = U_{\text{BX}} \cdot \kappa_1^n = U'_{\text{BHX}} \quad (3.24)$$

The end of the logarithmic amplitude characteristic of the amplifier corresponds to the input voltage at which the first non-linear stage begins to operate in quasilinear mode:

$$U_{\text{BX}} = U_{\text{B}} = U_{\text{BHX}} \cdot \kappa_1^n \quad (3.25)$$

Then output voltage is

$$U_{\text{BHX}} = n\kappa_1 U_{\text{B}} a_n \ln \kappa_1 + \kappa_1 U_{\text{B}} = U_{\text{BHX}} (na_n \ln \kappa_1 + 1) \quad (3.26)$$

The dynamic range of the amplifier with respect to input and output voltages, respectively, will be

$$D_{\text{BX}} = \frac{U_{\text{BHX}}}{U_{\text{BX}}} = \kappa_1^n = D_{\text{BX1}}^n \quad (3.27)$$

$$D_{\text{BHX}} = \frac{U_{\text{BHX}}}{U_{\text{BHX}}} = na_n \ln D_{\text{BX1}} + 1 \quad (3.28)$$

Consequently, the compression factor of amplifiable voltage can be written in the form

$$\kappa_{\text{CM}} = \frac{D_{\text{BX}}}{D_{\text{BHX}}} = \frac{D_{\text{BX1}}^n}{na_n \ln D_{\text{BX1}} + 1} \quad (3.29)$$

In a multistage logarithmic amplifier on intermediate frequency with shunting of anode loads of the stages by nonlinear elements, we use most frequently amplifiers consisting of stages to whose anode circuits are connected single or double-circuit filters. The equivalent circuit of a nonlinear resonance stage is presented in Fig. 3.4 [12]. The amplification factor of this stage is

$$\kappa_n = S_n \frac{R_2 R_{\text{BX}}}{R_0 + R_{\text{BX}}} \quad (3.30)$$

where S_n is tube steepness,

$$\frac{1}{R_0} = \frac{1}{R_{\text{вых}}} + \frac{1}{R_a} + \frac{1}{R_n} + \frac{1}{R_{\text{вх}}}$$

$R_{\text{вых}}$ is tube output resistance;

R_a is anode resistance;

R_n is equivalent circuit resistance;

$R_{\text{вх}}$ is input resistance of next tube.

Voltage at output of nonlinear stage is

$$U_{\text{вых}} = U_{\text{вх}} \cdot \kappa_n = S_n U_{\text{вх}} \frac{R_0 R_{\text{нел}}}{R_0 + R_{\text{нел}}} \quad (3.31)$$

When a stage is operating in linear mode, the resistance of the nonlinear element must be higher and must not shunt anode load, i.e., $R_{\text{нел}} \gg R_0$. In this case, $\kappa_1 = S_n R_0$.

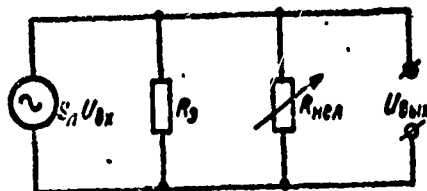


Fig. 3.4. Equivalent circuit of a nonlinear resonance stage.

The law of variations for resistance of a nonlinear element $R_{\text{нел} 2}$, as a function of the output voltage of the stage when the stage is operating in logarithmic mode, we find after equating the right sides of equations 3.11 and 3.31:

$$\kappa_1 U_{\text{вх}} \left(a_n \ln \frac{U_{\text{вых} 2}}{U_n} + 1 \right) = S_n U_{\text{вх} 2} \frac{R_0 R_{\text{нел} 2}}{R_0 + R_{\text{нел} 2}} \quad (3.32)$$

Introducing the designation

$$p_n = a_n \ln \frac{U_{\text{вых} 2}}{U_n} + 1$$

and performing the transformation, we obtain

$$R_{\text{нел}3} = \frac{R_0 p_n}{\exp\left(\frac{p_n - 1}{a_n} - p_n\right)} \quad (3.33)$$

With similar reasoning and using equations (3.17) and (3.31), we find the relationship between $R_{\text{нел}3}$ and the output voltage of the stage when it is operating in quasilinear mode:

$$R_{\text{нел}3} = \frac{R_0}{\frac{\kappa_1}{a_n p_n} (p_n - a_n \ln \kappa_1 - 1 + a_n) - 1} \quad (3.34)$$

When $p_n \gg \ln \kappa_1$, $R_{\text{нел}3} \rightarrow 1/S_n$ and, consequently, $k_3 = S_n R_{\text{нел}3} \rightarrow 1$.

In practice, in the design of amplifiers, by the input resistance of the nonlinear element $R_{\text{вх}} = R_{\text{нел}}$ we mean the ratio of the amplitude of applied voltage U_m to the current amplitude of the first harmonic, I_{m1} :

$$R_{\text{вх}} = R_{\text{нел}} = \frac{U_m}{I_{m1}} \quad (3.35)$$

The amplitude of the first harmonic of current flowing through the nonlinear element is determined based on the static volt-ampere characteristic of the element (semiconductor or vacuum diode), which can be given either graphically or analytically.

If the characteristic is given graphically, I_{m1} can be determined graphically by the method of five or twelve ordinates [25]. At high amplitudes of voltages this method has an accuracy of 5-8%. With low amplitudes the graphic method has considerable error; therefore, it is advisable to determine current amplitude I_{m1} analytically. These methods have been described in greater detail in reference [12] and we shall not examine them further.

Thus, the nonlinear element shunting the anode load of an amplifier stage in an n-stage logarithmic amplifier must satisfy the following requirements [12, 32].

1. With small input signal when the stage is operating in linear mode, the resistance of the nonlinear element must be high and constant so that anode load will not be shunted.

2. When the stage is operating in logarithmic mode, the resistance of the nonlinear element must change in accordance with (3.33). The nonlinear section of the volt-ampere characteristic of the nonlinear element must be within the range of

$$U_{\text{нел}} = U'_{\text{вых}} = \kappa_1 U_{\text{н}} \text{ до}$$
$$U_{\text{нел}} = U'_{\text{вых}} = \kappa_1 U_{\text{н}} (a_x \ln \kappa_1 + 1).$$

3. When the nonlinear stage is operating in quasilinear mode, the resistance of the nonlinear element must change according to the rule determined by expression (3.34). In order to fulfill this requirement, the nonlinear element must have a volt-ampere characteristic which has, at the beginning, a sharply pronounced nonlinear section with great steepness, gradually changing to linear.

4. Static characteristics of nonlinear elements shunting anode loads of various stages in an n-stage amplifier must be identical.

5. The nonlinear element must have low interelectrode capacitance, which has a particularly large significance when making a wide-band amplifier.

3.1.2. Logarithmic amplifiers with summation of stage output voltages. The method of obtaining the logarithmic amplitude characteristic in a i-f amplifier by the successive adding of voltages from the outputs of amplifier stages is known in literature as the method of successive detection [12].

Figure 3.5 illustrates the simplified diagram of a logarithmic amplifier with successive detection of signals and separate detectors in each channel. The high-frequency input voltage is amplified by n amplifier stages at whose output the detectors are connected. The detected signals are added on common loads. In order that the video-pulses moving from the outputs of all n detectors be added at the same time, it is necessary to use an artificial long line, each link of which delays the video-pulse for a period of time equal to the time of radiopulse passage through the amplifier stage. In order to exclude reflections, the delay line must be loaded at input and output to resistance equal to its wave impedance.

To examine the principle of obtaining a logarithmic amplitude characteristic in such an amplifier, we assume that all amplifier stages are identical and have an amplification factor in the linear mode k_1 ; upon saturation of a stage its output voltage remains constant regardless of the amplitude of the input signal. We shall also assume that signal in the summator are added linearly and the transmission factor of the summator is equal to one.

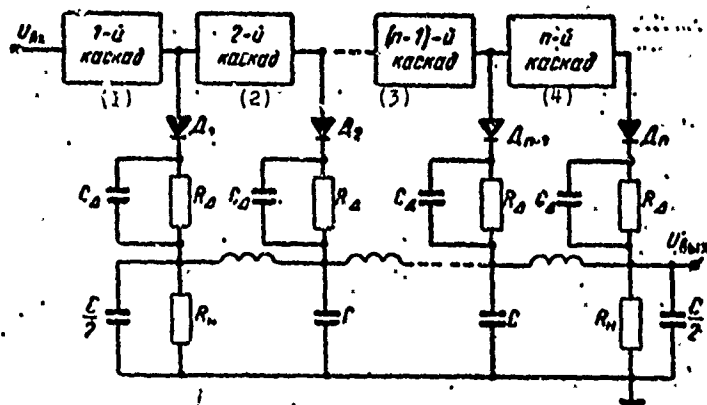


Fig. 3.5. Simplified diagram of a logarithmic amplifier with successive signal detection.
 KEY: (1) 1-st stage; (2) 2-st stage; (3) $(n - 1)$ -th stage; (4) n -th stage.

When low voltages are fed to amplifier input, all stages operate in linear mode and the voltage summator output is

$$U'_{\text{ВЛХ}} = U'_{\text{ВХ}} (\kappa_1^n + \kappa_1^{n-1} + \dots + \kappa_1^2 + \kappa_1) \quad (3.36)$$

If we designate the amplification factor in the linear part of the entire logarithmic amplifier in terms of $k_p = \kappa_1 + \kappa_1^2 + \dots + \kappa_1^{n-1} + \kappa_1^n$, equation (3.36) can be written as

$$U'_{\text{ВЛХ}} = U'_{\text{ВХ}} \cdot k_p \quad (3.37)$$

When voltage at amplifier input reaches the value $U'_{\text{ВХ}} = U_{\text{ВХН}}$, the last, the n -th stage, is saturated and the voltage at detector output of the last stage is

$$U_{\text{ВЛХН}} = U_{\text{ВХН}} \cdot \kappa_1^n$$

while voltage at summator output is,

$$U_{\text{ВЛХН}} = U_{\text{ВХН}} (\kappa_1^n + \kappa_1^{n-1} + \kappa_1^{n-2} + \dots + \kappa_1^2 + \kappa_1) = U_{\text{ВХН}} k_p \quad (3.38)$$

With an increase in input voltage to the value $U''_{\text{ВХ}} = \kappa_1 U_{\text{ВХН}}$ the next-to-the-last, the $(n-1)$ -th stage, is saturated and the voltage at summator output (when $n \gg 1$) is

$$U''_{\text{ВЛХ}} = \kappa_1^n U_{\text{ВХН}} + U_{\text{ВХН}} (\kappa_1^n + \kappa_1^{n-1} + \kappa_1^{n-2} + \dots + \kappa_1^2) \approx \kappa_1^n U_{\text{ВХН}} + U_{\text{ВХН}} k_p = U_{\text{ВЛХН}} + \kappa_1^n U_{\text{ВХН}}$$

When input voltage of the amplifier becomes equal to $U'''_{\text{ВХ}} = \kappa_1^2 U_{\text{ВХН}}$, the $(n-2)$ -th stage is saturated and voltage at summator output is

$$U_{\text{ВЫХ}}^{(n)} = 2\kappa_1^n U_{\text{ВХ}} + U_{\text{ВХ}} (\kappa_1^n + \kappa_1^{n-1} + \kappa_1^{n-2} + \dots + \kappa_1^2) \approx \\ \approx 2\kappa_1^n U_{\text{ВХ}} + U_{\text{ВХ}} \kappa_1^n = U_{\text{ВЫХ}} + 2\kappa_1^n U_{\text{ВХ}}$$

Similarly, when the first stage is saturated, we can write

$$U_{\text{ВХ}}^{(n)} = U_{\text{ВЫХ}} = \kappa_1^{n-1} U_{\text{ВХ}} \quad (3.39)$$

and, accordingly, voltage at summator output is

$$U_{\text{ВЫХ}}^{(n)} = U_{\text{ВЫХ}} = (n-1)\kappa_1^n U_{\text{ВХ}} + U_{\text{ВХ}} \kappa_1^n = n\kappa_1^n U_{\text{ВХ}} \quad (3.40)$$

From this analysis it is apparent that with the alternate transition of amplifier stages into saturation mode, input voltage of the amplifier changes exponentially and output voltages linearly. Consequently, between input and output voltages there is a logarithmic relationship.

Let us write equality (3.39) in the form

$$\ln U_{\text{ВХ}}^{(n)} = (n-1) \ln \kappa_1 + \ln U_{\text{ВХ}}$$

and we shall then find the value of n :

$$n = \frac{1}{\ln \kappa_1} \ln \frac{U_{\text{ВХ}}^{(n)}}{U_{\text{ВХ}}} + 1$$

If we substitute the obtained value of n into expression (3.40) we obtain

$$U_{\text{ВЫХ}} = \frac{\kappa_1^n U_{\text{ВХ}}}{\ln \kappa_1} \ln \frac{U_{\text{ВХ}}}{U_{\text{ВХ}}} + \kappa_1^n U_{\text{ВХ}} = \\ = \kappa_1^n U_{\text{ВХ}} \left(\frac{1}{\ln \kappa_1} \ln \frac{U_{\text{ВХ}}}{U_{\text{ВХ}}} + 1 \right) \quad (3.41)$$

After comparing expressions (3.2) and (3.41), we obtain

$$a_n = \frac{1}{\ln k_1}.$$

The dynamic range of an n-stage logarithmic amplifier with summation of the output voltages of the stages will be equal, respectively, for input and output voltages to

$$D_{\text{ВХ}} = \frac{U_{\text{ВХК}}}{U_{\text{ВХН}}} = k_1^{n-1}, \quad (3.42)$$

$$D_{\text{ВЫХ}} = \frac{U_{\text{ВЫХК}}}{U_{\text{ВЫХН}}} = \frac{n k_1^n}{k_p}. \quad (3.43)$$

When $k_1 \gg 1$, while $k_p \approx k_1^n$, $D_{\text{ВЫХ}} = n$.

The compression factor for amplifier voltage is

$$K_{\text{СЖ}} = \frac{D_{\text{ВХ}}}{D_{\text{ВЫХ}}} = \frac{k_1^{n-1} \cdot k_p}{n k_1^n}. \quad (3.44)$$

With the assumption made that the stages have linear characteristics up to saturation, the logarithmic amplitude characteristic of the amplifier will deviate from a precisely logarithmic characteristic. A precise LAC of an n-stage amplifier with successive signal detection can be obtained only with fully defined amplitude characteristics for the stages.

It is very difficult to find, analytically, the necessary form of the amplitude characteristic of a stage based on the given logarithmic amplitude characteristic of an amplifier. However, this can easily be done by the graphic-analytical method if the LAC of the amplifier is given $U_{\text{ВЫХ}} = f(U_{\text{ВХ}})$ and the number of stages n is known, as well as the amplification factor of each stage k_1 [32]. The values for voltages at amplifier output, at which all stages except the last operate in linear mode, are given.

The selected number of amplifier input voltage values will determine the number of points on the nonlinear section of the stage's amplitude characteristic.

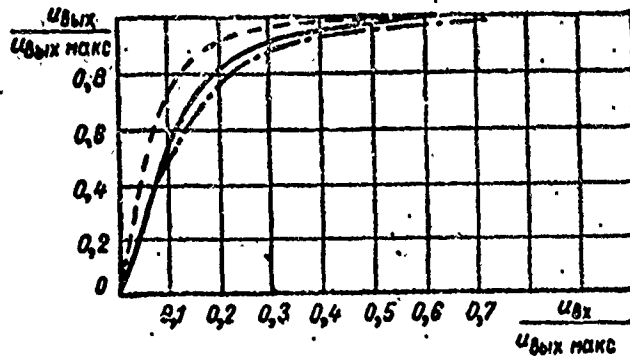


Fig. 3.6. Theoretical amplitude characteristics of a stage.
 - - - $k_1 = 10, n = 5$; — $k_1 = 5, n = 5$; -.-. $k_1 = 5, n = 4$.

Then for each voltage value at amplifier input the output voltage for the last n -th stage is

$$U_{\text{BWX}n} = f(U_{\text{BX}}) - \sum_{i=1}^{n-1} U_{\text{BWX}i}, \quad (3.45)$$

where $U_{\text{BWX}i}$ is the output voltage of the i -th stage which is equal to $U_{\text{BX}} \cdot k_1^i$.

Since all stages are identical, the nonlinear section calculated for the last stage is joined to the linear section of the amplitude characteristic of the next-to-last stage, at the moment it changes into nonlinear mode. With an increase in the values of voltage at amplifier input, the section thus constructed of the characteristic of the next-to-last stage is used for further calculation of the amplitude characteristic of the last stage. We should note that the nonlinear section of the amplitude characteristic of the stage plays an important role in forming the amplifier's LAC.

Figure 3.6 shows the stage characteristics calculated by this method for a logarithmic amplifier with successive signal detection at various values for n and k_1 . From this figure it is apparent that the form of the amplitude characteristic for this stage depends both on the number of stages in the amplifier and the amplification factor of the stage.

§ 3.2. PHASE DETECTOR

An important element in monopulse systems with phase and sum-difference angular detectors is the phase detector with whose aid the direction of target deviation from equisignal direction is determined.

Figure 3.7 presents the diagram of a vector-measuring phase detector which has $R_1 = R_2$ and $C_1 = C_2$.

The amplitude detector A_1 is fed the sum of voltages $u_1(t)$ and $u_2(t)$, and to detector A_2 is fed the difference of the voltages. In the case of sum-difference monopulse systems, $u_1(t)$ and $u_2(t)$ are, respectively, the standardized difference and sum voltages, while in the case of a phase system they are voltages from the linear i-f amplifier output. Voltages obtained as a result of detection are calculated by a special connection of the loads of the amplitude detectors A_1 and A_2 .

Considering amplitude detectors as devices which distinguish the envelope or the square of the envelope of the random input process, we can obtain the mathematical operations which are accomplished by a phase detector.

Voltages acting at phase detector inputs are written in the form

$$\left. \begin{aligned} u_1(t) &= U_1 \sin(\omega_{np}t + \varphi_1), \\ u_2(t) &= U_2 \sin(\omega_{np}t + \varphi_2). \end{aligned} \right\} \quad (3.46)$$

Figure 3.8 is the vector diagram of voltages which makes it possible to determine voltages which are detected by amplitude detectors A_1 and A_2 . These voltages, respectively, are equal to the vector sums

$$\begin{aligned}\vec{U}_+ &= \vec{U}_1 + \vec{U}_2, \\ \vec{U}_- &= -\vec{U}_1 + \vec{U}_2.\end{aligned}$$

(3.47)

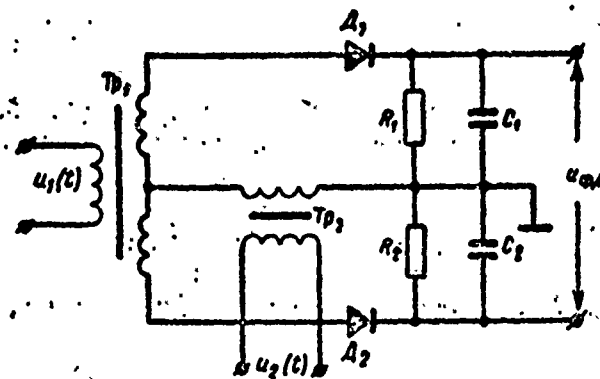


Fig. 3.7. Diagram of a vector measuring balance phase detector.

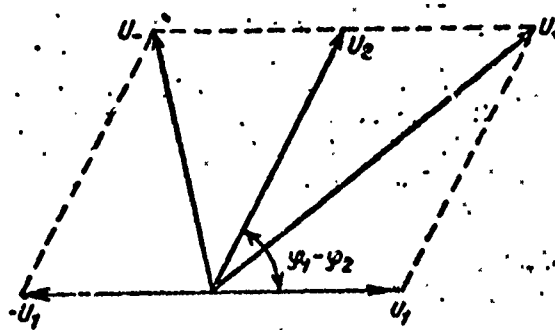


Fig. 3.8. Vector diagram of voltages for phase detector.

With linear characteristics of detectors, the output voltage of the phase detector will be

$$U_{\phi \kappa} = \kappa_{\phi \kappa} [|\vec{U}_+| - |\vec{U}_-|], \quad (3.48)$$

where $\kappa_{\phi \kappa}$ is the detection factor.

From the vector diagram (Fig. 3.8), it follows that

$$|\vec{U}_+| = \sqrt{U_1^2 + U_2^2 + 2U_1U_2 \cos(\varphi_1 - \varphi_2)}. \quad (3.49)$$

$$\begin{aligned} |\vec{U}_-| &= \sqrt{U_1^2 + U_2^2 + 2U_1U_2 \cos[180 - (\varphi_1 - \varphi_2)]} = \\ &= \sqrt{U_1^2 + U_2^2 - 2U_1U_2 \cos(\varphi_1 - \varphi_2)}. \end{aligned} \quad (3.50)$$

Consequently,

$$\begin{aligned} u_{\phi \kappa} &= \kappa_{\phi \kappa} \left[\sqrt{U_1^2 + U_2^2 + 2U_1U_2 \cos(\varphi_1 - \varphi_2)} - \right. \\ &\quad \left. - \sqrt{U_1^2 + U_2^2 - 2U_1U_2 \cos(\varphi_1 - \varphi_2)} \right]. \end{aligned} \quad (3.51)$$

If $U_1 \ll U_2$, which is valid for monopulse systems with a sum-difference angular discriminator, then, expanding each term of the expression (3.51) in a power series and limiting ourselves to two terms of the expansion, we obtain [26]

$$u_{\phi \kappa} = 2\kappa_{\phi \kappa} \frac{U_1U_2}{\sqrt{U_1^2 + U_2^2}} \cos(\varphi_1 - \varphi_2) = 2\kappa_{\phi \kappa} U_1 \cos(\varphi_1 - \varphi_2). \quad (3.52)$$

With equality of signal amplitudes $U_1 = U_2 = U$ (in the case of systems with a phase angular discriminator), voltage and phase detector output will have the form

$$\begin{aligned}
u_{\phi R} &= \kappa_{\phi R} (\sqrt{2U^2 [1 + \cos(\varphi_1 - \varphi_2)]} - \\
&- \sqrt{2U^2 [1 - \cos(\varphi_1 - \varphi_2)]}) = 2\kappa_{\phi R} U \left(\sqrt{\frac{1 + \cos(\varphi_1 - \varphi_2)}{2}} - \right. \\
&- \left. \sqrt{\frac{1 - \cos(\varphi_1 - \varphi_2)}{2}} \right) = 2\kappa_{\phi R} U \left[\cos \frac{(\varphi_1 - \varphi_2)}{2} - \right. \\
&- \left. \sin \frac{(\varphi_1 - \varphi_2)}{2} \right].
\end{aligned} \tag{3.53}$$

Figure 3.9 presents the dependence of output voltage on phase shift for the two examined cases. When $U_1 \ll U_2$ (or when $U_2 \ll U_1$), a cosinusoidal dependence of output voltage on phase difference is obtained and when $U_1 = U_2$ and variation in $(\phi_1 - \phi_2)$ is within 0 to π , this dependence is rectilinear.

With quadratic amplitude detectors A_1 and A_2 , the output voltage of the phase detector is proportional to the average value of the difference of currents passing through the diodes:

$$\begin{aligned}
u_{\phi R} &= \kappa_{\phi R} \{ [u_1(t) + u_2(t)]^2 - [u_1(t) - u_2(t)]^2 \} = \\
&= \kappa_{\phi R} u_1(t) u_2(t).
\end{aligned} \tag{3.54}$$

Substituting in (3.54) the values of $u_1(t)$ and $u_2(t)$ from (3.46), we obtain

$$\begin{aligned}
u_{\phi R} &= \kappa_{\phi R} U_1 U_2 \overline{\sin(\omega_{np}t - \varphi_1) \sin(\omega_{np}t + \varphi_2)} = \\
&= \frac{1}{2} \kappa_{\phi R} U_1 U_2 \cos(\varphi_1 - \varphi_2).
\end{aligned} \tag{3.55}$$

From expression (3.54) it is apparent that a phase detector with quadratic characteristics for diodes A_1 and A_2 is equivalent to a simple multiplier (when the highest harmonics ω_{np} are discarded) and the dependence of output voltage on phase shift has the form of a cosinusoid.

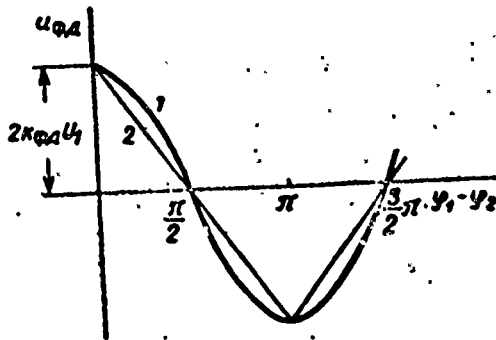


Fig. 3.9. Characteristics of a phase detector: 1 - when $U_1 \ll U_2$; 2 - when $U_1 = U_2$.

The disadvantage of this phase detector lies in the fact that it limits the range of approach angles to a quantity corresponding to a phase interval of 180° , whereas the maximum interval in single-value direction finding, determined by the angle-data transmitter, can frequently be greater than this value.

Another type of phase detector which makes it possible to broaden the range of approach angles is the Kirkpatrick phase detector [27, 41]. In this detector the angular range is broadened by decreasing sensitivity in the equisignal direction, which, however, slightly reduces measurement accuracy for angular coordinates since this sensitivity decrease is carried out at that point in the system where the signal level is greatest.

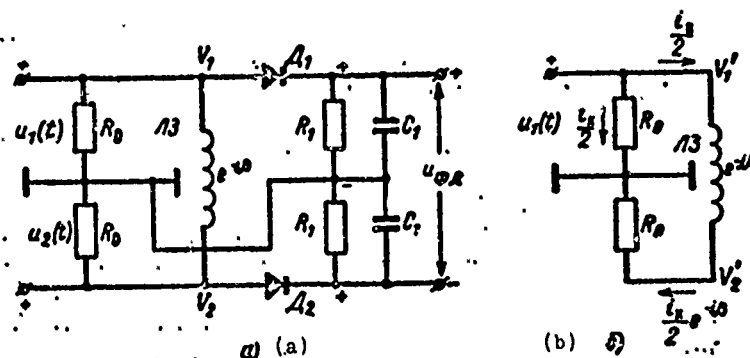


Fig. 3.10. The Kirkpatrick phase detector: a - simplified detector circuit; b - part of circuit illustrating the formation of voltages acting on diodes.

A diagram of the Kirkpatrick phase detector is presented in Fig. 3.10. From a comparison of diagrams presented in Figs. 3.7 and 3.10 it is apparent that the detecting part of the Kirkpatrick phase detector is precisely the same as in the usual phase detector and consists of two diodes and differentially connected loads. Both detectors have an output voltage which is formed by subtracting the voltages acting on the diode of the phase detector. However, although in the usual phase detector the sum and difference of input voltages act on the diodes, in the Kirkpatrick phase detector voltages which are a superposition of the components formed by each of the input voltages act on the diode.

Let us designate the voltages acting on diode inputs as V_1 and V_2 . Then voltage $u_1(t)$ forms the components V'_1 and V'_2 which act only at the points of the circuit indicated in Fig. 3.10b. Actually, current i_k , induced by the voltage $u_1(t)$, is fed to two parallel resistors, one of which is R_0 while the second is formed by the delay line loaded to wave impedance R_0 . Therefore, current i_k is divided evenly between these two resistors. As a result, the two components formed by voltage $u_1(t)$ will be

$$V'_1 = u_1(t) \text{ и } V'_2 = \ddot{u}_1(t) e^{-i\beta_0}.$$

[и = and]

Similarly, but in reverse order, the corresponding components of input voltage $u_2(t)$ are formed. Consequently, the output voltage of a Kirkpatrick phase detector in the case of linear diodes, which is a superposition of these components, will be

$$\begin{aligned} u_{\phi x} &= \kappa_{\phi x} \left[|u_1(t) + u_2(t) e^{-i\beta_0}| - |u_1(t) e^{-i\beta_0} + u_2(t)| \right] = \\ &= \kappa_{\phi x} \left[\sqrt{U_1^2 + U_2^2 + 2U_1U_2 \cos(\varphi_1 - \varphi_2 - \beta_0)} - \right. \\ &\quad \left. - \sqrt{U_1^2 + U_2^2 + 2U_1U_2 \cos(\varphi_1 - \varphi_2 + \beta_0)} \right] = \\ &= \kappa_{\phi x} \left[\sqrt{U_1^2 + U_2^2} \sqrt{1 + \frac{2U_1U_2}{U_1^2 + U_2^2} \cos(\varphi_1 - \varphi_2 - \beta_0)} - \right. \\ &\quad \left. - \sqrt{U_1^2 + U_2^2} \sqrt{1 + \frac{2U_1U_2}{U_1^2 + U_2^2} \cos(\varphi_1 - \varphi_2 + \beta_0)} \right]. \end{aligned} \tag{3.56}$$

For a system with a sum-difference angular discriminator ($U_1 \ll U_2$), expanding each term of expression (3.56) in a power series and using the first two terms, we obtain

$$\begin{aligned}
 u_{\phi \kappa} = \kappa_{\phi \kappa} & \left[\sqrt{U_1^2 + U_2^2} + \frac{U_1 U_2}{\sqrt{U_1^2 + U_2^2}} \cos(\varphi_1 - \varphi_2 - \beta_0) - \right. \\
 & \left. - \sqrt{U_1^2 + U_2^2} - \frac{U_1 U_2}{\sqrt{U_1^2 + U_2^2}} \cos(\varphi_1 - \varphi_2 + \beta_0) \right] \approx \\
 & \approx 2\kappa_{\phi \kappa} U_1 \sin(\varphi_1 - \varphi_2) \sin \beta_0.
 \end{aligned}
 \tag{3.57}$$

For a monopulse system with a phase angular discriminator ($U_1 = U_2 = U$) the output voltage of a Kirkpatrick detector will be

$$\begin{aligned}
 u_{\phi \kappa} = 2\kappa_{\phi \kappa} U & \left[\sqrt{\frac{1 + \cos(\varphi_1 - \varphi_2 - \beta_0)}{2}} - \right. \\
 & \left. - \sqrt{\frac{1 + \cos(\varphi_1 - \varphi_2 + \beta_0)}{2}} \right] = 4\kappa_{\phi \kappa} U \times \\
 & \times \sin \frac{\varphi_1 - \varphi_2}{2} \sin \frac{\beta_0}{2}.
 \end{aligned}
 \tag{3.58}$$

Figure 3.11 presents the characteristics of the output voltage of a Kirkpatrick detector. From a comparison of expressions (3.51) and (3.57), as well as (3.52) and (3.58) and of the presented characteristics, it is apparent that the output voltages of an ordinary phase detector and a Kirkpatrick detector, when $\beta_0 = \pi/2$, differ only by the $\pi/2$ shift, and the angular range of single-value direction finding is limited by the phase interval $-\pi/2 \ll \varphi_1 - \varphi_2 \gg \pi/2$. However, when $\beta_0 < \pi/2$, the angular range of the Kirkpatrick phase detector is broadened to 360° as β_0 approaches zero. As an example of broadening the angular range, Fig. 3.11 introduces the characteristic of output voltage for $\beta_0 = 0.1$; along with the substantial broadening of the angular range, steepness is severely reduced.

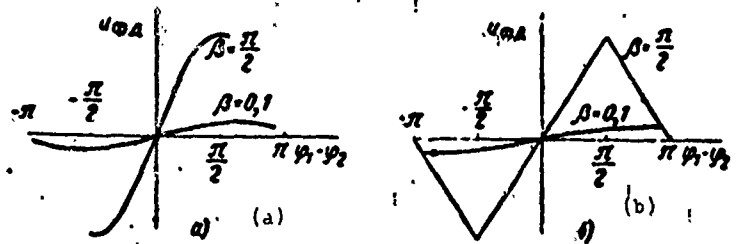


Fig. 3.11. Characteristics of the Kirkpatrick phase detector:
 a) when $U_1 \ll U_2$; b) when $U_1 = U_2$.

§ 3.3. SYSTEM OF AUTOMATIC AMPLIFICATION CONTROL

Most widely used in monopulse radar receivers is a pulse AGC system with feedback, illustrated in Fig. 3.12. Usually in such a system, delay voltage $U_{\text{зад}}$ is fed to the AGC detector, and because of this, amplification control begins when the signal exceeds quantity $U_{\text{зад}}$. An AGC system can be "amplified" or "unamplified" depending upon the presence or absence of an amplifier in the AGC circuit.

In amplified AGC systems amplification can be accomplished up to the AGC detector on alternating voltage (Fig. 3.12b) or after the AGC detector on direct current (Fig. 3.12c).

In contemporary monopulse radars, also frequently used are multiple-loop AGC systems with loops acting in parallel (Fig. 3.13). In these AGC systems, usually used as variable gain amplifiers are the first stages of the i-f amplifier, which ensures small nonlinear signal distortions in the i-f amplifier.

The main characteristics of the AGC system include the amplitude characteristic of the AGC circuit, the amplitude characteristic of the variable gain amplifier in the absence and in the presence of amplification control, and also its variable gain characteristic, [50].

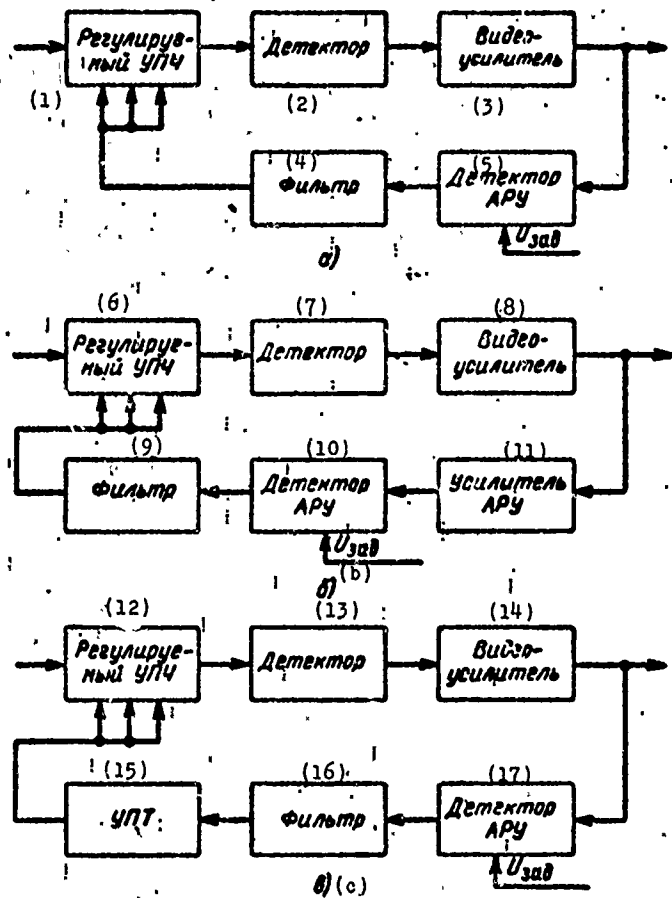


Fig. 3.12. Block diagram of pulse AGC system: a) "unamplified" AGC system; b) "amplified" AGC system with alternate voltage amplification; c) "amplified" AGC system with d-c amplification. KEY: (1) Variable gain i-f amplifier; (2) Detector; (3) Video amplifier; (4) Filter; (5) AGC detector; (6) Variable gain i-f amplifier; (7) Detector; (8) Video amplifier; (9) Filter; (10) AGC detector; (11) AGC amplifier; (12) Variable gain i-f amplifier; (13) Detector; (14) Video amplifier; (15) D-C amplifier; (16) Filter; (17) AGC detector.

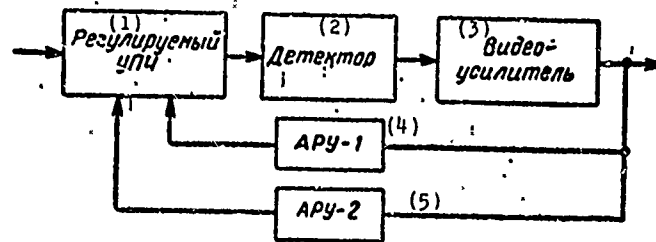
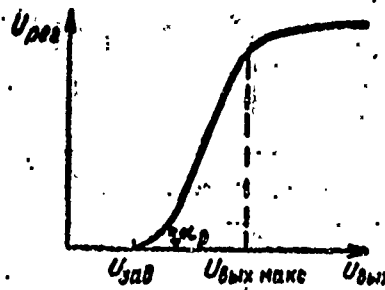


Fig. 3.13. Block diagram of a multiple-loop AGC system. KEY: (1) Variable gain i-f amplifier; (2) Detector; (3) Video amplifier; (4) AGC-1; (5) AGC-2.

Fig. 3.14. Amplitude characteristic of an AGC circuit.



The amplitude characteristic of an AGC circuit represents the dependence of the control voltage being fed to the variable gain amplifier on the amplitude of the signal at output of the variable gain amplifier $U_{\text{пер}} = f(U_{\text{вых}})$. The form of this dependence in the presence of delay voltage in the AGC system is presented in Fig. 3.14. Control voltage differs from zero when signal amplitude at amplifier output exceeds delay voltage. With a subsequent increase in $U_{\text{вых}}$ the working segment of the amplitude characteristic, with the proper choice of AGC circuit parameters, must be linear. The angle of slope to the axis of abscissas determines the amplification factor of the feedback circuit

$$\text{tg } \alpha_{\text{пер}} = K_{\text{обр}}$$

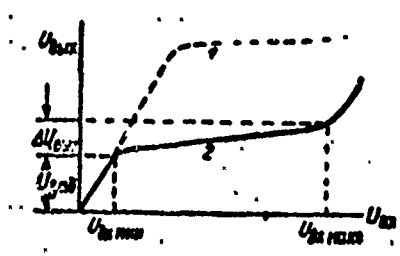


Fig. 3.15. Amplitude characteristics of amplifier: 1 - without AGC; 2 - with AGC.

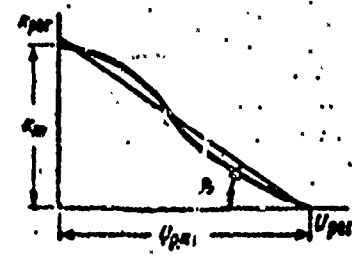


Fig. 3.16. Control characteristic of amplifier.

The amplitude characteristic of the variable gain i-f amplifier which determines the dependence of signal amplitude at amplifier output ($U_{\text{ВЫХ}}$) on signal amplitude at input ($U_{\text{ВХ}}$) with and without an AGC, is presented in Fig. 3.15.

The control characteristic of the amplifier determines the dependence of the amplification factor of the variable gain amplifier on control voltage:

$$K_{\text{пер}} = f(U_{\text{пер}}).$$

The form of this dependence is brought about by the anode-grid characteristics of the controlled tubes and the number of controlled stages. In view of the fact that usually there is a nonlinear dependence of tube steepness on bias, the control characteristic also has a nonlinear character, which appears, to a greater extent, when the number of controlled stages increases. However, in analyzing dynamic modes various approximations of the control characteristic are used: linear, exponential, polynomial, hyperbolic function, etc. The question of a rational approximation of the control characteristic must be solved individually in each case depending upon the study methods used.

In analytical calculations, it is usually considered linear since such an approach considerably simplifies analysis without leading to significant errors [26]. A typical form of control characteristic and its linear approximation are shown in Fig. 3.16.

Many works have been devoted to an analysis of AGC systems; they are examined thoroughly in reference [50]. However, we shall consider only the main dynamic properties of an AGC system with the introduction of a number of simplifying assumptions which, without distorting the essence of the phenomena, enable us to obtain more simply the necessary relationships.

We shall assume that there are no nonlinear distortions in the receiving device, and the bandwidth of the receiver is somewhat

wider than that of the AGC. We shall also assume that in the AGC circuit a single-section RC filter and an inertialess detector are used.

The behavior of an AGC system with a single-section filter can be described by the following system of equations [26]:

$$\begin{aligned}
 U_{\text{ВМХ}} &= \begin{cases} \kappa_m U_{\text{ВХ}} & \text{when } U_{\text{ВМХ}} < U_{\text{зад}}, \\ \kappa_{\text{рег}} U_{\text{ВХ}} & \text{when } U_{\text{ВМХ}} > U_{\text{зад}}. \end{cases} \\
 U_{\text{рег}} &= \kappa_{\text{обр}} F_A(p) (U_{\text{ВМХ}} - U_{\text{зад}}) \text{ при } U_{\text{ВМХ}} > U_{\text{зад}}, \quad (3.59)
 \end{aligned}$$

where κ_m is the maximum amplification factor of the amplifier when $U_{\text{рег}} = 0$;

$\kappa_{\text{обр}} = \kappa_{\text{д}} \kappa_{\text{А}}$ is the amplification factor of the feedback circuit, equal to the product of the transmission factors of the AGC amplifier and detector; $F(p) = \frac{1}{p T_A + 1}$ is the operator of the single-

section AGC filter;

T_A is the time constant of the AGC circuit.

With a linear approximation of the control characteristic

$$\kappa_{\text{рег}} = \kappa_m - b_A U_{\text{рег}}, \quad (3.60)$$

where $b_A = \text{tg } \phi_A = \frac{\kappa_m}{U_{\text{бм}}}$ is the angular coefficient of the control characteristic;

$U_{\text{бм}} = \frac{\kappa_m}{b_A}$ is voltage at which the receiver amplification factor reverts to zero.

With the introduction of approximation (3.60), system of equation (3.59) assumes the form

$$U_{\text{вых}} = \begin{cases} \kappa_m U_{\text{зад}} & \text{при } U_{\text{вых}} < U_{\text{зад}} \\ (\kappa_m - b_A U_{\text{рег}}) U_{\text{вых}} & \text{при } U_{\text{вых}} > U_{\text{зад}} \end{cases}$$

$$(pT_A + 1)U_{\text{рег}} = \kappa_{\text{обр}}(U_{\text{вых}} - U_{\text{зад}}) \text{ при } U_{\text{вых}} > U_{\text{зад}}.$$

(3.61)

(при = when)

We shall find the reaction of this system to a jump whose amplitude exceeds $U_{\text{вх мин}}$. When $U_{\text{вх}} = U_A = \text{const}$, system of equation (3.61) changes into a nonuniform linear differential equation of the first order with constant coefficients:

$$T_A \frac{dU_{\text{вых}}}{dt} + U_{\text{вых}}(1 + b_A \kappa_{\text{обр}} U_A) = b_A \kappa_{\text{обр}} U_A U_{\text{зад}} + \kappa_m U_A.$$

(3.62)

The solution to this equation has the form

$$U_{\text{вых}} = B_A + C_A e^{-\frac{t}{\tau_A}},$$

(3.63)

where B_A is the particular solution of the nonuniform equation, equal to

$$B_A = \frac{\kappa_m U_A + b_A \kappa_{\text{обр}} U_{\text{зад}}}{1 + \kappa_A},$$

(3.64)

τ_A is the length of the duration process, equal to

$$\tau_A = \frac{T_A}{1 + \kappa_s},$$

(3.65)

κ_s is the equivalent amplification factor of the AGC system, equal to

$$\kappa_s = b_A \kappa_{\text{обр}} U_A.$$

(3.66)

After prescribing the initial conditions, we shall find the integration constant C_A . Let us assume that at the initial moment when $t = 0$ voltage on the capacitor of the filter is zero. In this case, $U_{\text{пер}} = 0$ and $U_{\text{вых}} = k_m U_A$. Then the solution to equation (3.63) is written in the form

$$U_{\text{вых}} = U_A \left[\frac{b_A \kappa_{\text{обп}} U_{\text{зад}} + \kappa_m}{1 + \kappa_3} + \left(\kappa_m - \frac{b_A \kappa_{\text{обп}} U_{\text{зад}} + \kappa_m}{1 + \kappa_3} \right) e^{-\frac{t}{T_A}} \right]. \quad (3.67)$$

If we assume $U_{\text{зад}} = 0$, from equations (3.67) and (3.61) we find

$$U_{\text{вых}} = \kappa_m U_A \frac{1 + \kappa_3 e^{-\frac{t}{T_A}}}{1 + \kappa_3}, \quad (3.68)$$

$$U_{\text{пер}} = \frac{\kappa_m \kappa_{\text{обп}} U_A}{1 + \kappa_3} \left(1 - e^{-\frac{t}{T_A}} \right), \quad (3.69)$$

$$\kappa_{\text{пер}} = \kappa_m \frac{1 + \kappa_3 e^{-\frac{t}{T_A}}}{1 + \kappa_3}. \quad (3.70)$$

Calculated according to equations (3.68) and (3.69), the curves of input voltage and control voltage versus time are presented in Fig. 3.17.

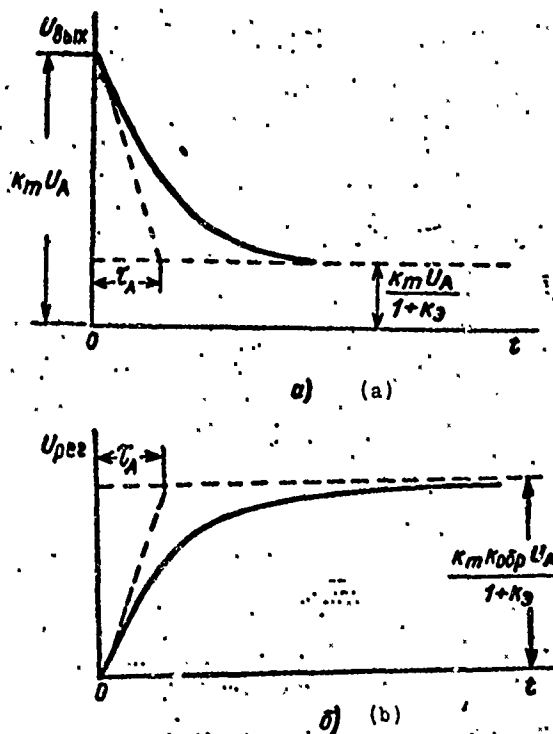
Output voltage when $t = 0$ grows abruptly to the quantity $\kappa_m U_A$, and then drops exponentially to a stable value $\frac{\kappa_m U_A}{1 + \kappa_3}$. Control voltage, on the other hand, grows exponentially to a stable value $\frac{\kappa_m \kappa_{\text{обп}} U_A}{1 + \kappa_3}$. The time of the transition process, in both cases, is identical and depends not only on the time constant of the AGC circuit

and the parameters of the AGC system (b_A and $k_{\text{одп}}$), but also on the amplitude of the jump U_A . As follows from equalities (3.65) and (3.66), with an increase in U_A the time of the transition process decreases and the fixing process proceeds more rapidly.

In conclusion, we shall study the works of an AGC system for an amplitude sum-difference monopulse radar, which makes it possible to ensure the independence of the error signal from the amplitudes of received signals, owing to the standardization of sum and difference signal amplitudes relative to the amplitude of the sum signal. A block diagram of one of the possible AGC circuits is presented in Fig. 3.18 [129].

The difference and sum signals are fed to the i-f amplifier from the converter. Each channel has its own AGC circuit. Automatic amplification control in each i-f amplifier is accomplished by feeding to its output short reference pulses of intermediate frequency, produced by a pulse oscillator whose amplitude varies in proportion to the necessary amplification. These pulses are fed with a time lead relative to the main pulse of the radar transmitter.

Fig. 3.17. Transition characteristics of an AGC system when the input signal acts intermittently.



The blocking oscillator generates signals which trigger the pulse oscillator. At the same time these signals are fed through the delay line to the modulator of the transmitter, which ensures the delay of the main pulse with respect to the reference pulses. Pulses from pulse oscillator output are fed to the two-stage i-f amplifier with variable amplification and then through the attenuator to the i-f amplifier of the sum and difference channels.

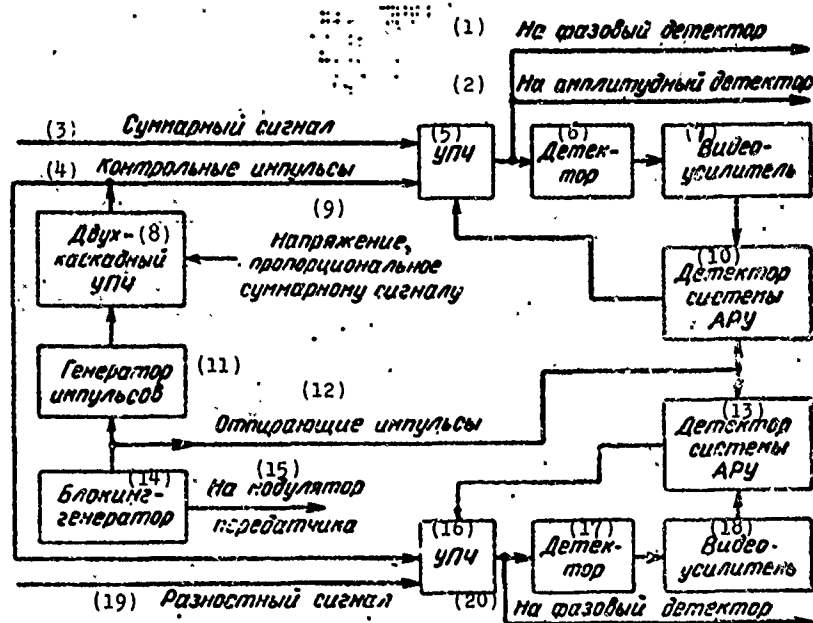


Fig. 3.18. Block diagram of an AGC system and an amplitude sum-difference monopulse radar.
 KEY: (1) Phase detector; (2) To amplitude detector; (3) Sum signal; (4) Reference pulses; (5) I-f amplifier; (6) Detector; (7) Video amplifier; (8) Two-stage i-f amplifier; (9) Voltage proportional to sum signal; (10) Detector of AGC system; (11) Pulse oscillator; (12) Trigger pulse; (13) Detector of AGC system; (14) Blocking oscillator; (15) To modulator transmitter; (16) I-f amplifier; (17) Detector; (18) Video amplifier; (19) Difference signal; (20) To phase detector.

Then the reference signals are detected by the detector and in the form of negative d-c voltage are removed from the filter to the grids of the tubes by the video amplifier. From video amplifier output voltage of negative polarity is fed to the grids of the tubes of the AGC system detectors. To these detectors, triggering pulses

from the blocking oscillator are also fed. To the cathodes of the tubes of the detectors, positive bias is fed and, therefore, only signals exceeding bias voltage are detected. The value of bias voltage (delay voltage) is controlled by cathode followers connected with detector tubes so that in the absence of echo signals the detectors maintain a constant noise level at the output of the i-f amplifier of the channels, i.e., act as noise limiters. When the automatic range tracking system picks up a target, to the two-stage i-f amplifier is fed positive voltage proportional to the sum signal, which causes amplification of the reference pulses. As a result, the AGC circuit accomplishes standardization of the sum and difference signals with respect to the amplitude of the sum signal and ensures an equality of the amplitudes of the referenced pulses fed to the i-f amplifier of the sum and difference channels, and, therefore, the amplification of the echos in these channels will be the same both when noise and echo are equal and when echo exceeds noise.

CHAPTER 4

RESOLUTION AND DIRECTION FINDING SENSITIVITY OF MONOPULSE RADARS WITH RESPECT TO ANGULAR COORDINATES

§ 4.1. THE CONCEPT OF ANGULAR COORDINATE RESOLUTION

By resolving power we mean the ability of a radar to distinguish separate targets in a group of targets with sufficient reliability. Quantitatively, angular coordinate resolution is evaluated by the minimum angle between directions to target at which it is still possible to measure separately the angular coordinates of targets which can not be resolved with respect to range and speed with the necessary accuracy.

It can be necessary to resolve many targets; however, we shall examine the resolution of only two targets as the simplest and most frequently encountered case.

As is apparent from the definition of resolution, the resolution process is indivisible from the detection process; therefore, in the simplest case, resolution is the detection of two signals corresponding to two targets. Hence, in the process of direction finding with a target pair, at receiver output there will be at least two signals, their resolution will depend upon the relative energy of the signals and the degree of their overlap with respect to the parameter being resolved, in this case, the angle. Obviously, the less overlap the greater the likelihood of tracking each target separately and the better the resolution of the radar.

Because of this, resolution can be judged based on the correlation function of the input signals carrying the corresponding information on the parameter involved. Obviously, resolution will be better the narrower the correlation function with respect to this parameter.

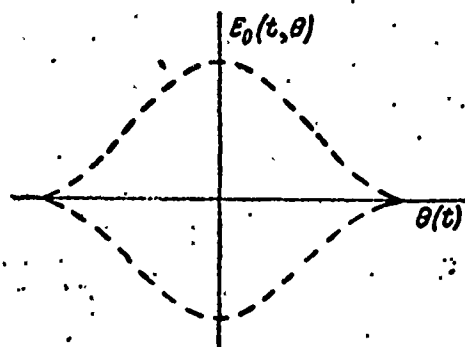


Fig. 4.1. Envelope of high-frequency signal received.

An analysis of angular coordinate resolution is easily performed with respect to the mode of space surveillance. We shall assume that the antenna of the radar system successively irradiates two point targets located at the same distance from the radar and spaced at an angle of $\Delta\theta$. Then, with respect to the case of interest, the autocorrelation function of the input signal in complex form can be written as

$$\dot{\Psi}(\Delta\theta) = \text{Re} \left[\int_0^T \dot{E}_0(t, \theta) \dot{E}_0^*(t, \theta + \Delta\theta) dt \right], \quad (4.1)$$

where $\dot{E}_0(t, \theta)$ is the input signal of the first target;
 $\dot{E}_0(t, \theta + \Delta\theta)$ is the input signal of the second target;
 $\theta, \theta + \Delta\theta$ are the angular coordinates of the target;
 T is the period of observation.

The input signals in this case are high-frequency signals with an envelope repeating the form of the radiation pattern (Fig. 4.1).

Obviously, with a single amplitude for signal sources

$$\dot{E}_e(t, \theta) = F(\theta) \exp(i\omega t), \quad (4.2)$$

$$\dot{E}_e^*(t, \theta + \Delta\theta) = F(\theta + \Delta\theta) \exp(-i\omega t), \quad (4.3)$$

where $F(\theta)$, $F(\theta + \Delta\theta)$ are the amplitude radiation patterns spaced at angle $\Delta\theta$.

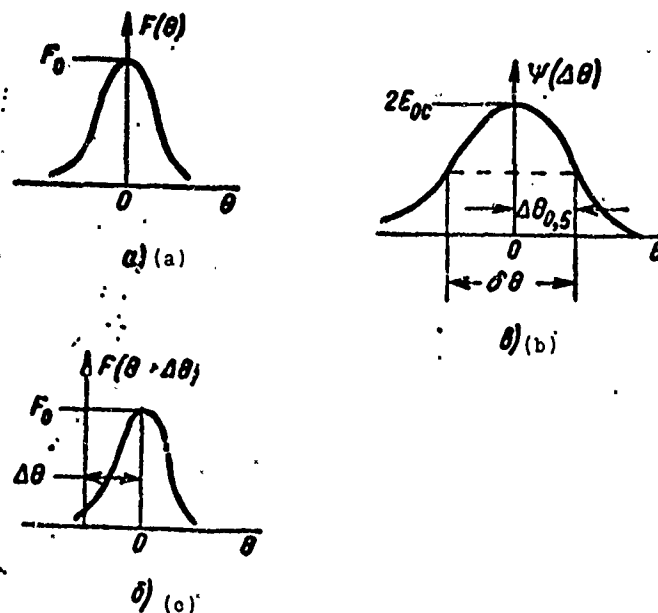


Fig. 4.2. Form of functions approximating radiation pattern. a) radiation pattern without angular displacements; b) radiation pattern with angular displacement by $\Delta\theta$; c) autocorrelation function of signal envelope.

An exponential factor characterizes the high-frequency signal filling. Substituting these values in (4.1) we obtain

$$\begin{aligned} \dot{\Psi}(\Delta\theta) &= \text{Re} \left[\int_0^T F(\theta) \exp(i\omega t) F(\theta + \Delta\theta) \exp(-i\omega t) d\theta \right] = \\ &= \int_0^T F(\theta) F(\theta + \Delta\theta) d\theta. \end{aligned} \quad (4.4)$$

When the form is bell-shaped, the radiation pattern (Fig. 4.2) is described by function

$$F(\theta) = \exp(-\gamma_0^2 \theta^2). \quad (4.5)$$

Then

$$F(\theta + \Delta\theta) = \exp[-\gamma_0^2 (\theta + \Delta\theta)^2]. \quad (4.6)$$

where γ_0 is the coefficient characterizing the width of the radiation pattern.

Substituting (4.5) and (4.6) into (4.4) and taking integration limits from $-\infty$ to ∞ , in accordance with the selected approximation of radiation pattern, we obtain

$$\begin{aligned} \Psi(\Delta\theta) &= \int_{-\infty}^{\infty} \exp(-\gamma_0^2 \theta^2) \exp[-\gamma_0^2 (\theta + \Delta\theta)^2] d\theta = \\ &= \exp(-\gamma_0^2 \Delta\theta^2) \int_{-\infty}^{\infty} \exp(-2\gamma_0^2 \theta^2 - 2\gamma_0^2 \Delta\theta\theta) d\theta. \end{aligned} \quad (4.7)$$

The unknown integral is a tabular integral in the form

$$\int_{-\infty}^{\infty} \exp(-p^2 x^2 - qx) dx = \exp \frac{\gamma_0^2 \Delta\theta^2}{2} \frac{\sqrt{\pi}}{\sqrt{2\gamma_0}}.$$

Substituting its value into (4.7), we obtain

$$\Psi(\Delta\theta) = \exp\left(-\frac{\gamma_0^2 \Delta\theta^2}{2}\right) \frac{\sqrt{\pi}}{\sqrt{2\gamma_0}}. \quad (4.8)$$

We can show that

$$\frac{\sqrt{\pi}}{\sqrt{2\gamma_0}} = 2E_{oc}$$

where E_{oc} is the energy of the high-frequency signal of the given form (Fig. 4.1).

Actually, if we take the time function $E_0(t)$ with a single amplitude and a bell-shaped envelope, then

$$\begin{aligned} E_{oc} &= \int_{-\infty}^{\infty} E_0^2(t) dt = \int_{-\infty}^{\infty} \exp(-2\gamma_0^2 t^2) \cos^2 \omega t dt = \\ &= \int_{-\infty}^{\infty} \exp(-2\gamma_0^2 t^2) \left(\frac{1}{2} + \frac{\cos 2\omega t}{2} \right) dt = \frac{\sqrt{\pi}}{2\sqrt{2}\gamma_0}. \end{aligned} \quad (4.9)$$

Hence it follows that

$$\Psi(\Delta\theta) = 2E_{oc} \exp\left(-\frac{\gamma_0^2 \Delta\theta^2}{2}\right). \quad (4.10)$$

The form of $\Psi(\Delta\theta)$ is shown in Fig. 4.2c.

Let us determine the width of the autocorrelation function, conditionally, at level 0.5 relative to maximum value. Substituting, for this purpose, the value of $\Psi(\Delta\theta) = E_{oc}$ into equation $\Delta\theta$ and solving it with respect to $\Delta\theta$, we obtain

$$\Delta\theta_{0.5} = \frac{1.17}{\gamma_0}. \quad (4.11)$$

Hence the width of the autocorrelation function at level 0.5 is

$$\delta\theta = 2 |\Delta\theta_{0.5}| = \frac{2.34}{\gamma_0}. \quad (4.12)$$

Let us express coefficient γ_0 through the width of the radiation pattern with respect to level 0.5 in accordance with the approximation made (4.5).

Obviously, when $|F(\theta)| = 0.5$ $\theta = \theta_{0.5}/2$. Taking this into account and solving equation (4.5) with respect to γ_0 , we find

$$\gamma_0 = 1.66/\theta_{0.5} \quad (4.13)$$

Hence

$$\delta\theta = \frac{2.34}{1.66} \theta_{0.5} = 1.40 \theta_{0.5} \quad (4.14)$$

A direct relationship has been obtained between the width of the autocorrelation function of signals received and the width of the radiation pattern. Since the width of the radiation pattern determines angular resolution, the width of the autocorrelation function also characterizes angular resolution and can be used in the approximate evaluation of a radar's resolution.

Expression (4.14) confirms the obvious conclusion that in order to improve angular resolution we must attempt to narrow the radiation pattern. Hence the dependence of signal strength on approach angle is the same during the operation of a radar on both scanning and tracking modes; the conclusions obtained are valid also for an automatic tracking radar.

We should note that resolution is characterized by the defined value only when signal energy substantially exceeds receiver noise energy. When this condition is not fulfilled, the value of the angle of resolution depends upon the signal/noise ratio and is characterized by the probability of both correct detection and false alarms.

However, in practice, for the value of potential resolution we use the width of the autocorrelation function of the signals of the target being resolved, read at a level of 0.5 from maximum. The probability approach to evaluating resolution is lost; however, this method is convenient because it is simple and easy to visualize.

The actual resolution of the radar can be considerably worse than its potential value because of energy loss and signal shape distortion in various units of the station. Therefore, the actual

value of angular resolution can be represented in the form

$$\delta\theta = \delta\theta_{\text{NOT}} + \sum_i \delta\theta_i = \gamma_\theta \delta\theta_{\text{NOT}} \quad (4.15)$$

where $\delta\theta_{\text{NOT}}$ is the value of potential angular resolution;

$\delta\theta_i$ is the additional impairment of angular resolution in the i -th element of the station;

γ_θ is the resolution impairment factor, equal to $1 + \frac{\sum \delta\theta_i}{\delta\theta_{\text{NOT}}}$.

Let us evaluate the resolution of monopulse radars and compare it to the resolution of single-channel radars with conical beam scanning.

§ 4.2. ANGULAR RESOLUTION OF MONOPULSE RADARS

4.2.1. An amplitude sum-difference monopulse system of direction finding in one plane. In this case, signals reflected from two point targets (Fig. 4.3) for the first and second receiving channels can be represented in complex form as

$$\dot{E}_1(t, \theta) = E_{m_1} F(\theta_0 - \theta_1) \exp i\omega t + E_{m_2} F(\theta_0 - \theta_2) \exp i(\omega t + \alpha). \quad (4.16)$$

$$\dot{E}_2(t, \theta) = E_{m_1} F(\theta_0 + \theta_1) \exp i\omega t + E_{m_2} F(\theta_0 + \theta_2) \exp i(\omega t + \alpha), \quad (4.17)$$

where $F(\theta_0 - \theta)$ and $F(\theta_0 + \theta)$ are the characteristics of antenna directivity for the corresponding receiving channels;

θ_0 is the value of the maximum deviation angle of the radiation pattern from equisignal direction;

$\theta_{1,2}$ are the angular positions of the first and second signal source relative to equisignal direction (Fig. 4.3);

$E_{m1,2}$ is the amplitude of the reflected signals from the first and second targets;

α is the phase shift caused by the difference in distances to targets.

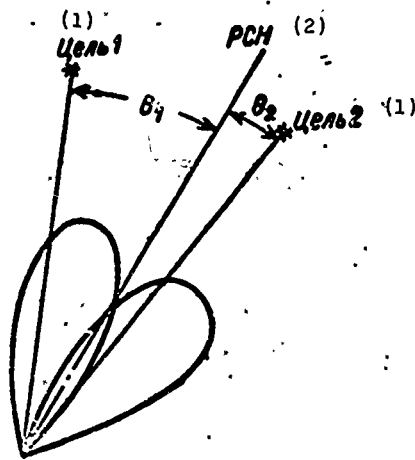


Fig. 4.3. Angles during direction finding of two point targets.
KEY: (1) Target; (2) ESD.

With sum-difference signal processing, at the input of the sum and difference channel we obtain

$$\begin{aligned} \dot{E}_c(t, \theta) = & \frac{E_{m1}}{\sqrt{2}} [F(\theta_0 - \theta_1) + F(\theta_0 + \theta_1)] \exp i \omega t + \\ & + \frac{E_{m2}}{\sqrt{2}} [F(\theta_0 - \theta_2) + F(\theta_0 + \theta_2)] \exp i(\omega t + \alpha), \end{aligned} \quad (4.18)$$

$$\begin{aligned} \dot{E}_p(t, \theta) = & \frac{E_{m1}}{\sqrt{2}} [F(\theta_0 - \theta_1) - F(\theta_0 + \theta_1)] \exp i \omega t + \\ & + \frac{E_{m2}}{\sqrt{2}} [F(\theta_0 - \theta_2) - F(\theta_0 + \theta_2)] \exp i(\omega t + \alpha). \end{aligned} \quad (4.19)$$

At the output of receiving channels with identical characteristics, we get the following with accuracy up to the constant coefficient;

$$\begin{aligned} \dot{u}_c(t, \theta) = & \frac{E_{m1}}{\sqrt{2}} [F(\theta_0 - \theta_1) + F(\theta_0 + \theta_1)] \exp i \omega_{np} t + \\ & + \frac{E_{m2}}{\sqrt{2}} [F(\theta_0 - \theta_2) + F(\theta_0 + \theta_2)] \exp i(\omega_{np} t + \alpha); \end{aligned} \quad (4.20)$$

$$\begin{aligned} \dot{u}_p(t, \theta) = & \frac{E_{m1}}{\sqrt{2}} [F(\theta_0 - \theta_1) - F(\theta_0 + \theta_1)] \exp i \omega_{np} t + \\ & + \frac{E_{m2}}{\sqrt{2}} [F(\theta_0 - \theta_2) - F(\theta_0 + \theta_2)] \exp i(\omega_{np} t + \alpha). \end{aligned} \quad (4.21)$$

At the output of a phase detector of the multiplying type, taking into account the amplitude standardization of the signal with the aid of a fast-acting AGC system and the averaging of the signal, error signal can be determined by expression

$$S(\theta) = \frac{\operatorname{Re} \dot{u}_c(t, \theta) \dot{u}_p^*(t, \theta)}{u_c(t, \theta) u_c^*(t, \theta)} \quad (4.22)$$

Substituting (4.20) and (4.21) into (4.22), after transformation we obtain

$$S(\theta) = \frac{E_{m1}^2 W_1 + 2E_{m1} E_{m2} (W_2 - W_3) + E_{m2}^2 W_4}{E_{m1}^2 W_5 + 2E_{m1} E_{m2} W_6 + E_{m2}^2 W_7} \quad (4.23)$$

where

$$\begin{aligned} W_1 &= F^2(\theta_0 - \theta_1) - F^2(\theta_0 + \theta_1), \\ W_2 &= F(\theta_0 - \theta_1) F(\theta_0 - \theta_2) \cos \alpha, \\ W_3 &= F(\theta_0 + \theta_1) F(\theta_0 + \theta_2) \cos \alpha, \\ W_4 &= F^2(\theta_0 - \theta_2) - F^2(\theta_0 + \theta_2), \\ W_5 &= [F(\theta_0 - \theta_1) + F(\theta_0 + \theta_1)]^2, \\ W_6 &= [F(\theta_0 - \theta_1) + F(\theta_0 + \theta_1)] [F(\theta_0 - \theta_2) + \\ &\quad + F(\theta_0 + \theta_2)] \cos \alpha, \\ W_7 &= [F(\theta_0 - \theta_2) + F(\theta_0 + \theta_2)]^2. \end{aligned}$$

In actual conditions, phase shift α changes rather rapidly with time even when the mutual displacement of target is small and the AGC system has a certain time delay with respect to these changes. Due to this, the low-frequency filter at phase detector output and in the AGC circuit filters all signal components formed by the terms of expression (4.23) containing $\cos \alpha$. This enables us to represent the direction finding characteristic, when there are two targets in the beam, in simplified form:

$$S_s(\theta) = \frac{[F^2(\theta_0 - \theta_1) - F^2(\theta_0 + \theta_1)] + a^2 [F^2(\theta_0 - \theta_2) - F^2(\theta_0 + \theta_2)]}{[F(\theta_0 - \theta_1) + F(\theta_0 + \theta_1)]^2 + a^2 [F(\theta_0 - \theta_2) + F(\theta_0 + \theta_2)]^2} \quad (4.24)$$

where $a = E_{m2}/E_{m1}$.

By equating the numerator of expression (4.24) to zero, we can find the condition for direction finding of two point targets. It is easy to see that, in this case, the radar will track from the power center of the sources and the equisignal direction will be nearer the direction to the source whose power is greater.

Of greatest interest is the case where one of the targets, for example, target number 1, is located at a small angle $\theta_1 = \Delta\theta$ to equisignal direction, which corresponds to the condition of target resolution.

In this case,

$$F(\theta_0 \pm \theta_1) \approx F(\theta_0) \mp \Delta\theta \left. \frac{dF(\theta_0 \pm \theta_1)}{d\theta_1} \right|_{\theta_1=\theta_0} = F(\theta_0) (1 \mp \mu \Delta\theta), \quad (4.25)$$

where μ is the direction finding sensitivity corresponding to the steepness of the linear part of the direction finding characteristic when a single target is involved in the direction finding, and is equal to

$$\mu = \frac{1}{F(\theta_0)} \left. \frac{dF(\theta_0 \pm \theta_1)}{d\theta_1} \right|_{\theta_1=\theta_0} \quad (4.26)$$

Substituting (4.25) into (4.24), we obtain after elementary transformations

$$S(\theta) = \frac{\mu \Delta\theta + a^2 \frac{F^2(\theta_0 - \theta_2) - F^2(\theta_0 + \theta_2)}{4F^2(\theta_0)}}{1 + a^2 \left[\frac{F(\theta_0 - \theta_2) + F(\theta_0 + \theta_2)}{2F(\theta_0)} \right]^2} \quad (4.27)$$

Since target resolution sets in at angular distances exceeding the radiation pattern width and angular direction finding errors for the resolved target, under normal conditions, do not exceed one tenth of the radiation pattern width, we can assume $\theta_2 \gg \Delta\theta$.

When these conditions are fulfilled, function $F(\theta_0 \pm \theta_2)$ in the first approximation can be considered independent of $\Delta\theta$. Then the value of the direction finding sensitivity at the operating point can be represented by the following expression:

$$\mu' = \left. \frac{dS(\theta)}{d\Delta\theta} \right|_{\Delta\theta=0} = \frac{\mu}{1 + \left[a \frac{F(\theta_0 - \theta_2) + F(\theta_0 + \theta_2)}{2F(\theta_0)} \right]^2} \quad (4.28)$$

hence it follows that

$$\frac{\mu - \mu'}{\mu'} = a^2 \left[\frac{F(\theta_0 - \theta_2) + F(\theta_0 + \theta_2)}{2F(\theta_0)} \right]^2 \quad (4.29)$$

Formula (4.29) makes it possible to evaluate the change in direction finding sensitivity due to the effect of an interfering target located at an angle θ_2 to the target being worked.

Equating $S(\theta)$ to zero, we can find the value of direction finding error

$$\mu\Delta\theta + a^2 \frac{F^2(\theta_0 - \theta_2) - F^2(\theta_0 + \theta_2)}{4F^2(\theta_0)} = 0; \quad (4.30)$$

hence

$$\Delta\theta = - \frac{a^2}{\mu} \frac{F^2(\theta_0 - \theta_2) - F^2(\theta_0 + \theta_2)}{4F^2(\theta_0)} \quad (4.31)$$

The expressions obtained (4.29) and (4.31) show that the effect of the second target is expressed in the change in direction finding sensitivity and the appearance of direction finding error for the selected target. Using these expressions, we can determine conditions for target resolutions.

Figure 4.4 presents a standardized curves of $\delta\theta_a$, $\delta\mu_a$, calculated according to formula (4.29) and (4.31) with an approximation of the antenna radiation patterns by function

$$F(\theta) = \frac{1}{2} \frac{\sin \kappa \frac{1}{2} d_n \theta}{\kappa \frac{1}{2} d_n \theta} \quad (4.32)$$

where d_n is the diameter of the antenna paraboloid.

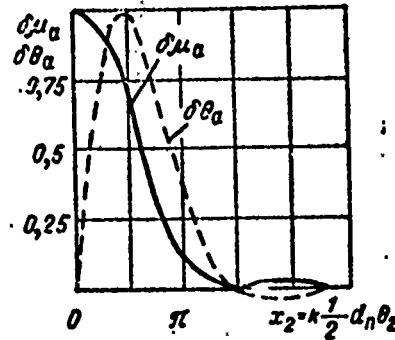


Fig. 4.4. Variation and direction finding sensitivity $\delta\mu_a$ and angular direction finding error $\delta\theta_a$ of an amplitude sum-difference monopulse radar because of interfering target.

The tilt angle of the beam θ_0 is determined from equation

$$\kappa \frac{1}{2} d_n \theta_0 = \frac{1}{2} \pi. \quad (4.33)$$

On the figure we assume the following standardization of relationships:

$$\delta\theta_a = \frac{\Delta\theta}{a^2 \kappa \frac{1}{2} d_n}, \quad (4.34)$$

$$\delta\mu_a = \frac{\mu - \mu'}{\mu'} \frac{1}{a^2}. \quad (4.35)$$

With the approximation used, the radiation pattern width with respect to the 3 dB level is equal to $\theta_{0.5} = \lambda/d_n$ and $\theta_0 = \theta_{0.5}/2$.

From Figure 4.4 it is apparent that with an increase in angle θ_2 the standardized direction finding sensitivity drops and reaches zero when

$$x_2 = \frac{\pi}{2} d_n \theta_2 = \frac{3\pi}{2}, \dots$$

which corresponds to $\theta_2 = 1.5 \theta_{0.5}$. When $x_2 = \pi/2$ ($\theta_2 = \theta_0$) the direction finding error is maximum and when $a = 1$, it reaches $\Delta\theta = 0.6 \theta_0$, which corresponds to an error equal, approximately, to the half-width of the angle between signal sources. Subsequent increase in θ_2 leads to a decrease in direction finding error to zero when $\theta_2 = 1.5 \theta_{0.5}$. Hence it follows that full target resolution in this case occurs when their angular separation is approximately $1.5 \theta_{0.5}$. This is near the condition for target resolution which takes into account the width of the autocorrelation function.

Naturally, if we select a less rigid criterion for resolution the requirements for target spacing are accordingly reduced.

4.2.2. A phase sum-difference monopulse system of direction finding in one plane. In this case, signals reflected from two point targets, received by the antennas of the first and second receiving channels, can be represented by the following expressions:

$$\dot{E}_1(t, \theta) = E_{m1} F(\theta_1) \exp i \omega t + E_{m2} F(\theta_2) \exp i (\omega t + \alpha), \quad (4.36)$$

$$\begin{aligned} \dot{E}_2(t, \theta) = & E_{m1} F(\theta_1) \exp i (\omega t + \varphi_1) + \\ & + E_{m2} F(\theta_2) \exp i (\omega t + \alpha + \varphi_2), \end{aligned} \quad (4.37)$$

where $F(\theta_1)$ and $F(\theta_2)$ are the amplification factors of the antennas in the direction to signal source;

ϕ_1 and ϕ_2 are the phase shifts of the signals, caused by angular errors in finding their sources, and equal to $\phi_{1,2} = k l \sin \theta_{1,2}$;

α is the phase shift of the signal, caused by target separation with respect to range.

With sum-difference processing, at the input of the sum and difference channels we obtain

$$\begin{aligned} \dot{E}_c(t, \theta) &= \frac{E_{m1}}{\sqrt{2}} F(\theta_1) [\exp i(\omega t + \varphi_1) + \exp i\omega t] + \\ &+ \frac{E_{m2}}{\sqrt{2}} F(\theta_2) [\exp i(\omega t + \alpha + \varphi_2) + \exp i(\omega t + \alpha)]; \end{aligned} \quad (4.38)$$

$$\begin{aligned} \dot{E}_p(t, \theta) &= \frac{E_{m1}}{\sqrt{2}} F(\theta_1) [\exp i(\omega t + \varphi_1) - \exp i\omega t] + \\ &+ \frac{E_{m2}}{\sqrt{2}} F(\theta_2) [\exp i(\omega t + \alpha + \varphi_2) - \exp i(\omega t + \alpha)]. \end{aligned} \quad (4.39)$$

At the output of receiving channels identical in characteristics, we get the following with accuracy up to the constant coefficient;

$$\begin{aligned} \dot{u}_c(t, \theta) &= \frac{E_{m1}}{\sqrt{2}} \{F(\theta_1) [\exp i(\omega_{np}t + \varphi_1) + \exp i\omega_{np}t] + \\ &+ aF(\theta_2) [\exp i(\omega_{np}t + \alpha + \varphi_2) + \exp i(\omega_{np}t + \alpha)]\}; \end{aligned} \quad (4.40)$$

$$\begin{aligned} \dot{u}_p(t, \theta) &= \frac{E_{m1}}{\sqrt{2}} \{F(\theta_1) [\exp i(\omega_{np}t + \varphi_1) - \exp i\omega_{np}t] + \\ &+ aF(\theta_2) [\exp i(\omega_{np}t + \alpha + \varphi_2) - \exp i(\omega_{np}t + \alpha)]\}. \end{aligned} \quad (4.41)$$

At the output of the multiplying-type detector, taking into account signal standardization with respect to sum-signal and additional phase shift of difference signal by 90° , the error signal can be determined by expression

$$\begin{aligned} S(\theta) &= \frac{\operatorname{Re} \dot{u}_c(t, \theta) \dot{u}_p^*(t, \theta) \exp i \frac{\pi}{2}}{\dot{u}_c(t, \theta) \dot{u}_c^*(t, \theta)} = \\ &= \frac{F^2(\theta_1) \sin \varphi_1 + a^2 F^2(\theta_2) \sin \varphi_2 - aF(\theta_1) F(\theta_2) [\sin(\alpha - \varphi_1) - \dots]}{F^2(\theta_1) + a^2 F^2(\theta_2) + F^2(\theta_1) \cos \varphi_1 + a^2 F^2(\theta_2) \cos \varphi_2 +} \\ &\dots \frac{- \sin(\alpha + \varphi_2)}{aF(\theta_1) F(\theta_2) [\cos(\alpha + \varphi_2 - \varphi_1) + \cos \alpha + \cos(\alpha + \varphi_2) + \cos(\alpha - \varphi_1)]} \end{aligned} \quad (4.42)$$

Phase shift α in actual conditions, changes rapidly and we can assume that the oscillation phases, which can be produced by the variations, of the error signal are fully filtered in the direction finding system. Then the expression (4.42) can be simplified by excluding components depending upon α :

$$S(\theta) = \frac{F^2(\theta_1) \sin \varphi_1 + a^2 F^2(\theta_2) \sin \varphi_2}{F^2(\theta_1) + a^2 F^2(\theta_2) + F^2(\theta_1) \cos \varphi_1 + a^2 F^2(\theta_2) \cos \varphi_2} \quad (4.43)$$

If target No. 1 is located at a small angle $\Delta\theta$ to equisignal direction, then $\theta_1 = \Delta\theta$, $F(\theta_1) \approx F(0)$ and $\sin \theta_1 = \Delta\theta$. Hence it follows that

$$S(\theta) = \frac{\left[\sin(\kappa l \Delta\theta) + a^2 \frac{F^2(\theta_2)}{F^2(0)} \sin(\kappa l \sin \theta_2) \right]}{1 + a^2 \frac{F^2(\theta_2)}{F^2(0)} + \cos(\kappa l \Delta\theta) + a^2 \frac{F^2(\theta_2)}{F^2(0)} \cos(\kappa l \sin \theta_2)} \quad (4.44)$$

For the area of interest to us $\theta_2 \gg \Delta\theta$ and functions $f(\theta_2)$ in the first approximation can be assumed independent of $\Delta\theta$. Therefore, the steepness of the direction finding characteristic at the working point can be calculated, approximately, according to formula

$$\begin{aligned} \mu' &= \left. \frac{dS(\theta)}{d\Delta\theta} \right|_{\Delta\theta=0} = \frac{\kappa l}{2 + a^2 \frac{F^2(\theta_2)}{F^2(0)} [1 + \cos(\kappa l \sin \theta_2)]} \\ &= 2 \left[1 + a^2 \frac{F^2(\theta_2)}{F^2(0)} \cos^2 \frac{\kappa l \sin \theta_2}{2} \right] \end{aligned} \quad (4.45)$$

With direction finding of a single source $a = 0$ and $\mu = \kappa l / 2$, which corresponds to standard direction finding sensitivity of a phase sum-difference monopulse system.

Solving equation (4.45) with respect to μ and μ' , we can find the formula which makes it possible to evaluate the change in the

direction finding characteristic of the system in the presence of an interfering signal source, in the form

$$\delta\mu_\phi = \frac{\mu - \mu'}{\mu' a^2} = \frac{F^2(\theta_2)}{F^2(0)} \cos^2(\kappa l \sin \theta_2). \quad (4.46)$$

Equating (4.44) to zero, we find the condition of direction finding in the presence of an interfering target:

$$\sin(\kappa l \Delta\theta) + a^2 \frac{F^2(\theta_2)}{F^2(0)} \sin^2(\kappa l \sin \theta_2) = 0$$

At small values of $\Delta\theta$ $\sin \kappa l \Delta\theta \approx \kappa l \Delta\theta$. Hence it follows that

$$|\delta\theta_\phi| = \frac{\Delta\theta}{a^2/\kappa l} = \frac{F^2(\theta_2)}{F^2(0)} \sin(\kappa l \sin \theta_2). \quad (4.47)$$

Figure 4.5 illustrates the dependence of the direction finding characteristic and the angular errors of a phase sum-difference monopulse system, designed according to formula (4.46) and (4.47) [55].

In the calculations, the radiation pattern was approximated by function

$$F(\theta) = \frac{1}{2} \frac{\sin \kappa \frac{l}{2} \theta}{\kappa \frac{l}{2} \theta}. \quad (4.48)$$

To simplify comparison, the dimensions of amplitude and the phase-type radar antennas were assumed identical and equal to $d_n = 2l$.

A comparison of calculated data presented in Figs. 4.4 and 4.5 shows that radar of the amplitude type is somewhat more sensitive to the presence of an interfering signal from a neighboring target

located within the main lobe of the sum directivity characteristic than a phase-type radar. If the interfering target lies beyond the main lobe of the sum radiation pattern, then a phase-type radar is more sensitive to interfering targets.

Analysis of the resolution of monopulse radars of the sum-difference type was carried out for the reception mode. If the radar is operating on reception and transmission, the amplitudes of the reflective signals E_{m1} and E_{m2} will be proportional to the corresponding radiation patterns on transmission. This should be taken into account when determining the direction finding characteristic $S(\theta)$ and the quantities $\Delta\theta$ and μ' .

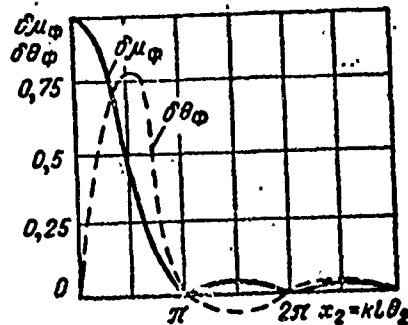


Fig. 4.5. Variation in direction finding sensitivity $\delta\mu_\phi$ and angular direction finding error $\delta\theta_\phi$ in a phase sum-difference monopulse radar because of an interfering ϕ target.

For simplification in analysis, it was assumed that one of the targets was located at a small angle relative to equisignal direction. In this case, when this condition is not fulfilled, analysis is complicated and it is simpler in determining radar resolution to go to graphics plotting the resulting direction finding characteristic at various angles between targets, given by certain approximations of radiation patterns.

As is apparent from equation (4.24), determining the direction finding characteristic are the sums of the difference and sum patterns

with respect to each of the signal sources, taken with a weight factor equal to the ratio of the powers of reflected signals from corresponding sources. Plotting the sum and difference patterns in corresponding scale (one on tracing paper, the other on a drawing grid) and summing them with various values of angular target separation, according to the expression determining the direction finding characteristic, we can, in each case of interest to us, plot graphically the resulting direction finding characteristic and, based on its behavior, determine the moment of target resolution.

The graphic method is convenient because of its immediate visibility and comparative simplicity. Below we shall examine the result of graphic analysis of radar resolution for various types of radars amplitude monopulse, with dual switching, with conical scanning and sequential switching of radiation patterns [102]. Partial patterns of the radars examined, presented in Fig. 4.6, were approximated in the region of the main lobe by function $\cos^2 56.25\theta$, where θ is the displacement angle in degrees. The width of the radiation pattern at the 3 dB level, with the approximation used, was 1.2° . In the analysis, the equality of amplitude for signals from targets ($a = 1$) was assumed.

Figure 4.7 presents standardized resulting direction finding characteristics of a monopulse radar with the reception of signals from a dual target for three values of angular target separation. In the figure it is apparent that with an angular separation of 1° , the radar does not differentiate the targets. In this case, the shape of the direction finding characteristic is typical for the case of a single target. The presence of the second target in the beam is manifested only by a certain dip in the direction finding characteristic in the equisignal direction.

With an angular separation of 1.1° there is a break in the direction finding characteristic in the region of the middle zero point, which points to the presence of two targets in the irradiation zone. However, in the region of the direction to each target, the steepness of the direction finding characteristic is low, which does

not provide the possibility of reliable tracking and determination of precise target coordinates. Only when $\psi_H = 1.6^\circ$ are there formed in the direction finding characteristic two stable points with high steepness; the monopulse radar fully distinguishes two targets and can reliably track either of them, giving accurate angular coordinates. Therefore, the angle at 1.6° , which is equal to $1.33\theta_{0.5}$, in the examined case, can be taken for the target resolution angle.

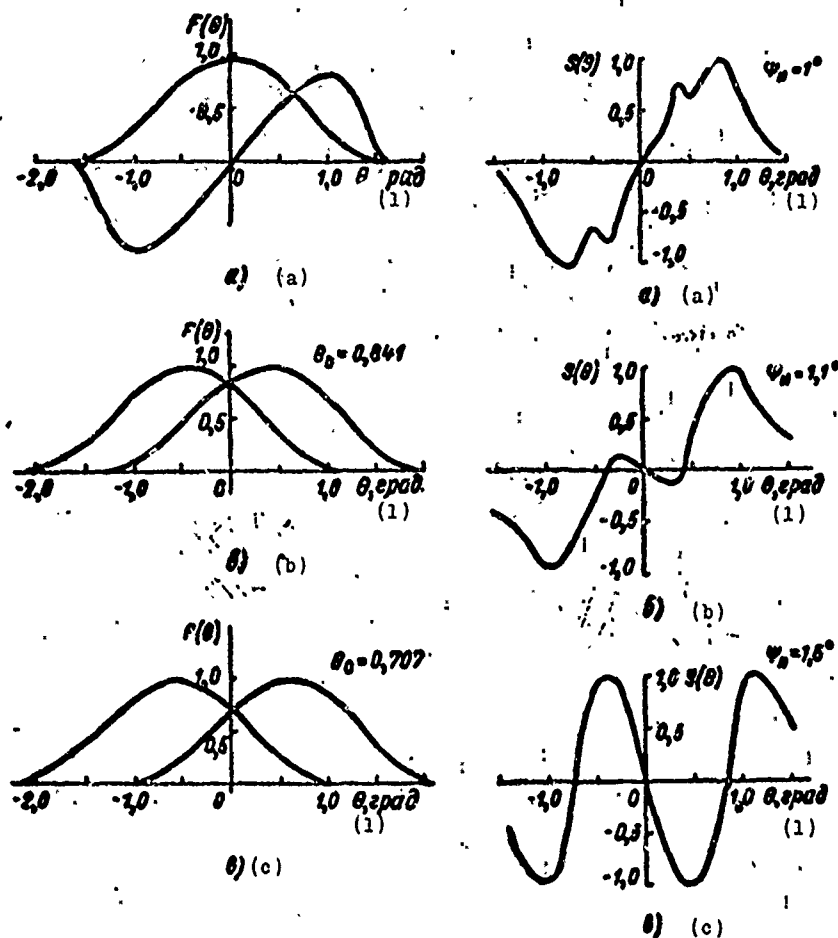


Fig. 4.6. Radiati pattern for compared coordinate system: a) a monopulse system and a system with dual switching of antenna radiation patterns; b) a system with conical beam scanning; c) a system with sequential switching of antenna radiation patterns.

Fig. 4.7. Standardized direction finding characteristics of a monopulse system with direction finding of a paired target for three values of target visibility angles ψ_H .
KEY: (1) 1.0 θ , deg.

A similar method of determining resolution was used with respect to systems with dual and sequential switching of antenna radiation patterns, and also systems with conical beam scanning. Direction finding characteristics for these systems are similar and are presented in Fig. 4.8. From the figure it is apparent that with angular target separation of 1.5° (upper curve) neither of the systems resolves the targets. In this case, all systems indicate the presence of one target instead of two.

With angular separation of 1.6° (middle curve) the direction finding characteristic of all three systems has its zero-steepness area at the origin of coordinates. This case can become similar to the case of single target direction finding for a radar station with a large region of insensitivity. When angular target separation is 1.7° , the direction finding characteristic indicates the presence of more than one target, but target separation is still insufficient for the separate tracking of either target.

The shape of direction finding characteristic for the radars studied, with full target resolution, is indicated in Fig. 4.9. Comparative resolution data for the stations studied are presented in Table 4.1.

In the table $\psi_{\text{н кр}}$ is the minimum angular target separation at which resolution of the targets occurs and the possibility is provided for separate tracking with errors not exceeding permissible quantities. The last column of the table contains data on angles of resolution, standardized with respect to radiation diagram width based on a level of half power.

From the data presented it is apparent that between a monopulse system and a system with dual switching of radiation patterns, there is little difference in resolution (less than 10%).

As for radars with conical scanning and sequential switching of patterns, they are inferior to the above systems, with respect to resolution, by approximately 30%.

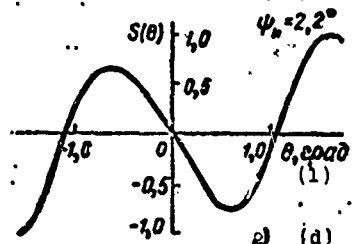
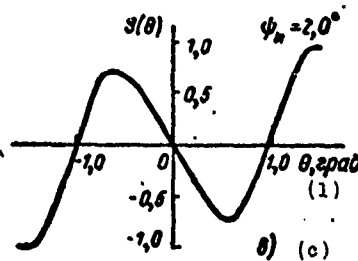
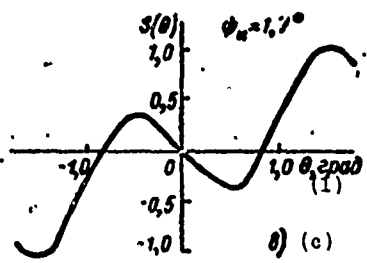
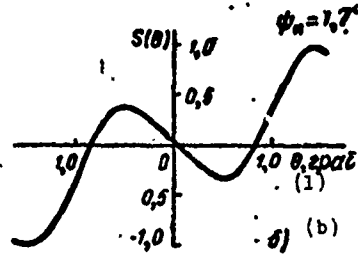
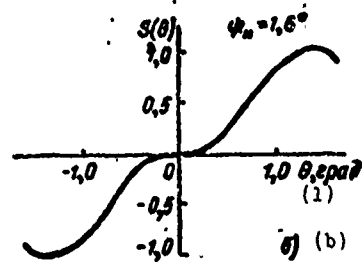
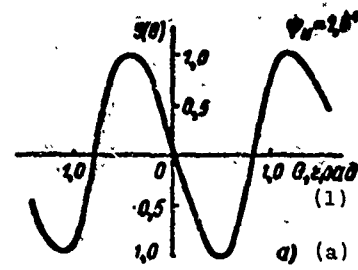
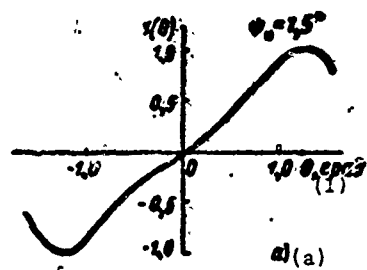


Fig. 4.8.

Fig. 4.9.

Fig. 4.8. Standardized direction finding characteristics of systems with dual switching of radiation patterns, with conical scanning and with sequential switching of the antenna radiation pattern during direction finding of paired targets for three values of target visibility angle ψ_n .

Fig. 4.9. Standardized direction finding characteristics containing minimum angular distances between targets, at which accurate tracking of either target is ensured: a) monopulse systems; b) system with dual switching of radiation patterns; c) system with conical scanning; d) system with sequential switching of antenna radiation patterns.
KEY: (1) 1.0 θ , deg.

Table 4.1.

(1) Тип РЛС	$\Phi_{\text{н}} - \Phi_{\text{д}}$	$\Phi_{\text{нр}}/\theta_{\text{с}}$
(2) Моноимпульсная	1,6	1,3
(3) С парным переключением диаграмм направленности	1,7	1,4
(4) С коническим сканированием	2,0	1,7
(5) С последовательным переключением диаграмм	2,2	1,8

KEY: (1) Type of radar; (2) Monopulse; (3) With dual switching of radiation pattern; (4) With conical scanning; (5) With sequential switching of patterns.

As a result of formula (4.24), it has been shown that the phase shifts of reflective signals can be disregarded on the basis that they give comparatively high-frequency components in error signals and are filtered at detector output.

In addition to phase changes, under actual conditions there will also be changes in reflected signal amplitudes due to the geometric differences in the targets and the fluctuation in the amount of effective reflecting surface. Amplitude ratios substantially affect the moment of target resolution. Since amplitude signal ratios, under actual conditions, are subject to random fluctuations, the evaluation of a radar's resolution, when operating on group targets, is generally a complex problem, and a radar's resolution, even for two targets, can be expressed only in the form of a probability.

Figure 4.10 presents the density distribution of direction probability for systems of tracking on each of two targets with different distances between them, expressed in fractions of radiation pattern width and taking into account the actual fluctuations in signal amplitude [19]. These data indicate that it is possible to distinguish two targets if they are separated by a distance corresponding to 0.85 of the width of the antenna radiation pattern. This agrees approximately with the moment of initial target resolution, obtained by the above described method, when during the equality of reflected

signals the presence of two targets can be determined; however, it is not possible as yet to perform accurate individual tracking of them due to the small steepness in the direction finding characteristics at the working points.

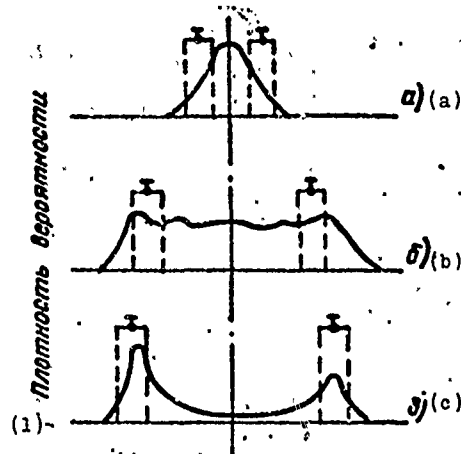


Fig. 4.10. Distribution of antenna direction probability during the tracking of two targets with different angular distances: a) $\psi_{\text{н}} = 0.3 \theta_{0.5}$; b) $\psi_{\text{н}} = 0.75 \theta_{0.5}$; c) $\psi_{\text{н}} = 0.85 \theta_{0.5}$.

KEY: (1) Probability density.

The side lobes of the radiation pattern impair angular resolution and can be the reason for the appearance of false targets.

§ 4.3. DIRECTION FINDING SENSITIVITY OF MONOPULSE RADARS

The direction finding sensitivity, by which we mean the steepness of the direction finding characteristic at the working point, is along with resolution, an important characteristic of a radar.

Figure 4.11 shows standardized direction finding characteristics during the operation of radars of various types on point targets, obtained by calculation [102]. In the calculations it was assumed that the direction finding systems have identical radiation patterns and equal signal-noise ratios for their receivers.

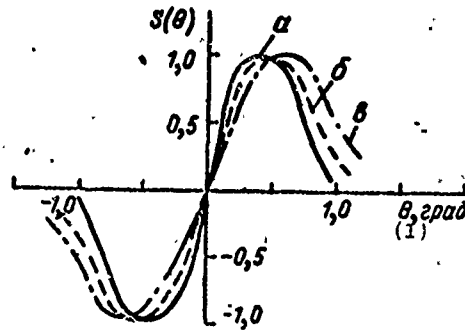


Fig. 4.11. Standardized direction finding characteristics of radars during the direction finding of a point source: a) monopulse systems; b) system with sequential and dual switching of antenna patterns; c) system with conical scanning.
KEY: (1) deg.

Table 4.2.

(1) Тип РЛС	(2) Крутизна, 1/град	(3) Нормированная крутизна
(4) Монопультсная суммарно-разностная	4,6	1
(5) С последовательным переключением диаграмм направленности	3,3	0,72
(6) С парным переключением диаграмм	3,1	0,67
(7) С коническим сканированием	2,7	0,59

KEY: (1) Type of radar; (2) Steepness, 1/deg; (3) Standardized steepness; (4) Monopulse sum-difference; (5) With sequential switching of radiation patterns; (6) With dual switching of patterns; (7) With conical scanning.

Comparative data on direction finding sensitivity of the selected systems for low signal/noise ratios are presented in Table 4.2. Steepness is standardized with respect to the amount of steepness of an amplitude monopulse system of the sum-difference type.

The data in the table show that a monopulse system with the comparatively low signal/noise ratios assumed possesses the highest direction finding sensitivity, approximately doubling the direction finding sensitivity of a radar with conical scanning. A similar conclusion was reached by Fellbrant [53].

Since the accuracy of direction finding, when we take into account the effect of the internal receiver noises (see Chapter 5), is inversely proportional to the steepness of the direction finding characteristic, a monopulse system, under these conditions, provides higher accuracy.

Under the conditions of a strong signal, when the signal/noise ratio is sufficiently high and answers the requirements for satisfactory operation of the target tracking system, there is no noticeable difference in direction finding sensitivity between monopulse radars and the systems examined.

Table 4.3.

(2) Тип углового дискриминатора	(1) Кривизна характеристик для трех методов пеленгации		
	(3) амплитудной	(4) фазовой	(5) комплексной
Амплитудный (6)	μ_a	μ_ϕ	μ_a
Фазовый (7)	μ_a	μ_ϕ	μ_ϕ
Суммарно-разностный (8)	$0,5\mu_a$	$0,5\mu_\phi$	$0,5\mu_a$ $0,5\mu_\phi$

KEY: (1) Steepness of characteristics for three methods of direction finding; (2) Type of angular discriminator; (3) amplitude; (4) phase; (5) complex; (6) Amplitude; (7) Phase; (8) Sum-difference.

Table 4.3 presents comparative data on the direction finding sensitivity of monopulse radars of various types [45]. It is apparent from the table that monopulse radars of the sum-difference type regardless of the direction finding method used, have half as much direction finding sensitivity as monopulse radars of other types. However, the latter is not evidence of less direction finding accuracy in sum-difference monopulse systems since a whole series of other important factors determining accuracy are not being taken into account.

Table 4.3 uses the following designations:

$$\mu_{\theta} = \left. \frac{dS(\theta)}{d\theta} \right|_{\theta=0}$$
$$\mu_{\phi} = \left. \frac{dS(\varphi)}{d\varphi} \right|_{\Delta\varphi=0}$$

We should keep in mind that the above indices of direction finding sensitivity and angular resolution cannot be assumed a completely sufficient basis for the selection of the best system. In addition to the parameters indicated, when selecting the type of coordinates system, it is necessary to take into account also range sensitivity, design complexity, noise protection with respect to natural and artificial noises, tactical operating conditions, and a number of other parameters.

§ 4.4. METHODS OF IMPROVING ANGULAR RESOLUTION IN MONOPULSE RADARS

The need to increase angular resolution arises when group targets are involved and also when countermeasures are being used by the enemy such as the dropping of chaff and decoys, which considerably confuse the aerial situation. Such a requirement also arises when working with low-flying targets where a mirror reflection of signals from earth begins to occur.

A well known method of increasing angular resolution is to decrease the λ/d ratio by using shorter waves and antennas with large aperture dimensions. However, this method is not always applicable since it requires that the size and weight of antenna systems be increased. Therefore, recently considerable attention has been given to the development of schematic methods of solving the problem of improving angular resolution in a radar and, in this respect, monopulse radars have definite advantages over other types of direction finding systems.

Monopulse systems not only have high angular resolution as compared with single-channel systems, but also, under certain conditions make it possible to accomplish the resolution of targets located within the antenna beam. This possibility is brought about by the use in monopulse radars of multichannel reception, making it possible to obtain additional target information.

As we know, the nonresolution of targets with respect to angular coordinates can appear in two ways. When the signals reflected from the targets are identical in level, the equisignal direction of the radar will be set in the direction of a point located midway between the targets. If low-frequency fluctuation of reflected signals occur and at times a stronger signal arrives from one target, the equisignal direction will be shifted in accordance with the changes in signal level from one target to the other. In both cases, the radar cannot properly indicate the location of the target; therefore, the flight of aircraft in groups is considered one of the countermeasures against the guidance systems of guided rockets with radar homing heads [103].

Since, under actual conditions, the reflected signal fluctuates, one of the methods for schematic solution to the target resolution problem for a group target is based on angle gating [103].

4.4.1. Methods for increasing resolution, based on angle gating. The essence of this method lies in desensitizing the angular-measurement servosystem with respect to error signals arising at the instant a stronger signal arrives from another direction, and tracking only the chosen target.

The gating principle can be used since the fluctuations of signals reflected from targets lead to rapid changes in error signals. Error variation during the tracking of a single target is a slower process; therefore, a certain threshold of angular information performance can be established in the system so that it will not respond to error signals from other targets which exceed this threshold. A block diagram of one of the versions of a multiple system, which

uses this principle of target resolution in a group, is presented in Fig. 4.12. Used in the system is a lens antenna with four horn feeds and two transmitters working on spaced frequencies or on one frequency but with a time shift.

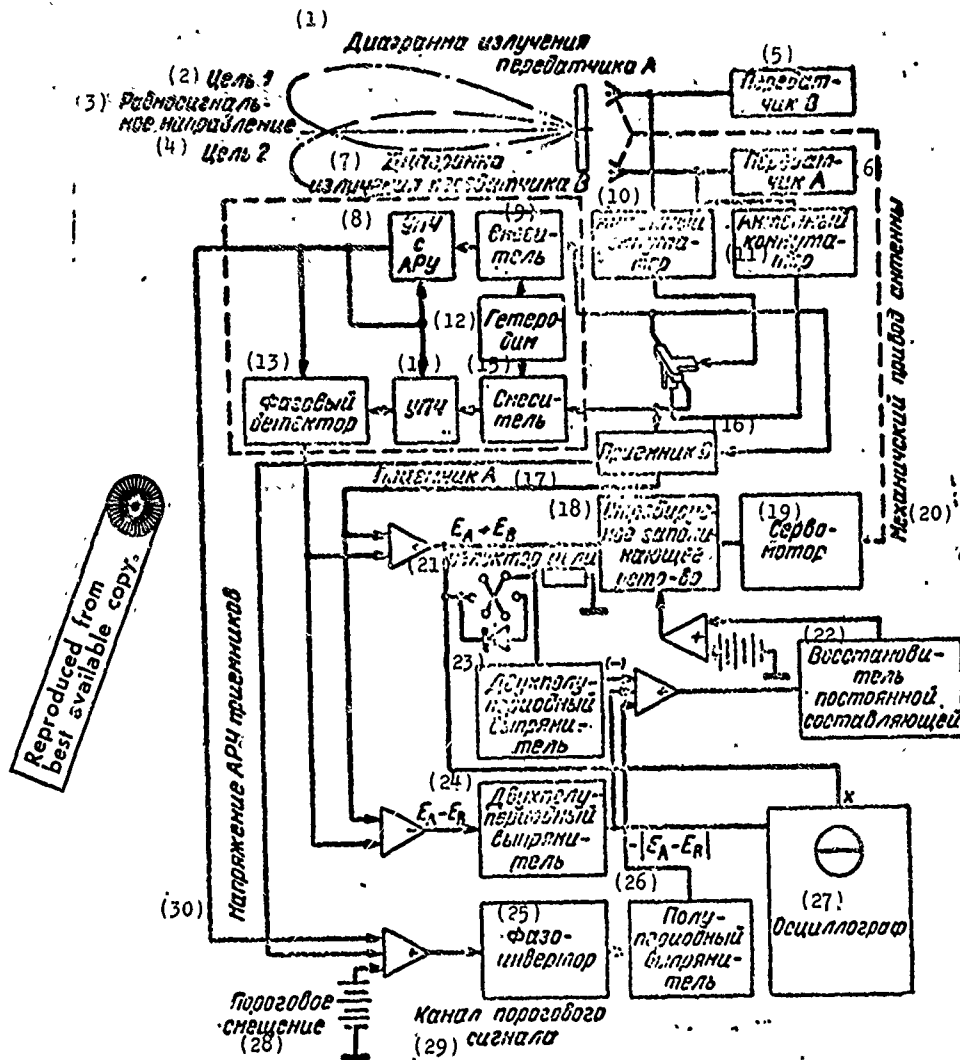


Fig. 4.12. Block diagram of a monopulse radar with high resolution.
 KEY: (1) Radiation pattern of transmitter A; (2) Target 1; (3) Equisignal direction; (4) Target 2; (5) Transmitter B; (6) Transmitter A; (7) Radiation pattern of transmitter B; (8) I-f amplifier with AGC; (9) Mixer; (10) Antenna switch; (11) Antenna switch; (12) Heterodyne; (13) Phase detector; (14) I-f amplifier; (15) Mixer; (16) Receiver B; (17) Receiver A; (18) Gated storage device; (19) Servomotor; (20) Mechanical antenna drive; (21) Target selector; (22) D-C restorer; (23) Full-wave rectifier; (24) Full-wave rectifier; (25) Phase inverter; (26) Wave rectifier; (27) Oscillograph; (28) Threshold bias; (29) Threshold signal channel; (30) Direction AGC receiver.

We should note that the frequency spacing of the transmitters must not be too great since the reflecting ability of a target depends upon frequency and this can affect the logic communication between error signals. In this respect, it is better to use transmitters on the same frequency but operating with a time shift. Thus, one transmitter can be used instead of two. A disadvantage of the method of time spacing of signals is the complication of target distance measurement since, in this case, additional ambiguity is introduced.

Thanks to frequency of time shift of transmitter signals, two independent error signal voltages are formed in the receiving system, each of which contains information on the location of the group target.

For simplicity let us examine a system of direction finding in one plane. As is apparent from the figure, the antenna radiation pattern consists of two separate patterns displaced equal angles relative to the antenna axis and formed by two feeds, each of which is excited by a separate transmitter (A or B). The presence of two separate patterns makes it possible to irradiate targets on different sides of the equisignal direction by signals from different transmitters. This ensures that additional information will be obtained on target position with the reception of reflected signals.

Two separate receivers are provided for the reception and corresponding processing of reflected signals. The receivers are similar in design; therefore, in the figure one of them is presented in greater detail (receiver A).

Signals from antenna output, through the send-receive switch are fed to the double balance bridge where sum-difference processing occurs, typical for amplitude sum-difference monopulse systems.

At input of the corresponding receivers are formed sum and difference signals which then are converted with respect to frequency, amplified in the i-f amplifier, standardized with the AGC system for a sum signal, and compared in the phase detector. Signals obtained at the output of each receiver are fed to common adding and subtracting devices and used for target selection.

To clarify the principle on which target resolution is based, let us examine analytically the processing of signals during direction finding of single and paired targets. We shall assume that one transmitter is used but radiation along independent channels is spaced in time. In this case, during the irradiation of a target by the upper antenna radiation pattern (pattern A), the signals received from the target at antenna channel output can be expressed as

$$\dot{E}_{1A}(t, \theta) = E_{m_A} F^2(\theta_0 - \theta) \exp i \omega t, \quad (4.49)$$

$$\dot{E}_{2A}(t, \theta) = E_{m_A} F(\theta_0 + \theta) F(\theta_0 - \theta) \exp i \omega t. \quad (4.50)$$

Hence, at the sum-difference processor output, with an accuracy up to the constant coefficient, we obtain

$$\begin{aligned} \dot{E}_{cA}(t, \theta) &= \dot{E}_{1A}(t, \theta) + \dot{E}_{2A}(t, \theta) = \\ &= E_{m_A} F(\theta_0 - \theta) [F(\theta_0 - \theta) + F(\theta_0 + \theta)] \exp i \omega t, \end{aligned} \quad (4.51)$$

$$\begin{aligned} \dot{E}_{pA}(t, \theta) &= \dot{E}_{1A}(t, \theta) - \dot{E}_{2A}(t, \theta) = \\ &= E_{m_A} F(\theta_0 - \theta) [F(\theta_0 - \theta) - F(\theta_0 + \theta)] \exp i \omega t. \end{aligned} \quad (4.52)$$

With identical channels and a conversion factor of one in the phase detector, error signal at receiver A output assumes the form

$$\begin{aligned} S_A(\theta) &= \frac{\operatorname{Re} \dot{E}_{cA}(t, \theta) \dot{E}_{pA}^*(t, \theta)}{\dot{E}_{cA}(t, \theta) \dot{E}_{cA}^*(t, \theta)} = \\ &= \frac{F(\theta_0 - \theta) - F(\theta_0 + \theta)}{F(\theta_0 - \theta) + F(\theta_0 + \theta)}. \end{aligned} \quad (4.53)$$

Similarly, we can obtain corresponding expressions for the case when the target is irradiated by the lower radiation pattern (pattern B):

$$\dot{E}_{1B}(t, \theta) = E_{mB}(\theta_0 + \theta) F(\theta_0 - \theta) \exp i(\omega t + \varphi), \quad (4.54)$$

$$\dot{E}_{2B}(t, \theta) = E_{mB} F^2(\theta_0 + \theta) \exp i(\omega t + \varphi), \quad (4.55)$$

$$\dot{E}_{cB}(t, \theta) = E_{mB} F(\theta_0 + \theta) [F(\theta_0 - \theta) + F(\theta_0 + \theta)] \exp i(\omega t + \varphi), \quad (4.56)$$

$$\begin{aligned} \dot{E}_{pB}(t, \theta) &= E_{mB} F(\theta_0 + \theta) [F(\theta_0 - \theta) - \\ &\quad - F(\theta_0 + \theta)] \exp i(\omega t + \varphi), \end{aligned} \quad (4.57)$$

$$\begin{aligned} S_B(\theta) &= \frac{\operatorname{Re} \dot{E}_{cB}(t, \theta) \dot{E}_{pB}^*(t, \theta)}{\dot{E}_{cB}(t, \theta) \dot{E}_{cB}^*(t, \theta)} = \\ &= \frac{F(\theta_0 - \theta) - F(\theta_0 + \theta)}{F(\theta_0 - \theta) + F(\theta_0 + \theta)}. \end{aligned} \quad (4.58)$$

As a result we obtain

$$S_A(\theta) = S_B(\theta),$$

hence

$$\Delta S(\theta) = S_A(\theta) - S_B(\theta) = 0. \quad (4.59)$$

Thus, when a single target is in the direction finding zone, at output of the monopulse system under study a zero difference signal is obtained, irregardless of target position relative to equisignal direction. This means that equality $\Delta S(\theta) = 0$ can serve as the criterion for the presence of only one target. Such a target can be found by the usual method, either using receiver A or receiver B.

With two or more targets in the unresolved volume equality $\Delta S(\theta) = 0$ becomes unfulfillable. We see this in the example of direction finding on two targets unresolved with respect to direction. Let us assume that the targets are identical in reflecting abilities.

If the targets are not too far apart, then, as experience shows, the direction finding system will track the power center which agrees, because of the equality of the reflected signals, with the geometric center of the targets and equality $|\theta_1| = |\theta_2| = |\theta|$ will be fulfilled where θ_1 and θ_2 are the displacement angles of the first and second targets with respect to equisignal direction. In this case, when targets are irradiated through the upper (A) and lower (B) patterns, at receiver channel output we obtain, respectively,

$$\begin{aligned} \dot{E}_{1A}(t, \theta) = E_m [F^2(\theta_0 - \theta) \exp i\omega t + \\ + F^2(\theta_0 + \theta) \exp i(\omega t + \varphi)], \end{aligned} \quad (4.60)$$

$$\begin{aligned} \dot{E}_{2A}(t, \theta) = E_m F(\theta_0 - \theta) F(\theta_0 + \\ + \theta) [\exp i\omega t + \exp i(\omega t + \varphi)], \end{aligned} \quad (4.61)$$

$$\dot{E}_{1B}(t, \theta) = E_m F(\theta_0 - \theta) F(\theta_0 + \theta) [\exp i\omega t + \exp i(\omega t + \varphi)], \quad (4.62)$$

$$\begin{aligned} \dot{E}_{2B}(t, \theta) = E_m [F^2(\theta_0 + \theta) \exp i\omega t + \\ + F^2(\theta_0 - \theta) \exp i(\omega t + \varphi)]. \end{aligned} \quad (4.63)$$

Accordingly, at output of the sum and difference channels (with accuracy up to the constant coefficient) we obtain

$$\begin{aligned} \dot{E}_{cA}(t, \theta) = E_m F_c [F(\theta_0 - \theta) \exp i\omega t + \\ + F(\theta_0 + \theta) \exp i(\omega t + \varphi)], \end{aligned} \quad (4.64)$$

$$\begin{aligned} \dot{E}_{pA}(t, \theta) = E_m F_p [F(\theta_0 - \theta) \exp i\omega t - \\ - F(\theta_0 + \theta) \exp i(\omega t + \varphi)], \end{aligned} \quad (4.65)$$

$$\begin{aligned} \dot{E}_{c_B}(t, \theta) = E_m F_c [F(\theta_0 + \theta) \exp i \omega t + \\ + F(\theta_0 - \theta) \exp i(\omega t + \varphi)], \end{aligned} \quad (4.66)$$

$$\begin{aligned} \dot{E}_{p_B}(t, \theta) = E_m F_p [F(\theta_0 + \theta) \exp i \omega t - \\ - F(\theta_0 - \theta) \exp i(\omega t + \varphi)], \end{aligned} \quad (4.67)$$

where

$$F_c = F(\theta_0 - \theta) + F(\theta_0 + \theta),$$

$$F_p = F(\theta_0 - \theta) - F(\theta_0 + \theta).$$

Error signals at output of receiver A and B, after elementary transformation, will be written as

$$S_A(\theta) = \frac{[F(\theta_0 - \theta) - F(\theta_0 + \theta)]^2}{F^2(\theta_0 - \theta) + 2F(\theta_0 - \theta)F(\theta_0 + \theta) \cos \varphi + F^2(\theta_0 + \theta)}, \quad (4.68)$$

$$S_B(\theta) = - \frac{[F(\theta_0 - \theta) - F(\theta_0 + \theta)]^2}{F^2(\theta_0 - \theta) + 2F(\theta_0 - \theta)F(\theta_0 + \theta) \cos \varphi + F^2(\theta_0 + \theta)}. \quad (4.69)$$

The resulting expressions for $S_A(\theta)$ and $S_B(\theta)$ are equal in modulus but opposite in sign. Hence

$$\Delta S(\theta) = S_A(\theta) - S_B(\theta) \neq 0. \quad (4.70)$$

Using this method, we can show that inequality (4.70) is also fulfilled when there are more than two targets with different reflecting surfaces in the unresolved volume c space. We can also show that when equisignal direction of the antenna of a monopulse system is shifted to the side of one of the targets and this target at some instant is more powerful source of reflected signals than the other target, the difference voltage of the error signal $\Delta S(\theta)$ will be near or equal to zero just as in the case of a single target.

Thus, the equality of error signal difference $\Delta S(\theta)$ to zero can be an indicator that the distinguished signal belongs to only one of the target and, based on this criterion, target resolution can be accomplished.

For an indication of the aerial situation in the zone of action of a direction finding system, in search mode, the difference of error signals $S_A(\theta) - S_B(\theta)$ is fed to input of the vertical sweep of the indicator tube, and their sum $S_A(\theta) + S_B(\theta)$ to the input of horizontal sweep. The image thus obtained on the screen is shown in Fig. 4.13a. The intersection points of the horizontal sweep line with the parabolic curve, forming the lower boundary of the image and corresponding to the zero values of the difference signal $\Delta S(\theta)$, indicate the location of each of the targets (on the figure these points are marked with boldfaced vertical lines).

If the difference voltage of the error signal is previously fed to the full-wave rectifier which produces negative voltage, on the screen the image changes (Fig. 4.13b) and becomes more suitable for determining target location and tracking either of them.

If there are three targets in the group, the image on the screen will have the form indicated in Fig. 4.13c. The outer edges of the oscillogram mark the outer targets of the group. This enables the radar operator to track these targets.

With automatic tracking of a selected target, the sum signal is fed to the servomotor of the antenna position control through the gated storage device, which blocks input signals not corresponding to the resolution criterion and passes signals from the selected target. In this radar diagram the gating device is unblocked by positive strobes and blocked by negative ones formed upon the appearance of undesirable or interference error signals.

The gating device at the same time provides memory of a signal which has passed through it in a certain period of time,

which removes the disconnection of the servosystem at the instant the gating device is blocking when error signals from an undesirable target are formed in the receiver.

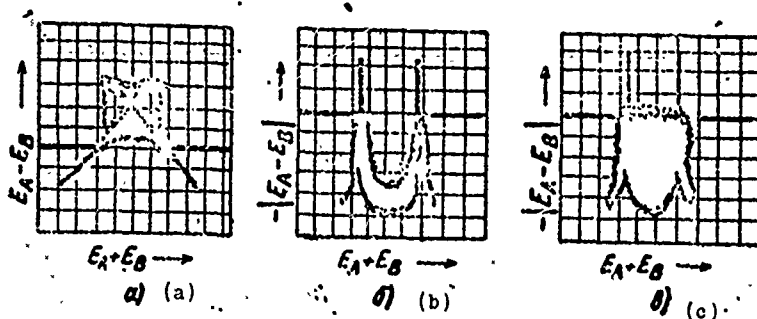


Fig. 4.13. Image on indicator screen: a) direction finding of a paired target (first version); b) direction finding of a paired target (better version); c) direction finding of a group of three targets.

As has been indicated, the resolution criterion is the equality to zero of the difference voltage of the error signal $\Delta S(\theta)$. At such instants the sum voltage of the error signal can be both positive and negative, depending upon which of the targets is at that instant the more intense source of signals. Therefore target selection for automatic tracking is accomplished by choosing the working polarity of the sum error signal with the aid of the target selector, consisting of a switch and a detector connected in series from the input load of the full-wave rectifier of the sum error signal. Depending upon the position of the switch, the polarity of the detector connection and the polarity of the signal transmitted through it change.

The full-wave rectifier of the sum error signal, regardless of the polarity of the input signal, develops at its output a voltage of negative polarity used for the blocking of the gating device. The blocking of the gating device also occurs if the difference error signal is zero, but the main signal source is an undesirable target.

In the system there are a number of additional devices not indicated in Fig. 4.12 but necessary for improving the quality of its operation.

Thus, for example, there is a threshold device which eliminates angular antenna drift in the case of small signals from targets, whose level is insufficient to use for tracking the target. A d-c restorer is also provided to ensure the unblocking of the gating device for certain minimum and maximum time intervals, thereby limiting the duration of the blocking of the servosystem. We can become acquainted with the work of these devices through the complete description of this system in reference [103].

It should be noted that this method of design solution for the problem of target resolution in a group cannot ensure high accuracies, for example, the accuracies which can be achieved when tracking single targets, since it is based on the blocking of the servosystem for certain time intervals during which the antenna moves from "inertia".

Nevertheless, its advantages are obvious, particularly, as will be shown in Chapter 7, in the protection from certain forms of active interferences.

From the point of view of achievable accuracy, preference should be given to another method of increasing resolution [72], which will be described below. The essence of this method reduces to the functional processing of signals received simultaneously along several independent receiving channels.

4.4.2. A method of increasing resolution, based on functional processing of signals. We know that the plane wave intensity phase ϕ at arbitrary point "H" relative to reference point "O" located at the origin of coordinates of the plane of the figure (Fig. 4.14) due to the difference in distances from radiation source A, is expressed by formula

$$\varphi = \kappa(R_0 - R_n) = -\kappa(\rho \cos \vartheta \cos \varepsilon \sin \theta + \rho \sin \vartheta \sin \varepsilon), \quad (4.71)$$

where R_0 and R_H is the distance from signal radiation source to points "O" and "H";

ρ, ϑ are the polar coordinates of point "H" relative to point "O" and the direction finding plane;

ϵ is the elevation of the radiation source;

θ is the azimuth of the radiation source.

If in the direction finding plane we use rectangular system of coordinates XY, connected with the polar system coordinates by relationships

$$y = \rho \sin \vartheta; \quad x = \rho \cos \vartheta,$$

then equation (4.71) assumes the form

$$\varphi = -\kappa (x \cos \epsilon \sin \theta + y \sin \epsilon). \quad (4.72)$$

In the presence of M sources the resulting field at the examined point in space is determined from the familiar expression

$$\dot{E}_r = \sum_{m=1}^M \dot{A}_m \exp -i\kappa (x \cos \epsilon_m \sin \theta_m + y \sin \epsilon_m), \quad (4.73)$$

where $\dot{A}_m = E_{om} \exp i (\omega_m t + \phi_{m0})$ is the complex amplitude of signal from the m-th source;

ω_m and ϕ_{m0} are frequency and initial phase of signal from the m-th source.

Expression (4.73) shows that the resulting field intensity at the examined point in space can be defined as the sum of M complex equations, each of which is determined only by the location of the correspondence source.

Obviously, if the receiving system is capable of forming the corresponding quantity of independent equations which characterize the mutual arrangement of the sources, then by solving these equations by familiar mathematical methods we can obtain parameters defining

the direction to each of the signal sources and thereby solve the problems of target resolution in space. This also involves the principle of increasing radar angular resolution by the functional method.

The necessary quantity of independent receiving channels for a direction finding system, when accomplishing the functional method of target resolution with respect to angular coordinates, is determined according to formula $N = 2M$, where M is the number of radiation sources with disagreeing angular coordinates.

A typical monopulse radar performing two-plane direction finding has four receiving channels and, therefore, can in principle successfully resolve a paired target by the method considered when targets are not being resolved with respect to range or speed.

The following system of equations is formulated for such a monopulse radar at input of the receiving channels;

$$\begin{aligned}
 \dot{E}_1 &= \dot{A}_1 \exp[-i(x_1 U_1 + y_1 V_1)] + \\
 &+ \dot{A}_2 \exp[-i(x_1 U_2 + y_1 V_2)], \\
 \dot{E}_2 &= \dot{A}_1 \exp[-i(x_2 U_1 + y_2 V_1)] + \\
 &+ \dot{A}_2 \exp[-i(x_2 U_2 + y_2 V_2)], \\
 \dot{E}_3 &= \dot{A}_1 \exp[-i(x_3 U_1 + y_3 V_1)] + \\
 &+ \dot{A}_2 \exp[-i(x_3 U_2 + y_3 V_2)], \\
 \dot{E}_4 &= \dot{A}_1 \exp[-i(x_4 U_1 + y_4 V_1)] + \\
 &+ \dot{A}_2 \exp[-i(x_4 U_2 + y_4 V_2)],
 \end{aligned}$$

(4.74)

where

$$\begin{aligned}
 V_1 &= \kappa \sin \alpha_1; \quad U_1 = \kappa \cos \alpha_1 \sin \theta_1; \\
 V_2 &= \kappa \sin \alpha_2; \quad U_2 = \kappa \cos \alpha_2 \sin \theta_2.
 \end{aligned}$$

If we select the position for antennas shown in Fig. 4.14 and their coordinates in a rectangular system are:

- 1) $y_1 = 0; x_1 = 0;$
- 2) $y_2 = l; x_2 = 0;$
- 3) $y_3 = 0; x_3 = l;$
- 4) $y_4 = l; x_4 = l;$

where l is the distance between the phase centers of the antennas, then the voltage in each antenna is expressed in the following manner:

$$\left. \begin{aligned} \dot{E}_1 &= A_1 + A_2, \\ \dot{E}_2 &= A_1 \exp(-iU_1) + A_2 \exp(-iU_2), \\ \dot{E}_3 &= A_1 \exp(-iV_1) + A_2 \exp(-iV_2), \\ \dot{E}_4 &= A_1 \exp[-il(U_1 + V_1)] + A_2 \exp[-il(U_2 + V_2)]. \end{aligned} \right\} \quad (4.75)$$

The equations obtained can be formed relative to $\varepsilon_1, \varepsilon_2, \theta_1$ and θ_2 by the method of wave division [72].

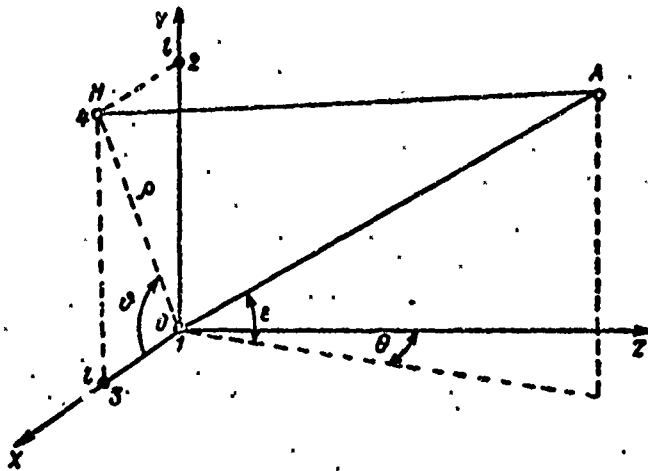


Fig. 4.14. The arrangement of antennas and radiation source in the selected system of coordinates.

Thus, a joint solution to the top pair of equations of system (4.75) gives

$$\dot{A}_1 = \frac{\dot{E}_1 \exp(-iU_2) - \dot{E}_2}{\exp(-iU_2) - \exp(-iU_1)} \quad (4.76)$$

$$\dot{A}_2 = \frac{\dot{E}_2 - \dot{E}_1 \exp(-iU_1)}{\exp(-iU_2) - \exp(-iU_1)} \quad (4.77)$$

Accordingly, we obtain from the joint solution of the bottom pair of equations from system (4.75)

$$\dot{A}_1 = \frac{\dot{E}_2 \exp(-iU_2) - \dot{E}_1}{\exp[-i(U_2 + V_1)] - \exp[-i(U_1 + V_1)]} \quad (4.78)$$

$$\dot{A}_2 = \frac{\dot{E}_2 - \dot{E}_1 \exp(-iU_1)}{\exp[-i(U_2 + V_2)] - \exp[-i(U_1 + V_2)]} \quad (4.79)$$

Equating in pairs the corresponding equations (4.76)-(4.79), after elementary transformation we obtain

$$\frac{\dot{E}_1 \exp(-iU_2) - \dot{E}_2}{\dot{E}_2 \exp(-iU_2) - \dot{E}_1} \exp(-iV_1) = 1, \quad (4.80)$$

$$\frac{\dot{E}_1 \exp(-iU_1) - \dot{E}_2}{\dot{E}_2 \exp(-iU_1) - \dot{E}_1} \exp(-iV_2) = 1. \quad (4.81)$$

Complex equations (4.80) and (4.81) give four actual equations and make it possible to determine unknowns U_1 , U_2 , V_1 and V_2 .

The values found for $U_{1,2}$ and $V_{1,2}$ enable us to calculate azimuth and elevation for each of the targets according to formulas

$$\varepsilon_{1,2} = \arcsin \frac{V_{1,2}}{\kappa}, \quad (4.82)$$

$$\theta_{1,2} = \arcsin \frac{U_{1,2}}{\sqrt{\kappa^2 - V_{1,2}^2}}. \quad (4.83)$$

All operations in calculating angular target coordinates can be performed by computers. Subtraction, comparison, and phase shift for signals, in accordance with formulas (4.80) and (4.81), can be performed both high and intermediate-frequency [72].

It should be noted that the functional method, unlike the design method examined above for increasing target resolution with respect to direction, enables us, in principle, to obtain higher angular measurement accuracy for targets in a group, but its realization is not a simple task. Thus, the suggested diagram of functional processing on high frequency [72] requires an increase in receiving channels of a monopulse radar from four to six and the introduction of 14 sum-difference bridges into the high-frequency circuit of the direction finding system. In connection with this, additional difficulties arise with the provision of identity and stability for the phase characteristics of the receiving channels, and power losses of signals received also rise considerably, which forces the additional amplification in receiving circuits. With functional processing of signals on intermediate frequency difficulties arise with the provision of linearity for the receiving circuits in a sufficiently wide dynamic range.

CHAPTER 5

ACCURACY PROBLEMS IN ANGULAR MEASUREMENT BY THE MONOPULSE METHOD

The accuracy of measuring angular coordinates is evaluated by direction finding errors caused by various factors.

Origins of direction finding errors are broken down into external origins, introduced by the target and the medium of radio wave propagation, and equipment origins, caused by imperfection in equipment, deficiencies in the measurement method, as well as internal noises of the receiver and servosystem. In character direction finding errors are divided into systematic and random.

In accordance with these sources of errors, Table 5.1 offers a list of the main components of errors determining angular measurement accuracy.

Direction finding errors caused by the effect of nonidentity of the amplitude-phase characteristics of receiving antennas are analyzed in Chapter 6. Below we examine the effect of a number of other reasons for the impairment of accuracy in angular measurement by the monopulse method.

§ 5.1. THE EFFECT OF RADIO WAVE PROPAGATION CONDITIONS ON DIRECTION FINDING ACCURACY

The main factors affecting the accuracy of angular measurement by the monopulse method and connected with radio wave propagation conditions are the surface of the earth and its atmosphere.

Reflections from earth create additional radiation sources which do not coincide with the radar-target direction, and the nonhomogeneities of the atmosphere lead to a distortion in the wave propagation trajectory and a misalignment between the apparent direction to the source of the reflected signals and the direction to the real source of signals.

Table 5.1.

Source of errors	Components of errors
Media in which radio waves are propagated	Errors caused by reflections of radio waves from ground and water, tropospheric and ionospheric refractions, diffractions, and depolarizations of radio waves.
Direction finding target	Errors caused by amplitude fluctuations of reflected signals, by straying of the reflection center (angular noise), depolarization of radio waves with reflection from a complex target.
Radar	Errors caused by nonidentity of receiving channels with respect to amplitude-phase characteristics, antenna deformations, cross-polarizations of receiving antennas, nonlinearities and clearances in antenna drives, internal receiver noises, structural deficiencies in various elements of the radar and their changes due to aging and mechanical and climatic effects, etc.

The effect of radio wave propagation conditions on direction finding error is analyzed in detail in a number of works [2, 18, 44, 48]. Therefore, in this book we shall only briefly review the results of these works.

5.1.1. The effect of the earth on direction finding accuracy. This effect is apparent, first of all, in the reflection of radio waves from the earth's surface and in interference phenomena. As

can be seen from Fig. 5.1, the radiated antenna energy falls on the target along two different paths: the direct path from the radar to the target, and after reflection from the earth's surface. The reflected wave can be considered direct radiation of a fictitious source which is a mirror reflection of the real source. The amount of resulting signal strength at the reception point will be determined by the amplitude and phase relationships of the direct and reflected signals and will reach maximum when they are cophased and minimum when they are antiphased.

Due to the effect of the reflecting surface, a one-lobe radar radiation pattern in the vertical plane is transformed into a multi-lobe pattern (Fig. 5.2). Because of this multilobe nature the quantity of equisignal zones in the direction finding characteristic of the system is accordingly increased and false equisignal directions (ESD) appear, located at different angles to the main equisignal direction. In a number of cases false ESD will fulfill the conditions of stability and then automatic target tracking with considerable angular errors is possible. The main equisignal direction with this also can be displaced [82, 132].

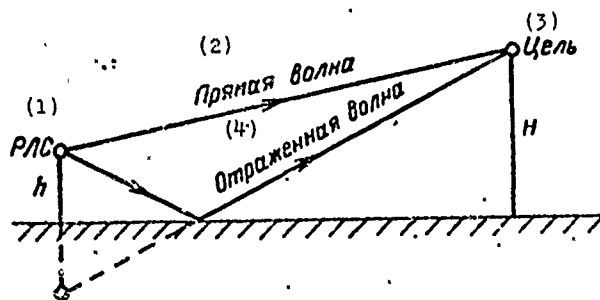


Fig. 5.1. Radio wave propagation over a flat reflecting surface.
KEY: (1) Radar; (2) Direct wave; (3) Target; (4) Reflected wave.

Direction finding error will also increase because of the fact that during the target's motion the multilobe structure of the radiation pattern changes because of changes in the propagation conditions and radio wave reflection. This leads to variations in

ESD position and rather irregular antenna movements in the target tracking process.

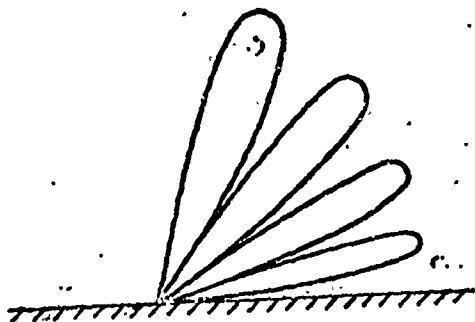


Fig. 5.2. Multilobe antenna radiation pattern caused by the effect of a flat reflecting surface.

The limits within which the radar antenna will be displaced are dependent upon the reflection factor, antenna beam width, and target elevation.

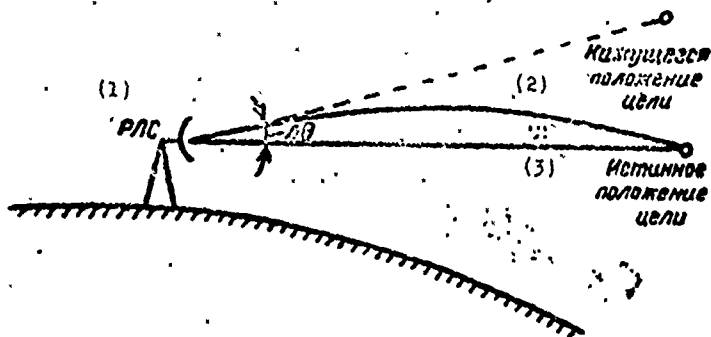


Fig. 5.3. Angular error caused by refractions.
KEY: (1) Radar; (2) Apparent position of target; (3) Real position of target.

5.1.2. The effect of refraction and diffraction on direction finding accuracy. Radio waves in free space are propagated rectilinearly but when passing through the atmosphere and, especially, its lower layer the troposphere, a distortion of radio waves occurs, which we call refraction. This leads to errors in determining target direction. The occurrence of angular error because of radio wave refraction is illustrated in Fig. 5.3.

We know that radio wave propagation rate in the atmosphere is determined by expression

$$c_s = \frac{c}{\sqrt{\epsilon}}, \quad (5.1)$$

where ϵ is the dielectric constant of the medium;
 c is the radio wave propagation rate in free space.

Hence it follows that the refraction factor, equal to the ratio of radio propagation rates in free space and in a given medium, can be found as

$$n = \frac{c}{c_s} = \sqrt{\epsilon}. \quad (5.2)$$

The dielectric constant of the atmosphere depends upon meteorological conditions. Knowing pressure, temperature, and humidity we can calculate the dielectric constant and the refraction factor in accordance with formula [2]:

$$(n - 1) 10^6 \approx \frac{77.6}{T} \left(p + \frac{4810}{T} e \right), \quad (5.3)$$

where p is the barometric pressure, mbar;
 e is the partial pressure of water vapor, mbar;
 T is absolute temperature, °K.

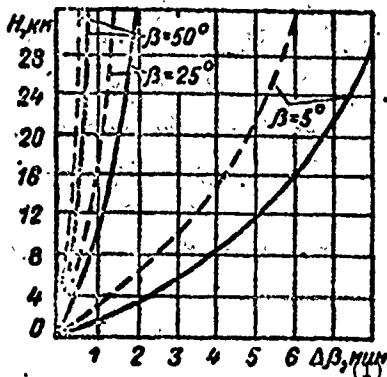


Fig. 5.4. Errors in measuring elevation in the lower atmospheric layers with a humidity of 100% (solid line) and 0° (dashes).

Since these parameters of the atmosphere change substantially with altitude, the greatest radio wave refraction occurs in the vertical plane. In the horizontal plane refraction phenomena appear to a considerably less extent than in the vertical plane.

The effect of refraction on direction measurement accuracy can be evaluated by the refraction angle, by which we mean the angle between the straight line connecting the radar and the target and the tangent to the radio wave propagation trajectory at the point under study. Figure 5.4 presents the calculated dependence [18] of elevation error measurement ($\Delta\beta$) in the lower layers of the atmosphere on the flight altitude of the target (H) and the slope of the radar antenna beam (β). As is seen from the figure, the greatest direction finding errors are noted with low target elevations.

In spite of the fact that the amount of direction finding error due to refraction is not great and is usually expressed by units of angular minutes, it should be taken into consideration in precision radars and compensated by introducing the proper corrections. The amount of correction, as a rule, is determined by the experimental method for each region involved.

Diffraction consists of the property of radio waves to bend around the curved surface of the earth, similarly to light waves. Because of diffraction the detection zone can be extended beyond the horizon. Since this phenomenon is connected with the distortion

of the radio wave propagation trajectory, as is refraction, target direction errors are also possible because of diffraction. However, the ability of electromagnetic waves to bend around earth's surface depends upon frequency and with an increase in frequency this ability rapidly lessens. Waves of the centimeter range have low diffraction ability. Since modern radars are predominantly of the centimeter range, the effect of radio wave diffraction on direction finding accuracy can be disregarded in the first approach.

§ 5.2. THE EFFECT OF AMPLITUDE AND ANGULAR FLUCTUATIONS IN REFLECTED SIGNALS ON DIRECTION FINDING ACCURACY

By fluctuations of signals reflected from a target we mean a large group of interference phenomena which occur during the irradiation of an object of complex form whose dimensions considerably exceed operating wavelength.

Modern monopulse radars operate generally in the centimeter and decimeter ranges and target dimensions can be hundreds of wavelengths; therefore, the interference pattern of secondary target radiation is rather complex and noticeably changes with small variations in target positions, generating fluctuations of signals reflected from the target.

Detailed studies have shown that the fluctuations of reflected signals can be divided into groups: fluctuations of reflected signals in amplitude and fluctuations of approach angle. These fluctuations differ both in nature and in the mechanism of the effect on radar instruments.

5.2.1. The effect of amplitude fluctuations on direction finding accuracy. Amplitude fluctuations appear in amplitude variations from pulse to pulse and are produced by fluctuations of the effective reflecting surface of the target due to its movement in space and change of position relative to the radar irradiating it, and also by fluctuations in the atmospheric nonhomogeneity, including those caused by variations of meteorological conditions on the path of radio wave propagation.

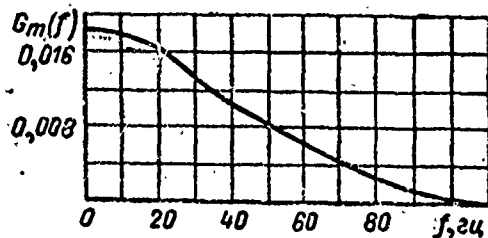
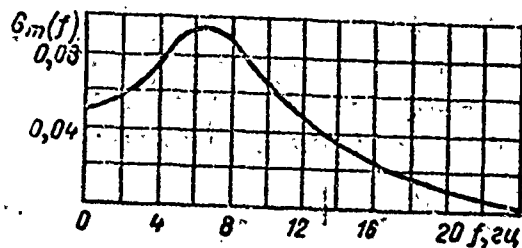


Fig. 5.5. Fluctuations spectrum for signals reflected from aircraft.

Fig. 5.6. Fluctuations spectrum for signals reflected from ship.

Depending upon the type of target, the spectral composition of amplitude fluctuations can change considerably, which is apparent, for example, from the standardized spectral densities of amplitude fluctuation for signals reflected from an aircraft and a ship, presented in Figs. 5.5 and 5.6, respectively, [18].

Since the monopulse method, in principle, makes it possible to determine angular coordinates with one pulse, and within the pulse there are no amplitude fluctuations, we might expect that direction finding error in monopulse radars could not be affected by amplitude fluctuations of signals. But this is not the case. Actually, amplitude fluctuations of the reflected signals have a disturbing effect on monopulse radars although considerably less than they do on radars with conical scanning or sequential beam switching.

This is explained first by the fact that contemporary monopulse radars do not use their potential capabilities for fast action but extract the angular target information from a series of sequential pulses. In order to eliminate the effect of the level of approaching signals on the quantity of angular error, signals are standardized usually with the aid of an AGC system operating on the sum signal. Since the AGC system has a finite bandwidth and, consequently, limited high-speed action, signal standardization proceeds with a

delay. This makes the error signal, to a certain extent, dependent upon the amplitude of signals received and it is modulated by the amplitude fluctuations of the signals.

Amplitude modulation components of the error signal, with frequencies lying within the bandwidth of the radar's servosystem, inevitably cause an increase in dynamic direction finding errors. In order to eliminate the effect of amplitude fluctuations in the reflected signal on direction finding accuracy, the AGC system must be fast-acting and capable of, at least, suppressing amplitude fluctuations whose spectra lie within the bandwidth of the servosystem. However, as will be seen later, the widening of the half-band of the AGC system leads to an increase in angular errors, caused by other sources and, particularly, angular noise. Therefore, the selection of AGC passband is a compromise.

The effect of the AGC system on angular errors caused by different sources is examined in greater detail in § 5.6.

5.2.2. The effect of angular fluctuations in reflected signals on direction finding and accuracy. By angular fluctuations we mean fluctuations in the approach angle of signals reflected from the target [5]. That such fluctuations exist in the reflected signal was established during the development and testing of the first monopulse radars [19].

In subsequent theoretical and experimental works it was established that angular fluctuations of signal (angular noise) are generated by fluctuations in the slope of the phase front of the wave. Since the work of any direction finding system for small targets is based on determining the position of normal to the phase front of the radio waves, variations in the position of the phase front during direction finding are one of the limitations on the accuracy of various angle-measuring coordinators, including those working on the monopulse method. This also pertains, to a certain extent, to the case of direction finding with extended targets although, in this case, there is no complete correspondence between

equisignal direction of the radar antenna and the direction of the normal to the phase front (see Section 5.2.3).

The appearance of angular noise is connected with the change in the apparent position of the target relative to its physical center. The reason for it lies in the multipoint structure of the reflecting surfaces of an extended target, causing the straying (flickering) of the reflection center both within the geometric dimensions of the target and beyond. Considering the universality of the action of angular noises, let us pause on their nature for more detail. With this aim in mind, we should examine the formation of a phase front by a target consisting of a set of reflected points. For simplicity, in the beginning let us examine a target consisting of two isotropic spaced point sources of signals.

A two-point target provides a visual method of representing the nature of angular noises and gives an approximate example of the form of such targets as, for example, a small interceptor with tanks on the wingtip or a group of targets consisting of two aircraft spaced at an angle within the width of the radar's antenna radiation pattern, i.e., resolvable with respect to angle.

The examined model of a target also describes quite well the phenomenon observed when tracking targets at low elevations, when, in addition to the actual target, the radar also observes its mirror image because of the effect of the earth's surface.

The phase front of the wave, as you know, is a locus of points of space with identical phases. Therefore, to find the phase front from a two-point target, it is sufficient to find an expression defining the phase of the resulting signal for any point of space and equate it to a constant quantity. Then the found equation determines the position of the phase front relative to the two-point signal source.

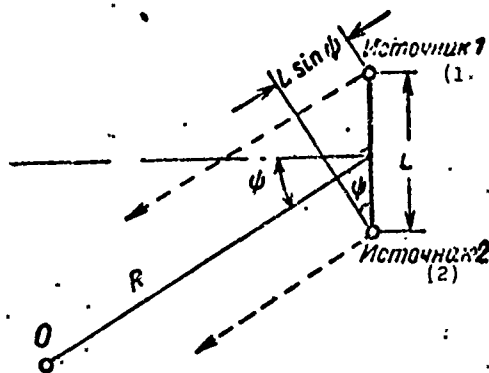


Fig. 5.7. Geometric relationships of a two-point signal source.
KEY: (1) Source 1; (2) Source 2.

With this aim, let us assume that the distance between point sources is L and the points are omnidirectional radiators with fixed phase shift (Fig. 5.7). At a distant point of space O with polar coordinates R and ψ , the radiators create field strength

$$\dot{E}_1(t) = E_{m1} \exp i \left(\omega t - \frac{2\pi R}{\lambda} + \frac{2\pi}{\lambda} \frac{L}{2} \sin \psi \right), \quad (5.4)$$

$$\dot{E}_2(t) = E_{m2} \exp i \left(\omega t - \frac{2\pi R}{\lambda} - \frac{2\pi}{\lambda} \frac{L}{2} \sin \psi - \alpha \right). \quad (5.5)$$

Phase shift between these oscillations is determined by the phase angle α and the difference of path $L \sin \psi$ depending upon the direction to point of reception. On Fig. 5.8 the signals of the radiators are represented in vector form. The strength of the resulting field can be expressed as

$$\dot{E}(t) = E_m \exp i \left[\omega t - \frac{2\pi R}{\lambda} - \Phi(\psi) \right]. \quad (5.6)$$

The phase angle of the resulting signal $\Phi(\psi)$ relative to the reference signal, corresponding to the direction passing through the middle of the distance between sources, can be found as an angle whose tangent is equal to the quotient from the division of the sum of the vertical component of two vectors by the sum of their

horizontal components, i.e.,

$$\Phi(\psi) = \arctg \frac{\sin \epsilon_a + a \sin(\epsilon_a + \pi)}{\cos \epsilon_a + a \cos(\epsilon_a + \pi)} \quad (5.7)$$

where

$$\epsilon_a = \frac{2\pi}{\lambda} \frac{l}{2} \sin \psi, \quad a = \frac{E_{m2}}{E_{m1}}$$

Assigning a constant phase to the resulting field in expression (5.6), we can obtain the relationship between R and ψ , which is the equation of the phase front in polar coordinates:

$$\frac{2\pi R}{\lambda} - \Phi(\psi) = 2\pi n \quad (5.8)$$

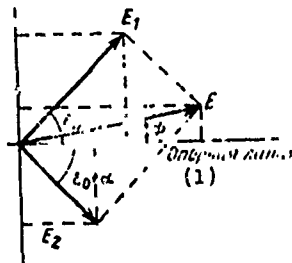


Fig. 5.8. Vector diagram of signals received from a two-point source. KEY: (1) Reference line.

When $n = 0$ the equation of the phase front assumes the form

$$\frac{2\pi R}{\lambda} = \Phi(\psi) \quad (5.9)$$

Figure 5.9 represents the calculated and experimental image of the phase front of waves caused by the presence of two point sources of signals of equal magnitude [97]. The experimental pattern of the phase front was obtained with an ultrasonic tank with the same relative phases, amplitudes, and distance between sources. A comparison of these diagrams shows that there is an almost complete analogy between the calculated and experimental data.

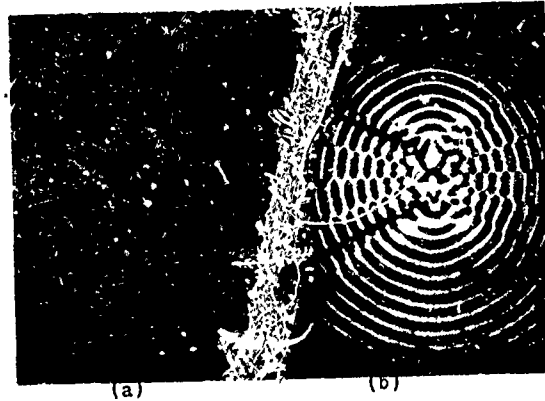


Fig. 5.9.. Phase front of waves radiated by a two-point source: a) calculated; b) experimental.

Of greatest interest is the slope of the phase front of the wave formed by two sources relative to the phase front of the individual signal source located in the middle between the sources studied. The slope of the phase front can be characterized by the angle formed between the normal to a given point of the phase front of a wave of a two-point signal source and the radius-vector drawn from the center between sources to the same point of the phase front and agreeing with the normal of the phase front of a single source.

Mathematically this angle is defined as

$$\operatorname{tg} \Delta\psi = \frac{dR/d\psi}{R}. \quad (5.10)$$

Taking into account expression (5.9), we obtain

$$\operatorname{tg} \Delta\psi = \frac{1}{R} \cdot \frac{\lambda}{2\pi} \frac{d\Phi(\psi)}{d\psi}. \quad (5.11)$$

The expression obtained determines the distortion of the phase front formed by a two-point signal source as compared with the spherical phase front peculiar to a single point source.

Differentiating (5.7) with respect to ψ and substituting it in (5.11), after simple transformations we obtain

$$\operatorname{tg} \Delta\psi = \frac{L}{2R} \cos\psi \frac{1-a^2}{1+a^2+2a \cos\left(\frac{2\pi L}{\lambda} \sin\psi + \alpha\right)}, \quad (5.12)$$

where $\frac{L}{R} \cos\psi = \psi_H$ is the angle of source sighting (angle base).

If $\Delta\psi$ is comparatively small, $\operatorname{tg} \Delta\psi \approx \Delta\psi$ and

$$\frac{\Delta\psi}{\psi_H} = \frac{1-a^2}{2 \left[1+a^2+2a \cos\left(\frac{2\pi L}{\lambda} \sin\psi + \alpha\right) \right]}. \quad (5.13)$$

When $\psi = 0$, when the base of the sources is located perpendicularly to the direction to reception point, formula (5.13) is simplified:

$$\frac{\Delta\psi}{\psi_H} = \frac{1-a^2}{2(1+a^2+2a \cos\alpha)}. \quad (5.14)$$

From expression (5.14) it follows that distortion in the phase front of the wave caused by the two-point structure of the target depends upon the relationship of signal amplitudes and phase shift between them and is maximum when they are in opposite phase ($\alpha = \pi$) and signal amplitudes ($a = 1$) are equal.

Generally when the case of reflected signals from a two-point target is considered, amplitude and phase relationships of the signals fluctuate which causes a fluctuation in the slope of the phase front of the wave reflected from the target. Variations in the slope of the phase front, in this case, are conveniently carried out by the probability method when the probabilities of errors exceeding a certain level are determined. For simplicity let us assume that there are no amplitude fluctuations and the phase shifts of reflected signals are distributed with equal probability in the range from $-\pi$ to π .

From the theory of random processes we know [34] that the probability of errors exceeding a certain level M is determined by expression

$$p(M) = \int_M^{M_{\text{макс}}} W(M) dM, \quad (5.15)$$

where $W(M)$ is the probability density of random quantity M

$$M = \left| \frac{\Delta\phi}{\phi_{\pi}} \right|,$$

$M_{\text{макс}}$ [макс = max] is the maximum possible error.

In this case

$$W(M) = W(\alpha) \frac{d\alpha}{dM}, \quad (5.16)$$

where $W(\alpha)$ is the probability density of the phase shift of the signals, equal to $1/2\pi$ in this case.

Solving equation (5.15) relative to α , we find

$$\alpha = \arccos \frac{1 - a^2 - 2M(1 + a^2)}{4aM}. \quad (5.17)$$

Hence after simple transformation we obtain

$$\frac{d\alpha}{dM} = \frac{1}{M \sqrt{-1 + \frac{4M(1+a^2)}{(1-a^2)} - 4M^2}}. \quad (5.18)$$

When calculating (5.15), we shall use the tabular integral [17]

$$\int \frac{dx}{x\sqrt{R}} = \frac{1}{\sqrt{-a}} \arcsin \frac{2a + bx}{x\sqrt{b^2 - 4ac}}, \quad (5.19)$$

where

$$R = a + bx + cx^2.$$

Substituting the values $a = -1$, $b = 4\frac{1+a^2}{1-a^2}$, $c = -4$ in (5.19), performing elementary transformations, and taking into account the fact that all possible changes in quantity M lie within α from 0 to π , we find

$$\begin{aligned}
 p(M) &= \frac{1}{\pi} \arcsin \left(\frac{1+a^2}{2a} - \frac{1-a^2}{4Ma} \right) \Big|_M^{M_{\max}} = \\
 &= \frac{1}{\pi} \left[\arcsin \left(\frac{1+a^2}{2a} - \frac{1-a^2}{4M_{\max}a} \right) - \right. \\
 &\quad \left. - \arcsin \left(\frac{1+a^2}{2a} - \frac{1-a^2}{4Ma} \right) \right].
 \end{aligned}
 \tag{5.20}$$

Analysis of expression (5.19) shows that M_{\max} occurs when $\alpha = \pi$ and is equal to

$$M_{\max} = \frac{1+a}{2(1-a)}.
 \tag{5.21}$$

Taking into consideration (5.21), we obtain the following calculations formula

$$p \left(\frac{\Delta\psi}{\psi_a} \right) = \frac{1}{2} - \frac{1}{\pi} \arcsin \left(\frac{1+a^2}{2a} - \frac{1-a^2}{4aM} \right).
 \tag{5.22}$$

Figure 5.10 represents the probability distribution, calculated according to formula (5.22), of a given deflection of the phase front of a wave of a two-point signal source relative to the position of the spherical front of the wave corresponding to the point force.

Since the antenna of any radar reacts to the phase distribution of the electromagnetic wave entering it, the distortion of the wave's phase front inevitably affects target finding accuracy. The character of this effect will be determined by the structure of the target and the parameter of the antenna and servosystem. When the target is a point target or a small one, target tracking can be identified with the tracking of the normal to the phase front of the wave of the signals entering antenna input, and direction finding

error will be determined by expression (5.14). In accordance with this, if the frequency spectrum of phase fluctuations in the signals received does not exceed the bandwidth of the radar servosystem, which is the case when tracking slowly moving (or immobile) targets, the calculated curves in Fig. 5.10 enable us, with fixed ratios of signal amplitudes, to determine the probability of obtaining direction finding errors exceeding the prescribed quantity. Thus, for example, the probability of angular deviation in the ESD from the direction to the centers of the base of the sources by a quantity equal to the base, when $a = 0.6$; 0.8 and 0.95 , is approximately 17, 14, and 7%, respectively. When $a = 0.2$ the probability of obtaining an error exceeding the base of the sources is zero.

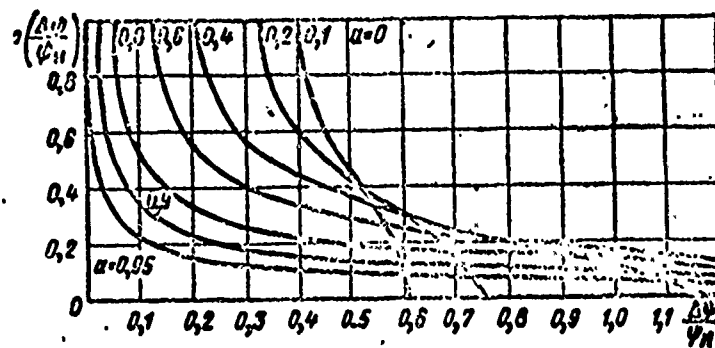


Fig. 5.10. Probability distribution of phase front error with various ratios of reflected signal intensity.

Table 5.2.

a	0.95	0.9	0.8	0.6	0.4	0.2	0.1
$[\overline{(\Delta\psi)^2}]^{1/2}/\psi_n$	2.2	1.6	1	0.8	0.6	0.52	0.505

If we know the law of probability density distribution $W(M)$, we can calculate standard error. For the case under study, table 5.2 presents the calculated dependences of standard direction finding errors, standardized with respect to the value of the source base for various ratios of reflected signal amplitude for a two-point target [18].

If the spectrum of phase fluctuations in signals from a two-point target exceeds the bandwidth of the direction finder's servosystem, the error calculation method changes. In this case, in seeking the expression determining the condition for target tracking, it is necessary to average beforehand the signal received in accordance with its statistical characteristic and the time lag of the servosystem.

We should mention that it is valid to identify the bearing with the direction of the normal to the face front of the resulting reflected signal only with linearization of the direction finding characteristic for the radar. The latter is permissible during the direction finding of small and point targets when angular deviations of the radar antenna axis from the direction to the geometric center of the reflected signals are small.

With large angular dimensions for the target being tracked, it is necessary to take into account the actual antenna radiation patterns. With this aim, let us examine, in general form, the direction finding of a complex extended target.

5.2.3. Errors and the direction finding of targets of complex form. In most practical cases the target cannot be represented in simple geometric form convenient for a mathematical description. Therefore, in analyzing the direction finding errors involved with a complex target, we replace the actual target with certain models. As such a model we usually use a multipoint target when the reflected signal from the complex target is a collection of reflections from a set of point targets characterizing the main reflecting elements

of the actual complex target [38]. It is assumed that amplitudes and phases of signals reflected from each point target are mutually independent.

For simplicity let us examine the direction finding of a complex target in one plane in static conditions. Let the complex target be sum M of elementary reflectors. Then the signal reflected from the complex target is defined as the sum of the signals of the elementary reflectors

$$\dot{E}(t) = \sum_{m=1}^M E_m \exp i(\omega t + \varphi_m), \quad (5.23)$$

where E_m is the amplitude of the signal from the m-th reflector;
 φ_m is the phase of the signal from the m-th reflector.

In accordance with this, at the output of the first and second antenna channel of an amplitude sum-difference monopulse system the reflected signal of a complex target can be represented by expression

$$\dot{E}_1(t, \theta) = \sum_{m=1}^M E_m F(\theta_0 - \theta_m) \exp i(\omega t + \varphi_m), \quad (5.24)$$

$$\dot{E}_2(t, \theta) = \sum_{m=1}^M E_m F(\theta_0 + \theta_m) \exp i(\omega t + \varphi_m), \quad (5.25)$$

where θ_m is the angular position of the m-th source relative to equisignal direction.

With sum-difference signal processing at the output of the sum and difference channels, respectively, we obtain

$$\dot{E}_c(t, \theta) = \frac{1}{\sqrt{2}} \sum_{m=1}^M E_m F_{cm}(\theta) \exp i(\omega t + \varphi_m), \quad (5.26)$$

$$\dot{E}_p(t, \theta) = \frac{1}{\sqrt{2}} \sum_{m=1}^M E_m F_{pm}(\theta) \exp i(\omega t + \varphi_m), \quad (5.27)$$

where

$$F_{c_m}(\theta) = F(\theta_0 - \theta_m) + F(\theta_0 + \theta_m),$$

$$F_{p_m}(\theta) = F(\theta_0 - \theta_m) - F(\theta_0 + \theta_m).$$

If the phase detector is of the multiplying type and the amplifier channels amplify without distortion, the standardized output voltage of the phase detector, as we know, is determined by expression

$$S(\theta) = \frac{\operatorname{Re} \dot{E}_c(t, \theta) \dot{E}_p^*(t, \theta)}{\dot{E}_c(t, \theta) \dot{E}_c^*(t, \theta)}. \quad (5.28)$$

Substituting into (5.28) expressions (5.26) and (5.27), we obtain

$$S(\theta) = \frac{\operatorname{Re} \sum_{m=1}^M \sum_{n=1}^M E_m E_n F_{c_m}(\theta) F_{p_n}(\theta) \exp i(\omega t + \varphi_m) \times \dots}{\sum_{m=1}^M \sum_{n=1}^M E_m E_n F_{c_m}(\theta) F_{c_n}(\theta) \exp i(\omega t + \varphi_m) \times \dots \times \exp -i(\omega t + \varphi_n) \dots \times \exp -i(\omega t + \varphi_n) \dots} =$$

$$= \frac{\sum_{m=1}^M \sum_{n=1}^M E_m E_n [F(\theta_0 - \theta_m) F(\theta_0 - \theta_n) - \dots]}{\sum_{m=1}^M \sum_{n=1}^M E_m E_n [F(\theta_0 - \theta_m) F(\theta_0 - \theta_n) + \dots - F(\theta_0 + \theta_m) F(\theta_0 + \theta_n)] \cos(\varphi_m - \varphi_n) \dots} \quad (5.29)$$

Given the proper approximation of the antenna radiation patterns and equating the numerator in expression (5.29) to zero, we can find the condition of servosystem equilibrium with the reception of signals from the given set of point radiators of a complex target and, consequently, the position of the point to be tracked by the radar system. Comparing the position of the point of equilibrium with the

position of the geometric center of the complex target, we can determine the error in direction finding in each specific case.

With small angular deviation θ_k , linearization of the antenna pattern is valid;

$$F(\theta_0 \pm \theta_k) = F(\theta_0)(1 \mp \mu \theta_k).$$

Then expression (5.29), which defines the equivalent direction finding characteristic of the system, assumes simplified form:

$$S(\theta) = \mu \frac{\sum_{m=1}^M \sum_{n=1}^M E_m E_n \theta_n \cos(\varphi_m - \varphi_n)}{\sum_{m=1}^M \sum_{n=1}^M E_m E_n \cos(\varphi_m - \varphi_n)} \quad (5.30)$$

We can show that expression (5.30) agrees with the expression for the phase front of the resulting wave of a multipoint target [21, 97]. Analysis also shows [43] that the equation defining the direction finding of a set of point sources, with small angular deviation, is identical to the equation of the resulting poynting vector.

In the general case, when angular deviations of sources are great and linearization of the antenna radiation pattern is not valid, the bearing will not coincide with the direction of the poynting vector and the normal to the face front. The reason for this noncorrespondence can be established by a comparison of expressions (5.29) and (5.30), determining the conditions for direction finding in both examined cases.

When taking into account nonlinearity of radiation pattern, as can be seen from expression (5.29), equisignal direction is generally determined by three factors; field intensity of each of the sources, position of sources in space, and characteristic (pattern) of antenna directivity. Depending upon the parameters of the antenna radiation pattern, the position of equisignal direction during direction

finding of a complex target can vary. This leads to corresponding variations in direction finding error. As for the position of the poynting vector, which can be determined by expression (5.30), it does not depend upon the radar antenna radiation pattern and is determined only by the intensities and special arrangement of the sources. Therefore, when direction finding with extended targets, where the angular dimensions exceed the linear part of a direction finding characteristic, noncorrespondence is inevitable between the bearing and the direction of the poynting vector (normal to phase front). This noncorrespondence is greater, the greater the target dimension and the narrower the antenna radiation pattern.

Under actual conditions, amplitude and phase relationships for signals from a set of sources changes during direction finding according to random law, while generating angular noise and direction finding error fluctuation. The calculation of errors, in this case, should be performed taking into account the spectral composition of angular noise, the parameters of the AGC system, and the bandwidth of the servosystem.

Basic conclusions with respect to complex target direction finding by an amplitude monopulse sum-difference system can be extended to monopulse systems of other types, as well as systems with conical beam scanning [38].

Taking into account the sphericity of phenomena connected with the nature of target noises and the importance of their examination during the evaluation of the accuracy of monopulse radar systems, we shall pause briefly on measurement methodology and target noise analysis.

5.2.4. Measurement methodology and target noise analysis.

Angular noises cannot be detected by a simple observation of reflected signals from a target of complex form and, in order to measure them, it is necessary to develop special methods.

As an example we shall examine experimental studies on fluctuation in a signal reflected from a target, presented in reference [19]. The studies were carried out with a modernized pulse radar of the Mk-50 type, under conditions of automatic aircraft tracking. The modernization of the radar consisted of using a double set of receivers, operating on one antenna. One of the sets was used for autotracking in the passive target finding mode on signals from a responder beacon installed on the aircraft, and the other for tracking the target on reflected signal. The servosystem of the latter set was released and did not participate in guiding the antenna to the target to be tracked.

The first set of the equipment made it possible to measure rather accurately the direction to target under the condition of no angular noise. Fluctuations of error signal at output of this set were caused only by the regular errors of tracking a virtually unfluctuating signal source. The second set had the capability of measuring error signal with angular and amplitude noises taken into account on the signals reflected from the target. By measuring voltages at error signal detector output and subtracting one result from the other, we can obtain the voltage whose value is proportional to angular error between directions to true and apparent target position.

Amplitude noise was measured by recording instantaneous oscillations in the level of signals reflected from target relative to average level. Since accurate determination of statistical quantities necessary in target noise analysis requires a very large amount of data, a magnetic record of errors was used with the subsequent reproduction and processing of it by special analyzers.

The block diagram of the recording device and error signal reproduction is illustrated in Fig. 5.11. To exclude the difficulty of direct magnetic recording of subsonic signals, amplitude modulation by a higher-frequency carrier signal was used. Recording rate was 12.7 mm/s; playback rate, 380 mm/s.

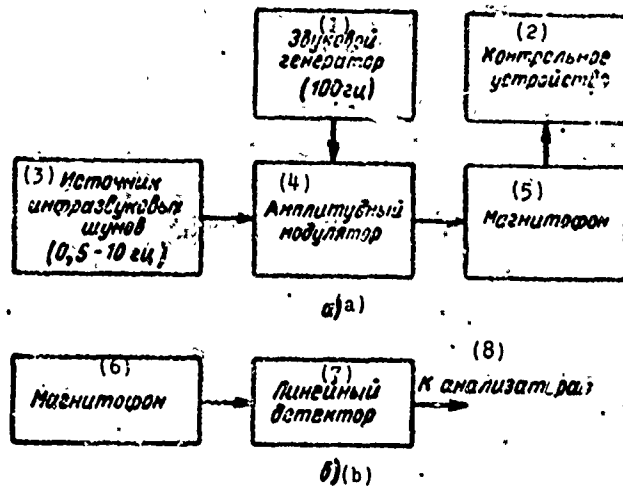


Fig. 5.11. Block diagram of installation: a) for recording subsonic noises; b) for reproducing them.

KEY: (1) Sonic generator (100 Hz); (2) Monitor; (3) Subsonic noise source (0.5-10 Hz); (4) Amplitude modulator; (5) Tape recorder; (6) Tape recorder; (7) Linear detector; (8) To analyzers.

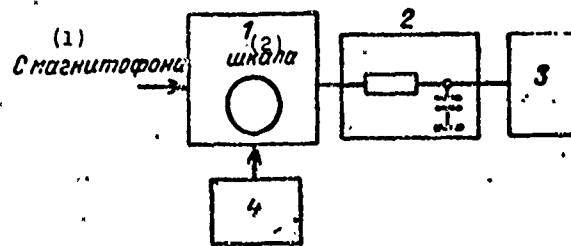


Fig. 5.12. Block diagram of equipment for analyzing noise power spectrum distribution: 1 - main spectral analyzer; 2 - integrator ($R = 20 \text{ k}\Omega$, $C = 50 \text{ }\mu\text{F}$); 3 - recorder; 4 - cam drive of analyzer for linear scan.

KEY: (1) From magnetic recorder; (2) Scale.

The block diagrams of equipment for analyzing noise power spectrum distribution and amplitude distribution are presented in Figs. 5.12 and 5.13. The curve at distribution analyzer output directly indicates amplitude distribution density.

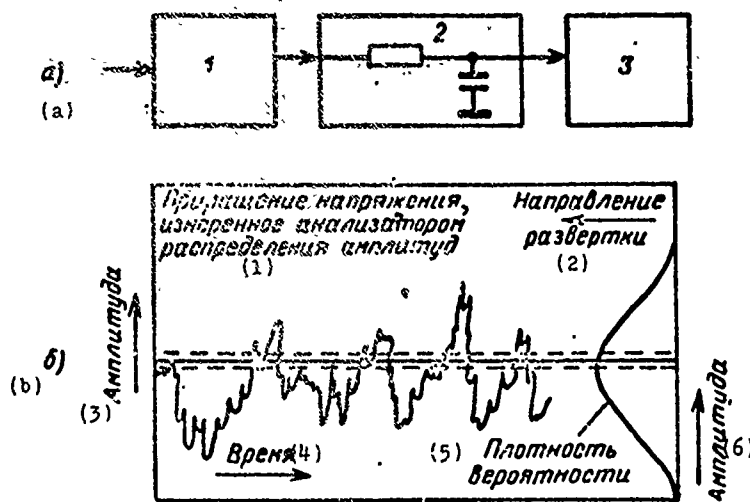


Fig. 5.13. Block diagram of the installation for analyzing amplitude distribution (a) and a sample of the working graph (b): 1 - amplitude distribution analyzer; 2 - integrator ($R = 100 \text{ k}\Omega$, $C = 50 \text{ }\mu\text{F}$); 3 - recorder.

KEY: (1) Increment of voltage measured by amplitude distribution analyzer; (2) Direction of scan; (3) Amplitude; (4) Time; (5) Probability density; (6) Amplitude.

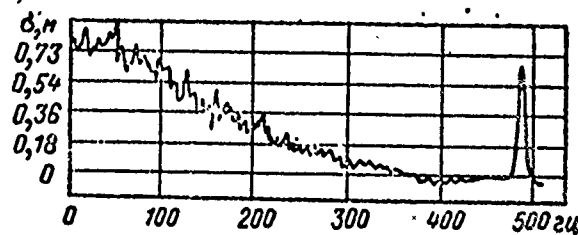


Fig. 5.14. Sample of recording of typical angular noise spectrum from aircraft.

An example of a recording of the angular target noises spectrum is presented in Fig. 5.14. Since, with reproduction, there occurred a broadening of the frequency spectrum by a factor of 30, the actual spectrum of noise components is obtained by dividing the scale along the axis of abscisses (Fig. 5.14) by 30. The jaggedness of the spectrum is caused by the insufficiently completed time integration of the reading period and can be ignored in analysis. The spike at the end corresponds to calibration signal.

By means of calibrating the radar station, voltage at detector output can be expressed in quantities of linear target tracking error. In Fig. 5.14, along the axis of ordinates are the mean values of noise (expressed in linear units of direction finding error) obtained at output of the analyzer with bandwidth 4 Hz.

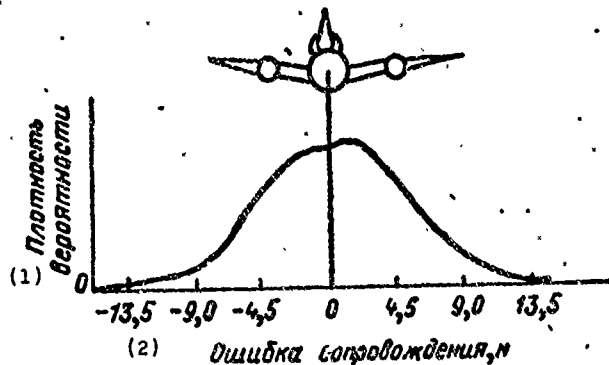


Fig. 5.15. Probability distribution of noise amplitudes plotted according to data on angular target noises.
KEY: (1) Probability density; (2) Tracking error, m.

Interpretation of the curves of angular noise amplitude distribution is relatively simple. Plotted in units of linear errors, the angular noise amplitude distribution curve enables us to evaluate the possibility of deviation in equisignal direction beyond the physical dimensions of the target (Fig. 5.15). As a result of experimental studies it has been established that the scattering of radio waves by the target from two reflectors, in a number of cases, causes a deviation of apparent position toward actual position at a distance several times exceeding target dimensions.

§ 5.3. THE EFFECT OF INTERNAL RECEIVER NOISES ON DIRECTION FINDING ACCURACY

The nature of internal noises is varied. The main reasons for their occurrence include thermal noises connected with the chaotic

motion of electrons in conductors at temperatures not equal to absolute zero, the shot effect caused by the random character of the arrival of electrons at the anode (grid) of electronic tubes and the passage of the barrier layer in semiconductors, and the flicker effect caused by the nonuniformity of electron emission in electronic and semiconductor instruments.

Because of their nature, noises always occur in a receiver and potentially represent the natural sensitivity boundary and the achievable measurement accuracy. Being amplified along with the useful signal, noises, to the same extent, disturb the structure of the error signal, cause fluctuation in it, and determine the zone of system insensitivity to the measured parameter.

In order to establish the character of the effect of internal receiver noises on direction finding accuracy, we shall examine an amplitude sum-difference monopulse system. In the examination we shall limit ourselves to the case of direction finding in one plane by a system with identical receiving channels. Because of the independence of errors in the receiving channel, such an examination enables us to judge errors in two planes of direction finding. Taking into account the allowances made, the signals at i-f amplifier output of the sum and difference channels, with accuracy up to the constant coefficient, can be presented in the accepted designations in the form of the following expressions:

$$u_c(t, \theta) = \sqrt{2} \kappa E_m F(\theta_0) \cos \omega_{np} t + u_{uc}(t), \quad (5.31)$$

$$u_p(t, \theta) = \sqrt{2} \kappa E_m F(\theta_0) \mu \theta \cos \omega_{np} t + u_{up}(t), \quad (5.32)$$

where $u_{uc}(t)$, $u_{up}(t)$ are noise voltages at i-f amplifier output of the sum and difference channels.

When a monopulse radar is operating in target tracking mode, the signal/noise ratio in the receiver is usually much greater than one and the displacement angle is small. This makes it possible to

disregard the effect of noises in the sum channel. Then expressions (5.31) and (5.32) can be rewritten in the form

$$\begin{aligned} u_c(t, \theta) &= \kappa E \cos \omega_{np} t, \\ u_p(t, \theta) &= \kappa E \mu \theta \cos \omega_{np} t + u_{np}(t), \end{aligned} \quad (5.33)$$

where

$$E = \sqrt{2} E_m F(\theta_0). \quad (5.34)$$

Error signal voltage at the output of a multiplication-type phase detector without taking into account standardization with respect to sum signal and taking into account the filtration of the high-frequency components, with accuracy up to the constant component, is defined as

$$S(\theta) = \frac{1}{2} \kappa^2 E^2 \mu \theta + \kappa E u_{np}(t) \cos \omega_{np} t. \quad (5.35)$$

The first term of the obtained expression is the useful component determining the displacement angle of the target relative to equisignal direction of the antenna. The second term determines the interference caused by the presence of internal noises in the difference channel of the receiver. Obviously the noise component of the error signal is created only by those frequency components of the noise spectrum which are grouped near the i-f amplifier tuning frequency and do not differ in frequency more than the bandwidth of the servosystem.

For a quantitative evaluation of this component let us find the spectral density of the error signal determined by the second term (5.35). We shall use the method based on determining the correlation function of the noise component of the error signal [18]

$$\begin{aligned} R(\tau) &= \kappa^2 E^2 \overline{u_{np}(t) u_{np}(t + \tau) \cos \omega_{np} t \cos \omega_{np} (t + \tau)} = \\ &= \frac{\kappa^2 E^2}{2} R_{np}(\tau) \cos \omega_{np} \tau, \end{aligned} \quad (5.36)$$

where $R_{\Pi\Upsilon}(\tau)$ is the correlation function of the internal noises of the difference channel at i-f amplifier output.

As we know, $R_{\Pi\Upsilon}(\tau)$ can be presented in the form

$$R_{\Pi\Upsilon}(\tau) = r(\tau) \cos \omega_{np}\tau, \quad (5.37)$$

where $r(\tau)$ is a slowly changing function whose character is determined by the width and the form of the frequency characteristic of the i-f amplifier.

Substituting (5.37) into (5.36) and taking into account the filtering of the frequency component $2\omega_{np}$ at phase detector output, we obtain

$$R(\tau) \approx \frac{1}{4} \kappa^2 E^2 r(\tau). \quad (5.38)$$

Hence we can find the dispersion of error signal fluctuations at phase detector output

$$\sigma^2 = R(0) = \frac{1}{4} \kappa^2 E^2 r(0). \quad (5.39)$$

Since $r(0)$ is the dispersion of noise voltage at i-f amplifier output, then

$$\sigma^2 = \frac{1}{4} \kappa^2 E^2 \sigma_w^2 = \frac{1}{4} \kappa^2 E^2 S_w \Delta f, \quad (5.40)$$

where Δf is the effective bandwidth of the i-f amplifier;

S_w is the spectral power density of noises at i-f amplifier input.

At output of the phase detector, in an automatic target tracking radar, taking into account standardization during an ideally operating

AGC or at standardization circuit output in surveillance radars (with the same μ) we can write

$$\sigma_H^2 = \frac{S_m \Delta f}{k^2 E^2 \mu^2}. \quad (5.41)$$

Then it reduces to finding the power spectrum of the fluctuation in the bandwidth of the servosystem of an automatic tracking radar or in the band of the smoothing filter (the device for secondary information processing) of a surveillance radar.

From the theory of random processes we know that with noise amplitude modulation the power spectrum of the process has the same form as the spectrum of a single pulse, but its intensity is proportional to the dispersion of noises and the pulse repetition frequency

$$G(\omega) = \frac{2}{T_n} |g(\omega)|^2 \sigma_H^2, \quad (5.42)$$

where $g(\omega)$ is the spectrum of a single pulse;
 T_n is the pulse repetition period.

If we assume that the phase detector operates on the principle of the so-called key peak detector when voltage at its output during each pulse repetition period is established practically instantaneously equal to the maximum value of input voltage and is then maintained unchanged to the end of the repetition period, after which it abruptly drops to zero; then the output voltage of the phase detector will have the form of a pulse with a length equal to the pulse repetition period T_n and its spectrum can be expressed as

$$g(\omega) = T_n \frac{\sin \frac{\omega T_n}{2}}{\frac{\omega T_n}{2}}. \quad (5.43)$$

Hence the power spectrum of the fluctuations of output error voltage

$$G(\omega) = 2\sigma_H^2 T_n \left(\frac{\sin \frac{\omega T_n}{2}}{\frac{\omega T_n}{2}} \right)^2. \quad (5.44)$$

Since the servosystem is narrow-band, random error will be caused by only those components of the fluctuation spectrum which adjoin zero frequency. In this case,

$$G(0) \approx 2\sigma_n^2 T_n. \quad (5.45)$$

Finding the spectral density of error signal fluctuations, we can find the average value of direction finding error caused by the effect of internal receiver noises according to formula

$$\sigma_\theta \approx \sqrt{G(0)\Delta F_{cc}}, \quad (5.46)$$

where ΔF_{cc} is the equivalent bandwidth of the servosystem or the smoothing filter.

Substituting into (5.46) expressions (5.41) and (5.45) and performing simple transformations, we obtain

$$\begin{aligned} \sigma_\theta &= \sqrt{\frac{2S_{\text{ш}}\Delta f}{\kappa^2 E^2 \mu^2} T_n \Delta F_{cc}} = \\ &= \frac{1}{\mu} \sqrt{\frac{P_{\text{ш}}}{P_{\text{ср}}}} = \frac{1}{\mu \sqrt{\frac{P_{\text{ср}}}{P_{\text{ш}}}}}, \end{aligned} \quad (5.47)$$

where $P_{\text{ш}} = S_{\text{ш}}\Delta f\Delta F_{cc}$ is the power of noises in the band of the servosystem;

$P_{\text{ср}} \approx \frac{\kappa^2 E^2}{2T_n}$ is the average power of the signal at receiver output.

As is apparent from the expression presented, the value of standard error caused by the effect of internal noises is inversely proportional to the steepness of the direction finding characteristic and the signal/noise ratio at receiver output.

For a monopulse system with amplitude direction finding, as shown in Chapter 2, intersection of radiation patterns at the half-power level is optimal, i.e., when $\theta_0 = \theta_{0.5}/2$.

In this case, $\mu \approx 1/\theta_0$ and

$$\sigma_s = \frac{0.5\theta_{0.5}}{\sqrt{\frac{P_{cp}}{P_m}}} \quad (5.48)$$

We should mention that internal receiver noises include the category of not fully removable factors which impair the processing of signals received and represent a natural barrier to improving direction finding accuracy. Therefore, angular errors caused by internal receiver noises determine the maximum possible accuracy of angular measurement radar systems. With high signal/noise ratios expression (5.48) determines the potential accuracy of direction finding in a monopulse system. With the purpose of establishing the connection between maximum accuracy and the bandwidth of the receiver and servosystem, we shall transform ratio P_{cp}/ω taking into account the radar radiation mode.

With pulsed radiation this ratio is

$$\frac{P_{cp}}{P_m} = \frac{P_n \tau f_n \Delta f}{S_m \Delta F_{ee} \Delta f} \quad (5.49)$$

where P_n is the pulse power of the signal at receiver input;
 τ is pulse duration;
 f_n is pulse repetition frequency.

Since the receiving system is matched and $\tau \Delta f \approx 1$, while $P_{\omega n} = S_m \Delta f$ is the power of the noise in the receiver bandwidth, expression (5.49) is transformed to

$$\frac{P_{cp}}{P_m} = \frac{P_n}{P_{zn}} \frac{f_n^2}{\Delta F_{ee}} \quad (5.50)$$

Ratio $f_n^2/\Delta F_{ee}$ is the number of integrated pulses of the signal received.

When the radar is operating in continuous radiation mode

$$\frac{P_{cp}}{P_{is}} = \frac{P_{cp}}{P_{is,n} \Delta F_{ce}} \quad (5.51)$$

Consequently,

$$\sigma_0 = \frac{C_{e,s}}{k_{\omega}} \quad (5.52)$$

where $k_{\omega} = 2 \sqrt{\frac{P_{ifn}}{P_{is,n} \Delta F_{ce}}}$ is for a pulsed radar and

$k_{\omega} = 2 \sqrt{\frac{P_{cp}}{P_{is,n} \Delta F_{ce}}}$ is for a continuous radar.

Obviously, the higher the coefficient k_{ω} the higher the maximum direction finding accuracy of the radar system.

We should mention that the effect of internal receiver noises on direction finding accuracy in monopulse radars and radars with conical scanning is somewhat different. This was explained by the quantitative difference of the receiver noises penetrating the servosystem bandwidth and the design of a different antenna system. In a monopulse system where the signals received are not artificially modulated, from the receiver noise spectrum only those of frequency components affect the servosystem, which appear within its doubled bandwidth, located symmetrically relative to each frequency component of the received signal spectrum (Fig. 5.16).

In direction finding systems with conical scanning the signals received are modulated with respect to amplitude with the scanning frequency, and the doubled pass bands of the servosystem, which determine the parts of the noise spectrum which will affect the servosystem, are located on both sides of each frequency component of the received signals at the distance of the scanning frequency (Fig. 5.17). As a result, in systems with conical scanning, as compared with a monopulse system, there is a doubling of the equivalent

bandwidth of the servosystem with respect to the internal receiver noises affecting it and, with identical values for the signal/noise ratio in the i-f amplifier and identical bandwidth of the servosystem, the power of noise at servosystem output for a radar with conical beam scanning will be twice as great as in a monopulse radar. Therefore, maximum accuracy of a monopulse radar is higher than it is for a radar with conical scanning.

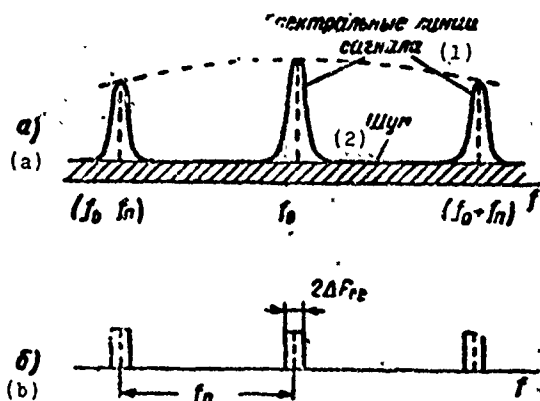


Fig. 5.16. Passage of signal and noise in monopulse radar: a) elements of the spectrum of signal and noise; b) servosystem bandwidth.

KEY: (1) Signal spectral lines; (2) Noise.

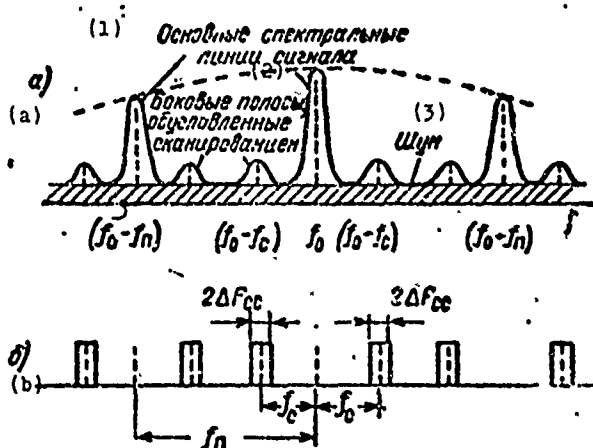


Fig. 5.17. Passage of signal and noise in radar with conical scanning: a) elements of spectrum of signal and noise; b) bandwidth of servosystem.

KEY: (1) Main signal spectral lines; (2) Side bands caused by scanning; (3) Noise.

The advantages of monopulse radars with respect to the effect of internal receiver noises on direction finding accuracy are also due to the fact that in the tracking process the target is irradiated by the maximum radiation pattern and signal losses due to nonagreement of the radiation pattern with the antenna axis, which occurs in radars with conical scanning, are virtually absent. This provides in the receiving channel of a monopulse system a higher signal/noise ratio than in systems with conical scanning.

Taking into account the higher steepness of the direction finding characteristic and the above listed factors enables us to evaluate the power advantage of a monopulse system with respect to internal receiver noises during target tracking from a reflected signal of 5.2 dB [4].

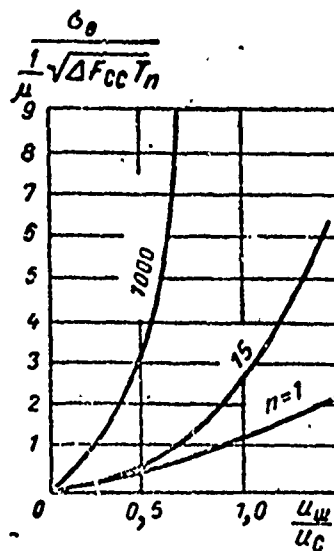


Fig. 5.18. The dependence of error in automatic tracking on the gating factor.

At great distances the signal/noise ratio is too low for normal target tracking and then target losses are possible. Because of this, the quality of receiver operation, in certain cases, is evaluated in terms of the loss norm, by which we mean the frequency (number of times per second) with which tracking error exceeds the maximum allowable value [44].

In deriving formula (5.48), we assumed the presence of ideal gating when noises act only during the reception of the useful signal. If this is the case and the gating duration exceeds signal pulse duration, average errors σ_θ increase. Figure 5.18 presents a graph showing the dependence of tracking error on gating factor [18], by which we mean the ratio of selected pulse duration to signal pulse duration. As is apparent from the figure, an increase in the gating factor can lead to a considerable increase in tracking errors. This method of evaluating tracking errors, valid when $P_c/P_m \gg 1$, can be used also for evaluating other types of monopulse systems. Analysis shows that tracking errors caused by the effect of internal receiving noises are of the same order for both phase and amplitude monopulse methods of direction finding.

Let us examine the effect of internal receiver noises on direction finding accuracy in monopulse radars with a phased antenna array, which occupies a rather unique position in the family of monopulse direction finders because of the multichannel structure of the angle-data transmitter.

§ 5.4. ERRORS CAUSED BY RECEIVER NOISES IN MONOPULSE RADARS WITH PHASED ANTENNA ARRAY

In our examination of errors in determining angular coordinates, caused by receiver noises in radars with phased antenna array, we shall assume that a plane wave falls on a linear array at angle θ_ϕ to its axis and at the output of each array element (Fig. 2.22) an amplifier is installed [6]. Then voltage at amplifier output in the k -th channel can be represented in the form

$$u_k = E_m \cos(\omega t + \varphi_{0n} + k\Delta\varphi) + n_k, \quad (5.53)$$

where φ_{0n} is the reference phase;

$\Delta\varphi$ is the phase difference in mixed channels

$$\Delta\varphi = \frac{2\pi l_p}{\lambda} \cos\theta_p,$$

n_k is the noise in the k -th channel.

We shall assume that reference phase $\phi_{0\pi}$ is unknown and noises in channels are independent, normally distributed, and can be written in the form

$$n_k = x_k \cos \omega t + y_k \sin \omega t, \quad (5.54)$$

where x_k and y_k is the quadrature in the k -th channel.

Average value of $\bar{x}_k = \bar{y}_k = 0$, and $\overline{x_k^2} = \overline{y_k^2} = \overline{n_k^2} = \sigma_w^2$.

The ratio of signal power to noise in each channel will be

$$q^2 = \frac{P_c}{P_w} = \frac{E_m^2}{2\sigma_w^2}. \quad (5.55)$$

Under these conditions we find the difference phase $\Delta\phi$ measurement error, according to which it is easy to find the angle value θ_p determination error. Let there be a series of readings u_k , obtained as a result of the instantaneous measurement of voltages at output N of array channels. If to calculate measurement error $\Delta\phi$ we use the theory of mathematical statistics and designate the approximate value of $\Delta\phi$ in terms of $\Delta\phi^*$, then for an antenna array having one beam the minimum value of variance for the quantity $\Delta\phi^*$ is determined by expression [6]

$$\sigma_{\Delta\phi^*}^2 = \frac{1^2 \sigma_w^2}{(N^2 - N) E_m^2} = \frac{6}{(N^2 - N) q^2}. \quad (5.56)$$

Error is calculated on an example of a monopulse system with amplitude direction finding. In such systems the antenna array forms two beams, as shown in Fig. 2.23. In order to distinguish angular information, two sum signals u_{ϕ_1} and u_{ϕ_2} are detected and then subtracted.

Sum voltage for each beam can be written in the form

$$u_{\phi_1} = \sum_{n=1}^N [E_n \cos(\omega t + \varphi_{0n} + \kappa \Delta \varphi + \kappa \delta \varphi) + x_n \cos(\omega t + \kappa \delta \varphi) + y_n \sin(\omega t + \kappa \delta \varphi)], \quad (5.57)$$

$$u_{\phi_2} = \sum_{n=1}^N [E_n \cos(\omega t + \varphi_{0n} + \kappa \Delta \varphi - \kappa \delta \varphi) + x_n \cos(\omega t - \kappa \delta \varphi) + y_n \sin(\omega t - \kappa \delta \varphi)], \quad (5.58)$$

where $\delta \varphi$ is the phase increment necessary for the beam to be displaced by angle θ_0 .

Under the condition of preserving information about relative phases of noises, the sum voltages can be presented in the form:

$$u_{\phi_1} = A_1 \cos \omega t + B_1 \sin \omega t, \quad (5.59)$$

$$u_{\phi_2} = A_2 \cos \omega t + B_2 \sin \omega t, \quad (5.60)$$

where

$$A_1 = \sum_{n=1}^N [E_n \cos(\varphi_{0n} + \kappa \Delta \varphi + \kappa \delta \varphi) + x_n \cos \kappa \delta \varphi + y_n \sin \kappa \delta \varphi],$$

$$B_1 = \sum_{n=1}^N [-E_n \sin(\varphi_{0n} + \kappa \Delta \varphi + \kappa \delta \varphi) - x_n \sin \kappa \delta \varphi + y_n \cos \kappa \delta \varphi], \quad (5.61)$$

$$-x_n \sin \kappa \delta \varphi + y_n \cos \kappa \delta \varphi], \quad (5.62)$$

$$A_2 = \sum_{n=1}^N [E_n \cos(\varphi_{0n} + \kappa \Delta \varphi - \kappa \delta \varphi) + x_n \cos \kappa \delta \varphi - y_n \sin \kappa \delta \varphi], \quad (5.63)$$

$$B_s = \sum_{s=1}^N [-E_m \sin(\varphi_{0s} + \kappa\Delta\varphi - \kappa\delta\varphi) + x_s \sin \kappa\delta\varphi + y_s \cos \kappa\delta\varphi]. \quad (5.64)$$

Let us examine square-law and linear detection. At output of square-law detectors we shall have

$$\rho_1^2 = A_1^2 + B_1^2; \quad \rho_2^2 = A_2^2 + B_2^2. \quad (5.65)$$

After subtraction we obtain

$$\rho_0 = \rho_1^2 - \rho_2^2. \quad (5.66)$$

Standard measurement error $\Delta\phi_1$ depends upon standard error σ_{ρ_0} in determining ρ_0 , caused by noise, and derivative ρ_0 with respect to $\Delta\phi$ in the absence of noises, i.e.

$$\sigma_{\Delta\phi} = \frac{\sigma_{\rho_0}}{d\rho_0/d\Delta\phi}. \quad (5.67)$$

With the substitution into equation (5.66) of the corresponding values determined by expressions (5.61)-(5.65), without taking noises into account, we obtain

$$\rho_0 = E_m^2 \left[\frac{\sin^2 \frac{N}{2} (\Delta\varphi + \delta\varphi)}{\sin^2 \frac{1}{2} (\Delta\varphi + \delta\varphi)} - \frac{\sin^2 \frac{N}{2} (\Delta\varphi - \delta\varphi)}{\sin^2 \frac{1}{2} (\Delta\varphi - \delta\varphi)} \right]. \quad (5.68)$$

Differentiating equation (5.68) with respect to $\Delta\phi$, we obtain in equisignal direction

$$\left. \frac{d\rho_0}{d\Delta\varphi} \right|_{\Delta\varphi=0} = \frac{E_m^2 \left[N \sin(N\delta\varphi) \sin^2 \left(\frac{\delta\varphi}{2} \right) - \sin \delta\varphi \sin^2 \left(\frac{N\delta\varphi}{2} \right) \right]}{\sin^4 \left(\frac{\delta\varphi}{2} \right)}. \quad (5.69)$$

Variance of error in determining ρ_0 , caused by noises, is determined by expression

$$\sigma_{\rho_0}^2 = \overline{(\rho_0 - \rho_a)^2}. \quad (5.70)$$

With a large signal/noise ratio this variance will be [6]

$$\sigma_{\rho_0}^2 = 2E_m^2 \sigma_m^2 \left[\frac{4N \sin^2\left(\frac{N\delta\varphi}{2}\right) \sin \delta\varphi + \sin(2N\delta\varphi) - 2 \sin(N\delta\varphi)}{\sin \delta\varphi \sin^2\left(\frac{\delta\varphi}{2}\right)} \right]. \quad (5.71)$$

Substituting the obtained values of $\sigma_{\rho_0}^2$ and $\frac{d\rho_0}{d\Delta\phi}$ into formula (5.67) and disregarding quantities of the second order, we obtain

$$\sigma_{\Delta\varphi}^2 \approx \frac{\sigma_m^2}{2N^2 E_m^2} F(\psi) = \frac{F(\psi)}{4N^2 q^2}, \quad (5.72)$$

where $\psi = N\delta\phi$

$$F(\psi) = \psi^2 \frac{4\psi \sin^2 \frac{\psi}{2} + \sin 2\psi - 2 \sin \psi}{\left(\psi \sin \psi - 4 \sin^2 \frac{\psi}{2}\right)^2}. \quad (5.73)$$

From formula (5.73) it is apparent that function $F(\psi)$ depends upon the phase $\delta\phi$ determining beam displacement by angle θ_0 from equisignal direction. When $\psi \approx \pi$ the patterns will be intersected at the half-power level. From the graph of function $F(\psi)$ presented in Fig. 5.19 it follows that with a variation in ψ from 0 to π angular coordinate measurement error does not depend upon displacement angle θ_0 . With an increase in displacement angle more than a half-width of the radiation pattern, this error will rise.

With beam displacement angle composing less than a halfwidth of the radiation pattern, $F(\psi) = 24$ and, consequently, can be written (with large N)

$$\sigma_{\Delta\varphi}^2 = \frac{6}{q^2 N^2}. \quad (5.74)$$

With small N the quantity $\sigma_{\Delta\phi_1}^2$ is determined by formula (5.56).

With linear detection and large signal/noise ratio variance $\sigma_{\Delta\phi_2}^2$ of the error in determining $\Delta\phi_2$, obtained similarly, is also determined by formula (5.72):

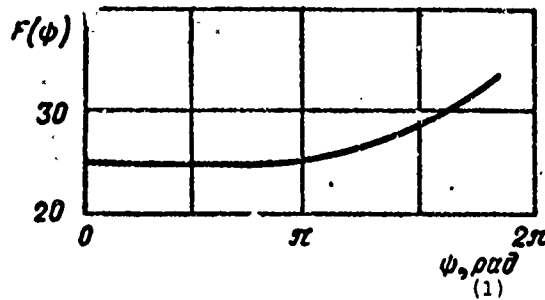


Fig. 5.19. Graph of function $F(\psi)$.
KEY: (1) ψ , rad.

§ 5.5. SUM ERROR IN DIRECTION FINDING CAUSED BY THE EFFECT OF TARGET AND RECEIVER NOISES

In order to present the overall character of the angular error components in a direction finding system, caused by different kinds of noises, qualitative dependences of relative values of errors of these components on relative distance to target are presented in Fig. 5.20 [19]. The position of the curve depends on many parameters and characteristics of specific radars and targets. The curves correspond to the typical case of a tracking radar. As is seen from the figure, only errors from angular noises and receiver noises depend upon range; the effect of receiver noises grows in proportion to the square of the distance to target up to the point at which receiver amplification becomes maximum (saturation sets in).

Amplitude noises represent the amplitude of signal modulation relative to its midlevel; therefore, angular errors caused by them do not depend upon distance to target if in the receiver circuit an AGC system is provided which maintains the midlevel of the received signal constant in a wide dynamic range of input signals.

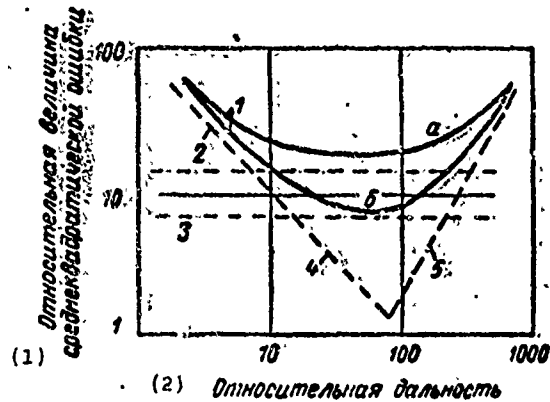


Fig. 5.20. Dependence of standard errors in automatic tracking on target range: 1 - sum error of radar with conical scanning (a) and monopulse radar (b); 2 - errors from amplitude fluctuations; 3 - errors of servosystem; 4 - errors from displacement of reflection center; 5 - errors from receiver noises.
KEY: (1) Relative value of standard error; (2) Relative range.

Angular noises are functions of the angular dimension of the target and the direction finding errors caused by them change in inverse proportion to distance.

In addition to these noises, there are also servosystem noises caused by the presence of zones of insensitivity, play and friction in the electrokinematic links of the antenna control mechanism, zero drift of the δ -c amplifiers, unbalance in the circuits of the drive amplifiers, etc. The value of angular errors caused by servosystem noises depends neither upon the character of the target nor upon range, but is wholly determined by the design peculiarities of the system, the class of accuracy of mechanisms being used, and the operational stability of the corresponding electronic circuits.

Sum error in radar direction finding can be defined as the mean-square value of all the mutually independent errors. Figure 5.20 presents the resulting dependence of angular error on range for a radar with conical beam scanning (a) and a monopulse type radar, for comparison, on the assumption that amplitude noises exceed servosystem noises (b). If the reverse relationship is valid, the advantage of a monopulse system over systems with an equisignal zone becomes insignificant.

These dependences show that at short ranges to target the angular noise is the determining factor in automatic tracking error. At medium ranges angular errors are mainly caused by the fluctuations in reflected signal amplitude and servosystem errors. With long ranges the predominating influence on automatic tracking error is internal receiver noise.

§ 5.6. EFFECT OF AUTOMATIC GAIN CONTROL ON DIRECTION FINDING ACCURACY

The target being tracked by the radar performs the function of an element of a closed tracking circuit; therefore, any changes in the amplitude of a signal reflected from the target can be considered a change in the amplification of such a closed circuit, which, in turn, can directly affect target coordinate measurement accuracy.

Thus, the automatic gain control system of the receiver, designed to keep the amplification of the entire tracking circuit constant with the necessary accuracy, is of great value. Slow-acting and fast-acting AGC systems differ in character.

With a slow-acting AGC system in the tracking circuit there is maintained a constant average amplification. In this case, the AGC does not react to fast changes in the level of reflected signal, because of which rapid signal amplitude fluctuations still have their effect on the amplification of the closed tracking circuit and the error signal fluctuations caused by this. A fast-acting AGC system reacts to most of the amplitude fluctuations and the reflected signal and keeps the tracking circuit amplification constant within a wide variation of reflected signal level.

The effect of the character of the AGC system on direction finding accuracy is examined as an example of an amplitude sum-difference monopulse system. We shall limit ourselves to the case of direction finding in one plane with errors not exceeding the linear part of the direction finding characteristic.

Earlier it was shown that the signal reflected from a complex target can be represented as a sum of signals M of the elementary reflectors forming the target:

$$\dot{E}(t) = \sum_{m=1}^M E_m \exp i(\omega t + \varphi_m). \quad (5.75)$$

In accordance with this, the signals received by the first and second channels of an amplitude monopulse system can be expressed in the following manner:

$$\dot{E}_1(t, \theta) = \sum_{m=1}^M E_m F(\theta_0 - \theta_m) \exp i(\omega t + \varphi_m), \quad (5.76)$$

$$\dot{E}_2(t, \theta) = \sum_{m=1}^M E_m F(\theta_0 + \theta_m) \exp i(\omega t + \varphi_m), \quad (5.77)$$

where with the approximation taken

$$\begin{aligned} F(\theta_0 - \theta_m) &= F(\theta_0)(1 + \mu\theta_m), \\ F(\theta_0 + \theta_m) &= F(\theta_0)(1 - \mu\theta_m). \end{aligned}$$

Angular position of the m -th reflector θ_m relative to the ESD of the direction finder's antenna can be represented in the form of a vector sum (Fig. 5.21)

$$\vec{\theta}_m = \vec{\theta} + \Delta\vec{\theta}_m, \quad (5.78)$$

where $\vec{\theta}$ is the angular position of the center of the target relative to the ESD;

$\Delta\vec{\theta}_m$ is the angular position of the m -th reflector relative to the center of the target.

For the direction finding plane under examination θ_m can be expressed in terms of an algebraic sum of the projections of the corresponding angles to this plane

$$\theta_m = -\theta + \Delta\theta_m. \quad (5.79)$$

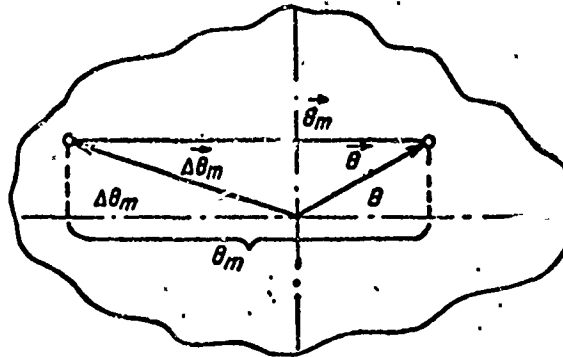


Fig. 5.21. Model of target.

Substituting (5.79) into expressions (5.76), and (5.77) and making the simplification $F(\theta_0) = 1$, we obtain

$$\begin{aligned} \dot{E}_1(t, \theta) &= \sum_{m=1}^M [1 + \mu(-\theta + \Delta\theta_m)] E_m \exp i(\omega t + \varphi_m) = \\ &= (1 - \mu\theta) \dot{E}(t) + \dot{E}_{y_m}(t), \end{aligned} \quad (5.80)$$

$$\begin{aligned} \dot{E}_2(t, \theta) &= \sum_{m=1}^M [1 - \mu(-\theta + \Delta\theta_m)] E_m \exp i(\omega t + \varphi_m) = \\ &= (1 + \mu\theta) \dot{E}(t) - \dot{E}_{y_m}(t), \end{aligned} \quad (5.81)$$

where

$$\begin{aligned} \dot{E}_{y_m}(t) &= \sum_{m=1}^M \mu \Delta\theta_m E_m \exp i(\omega t + \varphi_m) = E_{y_m} \exp i(\omega t + \varphi_m), \\ \dot{E}(t) &= \sum_{m=1}^M E_m \exp i(\omega t + \varphi_m) = E \exp i(\omega t + \varphi). \end{aligned}$$

where E , E_{y_m} are the resulting signal amplitudes;
 ϕ , ϕ_m are the resulting signal phases.

It is easy to see that the first terms contain useful information on the deviation of target center relative to ESD while the second are related to the finite dimensions of the target and are interfering components (angular noise). With slow variation in the mutual position of the radar as a target and relatively high M , the processes $E(t)$ and $E_{y \text{ ш}}(t)$ can be considered stationary normal processes [21] and

$$\overline{\dot{E}(t) \dot{E}_{y \text{ ш}}(t)} = 0.$$

Disregarding the effect of internal receiver noises at the input of the sum and difference channels, taking into account (5.80) and (5.81), we obtain

$$\dot{E}_c(t, \theta) = \sqrt{2} \dot{E}(t), \quad (5.82)$$

$$\dot{E}_p(t, \theta) = \sqrt{2} [\mu \dot{E}(t) - \dot{E}_{y \text{ ш}}(t)]. \quad (5.83)$$

Further processing of signals is carried out with respect to two types of AGC systems: inertialess and inertial.

With inertialess (instantaneous) gain control systems the standardizing signal can be represented as:

$$E_{\text{APY}} = \sqrt{2} E \kappa_c \kappa_{\text{APY}}, \quad (5.84)$$

where κ_c is the transmission factor of the sum channel;
 κ_{apy} is the transmission factor of the AGC circuit.

Taking standardization into account, signals at output of the sum and difference channels, with accuracy up to the constant coefficient, can be represented by expression

$$\dot{u}_c(t, \theta) = \frac{\dot{E}_c(t, \theta)}{E_{\text{APY}}} = \frac{1}{\kappa_{\text{APY}}} \exp i(\omega_{\text{np}} t + \varphi), \quad (5.85)$$

$$\dot{u}_p(t, \theta) = \frac{\dot{E}_p(t, \theta)}{E_{APY}} = \frac{\kappa_p}{\kappa_c \kappa_{APY}} \left[\mu \theta \exp i(\omega_{np} t + \varphi) - \frac{E_{ym}}{E} \exp i(\omega_{np} t + \varphi_m) \right], \quad (5.86)$$

where κ_p is the transmission factor of the difference channel.

Hence signal at phase detector output is

$$u(\theta) = \operatorname{Re} \dot{u}_c(t, \theta) \dot{u}_p^*(t, \theta) = \frac{\kappa_p}{\kappa_c \kappa_{APY}^2} \left[\mu \theta - \frac{E_{ym}}{E} \cos(\varphi - \varphi_m) \right]. \quad (5.87)$$

With an inertial AGC system, when the bandwidth of the AGC system is much less than the spectral band of reflected signal fluctuations, the standardizing signal assumes the form

$$E_{APY} = \sqrt{\bar{E}} \bar{E} \kappa_c \kappa_{APY}, \quad (5.88)$$

where \bar{E} is the average value of the envelope obtained as a result of signal passage through a narrow-band filter.

Then, taking into account expression (5.82) and (5.83), we obtain

$$\dot{u}_c(t, \theta) = \frac{\dot{E}_c(t, \theta)}{E_{APY}} = \frac{E}{\kappa_{APY} \bar{E}} \exp i(\omega_{np} t + \varphi), \quad (5.89)$$

$$\dot{u}_p(t, \theta) = \frac{\dot{E}_p(t, \theta)}{E_{APY}} = \frac{\kappa_p}{\kappa_c \kappa_{APY}} \left[\frac{E}{\bar{E}} \mu \theta \exp i(\omega_{np} t + \varphi) - \frac{E_{ym}}{E} \exp i(\omega_{np} t + \varphi_m) \right]. \quad (5.90)$$

Hence error signal in the presence of an inertial AGC system is

$$u(\theta) = \operatorname{Re} \dot{u}_c(t, \theta) \dot{u}_p^*(t, \theta) = \frac{\kappa_p}{\kappa_c \kappa_{APY}^2} \left[\frac{E^2}{\bar{E}^2} \mu \theta - \frac{E E_{ym}}{\bar{E}^2} \cos(\varphi - \varphi_m) \right]. \quad (5.91)$$

Comparison of expressions (5.87) and (5.91) shows that when $\theta = 0$, when equisignal direction coincides with direction to center of a complex target, error signal is not zero and, with an inertialess AGC system, is

$$u'(\theta) = \frac{\kappa_p}{\kappa_o \kappa_{\Delta \rho \gamma}} \frac{E_{y m}}{E} \cos(\varphi - \varphi_m), \quad (5.92)$$

with an inertial AGC system it is

$$u''(\theta) = \frac{\kappa_p}{\kappa_o \kappa_{\Delta \rho \gamma}} \frac{E E_{y m}}{E^2} \cos(\varphi - \varphi_m). \quad (5.93)$$

With target finding of a point target $\Delta \theta_m = 0$, $E_{y m} = 0$ and $u'(\theta) = u''(\theta)$.

Thus, the obtained expressions point to the fact that with direction finding of a complex target, direction finding errors occur because of angular noises of the target. The values of these errors with linearization of radiation patterns do not depend upon the angular target center tracking error but upon the type of AGC system. With a fast-acting AGC system the effect of angular noises on direction finding accuracy is somewhat greater than with an inertial AGC system. In practical circuits, this difference is usually not great and errors from the effect of angular noise with a fast-acting AGC system do not exceed errors with a slow AGC system by more than a factor of 2-3 [20].

With an inertial AGC, as follows from expression (5.91), the fluctuations of the sum signal affect direction finding accuracy. In order to reduce the effect of the fluctuations, we can limit the sum signal. In this case, error signal can be represented by expression

$$u(\theta) = \frac{\kappa_p U_0}{\kappa_{\Delta \rho \gamma} \kappa_o E} [E \mu \theta - E_{y m} \cos(\varphi - \varphi_m)], \quad (5.94)$$

where U_0 is the threshold signal limitation at sum channel output.

Obviously, with an inertial AGC system, the effect of signal amplitude fluctuation on direction finding accuracy is apparent.

Representing the amplitude of the reflected signal as a sum of the mean and fluctuating components, expression (5.94) can be changed to the form

$$u(\theta) = \frac{\kappa_p U_0}{\kappa_{APY} \kappa_c B} [\bar{E} \mu \theta + \tilde{E} \mu \theta - E_{ym} \cos(\varphi - \varphi_m)], \quad (5.95)$$

where \tilde{E} is the fluctuation component of reflected signal amplitude relative to the mean value \bar{E} .

With a fluctuating signal from a point target

$$u(\theta) = \frac{\kappa_p U_0}{\kappa_{APY} \kappa_c B} [E \mu \theta + \tilde{E} \mu \theta]. \quad (5.96)$$

Hence it follows that with an inertial AGC system amplitude signal fluctuations affect direction finding accuracy and the direction finding system virtually ceases to be a monopulse system since the requirements for signal standardization are not met. The value of error caused by amplitude fluctuations, unlike errors from the effect of angular noises depends upon angular target tracking error and increases with an increase in the latter.

We can evaluate quantitatively the direction finding error from amplitude and angular fluctuations if the corresponding fluctuation distributions and the AGC system parameters are given.

We can use calculation formulas obtained from expressions (5.87) and (5.95) while equating them to zero:

$$\mu \theta = \frac{E_{ym}}{E} \cos(\varphi - \varphi_m). \quad (5.97)$$

$$\mu \theta = \frac{E_{ym}}{B + \tilde{E}} \cos(\varphi - \varphi_m). \quad (5.98)$$

Comparison of expressions (5.97) and (5.98) shows that with a fast-acting AGC error caused by amplitude fluctuations in the reflected signal is zero. As for errors caused by the change in the slope of the reflected signal phase front, they are somewhat greater with a slow AGC. However, with a slow AGC the effect of reflected signal amplitude fluctuations increases.

Figure 5.22 presents the experimental dependences of sum tracking error, caused by amplitude and angular fluctuations of reflected signals, on antenna pointing error in a monopulse system with various values for the AGC bandwidth [20]. Errors are expressed in units of target dimension L_u as a function of errors in the pointing of the direction finding antenna to the center of the target. As a result of experiments, it has been established that with tracking errors equal to half the linear dimension of the target, the level of error with slow and fast AGC is approximately the same. On average and long ranges, when angular target dimensions are small and the effect of internal noises of the autotracking system increases, the effect of angular noises on direction finding accuracy becomes insignificant. With small angles of antenna deviation from direction to target center, direction finding error with a fast-acting AGC system exceeds error with a slow AGC. With short ranges to target, due to an increase in the effect of angular fluctuations, in a number of cases the use of a slow AGC can be advisable.

In the course of experiments it was also noted that low-frequency components of amplitude fluctuations penetrated into the band of the servosystem and additional angular errors occurred because of them. Thus it was indicated that amplitude fluctuations of very low frequency lying within the servosystem bandwidth affect all radar direction finding systems, including monopulse. The degree of their effect depends upon the characteristics of AGC and the bandwidth of the servosystem.

Since the tracking time lag with a slow AGC increases tracking error, the servosystem bandwidth must be increased so as to reduce to minimum the processing time of angular error. However, an increase

in servosystem bandwidth heightens the effect of noises on the system and under certain conditions can lead to loss of target (Fig. 5.23). The effect of internal autotracking system noises rises, which, in turn, with a slow AGC increases error from amplitude fluctuations of reflected signals.

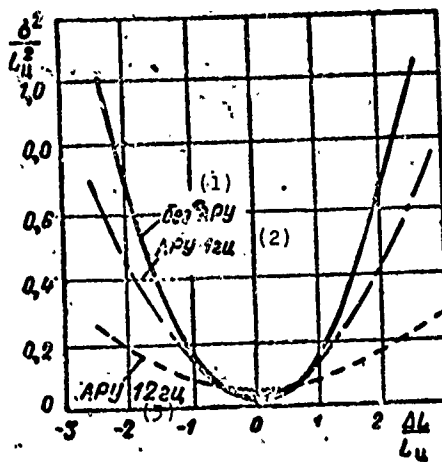


Fig. 5.22. Dependence of standard error caused by amplitude and angular signal fluctuations on error of antenna pointing to target with different AGC bandwidth.

KEY: (1) Without AGC; (2) AGC 1 Hz; (3) AGC 12 Hz.

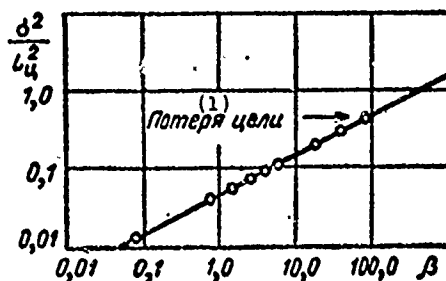


Fig. 5.23. Experimental dependence of standard tracking error on servosystem bandwidth in a radar with low AGC and zero delay error. β - ratio of servosystem bandwidth to width of amplitude spectrum of fluctuations at half power.

KEY: (1) Loss of target.

The advantages of using a fast-acting AGC as compared with a slow-acting one will be the more substantial the greater the internal radar noises and the wider the servosystem bandwidth is required to be with respect to tactical considerations.

Thus, theoretical and experimental studies show that error caused by angular noises decreases with an increase in the time constant of the AGC system. However, with the increase in this constant, error caused by low-frequency amplitude fluctuations of reflected signals, modulating any error signal, also increases. This component is proportional to tracking error and rapidly rises with an increase in the latter. Internal autotracking system noises impair even more the work of the servosystem with a low AGC.

The work of the direction finding servosystem improves with the use of a fast-acting AGC, effectively eliminating the effect of amplitude fluctuations in signals reflected from target. Since the effect of angular target noise on direction finding accuracy rises with this, the selection of AGC parameters must be a compromise. We should try for the minimum possible servosystem bandwidth since an expansion in this bandwidth leads to an increase in the reaction of the angular-measurement radar coordinator to internal and external error sources and thus worsens direction finding accuracy.

§ 5.7. THE EFFECT OF THE DEPOLARIZATION OF REFLECTED SIGNALS ON DIRECTION FINDING ACCURACY

The polarization of waves is determined by the direction of the vector of the electrical field. Most radar antennas operate with linear polarization, with which the direction of the vector of the electrical field is either vertical or horizontal. This is partially explained by the fact that linear polarization is structurally easier to accomplish in equipment.

In addition to linear polarization, we find, although considerably more rarely, the use of circular polarization when the vector of the electrical field turns with the frequency of the signal in a

plane perpendicular to the direction of radio wave propagation, to the right or left. Circular polarization, in addition to the electrical advantages, has other advantages when operating where radio waves pass through layers of the ionosphere and where there are severely disturbing meteorological factors, rain, snow, thunderheads, etc.

However, the polarization formed during the emission of signals, as a rule, is not kept constant and undergoes some sort of distortion, which varies depending upon the operating conditions of the radar. Let us examine reasons for the depolarization of signals and the impairment of direction finding accuracy connected with it.

5.7.1. Reasons for the depolarization of reflected signals. One of the reasons for depolarization is the medium of radio wave propagation. If the radio waves are propagated in a vacuum or in plasma (in the absence of a magnetic field), their polarization is maintained constant.

Actually, radio waves are propagated in atmosphere where different types of inhomogeneities occur including regions of plasma (ionized gas) found in earth's magnetic field. This generates various changes in signal polarization. Thus, for example, during the passage of linearly polarized radio waves through ionized sections, the slope of the polarization plane changes. The direction of polarization rotation for radiated and reflected waves is the same; therefore, the total angle of rotation will be twice as large as it is with radio wave propagation in one direction. Since the value of the angle of polarization plane rotation is not constant and cannot be determined beforehand, linearly polarized waves, returning after reflection from target to radar antenna can have a polarization orthogonal to the radiated wave, as a result of which signal reception and target detection becomes either impossible or target direction finding will have large errors. To avoid this, radars designed for the detection of space targets when the passage of radio waves through sections of the ionosphere is inevitable, as a rule, use circular polarization. A wave with circular polarization, in spite

of the effect of additional rotation of polarization, maintains a polarization near circular; which ensures reliable target tracking.

However, the propagation medium is not the only reason for radio wave depolarization. Another even more important reason is the target itself, reflecting the radio wave. The actual target in the overwhelming majority of cases is a complex reflecting surface. During irradiation, currents with a complex special structure are induced on its surface. As a result of interference phenomena, the resulting radiation field (reflected signal) generated by the currents induced on the target's surface will have a complex structure, as will its polarization. Instead of the radio waves with a stationary polarization state, there will occur the so-called partially polarized waves where, along with regular polarization components, there will be components of a fluctuation character which do not have, because of their indeterminacy, representation on a Poincare polarization sphere. The degree of radio wave depolarization which occurs in this case will be determined mainly by the structure of the target, the parameters and dynamics of its motion; therefore, the depolarizing properties of targets are being widely studied at present and attempts are made to use them for classification and identification of targets [28, 83, 84, 106].

In operations with low-flying targets, when elevation angles are rather small, reflections from ground or water can affect radio signal depolarization. Reflection and refraction factors of radio waves, as we know, depend to a considerable extent upon polarization. Representing the polarization of the incident field in the form of two polarization components - one parallel to the surface of reflection and one orthogonal to it - we can show that the reflected wave will have a distorted (generally elliptical) polarization. Being summed at the reception point with the direct wave from the target, the wave reflected from the ground (water) can further deform the polarization structure of signals received by the radar antenna.

Thus, a radio wave reflected from the target is generally depolarized, i.e., has a polarization unlike the working polarization

of the radar. Along with components agreeing with the radar antenna polarization there can appear regular components significantly different from the main (working) polarization and also irregular (chaotic) components of polarization.

Let us consider to what extent signal depolarization can affect the direction finding accuracy of monopulse radars.

5.7.2. The character of the effect of reflected signal depolarization on direction finding accuracy. The effect of reflected signal of depolarization on direction finding accuracy is mainly caused by the crosspolarization of the receiving antennas.

As was shown in Chapter 2, most antennas used in modern radars have crosspolarization, because of which the radiation pattern of the receiving antenna has a complex polarization structure. Due to this, the parameters of the radiation pattern for the receiving antenna are independent of the polarization of radio waves received.

The calculated radiation pattern occurs in practice with the polarization of signals corresponding to the main (working) polarization of the antenna. In the other cases, the radiation pattern is distorted and is the more noticeably so the more substantially the polarization of signals received differs from the working polarization of the antenna. With signal polarization agreeing with the crosspolarization of the antenna, the expected distortion of the radiation pattern is maximum. In this case, the antenna radiation pattern will be fully determined by the structure of the crosspolarization of the radiation of a given antenna.

Since the radiation pattern on crosspolarization, as can be seen from the figures presented in Chapter 2, agrees neither in form nor position with the radiation pattern on main polarization, such a deformation of pattern inevitably affects direction finding accuracy.

Analysis shows [104] that for linearly polarized antennas a noncorrespondence of polarization in radio waves received with the

working polarization leads to displacement of their equisignal direction with respect to the optical axis of the antenna; the value of the displacement depends both on the value of polarization non-correspondence and the angle of displacement with the tracked source. Beam displacement due to crosspolarization is noticeable also when the direction finding antenna has a beam of circular cross-section. As a rule, the radiation pattern with the alternate reception of signals radiated by orthogonal dipoles is displaced in opposite directions relative to the optical axis of the antenna. On the basis of this we conclude that direction finding errors are approximately double if the radar antenna is designed for the reception of both polarizations.

The dependence of antenna beam direction on the polarization of signals received affects the accuracy of direction finding systems of various types, including those operating on the monopulse method. This is apparent in the example of the transformation of direction finding characteristics depending upon the polarization of reflected signals in an amplitude sum-difference monopulse radar. As a receiving antenna we shall take an antenna of the truncated paraboloid type, designed for tracking a target in one plane.

As we know [41], the direction finding characteristic of an amplitude monopulse radar of the sum-difference type with an instantaneous AGC system can be determined according to formula

$$S(\theta) = \frac{\operatorname{Re} \dot{u}_s(t, \theta) \dot{u}_p^*(t, \theta)}{\dot{u}_s(t, \theta) \dot{u}_s^*(t, \theta)}, \quad (5.99)$$

where $\dot{u}_s(t, \theta)$ and $\dot{u}_p(t, \theta)$ are the complex expressions for signals of the sum and difference receiving channels.

Let us assume that the antenna is linear and the field distribution along its aperture is determined by functions

$$\vec{\psi}_1(x) = \vec{\psi}_{1x}(x) \vec{e}_x + \vec{\psi}_{1y}(x) \vec{e}_y \quad \text{for the first channel} \quad (5.100)$$

$$\vec{\psi}_2(x) = \vec{\psi}_{2x}(x)\vec{e}_x + \vec{\psi}_{2y}(x)\vec{e}_y \quad \text{for the second channel} \quad (5.101)$$

where $\dot{\psi}_{1x}(x)$; $\dot{\psi}_{2x}(x)$ are functions determining the excitation field with respect to the main component of polarization for signals received;

$\dot{\psi}_{1y}(x)$; $\dot{\psi}_{2y}(x)$ are functions determining the excitation field with respect to the crosspolarization component of the signals received;

\vec{e}_x and \vec{e}_y are unit vectors.

We shall define functions $\dot{\psi}_{1x}(x)$ and $\dot{\psi}_{2x}(x)$ as

$$\left. \begin{aligned} \dot{\psi}_{1x}(x) &= \exp i(\kappa x \cos \alpha_0) f_1(x) \\ \dot{\psi}_{2x}(x) &= \exp i(-\kappa x \cos \alpha_0) f_2(x) \end{aligned} \right\} -d \leq x \leq d. \quad (5.102)$$

Assuming the given functions $\dot{\psi}_{1x}(x)$ and $\dot{\psi}_{2x}(x)$ and opposite phase for the lobes of the crosspolarization radiation pattern lying on different sides of the main planes of the antenna aperture, functions $\dot{\psi}_{1y}(x)$ and $\dot{\psi}_{2y}(x)$ for this case can be represented by the following expressions:

$$\left. \begin{aligned} \vec{\dot{\psi}}_{1y}(x) &= a_x \exp i(\kappa x \cos \alpha_0 + \varphi_1) f_1(x) \\ \vec{\dot{\psi}}_{2y}(x) &= a_x \exp i(-\kappa x \cos \alpha_0 + \varphi_1) f_2(x) \end{aligned} \right\} -d \leq x \leq 0, \quad (5.103)$$

$$\left. \begin{aligned} \vec{\dot{\psi}}_{1y}(x) &= a_x \exp i(\kappa x \cos \alpha_0 + \varphi_1 + \pi) f_1(x) \\ \vec{\dot{\psi}}_{2y}(x) &= a_x \exp i(-\kappa x \cos \alpha_0 + \varphi_1 + \pi) f_2(x) \end{aligned} \right\} 0 \leq x \leq d. \quad (5.104)$$

In the above functions the following designations are used:

$2d$ is the antenna aperture dimension;

α_0 is the angle accounting for the asymmetry of the radiation pattern in space relative to equisignal direction;

a_H is the relative amplitude of the field which can be excited with respect to the crosspolarization component of the signals received;

ϕ_1 is the phase shift of fields excitable in the antenna aperture with respect to the main and crosspolarization component.

For the sake of simplification, amplitude distribution of the field along the antenna will be considered uniform and equal to

$$f_1(x) = f_2(x) = 1/2d. \quad (5.105)$$

Let the signal received be defined by the expression

$$\vec{E} = \vec{E}_x \vec{e}_x + \vec{E}_y \vec{e}_y, \quad (5.106)$$

where

$$\vec{E}_x = E_0 \exp i \kappa (x \cos \alpha + y \cos \beta + z \cos \gamma) \quad (5.107)$$

- is the component of the signal agreeing with the main polarization of the antenna,

$$\vec{E}_y = b E_0 \exp i [\kappa (x \cos \alpha + y \cos \beta + z \cos \gamma) + \phi_2] \quad (5.108)$$

- is the component of the signal with polarization orthogonal to the main polarization of the antenna.

Here E_0 is the amplitude of the incident field;

b is the ratio of incident field amplitude to two mutually orthogonal polarizations;

ϕ_2 is the phase shift between orthogonal components of the incident field;

$\cos \alpha$, $\cos \beta$, $\cos \gamma$ are the direction cosines of a spherical system of coordinates.

With direction finding in one plane $y = z = 0$, and

$$\vec{E}_x = E_0 \exp i \kappa x \cos \alpha, \quad (5.109)$$

$$\vec{E}_y = b E_0 \exp i (\kappa x \cos \alpha + \varphi_2). \quad (5.110)$$

Let us determine, under the given conditions, the signals at output of antenna channels:

$$\begin{aligned} \dot{u}_1(\theta) &= \int_S \vec{\psi}_1(x) \vec{E} dx = \int_S [\vec{\psi}_{1x}(x) \vec{E}_x + \vec{\psi}_{1y}(x) \vec{E}_y] dx = \\ &= \frac{E_0}{L} \left\{ \int_{-d}^d \exp i \kappa x (\cos \alpha + \cos \alpha_0) dx + \right. \\ &\quad \left. + a_x b \exp i \Phi \left[\int_{-d}^0 \exp i \kappa x (\cos \alpha + \cos \alpha_0) dx - \right. \right. \\ &\quad \left. \left. - \int_0^d \exp i \kappa x (\cos \alpha + \cos \alpha_0) dx \right] \right\}. \end{aligned} \quad (5.111)$$

$$\begin{aligned} \dot{u}_2(\theta) &= \int_S \vec{\psi}_2(x) \vec{E} dx = \int_S [\vec{\psi}_{2x}(x) \vec{E}_x + \vec{\psi}_{2y}(x) \vec{E}_y] dx = \\ &= \frac{E_0}{L} \left\{ \int_{-d}^d \exp i \kappa x (\cos \alpha - \cos \alpha_0) dx + \right. \\ &\quad \left. + a_x b \exp i \Phi \left[\int_{-d}^0 \exp i \kappa x (\cos \alpha - \cos \alpha_0) dx - \right. \right. \\ &\quad \left. \left. - \int_0^d i \kappa x (\cos \alpha - \cos \alpha_0) dx \right] \right\}. \end{aligned} \quad (5.112)$$

As a result of integration, we obtain

$$\begin{aligned} \dot{u}_1(\theta) &= 2E_0 \left[\frac{\sin m}{m} + 2a_x b \exp i \Phi \frac{\sin^2 m/2}{im} \right] = \\ &= 2E_0 \left[\frac{\sin m}{m} - i 2a_x b \exp i \Phi \frac{\sin^2 m/2}{m} \right], \end{aligned} \quad (5.113)$$

$$\begin{aligned} \dot{u}_2(\theta) &= 2E_0 \left[\frac{\sin n}{n} + 2a_x b \exp i\Phi \frac{\sin^2 n/2}{n} \right] = \\ &= 2E_0 \left[\frac{\sin n}{n} - i2a_x b \exp i\Phi \frac{\sin^2 n/2}{n} \right], \end{aligned} \quad (5.114)$$

where

$$\begin{aligned} m &= kd(\cos a - \cos a_0), \\ n &= kd(\cos a + \cos a_0), \\ \Phi &= \varphi_1 + \varphi_2. \end{aligned}$$

Hence it follows that

$$\begin{aligned} \dot{u}_c(\theta) = \dot{u}_1(\theta) + \dot{u}_2(\theta) &= 2E_0 \left[\frac{\sin m}{m} + \frac{\sin n}{n} - \right. \\ &\left. - i2a_x b \exp i\Phi \left(\frac{\sin^2 \frac{m}{2}}{m} + \frac{\sin^2 \frac{n}{2}}{n} \right) \right], \end{aligned} \quad (5.115)$$

$$\begin{aligned} \dot{u}_p(\theta) = \dot{u}_1(\theta) - \dot{u}_2(\theta) &= 2E_0 \left[\frac{\sin m}{m} - \frac{\sin n}{n} - \right. \\ &\left. - i2a_x b \exp i\Phi \left(\frac{\sin^2 \frac{m}{2}}{m} - \frac{\sin^2 \frac{n}{2}}{n} \right) \right]. \end{aligned} \quad (5.116)$$

Calculation of the numerator and denominator of the direction finding characteristic, respectively, gives the following:

$$\begin{aligned} \operatorname{Re} \dot{u}_c(\theta) \dot{u}_p^*(\theta) &= 4E_0^2 \left[\left(\frac{\sin^2 m}{m^2} - \frac{\sin^2 n}{n^2} \right) + \right. \\ &+ 4a_x b \left(\frac{\sin^2 \frac{m}{2}}{m} \frac{\sin m}{m} - \frac{\sin^2 \frac{n}{2}}{n} \frac{\sin n}{n} \right) \sin \Phi + \\ &\left. + 4a_x^2 b^2 \left(\frac{\sin^4 \frac{m}{2}}{m^2} - \frac{\sin^4 \frac{n}{2}}{n^2} \right) \right], \end{aligned} \quad (5.117)$$

$$\begin{aligned} \dot{u}_c(\theta) \dot{u}_c^*(\theta) &= 4E_0^2 \left[\left(\frac{\sin m}{m} + \frac{\sin n}{n} \right)^2 + \right. \\ &+ 4a_x b \left(\frac{\sin m}{m} + \frac{\sin n}{n} \right) \left(\frac{\sin^2 \frac{m}{2}}{m} + \frac{\sin^2 \frac{n}{2}}{n} \right) \sin \Phi + \\ &\left. + 4a_x^2 b^2 \left(\frac{\sin^2 \frac{m}{2}}{m} + \frac{\sin^2 \frac{n}{2}}{n} \right)^2 \right]. \end{aligned} \quad (5.118)$$

We know that

$$\begin{aligned}\cos \alpha &= \cos \vartheta \sin \theta, \\ \cos \alpha_0 &= \cos \vartheta \sin \theta_0.\end{aligned}$$

For the case of tracking in one plane $\vartheta = 0$ and $\cos \alpha = \sin \theta$, $\cos \alpha_0 = \sin \theta_0$.

Usually $\theta_0 = \theta_{0.5}/2$ where

$$\theta_{0.5} = \frac{A\lambda}{2d}$$

Coefficient A depends upon the type of antennas and for parabolic antennas $A \approx 0.8$.

In accordance with this, expressions m and n can be represented in the forms

$$m = \frac{0.8\pi}{\theta_{0.5}} (\sin \theta - \sin \theta_0), \quad (5.119)$$

$$n = \frac{0.8\pi}{\theta_{0.5}} (\sin \theta + \sin \theta_0). \quad (5.120)$$

After dividing expression (5.117) by (5.118), we obtain an equation defining the direction finding characteristic of the studied monopulse system as a function of the polarization of signals received and the polarization characteristic of the receiving antenna. In accordance with this equation, calculations were made on a computer.

Figure 5.24 illustrates calculated direction finding characteristics for different values of $a_{\kappa} b$ when $\theta_{0.5} = 1^\circ$ and $\varphi = 90^\circ$.

As seen from the figure, an increase in $a_{\kappa} b$ leads to the transformation of direction finding characteristics, which is manifested in a displacement of zero, as well as a change in steepness and form. With an increase in $a_{\kappa} b$ the value of zero displacement for the direction finding characteristic also increases and when $(a_{\kappa} b \rightarrow \infty)$ tends toward the width of the radiation pattern (Fig. 5.25). Beginning

with $a_h b = 0.5$, there is a noticeable asymmetry of the direction finding characteristic. The lobe of the characteristic in whose direction displacement of zero occurs is severely reduced with respect to amplitude.

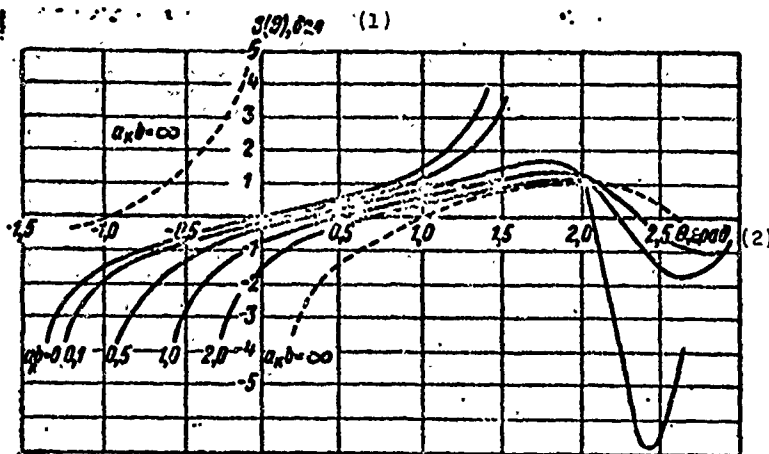


Fig. 5.24. Calculated direction finding characteristics as a function of the value of $a_h b$ when $\phi = 90^\circ$, $\theta_{0.5} = 1^\circ$ and $\theta_0 = 0.5^\circ$.

KEY: (1) div; (2) deg.

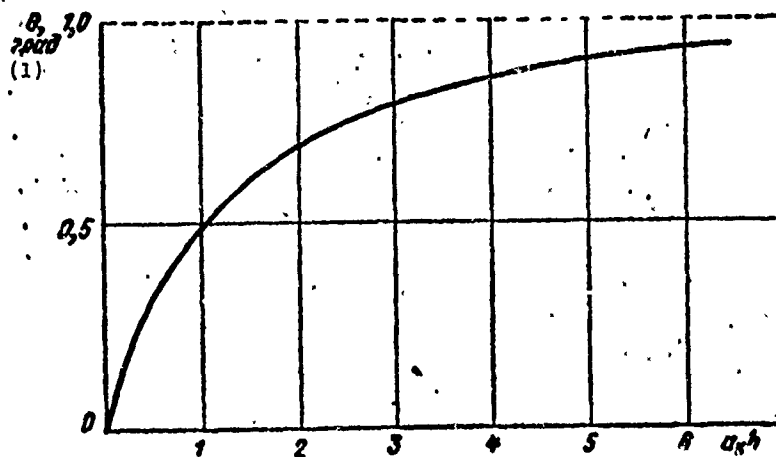


Fig. 5.25. Calculated dependence of the displacement of equisignal direction on the value of $a_h b$ when $\theta_{0.5} = 1.0^\circ$ and $\theta_0 = 0.5^\circ$.

KEY: (1) deg.

The product of $a_H b$ with direction finding of a single signal source physically denotes the ratio of signal amplitude at receiving antenna output, received on crosspolarization, to signal amplitude received on main polarization. Therefore, $a_H b = \infty$ when $a_H < 1$ corresponds to the case where the received signals pass only through the crosspolarization of the antenna and have linear polarization turned precisely 90° relative to the working polarization of the receiving antenna.

The fact of reflected signal depolarization and the related appearance of additional direction finding errors because of the crosspolarization of receiving antennas has been experimentally noted. Thus, in one of the works [130] there are results presented on the radiation pattern measurements in an amplitude sum-and-difference monopulse system on main polarization and crosspolarization. As is apparent from Fig. 5.26 illustrating these measurement results, with the reception of signals with polarization agreeing with the crosspolarization of the receiving antenna, partial patterns of a monopulse system are deformed, as a result of which an equisignal direction is formed which deviates 2° from normal, corresponding to a displacement of 0.45 radiation pattern width at half power.

The presence of nonidentity of amplitude-phase characteristics of receiving channels and the initial tracking errors can intensify the effect of antenna crosspolarization on direction finding accuracy.

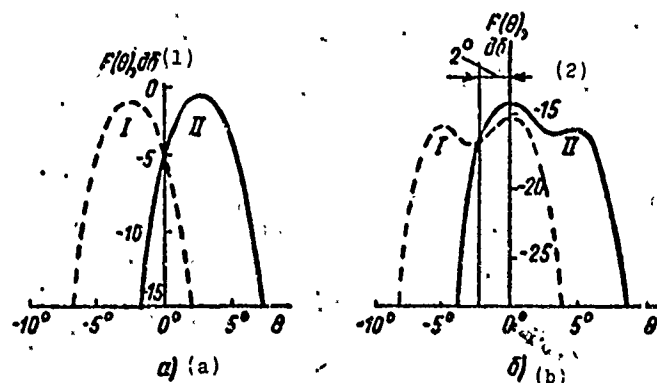


Fig. 5.26. Antenna radiation pattern on an amplitude sum-difference monopulse system: a) for main polarization; b) for crosspolarization. KEY: (1) $F(\theta), \text{dB}$; (2) $F(\theta), \text{dB}$.

Figure 5.27 presents the dependence of equisignal direction displacement on polarization orientation and working frequency, obtained experimentally with the AN/FPS-16 modified monopulse radar with circular polarization under conditions of signal reception with linear polarization [49]. From the figure it is apparent that the value of equisignal direction displacement with a change in the angle of linear polarization orientation and working frequency of received signals changes both in magnitude and in sign and reaches $1.5'$. If we consider that the normal accuracy of angular measurements for the AN/FPS-16 is evaluated by tenths of an angular minute [74], we cannot disregard the displacements obtained in equisignal direction of radiation patterns for the receiving antenna.

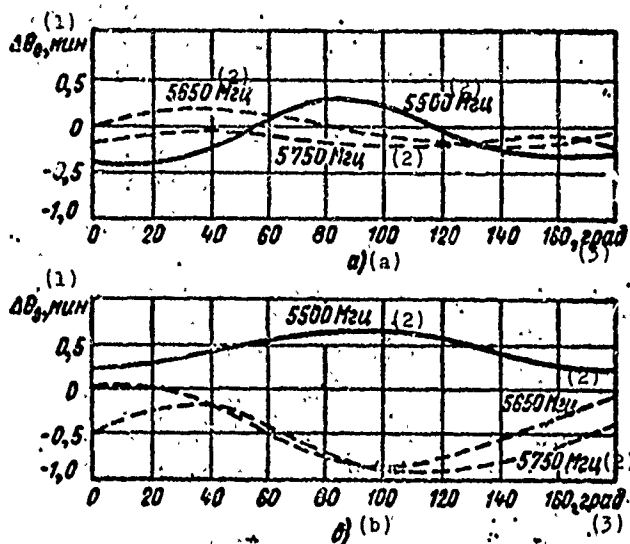


Fig. 5.27. Dependence of equisignal displacement on the angle of slope in the polarization plane of received signals: a) in azimuth; b) in elevation.

KEY: (1) $\Delta\theta_0$ min; (2) Mhz, (3) deg.

Thus, the experimental results substantiate calculated data on the effect of crosspolarization of receiving antennas in a monopulse system on direction finding accuracy. We should mention that a

change in the orientation of the linear polarization of a wave is also expressed in a change of the depth of the minimum difference radiation pattern as well as the level of its side lobes.

Under actual conditions, reflected signals have a partially polarized structure. Therefore, a deformation in the radiation pattern will have a random character, as a result of which the final effect will be determined by the spectral density of the variations in polarization and servosystem bandwidth. Under these conditions, we can expect a reduction in direction finding sensitivity of the system and an increase in its standard errors.

5.7.3. Methods of lessening the effect of antenna crosspolarization on direction finding accuracy. Since crosspolarization is generally caused by the very principle of radiation pattern formation, to improve design quality and increase manufacturing precision for direction finding systems is necessary but insufficient to reduce crosspolarization radiation.

More effective measures for the reduction of crosspolarization effects are compensation and polarization filtration.

The first method is based on the selection of an irradiator capable of compensating the crosspolarization components of the field in the aperture of the mirror. One of the simplest irradiators is a sum of electrical and magnetic dipoles with different moments, located at right angles to each other. An analog of such an irradiator is a pyramidal horn [100]. For compensating crosspolarization we can also use an installation of special correcting plates at the maxima of the antenna's electrical field [133, 134].

The second method for reducing the effect of crosspolarization on direction finding accuracy lies in the use of mesh reflectors and in the installation in antenna apertures of polarization grids which are ordinary grids of close parallel wires or metal plates [1, 63, 77, 111, 112]. Such reflectors and grids reflect waves with a polarization parallel to the wires (plates) and pass wave

with an orthogonal polarization direction. This makes it possible, to a certain extent, to filter the components of the reflected signal whose polarization is near the cross polarization of the antenna and, as a consequence, to lessen their harmful effect on direction finding accuracy.

With values of wire radius $r_0 < 0.05\lambda$ and spacing between wire axes $S < 0.2\lambda$, the attenuation factor for radio waves with a polarization parallel to the wires of the grid can be calculated according to formula [1].

$$T_0 \approx \frac{1}{1 + \left(\frac{\lambda}{2S} \frac{1}{\ln 2\pi r_0/S} \right)^2}, \quad (5.121)$$

where T_0 is the ratio of the power of a wave which has passed through the grid to the power of an incident wave.

When $r_0/\lambda = 0.1$ and 0.05 , calculation according to the cited formula gives the following, respectively:

$$T_0 = 0,05 \overset{\text{db}}{(-13 \text{ dB})}; 0,002 \overset{\text{db}}{(-26 \text{ dB})}.$$

Reduction in phase errors of field distribution in the aperture of the antenna by reducing the illumination of the edges of the mirror during its excitation leads to a decrease in the crosspolarization of the antennas. However, the amplification of the antenna is also reduced and the main lobe of the radiation pattern is broadened [100, 121].

CHAPTER 6

THE EFFECT OF IMPERFECTIONS IN ELEMENTS OF THE RECEIVING CIRCUIT ON THE ACCURACY OF MEASURING ANGULAR COORDINATES BY THE MONOPULSE METHOD

§ 6.1. MAIN SOURCES OF EQUIPMENT ERRORS

The monopulse method is based, as indicated earlier, on the reception of signals simultaneously by two or more receiving channels with their subsequent comparison with respect to amplitude or phase. In accordance with this, the accuracy of direction finding using the monopulse method, in many cases, will be determined by the identity of the characteristics of each pair of receiving channels which together provide direction finding in any coordinate plane.

Hitherto, when examining the reception and processing of signals in monopulse direction finding systems, we have based our assumption on the fact that the characteristics of receiving channels are identical. This enabled us to study the principles involved in constructing monopulse systems under conditions which ensure the achievement of the potential capabilities of the monopulse direction finding method. Actually, however, the structural and circuit makeup of a monopulse radar can have certain disadvantages which disturb the identity of receiving circuit characteristics. In a number of cases, such disruption can occur during the operation of the equipment because of element aging as well as climatic and mechanical effects. In these cases, direction finding accuracy, to a certain extent, will be determined by the value and character of equipment error.

Among the main sources of equipment error in monopulse radar systems are inadequacies in the formation of antenna radiation patterns, nonidentity of amplitude-phase characteristics for receiver-amplifier channels, imperfect operation of the AFC and AGC systems.

Below we examine the character of the effect of certain sources of equipment error on direction finding accuracy.

§ 6.2. THE EFFECT OF IMPERFECT FORMATION OF ANTENNA RADIATION PATTERNS OF MONOPULSE SYSTEMS ON DIRECTION FINDING ACCURACY.

The character of an antenna radiation pattern is determined by the amplitude-phase distribution of the excitation field in the aperture [52, 62]. Since antennas of monopulse radars must form symmetric pairs of radiation patterns in each direction finding plane, this assumes certain requirements on the function of the field distribution in the aperture (requirement of the function of the field distribution in the antenna aperture for amplitude and phase direction finding were examined in § 2.1). The nonfulfillment of these requirements inevitably leads to the noncorrespondence of radiation patterns to the principles of direction finding, to the appearance of asymmetry in amplitude and phase, and to a number of other disturbances. This, in turn, generates additional direction finding errors.

One of the main reasons for nonfulfillment of required excitation field symmetry is the inaccuracy of antenna building. Errors incurred in the building of antennas bring about irremovable distortions in field distribution along the aperture and, as a consequence, lead to the formation of radiation patterns unlike those calculated.

Errors in field distribution along the aperture can be broken down into systematic and random. The reasons for systematic error can include shading of mirror aperture by the feeds and fastening elements, the diffraction of radio waves on the edges of the mirror and the feeds, and channel cross-talk. Reasons for random error include random deformations of antenna mirror surface, temperature

drops or wind force changes around the antenna, which lead to fluctuations in excitation field phase, errors in building antenna, etc.

Systematic errors, as a rule, are identical or near in value to those of single-type antennas made according to established technology and, therefore, can be studied beforehand with a certain accuracy. As for random errors, they cannot be studied in advance since they vary in magnitude within wide limits from sample to sample. Therefore, an evaluation of random errors usually is done by the statistical method.

The effect of systematic errors on radiation pattern can be determined by introducing them into the field distribution along the aperture according to familiar methodology [62]. We can show that the presence of linear phase error along the antenna aperture leads to the corresponding deviation of radiation pattern from the prescribed direction. If the phase error changes according to square law, antenna beam defocusing sets in.

Random phase and amplitude errors in field distribution along the aperture cause an increase in the level of the side lobes, angular displacement of radiation pattern, and decrease in the coefficient of antenna directional action. The effect of random phase and amplitude errors in field distribution along the aperture on the indicated characteristics of antennas was studied by the statistical method in a number of works [40, 60, 71, 88, 107, 116, and 119].

In order to explain the results, let us examine two examples corresponding to a two-dimensional antenna array [116] and an antenna of the parabolic type [40].

6.2.1. The effect of errors in field distribution along the aperture of an antenna array on direction finding accuracy. In analyzing direction finding errors introduced by the elements of a phased array, we shall assume that the antenna is a rectangular array

arranged in plane XY, and the monopulse system is an amplitude sum-difference system.

Displacement of equisignal direction created by errors of array excitation leads to direction finding error in plane XZ, equal to

$$\Delta\theta_{x_0} = \theta'_{x_0} - \theta_{x_0} \quad (6.1)$$

where θ_{x_0} is the angle defining equisignal direction in the absence of errors;

θ'_{x_0} is the angle defining equisignal direction in the presence of errors.

Usually in monopulse systems with antenna arrays tracking is accomplished on error signal value without converting the signal $S(\theta)$ to zero. In this case, an additional source of direction finding error appears because of the change in direction finding sensitivity. If the direction finding characteristic is assumed linear, defined by relationship $S(\theta) = \mu\theta_x$, tracking error can be determined by equality

$$\Delta\theta_x = \theta'_{xp} - \theta_{xp} = \Delta\theta_{x_0} + \frac{\Delta\mu}{\mu} \theta_x \quad (6.2)$$

where θ'_{xp} is true direction to target;

θ_{xp} is apparent direction to target, taking error into account;

$\Delta\mu/\mu$ is the relative change in sensitivity during target tracking;

θ_x is the displacement of the target relative to equisignal direction in the direction finding plane X, equal to $(\theta'_{xp} - \theta'_{x_0})$.

From equation (6.2) it is apparent that tracking error consists of two components: the first is caused by the displacement of equisignal direction, while the second by change in direction finding sensitivity.

Sum tracking error will be maximum at maximum displacement of target from equisignal direction. If we assume that the maximum

displacement of target will reach half the radiation pattern width, equation (6.2) is written in the form

$$[\Delta\theta_x]_{\max} = \Delta\theta_{x_0} + \frac{\Delta\mu}{\mu} \frac{\lambda}{2X \sin \theta_{x_0}}, \quad (6.3)$$

where X is the dimension of the array in direction x .

The value of the sum tracking error depends upon type and magnitude of errors of amplitude-phase excitation field distribution. Let us examine each component of tracking error. For example, we find even excitation creating sum pattern $F_c(\theta)$ with amplitude-phase distribution along the array in the form

$$\hat{\gamma}_{nm} = \gamma_{nm} (1 + \Delta\gamma_{nm}) \exp[-i(\beta x_n \cos \theta_{x_0} + \beta y_m \cos \theta_{y_0} - \vartheta_{nm})], \quad (6.4)$$

where x_n, y_m are the coordinates of the radiators;

γ_{nm} is the excitation amplitude in the absence of error;

$\Delta\gamma_{nm}$ is amplitude error;

ϑ_{nm} is phase error.

Similarly, with uneven excitation with respect to x and y , creating difference pattern $F_p(\theta)$ in plane XZ , amplitude-phase distribution is described by expression

$$\hat{\eta}_{nm} = \eta_{nm} (1 + \Delta\eta_{nm}) \exp[-i(\beta x_n \cos \theta_{x_0} + \beta y_m \cos \theta_{y_0} - \xi_{nm})]. \quad (6.5)$$

Phase error for any array element consists of error in the position of this element and error in phase during its excitation:

$$\vartheta_{nm} = \vartheta'_{nm} + \beta(\Delta x_{nm} \cos \theta_{x_0} + \Delta y_{nm} \cos \theta_{y_0} + \Delta z_{nm} \cos \theta_{z_0}). \quad (6.6)$$

where $\Delta x_{nm}, \Delta y_{nm}, \Delta z_{nm}$ are errors in location of excited element;
 ϑ'_{nm} is phase error of excited element.

Similarly, for phase error in excitation field distribution during the formation of difference diagram

$$\xi_{nm} = \xi'_{nm} + \beta (\Delta x_{nm} \cos \theta_{x_0} + \Delta y_{nm} \cos \theta_{y_0} + \Delta z_{nm} \cos \theta_{z_0}). \quad (6.7)$$

For antenna arrays having a large number of elements, excitation can be represented in the form of continuous functions $\gamma(x, y)$ and $\eta(x, y)$.

Under this condition, expressions for both tracking error components assume the form [116]

$$\Delta \theta_{x_0} = \frac{1}{\beta \sin \theta_{x_0}} \frac{\iint \xi(x, y) \eta(x, y) dA}{\iint x \eta(x, y) dA}, \quad (6.8)$$

$$\begin{aligned} \frac{\Delta \mu}{\mu} \frac{\lambda}{2X \sin \theta_{x_0}} &= \frac{1}{2} \left(\frac{\iint \theta^2 \gamma dA}{\iint \gamma dA} - \frac{\iint \xi^2 x \eta dA}{\iint x \eta dA} \right) \frac{\pi}{\beta X \sin \theta_{x_0}} \\ &= - \left(\frac{\iint \Delta \gamma \gamma dA}{\iint \gamma dA} - \frac{\iint \Delta \eta x \eta dA}{\iint x \eta dA} \right) \frac{\pi}{\beta X \sin \theta_{x_0}}. \end{aligned} \quad (6.9)$$

Let us note that integration is carried out over an equivalent aperture of the array, having dimensions X , Y , and none of the amplitude and phase excitation errors γ are introduced into formula (6.8).

Formulas (6.8) and (6.9) can be used for calculating tracking errors arising both from systematic and from random amplitude and phase excitation errors [116].

Systematic tracking error is considered for uniform amplitude distribution of excitation η , when

$$\eta(x, y) = \begin{cases} -1 & \text{при } x < 0; \\ 1 & \text{при } x > 0, \end{cases} \quad (6.10)$$

(при = when)

while the systematic phase error which occurs has the form

$$\xi = -\xi_0 \left(\frac{2x}{X} \right)^2, \quad \text{where } \xi_0 \text{ is the maximum value of phase error}$$

on the edge of the array. The components of tracking error, in accordance with equations (6.8) and (6.9), will be equal, respectively, to

$$\Delta\theta_{x_0} = -\frac{\lambda}{X \sin \theta_{x_0}} \left(\frac{\xi_0}{2\pi} \right), \quad (6.11)$$

$$\frac{\Delta\mu}{\mu} = \frac{\lambda}{2X \sin \theta_{x_0}} = -\frac{\lambda}{X \sin \theta_{x_0}} \left(\frac{\xi_0}{4} \right)^2. \quad (6.12)$$

Consequently, sum error, expressed in fractions of radiation pattern width is determined by expression

$$\frac{\Delta\theta_x}{\lambda/X \sin \theta_{x_0}} = \frac{\xi_0}{2\pi} \left(1 + \frac{\pi}{8} \xi_0 \right). \quad (6.13)$$

From the graphs showing the dependence of tracking errors on cubic phase error (Fig. 6.1), it is apparent that displacement of equisignal direction is the predominant tracking error in the presence of phase errors.

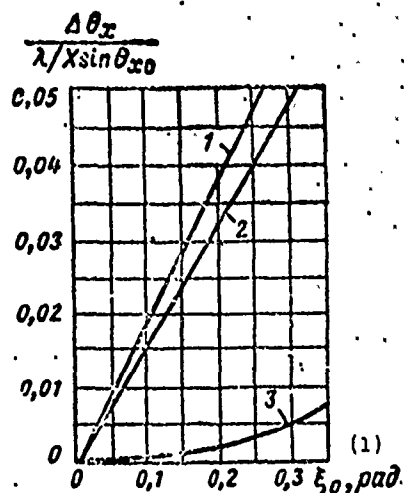


Fig. 6.1. Dependence of standard tracking error on the value of cubic phase antenna excitation error: 1 - sum error; 2 - error from displacement of equisignal direction; 3 - error from change in direction finding sensitivity.

KEY: (1) ξ_0 , rad.

Random tracking errors are examined for the case when phase and amplitude excitation field errors have normal distribution. With average values of phase errors equal to zero, uniform distribution of γ , and step-uniform distribution of η , the mean-square values of sum tracking error and its components, in this case, will be equal to [116]

$$\sigma_{\theta_{x0}} = \left(\frac{\lambda}{X \sin \theta_{x0}} \right) \frac{0.64}{\sqrt{NM}} \sigma_{\xi}^2 \quad (6.14)$$

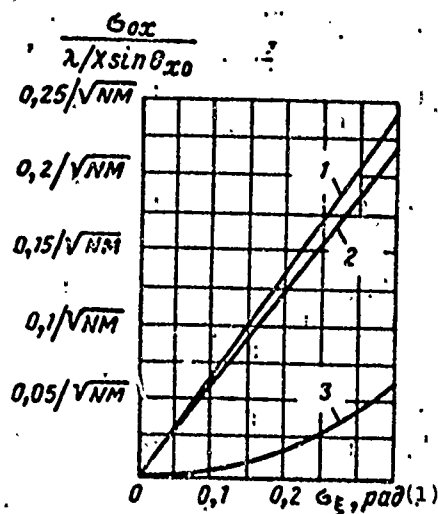
$$\frac{\sigma_{\mu}^2}{\mu^2} \left(\frac{\lambda}{2X \sin \theta_{x0}} \right) = \left(\frac{\lambda}{X \sin \theta_{x0}} \right) \frac{0.54}{\sqrt{NM}} \sigma_{\xi}^2 \quad (6.15)$$

$$\sigma_{\theta_x}^2 = \sigma_{\theta_{x0}}^2 + \frac{\sigma_{\mu}^2}{\mu^2} \left(\frac{\lambda}{2X \sin \theta_{x0}} \right)^2 \quad (6.16)$$

when N is the number of array elements along axis x ;
 M is the number of array elements along axis y ;
 σ_{ξ} is the variance of phase error in radians.

Figure 6.2 presents the dependence of these errors on σ_{ξ} . In this case, also predominant is the error from displacement of equisignal direction.

Fig. 6.2. Dependence of standard tracking error on the value of standard phase error in antenna excitation: 1 - sum error; 2 - error from displacement of equisignal direction; 3 - error from change in direction finding sensitivity.
 KEY: (1) rad.



The standard value of sum tracking error, caused by random amplitude errors, is determined by expression [116]

$$\sigma_{\theta_z} = \left(\frac{\lambda}{X \sin \theta_{z0}} \right) \frac{1.56}{\sqrt{NM}} \sigma_a \quad (6.17)$$

where $\sigma_a = \sigma_{\Delta\gamma} = \sigma_{\Delta\eta}$ is the standard value of amplitude error.

Graphs showing the dependence of standard sum error on σ_a are presented in Fig. 6.3.

The above expressions for errors were obtained for tracking in one plane; however, they are also valid for tracking in another plane.

The effect of amplitude and phase errors can also be evaluated from the point of view of variations in antenna radiation pattern. It is convenient to use the statistical method of calculating antennas [40, 60]. Thus, with uniform current amplitude distribution of the element along the aperture and normal phase error distribution statistical calculation [40, 44] gives the following generalized expression for the averaged antenna radiation pattern of the array with respect to power:

$$\overline{F(\theta, \varphi)} = F(\theta, \varphi) + \mu(\theta, \varphi) \sigma_0^2 \frac{\sum_{m=1}^M \sum_{n=1}^N I_{mn}^2}{\sum_{m=1}^M \sum_{n=1}^N I_{mn}^2} \quad (6.18)$$

where $F(\theta, \varphi)$ is the antenna radiation pattern of the array in the absence of random errors;

$\mu(\theta, \varphi)$ is the coefficient of radiation pattern slope, equal to

$$\mu(\theta, \varphi) = \cos \theta (\cos^2 \theta \cos^2 \varphi + \sin^2 \varphi),$$

σ_0^2 is the mean square of sum error, equal to

$$\sigma_0^2 = \sigma_a^2 + \sigma_\phi^2$$

σ_a^2 is the mean square of relative amplitude error;

σ_ϕ^2 is the mean square of phase error;

I_{mn} is the current in the mn-th element of the antenna, determined by the given distribution in the aperture;

θ, ϕ are the angles determining beam orientation in a selected system of coordinates (Fig. 6.4)

Fig. 6.3. Dependence of standard tracking error on the value of standard amplitude error in antenna excitation.

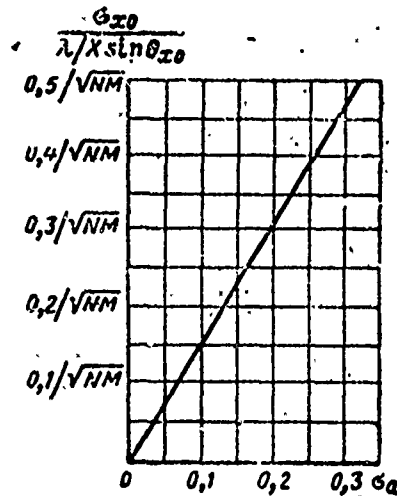
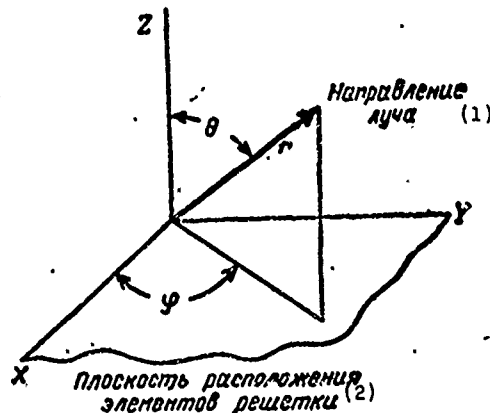


Fig. 6.4. System of coordinates for determining angle θ and ϕ .
KEY: (1) Beam direction; (2) Plane of array elements.



From expression (6.18) it is apparent that the effect of amplitude and phase errors leads to secondary radiation determined by the second term of the expression, and, as a consequence, to a decrease in the coefficient of directional action. The latter can be determined from the following approximation formula [40, 44]:

$$\frac{G}{G_0} \approx \frac{1}{1 + \frac{3}{4} \pi \left(\frac{l_p}{\lambda} \right)^2 \sigma_0^2} \quad (6.19)$$

where G_0 , G is the coefficient of directional action for the antenna in the absence of errors and with errors taken into account, respectively;

l_p is the distance between elements of the antenna lattice.

6.2.2. The effect of errors in field distribution along the aperture of a parabolic antenna on direction finding accuracy. With respect to parabolic mirror antennas the statistical method with small phase errors σ_ξ and normal law of distribution gives [40, 44]

$$\overline{F(\theta, \varphi)} = F(\theta, \varphi) + \mu(\theta, \varphi) \frac{4\tau_0^2 \pi^2 \sigma_\xi^2}{\lambda^2 G_0} \exp\left(-\frac{\pi^2 u^2 \tau_0^2}{\lambda^2}\right), \quad (6.20)$$

where $u = \sin \theta$;

τ_0 is the correlation interval expressed in wavelengths and corresponding to the average interval in which errors in excitation currents cannot be considered independent.

Just as in expression (6.18) the first term of expression (6.20) characterizes the radiation pattern in the absence of errors, while the second term describes this distortion caused by phase error in field distribution along the aperture. Secondary radiation is proportional to the mean square of the error, just as in an antenna array, and also proportional to the square of the correlation interval expressed in wavelengths.

With small errors and a small correlation interval the decrease in the coefficient of directional action is determined by the approximation expression

$$\frac{G}{G_0} \approx 1 - \frac{3}{4} \frac{\sigma_{\epsilon}^2 \tau_0^2}{\lambda^2}, \quad \frac{\tau_0}{\lambda} \ll 1 \quad (6.21)$$

and with a large correlation interval by expression

$$\frac{G}{G_0} \approx 1 - \sigma_{\epsilon}^2, \quad \frac{\tau_0}{\lambda} \gg 1. \quad (6.22)$$

Thus, amplitude and phase errors in excitation field distribution along the antenna aperture lead to the distortion of the radiation pattern, which can be manifested, specifically, in a decrease in the coefficient of directional action. Due to this, nonidentity of amplitude characteristics for the receiving channels of a monopulse system and an increase in direction finding errors can occur.

In order to evaluate the effect of nonidentity of radiation patterns on target direction finding accuracy, we shall assume that the amplification of one of the receiving antennas differs from the other by quantity ΔG . As is apparent in Fig. 6.5, a variation in the amplification of one of the antennas of a monopulse radar involves the displacement of equisignal direction (ESD) by quantity $\Delta\theta_0$ and is a source of systematic direction finding error, linearly connected with the quantity of antenna nonidentity with respect to amplification.

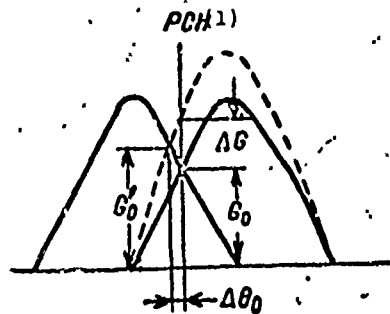


Fig. 6.5. Displacement of equisignal direction with a change in the amplification of one of the antennas.
KEY: (1) ESD.

The value of systematic error can be determined in the following manner. Let G_0 be the amplification factor in equisignal direction under the condition of identity for radiation patterns; G'_0 is the amplification factor in equisignal direction during a change in the amplification of one of the antennas by quantity ΔG , and μ and μ' are the steepness of the radiation pattern at the working point for these conditions. Then we can write the following relationship:

$$G'_0 = G_0 (1 \pm \mu \Delta \theta_0), \quad (6.23)$$

$$G_0 \pm \Delta G = G'_0 (1 \pm \mu' \Delta \theta_0). \quad (6.24)$$

Substituting (6.23) into (6.24) and disregarding the quantity of the second order of smallness, after elementary transformation, we obtain

$$\Delta \theta_0 = \frac{\Delta G_0}{G_0 (\mu + \mu')} \approx \frac{\Delta G}{G_0} \frac{1}{2\mu}. \quad (6.25)$$

or

$$\mu \Delta \theta_0 \approx \frac{\Delta G}{2G_0}. \quad (6.26)$$

If we assume the values of the steepness of the direction finding characteristic and the nonidentity of radiation patterns with respect to amplitude, we can determine the value of angular error. Calculations show that with a direction finding characteristic steepness of 0.25 1/deg, radiation pattern nonidentity with respect to amplification of 10% leads to systematic angular error or 0.2°. If permissible angular error, in this case, is taken as one minute, antenna disagreement with respect to amplification must not exceed 0.8%.

Using formulas (6.22), we can calculate permissible standard error with respect to excitation field phase for a parabolic antenna. Thus, with a large correlation interval,

$$\sigma_{\xi}^2 = 1 - \frac{G}{G_0} = \frac{\Delta G}{G_0}, \quad (6.27)$$

$$\sigma_{\xi} = \left(\frac{\Delta G}{G_0} \right)^{\frac{1}{2}}. \quad (6.28)$$

When $\Delta G/G_0 = 0.1$, $\sigma_{\xi} = 0.32 \text{ rad} = 18.3^\circ$. With a permissible error of $\Delta\theta_0 = 1 \text{ min } \Delta G/G_0 = 0.8\%$. Permissible standard error with respect to phase, in this case, is

$$\sigma_{\xi} = (0.008)^{\frac{1}{2}} = 0.09 \text{ rad} = 5^\circ.$$

These are rather high requirements for an antenna excitation field. Therefore, higher requirements are imposed on accuracy in building and ensuring rigidity of antennas for monopulse systems.

If unbalance of the antenna with respect to amplification occurs because of random errors, in the calculation of permissible phase and amplitude errors in the excitation field distribution of array and parabolic antennas, we can use formulas (6.19), (6.21), and (6.22).

Let us examine the effect on direction finding accuracy of non-identity of amplitude-phase characteristics for receiving channels of monopulse systems.

§ 6.3. THE EFFECT OF NONIDENTITY OF AMPLITUDE-PHASE CHARACTERISTICS FOR RECEIVING CHANNELS OF MONOPULSE SYSTEMS ON DIRECTION FINDING ACCURACY

The appearance of nonidentity of amplitude-phase characteristics for receiving channels is caused by the difficulties involved in making parts with strictly prescribed allowances, the inevitable

processes of aging, and the related changes in their parameters, a possible detuning of circuits during equipment operation, and various types of mechanical and climatic effects.

In studying the effect of nonidentity of amplitude-phase characteristics, it is expedient that the receiving circuit be divided into two parts: into the high-frequency part including the antenna-waveguide receiving circuit up to the i-f mixer and the part of the receiving circuit operating on intermediate frequency. The advantage of this division ensues from the fact that in studying the effect of imperfection in the channels of the h-f amplifier, we can disregard the pulsed character of the signal received since the bandwidth of these channels is virtually always greater than the spectral width of the signal. As for i-f amplifier channels, this is not always valid and we should take into account the relationship between the spectral width of the signal and the bandwidth of the i-f amplifier [55].

To simplify the analysis of the effect of nonidentity in the amplitude-phase characteristics, we shall first examine the case of direction finding in a continuous signal emission mode when we do not take into account limitations on the bandwidth of the i-f amplifier. Since the degree and character of the effect of imperfections in the amplitude-phase characteristics depends, to a certain extent, upon the construction of the direction finding system, we shall perform analysis with respect to the most commonly used types of monopulse systems.

6.3.1. The effect of nonidentity of amplitude-phase characteristics in an amplitude-amplitude monopulse system on direction finding accuracy. A simplified block diagram of an amplitude-amplitude monopulse system is presented in Fig. 1.7. We shall assume that the target is tracked with small angular errors θ and linearization of the radiation pattern in the region of equisignal direction is valid. If the receiving channels have out-of-phase quantity ψ and high-frequency transmission factors (up to the i-f amplifier)

k_1 and k_2 , signals at the output of the i-f amplifier with logarithmic characteristics can be represented in the form of the following expression:

$$\dot{u}_1(t, \theta) = \kappa_{01} \ln \kappa_1 E_m F(\theta_0) (1 + \mu\theta) \exp i(\omega_{np} t + \psi), \quad (6.29)$$

$$u_2(t, \theta) = \kappa_{02} \ln \kappa_2 E_m F(\theta_0) (1 - \mu\theta) \exp i \omega_{np} t, \quad (6.30)$$

where κ_{01} and κ_{02} are coefficients characterizing the steepness of the amplitude characteristics of the first and second i-f amplifiers.

At i-f amplifier output, signals are detected and compared with respect to amplitude by subtraction, forming, with linear signal detection, errors in accordance with expression

$$S(\theta) = |\dot{u}_1(t, \theta)| - |\dot{u}_2(t, \theta)|. \quad (6.31)$$

Substituting expressions (6.29) and (6.30), we obtain

$$S(\theta) = \kappa_{02} [g_0 \ln \kappa_1 E_0 (1 + \mu\theta) - \ln \kappa_2 E_0 (1 - \mu\theta)], \quad (6.32)$$

where

$$g_0 = \frac{\kappa_{01}}{\kappa_{02}}, \quad E_0 = E_m F(\theta_0).$$

Taking into account the earlier assumptions on smallness of target finding errors, expression (6.32) can be simplified:

$$S(\theta) = \kappa_{02} [g_0 \ln \kappa_1 E_0 + g_0 \ln(1 + \mu\theta) - \ln \kappa_2 E_0 - \ln(1 - \mu\theta)] = \kappa_{02} \left[\ln \frac{(\kappa_1 E_0)^{g_0}}{\kappa_2 E_0} + (g_0 + 1) \mu\theta \right]. \quad (6.33)$$

Equating (6.33) to zero and solving relative to $\mu\theta$, we find the direction finding condition in the form

$$\mu\theta = - \frac{\ln \frac{(k_1 E_0)^{g_0}}{\kappa_2 E_0}}{(g_0 + 1)}. \quad (6.34)$$

With identical amplitude characteristics for the receiving channels ($g_0 = 1$; $k_1 = k_2$)

$$S(\theta) = \kappa_0 \ln \frac{1 + \mu\theta}{1 - \mu\theta} \approx 2\kappa_0 \mu\theta. \quad (6.35)$$

In this case $S(\theta) = 0$ when $\theta = 0$, which corresponds to the condition of direction finding without equipment error.

A comparison of expressions (6.34) and (6.35) shows that non-identity of amplitude characteristics for receiving circuits of amplitude-amplitude monopulse systems leads to the appearance of systematic direction finding errors whose value depends upon the value of nonidentity.

If nonidentity occurs only in high-frequency receiver circuits ($g_0 = 1$ and $k_1 \neq k_2$), the value of direction finding error is determined by expression

$$\mu\theta = - \frac{\ln g}{2}, \quad (6.36)$$

where $g = k_1/k_2$.

When $k_1 = k_2 = k$ and $g_0 \neq 1$ direction finding errors can be calculated from formula

$$\mu\theta = - \frac{\ln (\kappa E_0)^{g_0 - 1}}{(g_0 + 1)} = - \frac{g_0 - 1}{g_0 + 1} \ln \kappa E_0. \quad (6.37)$$

From expression (6.37) it follows that with nonidentity of amplitude characteristics of logarithmic receivers, signal standardization is disturbed and error signal becomes dependent upon the level of signals received. Thus, an increase in the input signal to the square leads to a doubling of direction finding errors.

Figure 6.6 presents the dependence of generalized angular error on nonidentity of receiving channel transmission factors, calculated from formula (6.36). If we know the steepness of the direction finding characteristic with respect to generalized direction finding error, we can determine the absolute value of angular direction finding error with any given nonidentity of amplitude characteristics for receiving channels. Thus, for example, if $\mu = 0.25$ 1/deg, nonidentity of channels with respect to high frequency is 10% ($g = 1.1$), equipment error in direction finding is 0.2 deg. It is easy to calculate the permissible nonidentity of amplitude characteristics for high-frequency channels with any given allowable error.

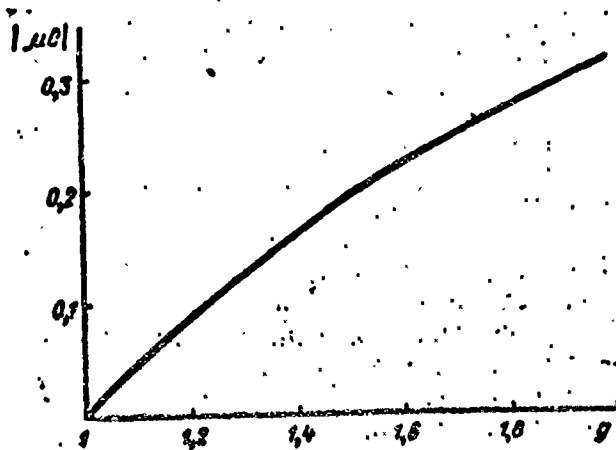


Fig. 6.6. Dependence of generalized angular error in direction finding on nonidentity of transmission factors of receiving channels in an amplitude monopulse radar.

The dependence in Fig. 6.6 can be used for evaluating direction finding errors when $g = 1$ and $g_0 \neq 1$ if by the quantity $|\mu\theta|$

we mean the standardized quantity $\frac{|\mu\theta|}{\ln kE_0}$, and instead of g we use g_0 .

The obtained results of analysis also show that phase non-identity of receiving channels does not affect the accuracy of amplitude-amplitude monopulse systems. We can see that the conclusions with respect to the effect of nonidentity of amplitude-phase characteristic for receiving channels in amplitude-amplitude monopulse systems with logarithmic receivers are valid also for cases when receivers are used with linear and quadratic characteristics.

We have examined the case of small angular deviations when the direction finding system operates in linear mode. In a number of cases because of considerable unbalance of receiving channels with respect to amplitude, direction finding errors can go in value beyond the linear section of the direction finding characteristic. In this case, the problem of finding direction finding errors is solved in general form, approximating the radiation pattern with the appropriate functions. Since in the great majority of cases equipment errors are small, such a complication of calculations is not necessary and we will not attempt it here.

Let us proceed to an examination of another type of monopulse system.

6.3.2. The effect of nonidentity of amplitude-phase characteristics for receiving channels of an amplitude sum-difference monopulse system on direction finding accuracy. A simplified block diagram of an amplitude sum-difference monopulse direction finding system is presented in Fig. 1.9. Let the transmission factors of the high-frequency receiving circuits up to the sum-difference converter be, respectively, k_1 and k_2 , and nonidentity with respect to phase be expressed by quantity ψ . Then the sum and difference signals at summator output can be represented by the following expressions:

$$\begin{aligned} \dot{E}_c(t, \theta) &= \frac{1}{\sqrt{2}} [\dot{E}_1(t, \theta) + \dot{E}_2(t, \theta)] = \\ &= E_0 [(1 + \mu\theta) \exp i(\omega t + \psi) + g(1 - \mu\theta) \exp i\omega t], \end{aligned} \quad (6.38)$$

$$\begin{aligned} \dot{E}_p(t, \theta) &= \frac{1}{\sqrt{2}} [\dot{E}_1(t, \theta) - \dot{E}_2(t, \theta)] = \\ &= E_0 [(1 + \mu\theta) \exp i(\omega t + \psi) - g(1 - \mu\theta) \exp i\omega t], \end{aligned} \quad (6.39)$$

where $\dot{E}_1(t, \theta)$ and $\dot{E}_2(t, \theta)$ are mathematical expressions of signals received by the first and second high-frequency receiving channels:

$$E_0 = \frac{1}{\sqrt{2}} E_m F(\theta_0) \kappa_1.$$

At 1-f amplifier output of the sum and difference channels, respectively, we obtain

$$\begin{aligned} \dot{u}_c(t, \theta) &= E_0 \kappa_c [(1 + \mu\theta) \exp i(\omega_{np} t + \psi + \gamma) + \\ &+ g(1 - \mu\theta) \exp i(\omega_{np} t + \gamma)], \end{aligned} \quad (6.40)$$

$$\begin{aligned} \dot{u}_p(t, \theta) &= E_0 \kappa_p [(1 + \mu\theta) \exp i(\omega_{np} t + \psi) - \\ &- g(1 - \mu\theta) \exp i\omega_{np} t], \end{aligned} \quad (6.41)$$

where κ_c and κ_p are the transmission factors of the sum and difference channels, respectively;

γ is the quantity of phase nonidentity for sum and difference channels.

In the error signal detector of the direction finding system the sum and difference signals are multiplied and high-frequency components filtered. Because of this, error signal, taking standardization with respect to sum signal into account, can be represented as

$$\begin{aligned} S(\theta) &= \frac{\operatorname{Re} \dot{u}_c(t, \theta) \dot{u}_p^*(t, \theta)}{\dot{u}_c(t, \theta) \dot{u}_c^*(t, \theta)} = \\ &= \kappa_p \kappa_c \frac{\kappa_p \{[(1 + \mu\theta)^2 - g^2(1 - \mu\theta)^2] \cos \gamma + 2g(1 - \mu^2\theta^2) \sin \psi \sin \gamma\}}{\kappa_c \{[(1 + \mu\theta)^2 + g^2(1 - \mu\theta)^2 + 2g(1 - \mu^2\theta^2) \cos \psi\]}. \end{aligned} \quad (6.42)$$

Hence the condition for target finding is determined by equation

$$[(1 + \mu\theta)^2 - g^2(1 - \mu\theta)^2] \cos \gamma + 2g(1 - \mu^2\theta^2) \sin \psi \sin \gamma = 0. \quad (6.43)$$

Solving this equation with respect to $\mu\theta$, we obtain the following expression determining the value of generalized angular direction finding error as a function of the character and value of nonidentity of amplitude-phase characteristics for receiving channels in an amplitude sum-difference monopulse system:

$$\mu\theta = \frac{-(1 + g^2) \pm 2g \sqrt{1 + tg^2 \gamma \sin \psi}}{(1 - g^2) \mp 2g tg \gamma \sin \psi}. \quad (6.44)$$

Of practical value is the solution with a plus sign determining the steady state of the direction finding system with comparatively small angular errors. Solution with a minus sign gives higher value of generalized errors and is not valid with the assumption made on operation in a linear region of the direction finding characteristic.

With identical characteristics of receiving channels expression (6.42) is transformed into the familiar expression corresponding to the case of direction finding without equipment errors:

$$S(\theta) = \mu\theta. \quad (6.45)$$

Differentiating expression (6.42) with respect to θ , we find the expression for steepness of direction finding characteristic at the working point:

$$\left. \frac{dS(\theta)}{d\theta} \right|_{\theta=0} = \frac{\kappa_p}{\kappa_0} \frac{4\mu g [2g \cos \gamma + \cos(\psi + \gamma) + g^2 \cos(\psi - \gamma)]}{(1 + g^2 + 2g \cos \psi)^2}. \quad (6.46)$$

Comparing expressions (6.42) and (6.45), we see that nonidentity of amplitude-phase characteristics for receiving channels affects

direction finding errors. In order to understand the character of the dependence of direction finding errors on nonidentity of receiving channels, we shall examine a number of particular cases.

Case 1. Amplitude-phase characteristics of sum and difference channels are identical; high-frequency channels are identical with respect to phase but nonidentical with respect to transmission factor. In this case $k_p = k_c = k$; $\gamma = 0$; $\psi = 0$; $g \neq 1$.

Substituting these values into expression (6.44) and performing elementary transformations, we obtain the equality

$$\mu\theta = \frac{g-1}{g+1}, \quad (6.47)$$

indicating that nonidentity of amplitude characteristics for high-frequency channels in an amplitude sum-difference monopulse system leads to a displacement of equisignal direction and additional direction finding errors.

Since high-frequency receiving circuits in a sum-difference direction finding system usually do not contain effective elements, their identity generally will depend upon the identity of their matching and electrical length in the operating frequency band. Therefore, when designing and making the waveguide-feeder lines which are the high-frequency channels of a direction finding system, we should give particular attention to their quality and accuracy.

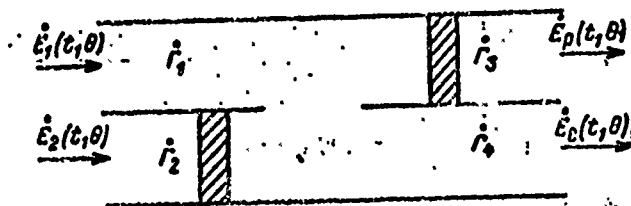


Fig. 6.7. Diagram of a slotted balance bridge.

One of the important elements of high-frequency circuits in monopulse radars is the waveguide bridge for sum-difference signal processing. This bridge is illustrated in Fig. 6.7 where matching in the arms is characterized by complex reflection factors Γ_1 , and the elements of phase tuning are conditionally illustrated by the shaded inserts.

In reference [131] it is shown that taking into account imperfect agreement of arms, the sum and difference signals at bridge output can be represented in the form of the following complex expressions:

$$E_c(t, \theta) = \frac{1[E_1(t, \theta)(1 + \Gamma_2 \Gamma_3) + E_2(t, \theta)(1 + \Gamma_1 \Gamma_4)]}{\sqrt{2} \left[1 + \Gamma_1 \Gamma_2 \Gamma_3 \Gamma_4 + \frac{1}{2} (\Gamma_1 + \Gamma_2)(\Gamma_3 + \Gamma_4) \right]} \quad (6.48)$$

$$E_p(t, \theta) = \frac{1[E_1(t, \theta)(1 + \Gamma_2 \Gamma_3) - E_2(t, \theta)(1 + \Gamma_1 \Gamma_4)]}{\sqrt{2} \left[1 + \Gamma_1 \Gamma_2 \Gamma_3 \Gamma_4 + \frac{1}{2} (\Gamma_1 + \Gamma_2)(\Gamma_3 + \Gamma_4) \right]} \quad (6.49)$$

where, with respect to amplitude direction finding,

$$E_1(t, \theta) = E_m F(\theta_0) (1 + \mu \theta) \exp i \omega t, \quad (6.50)$$

$$E_2(t, \theta) = E_m F(\theta_0) (1 - \mu \theta) \exp i \omega t. \quad (6.51)$$

Because of the fact that the quantities Γ_1 are complex quantities, unmatching of bridge arms causes not only a change in amplitudes of sum and difference signal, but also a phase shift between these signals.

Disregarding phase signals for the sake of simplification, the direction finding characteristic of an amplitude sum-difference monopulse system taking into account matching in the waveguide bridge can be represented in the form

$$\begin{aligned}
S(\theta) &= \frac{\operatorname{Re} \dot{E}_e(t, \theta) \dot{E}_e^*(t, \theta)}{\dot{E}_e(t, \theta) \dot{E}_e^*(t, \theta)} = \\
&= \frac{[(1 + \mu\theta)(1 + \Gamma_1\Gamma_2) - (1 - \mu\theta)(1 + \Gamma_1\Gamma_2)](1 + \mu\theta)(1 + \Gamma_1\Gamma_2)}{[(1 + \mu\theta)(1 + \Gamma_1\Gamma_2) + (1 - \mu\theta)(1 + \Gamma_1\Gamma_2)]^2} \dots
\end{aligned}
\tag{6.52}$$

Equating the numerator to zero and solving the equality with respect to $\mu\theta$, we find the dependence determining direction finding error caused by the nonidentity of waveguide bridge channel matching:

$$\mu\theta = \frac{\Gamma_1(\Gamma_1 - \Gamma_2)}{2 + \Gamma_1(\Gamma_1 + \Gamma_2)}
\tag{6.53}$$

Since the reflection factor is connected with the standing wave ratio (SWR) by the familiar expression

$$\Gamma = \frac{\text{KCB} - 1}{\text{KCB} + 1}
\tag{6.54}$$

The relationship $\mu\theta = f(\Gamma)$ can be considered $\mu\theta = f(\text{SWR})$ and possible errors from arm mismatch in the waveguide bridge can be evaluated directly in terms of the permissible values of the corresponding standing wave ratios.

Case 2. Sum and difference channels are identical with respect to characteristics; high-frequency channels are identical with respect to transmission factor but nonidentical with respect to phase. In this case $k_c = k_p = k$; $\gamma = 0$; $g = 1$; $\psi \neq 0$ and expression (6.44) assumes the form $\mu\theta = 0$. This means that regardless of the value of phase nonidentity for high-frequency channels, there is no zero shift for the direction finding characteristic. But this still does not mean that the operational capability of an amplitude-difference monopulse direction finding system, under the examined

conditions, remains normal since it is unknown how steepness of the direction finding characteristic changes in this case.

Using expression (6.46) and applying it to this case, we obtain

$$\left. \frac{dS(\theta)}{d\theta} \right|_{\theta=0} = \frac{2\mu}{(1 + \cos \psi)}. \quad (6.55)$$

In normal direction finding conditions $\psi = 0$, and

$$\left. \frac{dS(\theta)}{d\theta} \right|_{\theta=0} = \mu.$$

When $\psi = \pi$ expressions (6.38) and (6.39) are transformed as

$$E_c(t, \theta) = E_0 [g(1 - \mu\theta) \exp i\omega t - (1 + \mu\theta) \exp i\omega t], \quad (6.56)$$

$$E_p(t, \theta) = -E_0 [g(1 - \mu\theta) \exp i\omega t + (1 + \mu\theta) \exp i\omega t]. \quad (6.57)$$

Functionally the channels change places; the sum channel becomes difference and the difference channel sum. Due to this, the operational ability of the direction finding system breaks down completely.

Substituting $\psi = \pi$ into (6.55), we find

$$\left. \frac{dS(\theta)}{d\theta} \right|_{\theta=0} = \infty, \quad (6.58)$$

which is a consequence of standardization with respect to difference signal, equal to zero when $\theta = 0$. This case is illustrated in Fig. 6.8 where radiation patterns with respect to sum and difference channels are presented schematically. There, however, for comparison are presented the corresponding radiation patterns when $\psi = 0$, corresponding to the normal operating conditions of a direction finding system.

When $\psi < \pi$, as we can see from the expression (6.55), the steepness of the direction finding characteristic increases. If $\theta = \frac{\pi}{2}$, complication in the waveguide balance bridge occurs in quadrature, due to which at output of the sum and difference arms of the bridge equal signals are obtained regardless of the ratio of received signal amplitudes, i.e., regardless of the angle of displacement (Fig. 6.9). The operational capacity of the servosystem, in this case, is not hampered since angular information contained in the amplitude ratio of signals received by independent channels converts to phase difference of sum and difference signals. Since this phase difference in equisignal direction is 90° , the output signal of the phase detector in the absence of mismatch is zero and the servosystem maintains its operational ability.

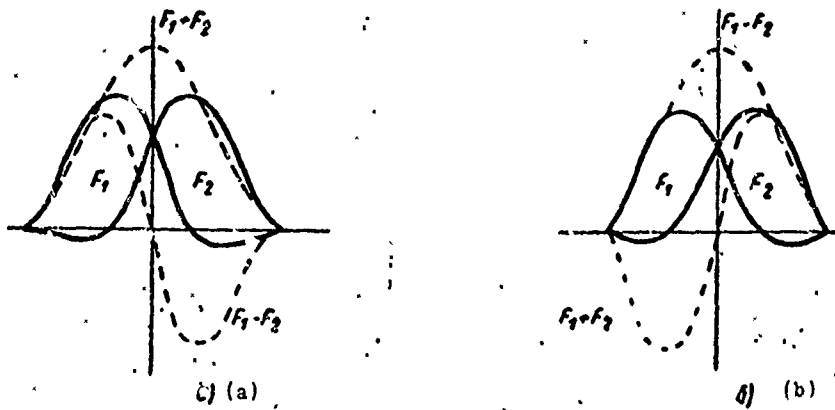
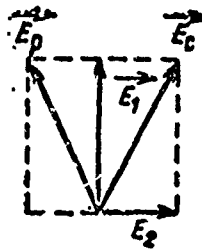


Fig. 6.8. Radiation patterns for difference and sum channels: a) when $\psi = 0$; b) when $\psi = \pi$.

Fig. 6.9. Vector diagram illustrating the formation of sum and difference signal when $\psi = \pi/2$.



We should mention that a 90° shift of signal circuit preceding the sum-difference processor, in a number of cases, is specially used for information conversion [45, 122].

When $\psi \neq \frac{\pi}{2}$ and $\psi \neq 0$ the sum and difference signals are out of phase. The state of the direction finding system with which channels are out of phase can be considered undesirable, leading to a crossover of channels and a disruption to some degree of its stability.

Case 3. High-frequency circuit of receiving channels are identical in amplitude-phase characteristics; sum and difference channels are identical in amplitude but nonidentical in phase. In this case, $g = 1$; $k_c = k_p = k$; $\psi = 0$; $\gamma \neq 0$ and direction finding conditions are determined in accordance with (6.42) and (6.46) by expression

$$S(\theta) = \mu \theta \cos \gamma, \quad (6.59)$$

$$\left. \frac{dS(\theta)}{d\theta} \right|_{\theta=0} = \mu \cos \gamma. \quad (6.60)$$

Equality $S(\theta) = 0$ is fulfilled when $\theta = 0$. This means that zero shift of direction finding characteristic is absent. The presence of phase nonidentity affects direction finding sensitivity and steepness.

When $\gamma = \pm 90^\circ$ error signal in the direction finding system becomes equal to zero regardless of the value of the displacement angle. Operation of an automatic tracking system, in this case becomes impossible. When $90^\circ < \gamma < 270^\circ$ the steepness of the direction finding characteristic becomes negative, which is equivalent to out-of-phase condition and loss of stability in the servosystem of the direction finder.

Thus, it is impossible to disregard phase nonidentity of sum and difference channels. Although it does not lead to direct dis-

placement of equisignal direction, its value must lie within a certain permissible range. The value of permissible nonidentity can be determined based on the permissible decrease in direction finding sensitivity. Thus, for example, if the permissible sensitivity drop is 50%, then the permissible out-of-phase condition for sum and difference channels must not exceed $\gamma = \pm 60^\circ$.

Case 4. High-frequency circuits for receiving channels are identical in amplitude-phase characteristic; sum and difference channels are identical in phase but nonidentical in amplitude. In this case $g = 1$; $\psi = 0$; $\gamma = 0$; $k_c \neq k_p$ and direction finding conditions are determined by expressions

$$S(\theta) = \frac{\kappa_p}{\kappa_c} \mu \theta, \quad (6.61)$$

$$\left. \frac{dS(\theta)}{d\theta} \right|_{\theta=0} = \mu \frac{\kappa_p}{\kappa_c}. \quad (6.62)$$

Error signal equals zero when $\theta = 0$ and a shift in equisignal direction of the direction finding characteristic does not occur.

The effect of nonidentity of sum and difference channels is apparent only on direction finding sensitivity, which can be characterized by formula

$$\frac{\kappa_p}{\kappa_c} = \frac{\kappa_c \pm \Delta\kappa}{\kappa_c} = 1 \pm \frac{\Delta\kappa}{\kappa_c}. \quad (6.63)$$

Change in sensitivity is directly proportional to unbalance of one of the channels with respect to transmission factor. Thus, if the permissible sensitivity loss is expressed by quantity 0.5, the transmission factor of the difference channel must not be less than half the transmission factor of the sum channel.

Case 5. Receiving channels before and after sum-difference converter are identical in amplitude characteristics but nonidentical

in phase characteristics. In this case, $g = 1$; $k_c = k_D = k$; $\psi \neq 0$, $\gamma \neq 0$ and direction finding conditions for the system, as follows from (6.44) and (6.46), are determined by expressions

$$\mu\theta = \frac{1 \pm \sqrt{1 + \sin^2 \psi \operatorname{tg}^2 \gamma}}{\sin \psi \operatorname{tg} \gamma}, \quad (6.64)$$

$$\left. \frac{dS(\theta)}{d\theta} \right|_{\theta=0} = \frac{2\mu \cos \gamma}{(1 + \cos \psi)}. \quad (6.65)$$

Expression (6.64) is analogous to the expression obtained by a somewhat different method in reference [86].

When $\psi = 0$, $\gamma \neq 0$ (case 3) $\mu\theta = 0$.

The effect of phase unbalance is apparent only in the direction finding sensitivity. When $\gamma = 0$, $\psi \neq 0$ (case 2); similarly $\mu\theta = 0$. Thus, systematic selection finding errors appear only during phase nonidentity of high-frequency circuits and sum and difference channels simultaneously.

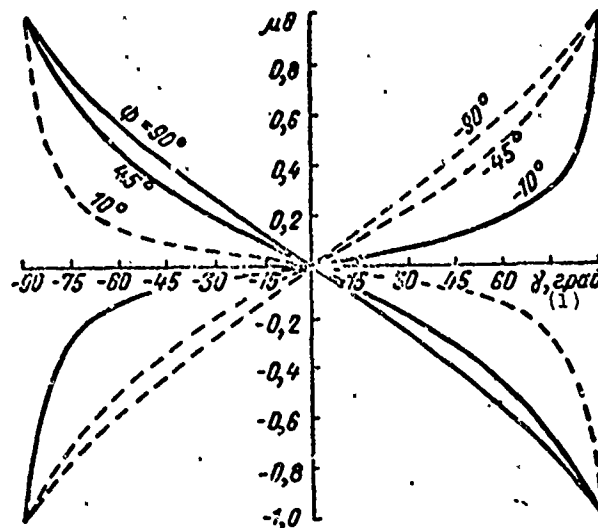


Fig. 6.10. Dependence of generalized direction finding error on value of out-of-phase condition for sum and difference receiving channels calculated with various values for out-of-phase condition of high-frequency channels.
KEY: (1) deg.

Figure 6.10 presents the values of generalized errors calculated according to formula (6.64) for various values of out-of-phase condition for receiving channels. Using calculated data and prescribing the value of direction finding sensitivity, we can determine angular systematic error as a function of the value of phase nonidentity of channels in an amplitude sum-difference monopulse system. Thus, for example, when $\mu = 0.25$ 1/deg, $\gamma = 45^\circ$, $\psi = 10^\circ$ and 45° , systematic angular error, respectively; is 0.35° and 1.27° . If permissible error is taken as one minute, nonidentity in phase of high-frequency circuits with $\gamma = 45^\circ$ must not exceed $\psi = 0.5^\circ$.

Results of analysis show that amplitude sum-difference monopulse systems unlike amplitude-amplitude monopulse systems require a rather high-quality in-phase condition for high-frequency receiving channels.

Taking into account the substantial effect of phase unbalance in high-frequency circuits on target finding accuracy, in designing a radar the waveguide bridge intended for sum-difference signal processing should be located as near as possible to the antenna in order to reduce the possible nonidentity with respect to phase in high-frequency circuits.

Without going into a detailed analysis, we should examine a method for analyzing the effect on direction finding accuracy of nonidentity in amplitude phase characteristics of receiving channels, taking into account the nonlinearity of the direction finding characteristic. For this we shall approximate the amplitude radiation pattern with respect to voltage by a Gaussian curve [44]:

$$F(\theta) = \exp\left(-\frac{a_0^2 \theta^2}{2}\right), \quad (6.66)$$

where $a_0^2 = 2,776/\theta_{0.5}^2$,

$\theta_{0.5}$ is the width of the antenna beam with respect to half-power level.

For the case of mutually independent feeds, signals at antenna output in each channel will be proportional

$$\dot{E}_1(t, \theta) = \dot{E}(t) \exp \left[-\frac{a_0^2}{2} (\theta_0 - \theta)^2 \right], \quad (6.67)$$

$$\dot{E}_2(t, \theta) = \dot{E}(t) \exp \left[-\frac{a_0^2}{2} (\theta_0 + \theta)^2 \right], \quad (6.68)$$

where $\dot{E}(t)$ is a function determining the signal entering antenna system input from the target.

The signal in the sum and difference channel can be expressed as

$$\dot{E}_c(t, \theta) = \dot{E}(t) F_c(\theta_0, \theta), \quad (6.69)$$

$$\dot{E}_p(t, \theta) = \dot{E}(t) F_p(\theta_0, \theta), \quad (6.70)$$

where $F_c(\theta_0, \theta)$, $F_p(\theta_0, \theta)$ are the sum and difference radiation patterns with respect to voltage.

Obviously,

$$\begin{aligned} F_c(\theta_0, \theta) &= \frac{1}{\sqrt{2}} \left\{ \exp \left[-\frac{a_0^2}{2} (\theta_0 - \theta)^2 \right] + \right. \\ &\quad \left. + \exp \left[-\frac{a_0^2}{2} (\theta_0 + \theta)^2 \right] \right\} = \\ &= \sqrt{2} \exp \left[-\frac{a_0^2}{2} (\theta_0^2 + \theta^2) \right] \operatorname{ch}(a_0^2 \theta_0 \theta). \end{aligned} \quad (6.71)$$

Analogously we can show that the difference radiation pattern

$$F_p(\theta_0, \theta) = \sqrt{2} \exp \left[-\frac{a_0^2}{2} (\theta_0^2 + \theta^2) \right] \operatorname{sh}(a_0^2 \theta_0 \theta). \quad (6.72)$$

With a given approximation of radiation patterns the direction finding characteristic of the system, without taking into account nonidentities of the amplitude-phase characteristics for receiving channels, can be represented in the form

$$S(\theta) = \frac{\operatorname{Re} \dot{E}_e(t, \theta) \dot{E}_p^*(t, \theta)}{\dot{E}_e(t, \theta) \dot{E}_e^*(t, \theta)} = \operatorname{th}(a_0^2 \theta_0 \theta). \quad (6.73)$$

The expression obtained shows that error signal is related by nonlinear dependence with the angle of target deviation from equisignal direction and only with small angular errors can it be expressed by linear function

$$S(\theta) \approx a_0^2 \theta_0 \theta. \quad (6.74)$$

Steepness of direction finding characteristics in equisignal direction is defined as

$$\mu = \left. \frac{dS(\theta)}{d\theta} \right|_{\theta=0} = \left. \frac{a_0^2 \theta_0}{\operatorname{ch}^2(a_0^2 \theta_0 \theta)} \right|_{\theta=0} = a_0^2 \theta_0. \quad (6.75)$$

Substituting the value of a_0 in (6.75) and assuming $\theta_0 = \frac{\theta_{0.5}}{2}$, we find

$$\mu \approx \frac{1.4}{\theta_{0.5}}. \quad (6.76)$$

Given the width of the radiation pattern with respect to half power level, we can determine the value of direction finding characteristic steepness, and knowing the steepness, it is easy to calculate from the above calculated dependences direction finding errors with any possible nonidentities of amplitude-phase characteristics for receiving channels of the system. The dependence of direction finding characteristic steepness on radiation pattern width and the amount of its maximum deviation from antenna axis can be determined by this method for any approximation of radiation pattern taking into account the nonidentity of characteristics for receiving channels.

6.3.3. The effect of nonidentity in amplitude-phase characteristics of receiving channels for a phase-phase monopulse system on direction finding accuracy. A simplified block diagram of a phase-phase monopulse system is presented in Fig. 1.8.

Earlier it was shown that signals at output of the first and second channels of the antenna in such a system can be represented by expression

$$E_1(t, \theta) = E_m F(\theta) \exp i \left(\omega t + \frac{\Delta\varphi}{2} \right), \quad (6.77)$$

$$E_2(t, \theta) = E_m F(\theta) \exp i \left(\omega t - \frac{\Delta\varphi}{2} \right). \quad (6.78)$$

Let us assume that transmission factors for receiving channels are k_1 and k_2 , respectively, and phase shift in one channel is $90^\circ + \psi$. Then at the amplifier channel output we have

$$\dot{u}_1(t, \theta) = U_{\text{орп}} \exp i \left(\omega_{\text{орп}} t + \frac{\Delta\varphi}{2} \right), \quad (6.79)$$

$$\dot{u}_2(t, \theta) = U_{\text{орп}} \exp i \left(\omega_{\text{орп}} t - \frac{\Delta\varphi}{2} + 90 + \psi \right), \quad (6.80)$$

and at phase detector output, taking into account limitation of signals with respect to amplitude in the receiving circuits

$$S(\theta) = \text{Re} \dot{u}_1(t, \theta) \dot{u}_2^*(t, \theta) = \text{Re} \kappa_{\phi \mu} U_{\text{орп}}^2 \exp i (\Delta\varphi - 90 - \psi) = \kappa_{\phi \mu} U_{\text{орп}}^2 \sin(\Delta\varphi - \psi). \quad (6.81)$$

Substituting into (6.81) the value of $\Delta\varphi$ and equating error signal to zero, we obtain

$$\frac{2\pi\lambda}{\lambda} \sin \theta = -\psi \quad (6.82)$$

or

$$\sin \theta = -\frac{\phi}{2\pi} \frac{\lambda}{l}. \quad (6.83)$$

With automatic target tracking angular errors are comparatively small and $\sin \theta \approx \theta$. Hence it follows that

$$\theta = -\frac{\phi}{2\pi} \frac{\lambda}{l} \approx -\frac{\phi}{2\pi} \theta_{0.5} \quad (6.84)$$

or

$$\frac{\theta}{\theta_{0.5}} = -\frac{\phi}{2\pi}. \quad (6.85)$$

Equality (6.85) shows that phase unbalance of receiving channels leads to the appearance of angular direction finding errors directly proportional to the value of phase unbalance. Direction finding errors for phase servosystems do not depend upon the value of the measurable phase difference caused by target deviation from equisignal direction [65].

As for amplitude unbalance of receiving channels, the use of limitation excludes its effect on direction finding accuracy in phase-phase monopulse systems. This agrees with the conclusion in reference [55].

6.3.4. The effect of nonidentity of amplitude phase characteristics for receiving channels of a phase sum-difference monopulse system on direction finding accuracy. A simplified block diagram of a phase sum-difference monopulse system is presented in Fig. 1.11. The same designations for phase and amplitude nonidentity are used as were used in our study of amplitude sum-difference monopulse systems. Signals at waveguide bridge output can be represented in a form of the following expressions:

$$\begin{aligned} \dot{E}_c(t, \theta) = E_0 \left[\exp i \left(\omega t + \frac{\Delta \varphi}{2} + \psi \right) + \right. \\ \left. + g \exp i \left(\omega t - \frac{\Delta \varphi}{2} \right) \right], \quad (6.86) \end{aligned}$$

$$\begin{aligned} \dot{E}_p(t, \theta) = E_0 \left[\exp i \left(\omega t + \frac{\Delta\varphi}{2} + \psi \right) - \right. \\ \left. - g \exp i \left(\omega t - \frac{\Delta\varphi}{2} \right) \right]. \end{aligned} \quad (6.87)$$

where

$$E_0 = \frac{1}{\sqrt{2}} E_m F(\theta) \kappa_1.$$

At the output of the sum and difference channel

$$\begin{aligned} \dot{u}_c(t, \theta) = E_0 \kappa_c \left[\exp i \left(\omega_{np} t + \frac{\Delta\varphi}{2} + \psi \right) + \right. \\ \left. + g \exp i \left(\omega_{np} t - \frac{\Delta\varphi}{2} \right) \right], \end{aligned} \quad (6.88)$$

$$\begin{aligned} \dot{u}_p(t, \theta) = E_0 \kappa_p \left[\exp i \left(\omega_{np} t + \frac{\Delta\varphi}{2} + \right. \right. \\ \left. \left. + \psi + \gamma - \frac{\pi}{2} \right) - g \exp i \left(\omega_{np} t - \frac{\Delta\varphi}{2} + \gamma - \frac{\pi}{2} \right) \right]. \end{aligned} \quad (6.89)$$

At phase detector output, taking into account sum signal standardization,

$$\begin{aligned} S(\theta) &= \frac{\operatorname{Re} \dot{u}_c(t, \theta) \dot{u}_p^*(t, \theta)}{\dot{u}_c(t, \theta) \dot{u}_c^*(t, \theta)} = \\ &= \frac{\kappa_p [(1-g)^2 \sin \gamma + 2g \sin(\Delta\varphi + \psi) \cos \gamma]}{\kappa_c (1+g)^2 + 2g \cos(\Delta\varphi + \psi)}. \end{aligned} \quad (6.90)$$

Hence the condition of equilibrium for the direction finding system is determined by equation

$$(1-g^2) \sin \gamma + 2g \sin(\Delta\varphi + \psi) \cos \gamma = 0. \quad (6.91)$$

Solving this equation relative to $\Delta\phi$, we find

$$\Delta\varphi = \arcsin \left[\frac{(g^2 - 1)}{2g} \operatorname{tg} \gamma \right] - \psi. \quad (6.92)$$

Substituting into (6.92) the value of $\Delta\phi = \frac{2\pi}{\lambda} z\theta$ and taking into account equality $\theta_{0.5} = \lambda/z$, we obtain the following formula for direction finding error:

$$\frac{\theta}{\theta_{0,s}} = \frac{1}{2\pi} \left[\arcsin \left(\frac{g^2 - 1}{2g} \operatorname{tg} \gamma \right) - \psi \right]. \quad (6.93)$$

Let us examine a number of practical cases.

Case 1. High-frequency circuits are identical in phase but non-identical in transmission factor; sum and difference channels have identical amplitude-phase characteristics. In this case; $\psi = 0$; $g \neq 1$; $k_c = k_p = k$; $\gamma \neq 0$.

Substituting these values into equations (6.90) and (6.93), we find

$$S(\theta) = \frac{2g \sin \Delta\varphi}{(1 + g^2) + 2g \cos \Delta\varphi}, \quad (6.94)$$

$$\frac{\theta}{\theta_{0,s}} = 0.$$

Consequently, amplitude unbalance for the high-frequency part of the receivers in a phase sum-difference system does not especially affect direction finding accuracy; the zero of the direction finding characteristic is not shifted and only direction finding sensitivity changes, but insufficiently.

Case 2. Sum and difference channels are identical in characteristics; high-frequency channels are identical in transmission factor but nonidentical in phase shifts. In this case, $k_p = k_c = k$; $\gamma = 0$; $g = 1$; $\psi \neq 0$ and for comparatively small direction finding errors

$$S(\theta) = \frac{\sin(\Delta\varphi + \psi)}{1 + \cos(\Delta\varphi + \psi)} = \operatorname{tg} \frac{\Delta\varphi + \psi}{2}. \quad (6.95)$$

$$\frac{\theta}{\theta_{0,s}} = -\frac{\psi}{2\pi}. \quad (6.96)$$

As in a phase-phase monopulse system, direction finding error is directly proportional to the value of phase nonidentity for high-frequency channels. The sign of the error depends upon what channel has the greater phase delay.

Case 3. High-frequency circuits are identical in characteristics; sum and difference channels are identical in phase but nonidentical in transmission factors. In this case,

$$g = 1; \psi = 0; \gamma = 0; \kappa_c \neq \kappa_p, \\ S(\theta) = \frac{\kappa_p}{\kappa_c} \operatorname{tg} \frac{\Delta\varphi}{2}, \quad (6.97)$$

$$\mu' = \left. \frac{dS(\theta)}{d\theta} \right|_{\theta=0} = \frac{\kappa_p}{\kappa_c} \frac{\pi l}{\lambda} = \frac{\kappa_p}{\kappa_c} \mu, \quad (6.98)$$

where μ is the steepness of the direction finding characteristic of the system with identical receiving channel.

Obviously, unbalance of sum and difference channels with respect to transmission factors does not give a zero shift of direction finding characteristic and only somewhat affects direction finding sensitivity of the system.

Case 4. High-frequency circuits are identical in characteristics; sum and difference channels are identical in transmission factors but nonidentical in phase. In this case, $g = 1; \psi = 0; \kappa_p = \kappa_c = k; \gamma \neq 0$ and according to expression (6.95) $\theta/\theta_{0.5} = 0$, which corresponds to the absence of shift of equisignal direction.

The direction finding characteristics and its steepness for this case, in accordance with expression (6.90), can be represented by equation

$$S(\theta) = \frac{\sin \Delta\varphi}{1 + \cos \Delta\varphi} \cos \gamma = \operatorname{tg} \frac{\Delta\varphi}{2} \cos \gamma, \quad (6.99)$$

$$\left. \frac{dS(\theta)}{d\theta} \right|_{\theta=0} = \frac{\pi}{\theta_{0.5}} \cos \gamma. \quad (6.100)$$

The effect of phase nonidentity for sum and difference channels is manifested, as can be seen from expressions (6.99) and (6.100), in the change in direction finding sensitivity.

When $\gamma = \pm \frac{\pi}{2}$ $S(\theta) = 0$ and $\left. \frac{dS(\theta)}{d\theta} \right|_{\theta=0} = 0$, error signal becomes equal to zero regardless of antenna displacement angle with target direction. When $90 < \gamma < 270^\circ$ the sign of the direction finding characteristic steepness and the error signal change to the reverse. Out-of-phase condition of the coordinate system sets in, leading to its unstable state. With phase shift $\gamma \leq 60^\circ$ direction finding sensitivity drops no more than half as compared with the case when amplitude-phase characteristics of channels are identical.

We should note that the character of the effect of amplitude and phase nonidentity for sum and difference channels on direction finding accuracy in amplitude and phase systems is identical since in those types of systems the same angle discriminator is used.

Case 5. Receiving channels before and after sum-difference converters are identical in amplitude but nonidentical in phase characteristics. In this case, $g = 1$, $k_c = k_p = k$; $\psi \neq 0$; $\gamma \neq 0$ and the basic direction finding properties of the system are determined by the following expressions:

$$S(\theta) = \frac{\sin(\Delta\varphi + \psi)}{1 + \cos(\Delta\varphi + \psi)} \cos \gamma = \operatorname{tg} \frac{\Delta\varphi + \psi}{2} \cos \gamma, \quad (6.101)$$

$$\left. \frac{dS(\theta)}{d\theta} \right|_{\theta=\theta_p} = \frac{\pi}{\theta_{0.5}} \cos \gamma, \quad (6.102)$$

where $\theta_p = -\frac{\psi}{2\pi} \theta_{0.5}$ is the working point of the direction finding characteristic, determined in accordance with the expression obtained from (6.93):

$$\frac{\theta}{\theta_{0.5}} = -\frac{\psi}{2\pi}. \quad (6.103)$$

These expressions show that with phase nonidentity for receiving channels before and after the sum-difference converter in a phase sum-difference monopulse system there occurs zero shift of the direction finding characteristic (systematic error) and the direction finding sensitivity drops (dynamic errors increase).

A comparison of results of this analysis enables us to conclude that in systems with sum-difference angular discriminators we can impose less rigid requirements on amplitude and phase stability of i-f amplifiers than we do in systems with amplitude and phase angular discriminators.

§ 6.4. SUPPLEMENTARY REQUIREMENTS FOR IDENTITY OF AMPLITUDE-PHASE CHARACTERISTICS OF RECEIVING CHANNELS DURING THE USE OF WIDE-BAND, CONTINUOUS AND QUASICONTINUOUS SIGNALS

The use in monopulse systems of wide-band sounding signals (frequency-modulated pulses, continuous signals with frequency modulation) leads to additional requirements in the design of these systems. This is connected with the fact that in practice signal processing differs from optimal and with various forms of signal there occur additional angular errors [45].

Usually the antenna system is sufficiently wide-band and does not distort the form of the signals received and, consequently, additional requirements generally pertain to information converters and angular discriminators.

We shall examine briefly these requirements with respect to several forms of sounding signals.

6.4.1. Direction finding on signals with frequency modulation. When using frequency modulation, information converters must perform their function on any frequency contained in the spectrum of the signal received.

The use of a double waveguide T-joint ensures sufficient wide-band conditions for an information converter. As for phase switchers they perform their function only with small relative frequency deviations. We see this in the example in [45].

Let at input of a monopulse system a signal with linear frequency modulation enter

$$\dot{E}(t) = E_m \exp i \omega t, \quad (6.104)$$

where $\omega = \omega_0 + \omega'(t - 0.5T_q)$ is instantaneous frequency;

ω_0 is mean signal frequency;

$\omega' = \frac{d\omega}{dt}$ is the signal frequency change rate;

T_q is the frequency modulation period.

The instantaneous phase of this signal is

$$\varphi = \int \omega dt = (\omega_0 - 0.5\omega'T_q)t + 0.5\omega't^2 + \varphi_0. \quad (6.105)$$

The phase switcher can be similar to the delay device. Then the phase of the signal delayed by time τ is determined by expression

$$\varphi_\tau = (\omega_0 - 0.5\omega'T_q)(t + \tau) + 0.5\omega'(t + \tau)^2 + \varphi_0. \quad (6.106)$$

and phase difference corresponding to time shift τ is determined by the following time function:

$$\Delta\varphi = \varphi_\tau - \varphi = (\omega_0 - 0.5\omega'T_q)\tau + \omega'\tau + 0.5\omega'\tau^2. \quad (6.107)$$

In accordance with this, error signal at output of angular discriminator during target finding on signals with frequency modulation will also be a function of time, which reduces direction finding accuracy and the interference immunity of the system.

To exclude the dependence of phase difference on time, it is necessary to have either a signal delay time variable provided by the phase switcher with phase shift independent of frequency (within the frequency spectrum of the signal) or small relative frequency deviations when $\Delta\phi \approx \omega_0\tau$.

If the carrier frequency of signals received is modulated according to harmonic law:

$$\omega = \omega_0 + \Delta\omega \sin \Omega t, \quad (6.108)$$

where $\Delta\omega$ is frequency deviation and Ω is modulation frequency, phase difference corresponding to time shift τ , taking into account inequality $\omega \gg \Omega$, is determined by expression

$$\Delta\phi = \omega_0\tau + \Delta\omega\tau \sin \Omega \left(\frac{t}{2} + \tau \right). \quad (6.109)$$

In a phase-phase monopulse system time delay τ between signals received is determined by the angular position of the target and error signal with identical receiving channels, as we know, is formed according to $S(\theta) = \sin \Delta\phi$. In accordance with this, the expression for error signal in the examined case when $\theta = 0$ assumes the form

$$S(0) = \sin \left[\omega_0\tau + \Delta\omega\tau \sin \Omega \left(\frac{t}{2} + \tau \right) \right]. \quad (6.110)$$

Hence it follows that with frequency modulation of signals received there occurs parasitic amplitude modulation of error signal even with identical characteristics of receiving channels.

We obtain a similar result in a phase sum-difference system where

$$S(\theta) = \operatorname{tg} \frac{\Delta\phi}{2} = \operatorname{tg} \frac{1}{2} \left[\omega_0\tau + \Delta\omega\tau \sin \Omega \left(\frac{t}{2} + \tau \right) \right]. \quad (6.111)$$

Thus, when using a frequency-modulated signal in monopulse systems with phase direction finding, the character of the direction

finding function is distorted and parasitic amplitude modulation of error signal appears, reducing direction finding accuracy. Therefore, in systems with phase direction finding it is permissible to use a frequency-modulated signal with a small relative frequency deviation.

In monopulse systems with amplitude direction finding and identical receiving channels the effect of a frequency-modulated signal appears in the dependence of the amplitude radiation patterns on frequency and in the parasitic amplitude modulation of error signal and, as a consequence, reduces accuracy.

With nonidentical amplitude-phase characteristics for receiving channels the effect of a frequency-modulated signal on direction finding accuracy intensifies and error increases. Therefore, when operating with frequency-modulated signals, requirements for identity of amplitude-phase characteristics for receiving channels are higher than with signals discussed earlier. These requirements can be evaluated with the method described above for each case.

6.4.2. Direction finding on continuous and quasi-continuous signals with speed selection. Examples of monopulse direction finders with speed selection are presented in Chapter 1. The characteristic peculiarity of such systems is the measurement of angular target coordinates after the selection of signals with respect to doppler frequencies. Therefore, each receiving channel includes a doppler filter terminating in a phase detector.

Since the doppler shift of signal frequency depends upon speed, course parameters, and aerodynamic properties of the target and, under actual conditions, varies within a wide range, in direction finding systems using speed selection there are imposed particularly high requirements on identity of doppler filter characteristics. Having a narrow band and great steepness of phase-frequency characteristics, such filters, with insufficient identity of characteristics and a change in doppler frequency shift during target tracking based on speed, can create large equipment errors in the direction

finding system. To lessen this we must turn to frequency stabilization of signals entering the doppler filter to the phase detector.

Requirements for identity of receiving channels during operation on signals of quasi-continuous and continuous type are similar.

6.4.3. Direction finding during the use of pulsed signal compression. As we know, for the purpose of preserving high resolution with respect to range and of improving the power ratios with limited peak power, we resort to an expansion of the working pulse and interpulse frequency (phase) modulation. Such a pulsed signal, after having passed through the optimal filter of the receiver, undergoes compression with respect to width.

Pulse width compression is brought about by the fact that the optimal filter creates delay of each central component of the signal in accordance with its frequency in such a manner that the low-frequency components are delayed longer and the high-frequency components are delayed less. This ensures, at a certain moment of time, phase addition of all frequency components and formation of a short pulse of high amplitude.

Nonidentity of medium tuning frequencies for optimal filters leads to a variation in the signal amplitude ratio, the appearance of parasitic phase shift, and frequency modulation, which causes a corresponding variation in error signal and a reduction of direction finding accuracy. If the medium frequency of the signal and the nonidentity of optimal filter tuning are stable in time, error signal distortion in a direction finding system can be removed by tuning the equipment. In the opposite case, a reduction in both accuracy and interference immunity is inevitable.

Nonidentity of filters can be apparent in the nonagreement of frequency change rates and the envelope of pulse filter response with the corresponding parameters of the input signal. In this case, even with identity of filter medium frequency tuning, parasitic phase shifts and residual frequency modulation can reach a significant value.

Hence, it follows that the provision of a certain degree of optimal filter identity in monopulse direction finding systems operating on pulsed signals with frequency modulation is very important.

Given the values of permissible parasitic phase shifts and residual frequency modulation, we can determine the requirements for identity of optimal filters from formulas [45].

$$\Delta\varphi = 0,5 \left(\operatorname{arctg} \frac{C_{\phi_1}}{B_{\phi_1}} - \operatorname{arctg} \frac{C_{\phi_2}}{B_{\phi_2}} \right), \quad (6.112)$$

$$\Delta h = \frac{1}{4} \left(\frac{C_{\phi_1}}{B_{\phi_1}^2 + C_{\phi_1}^2} - \frac{C_{\phi_2}}{B_{\phi_2}^2 + C_{\phi_2}^2} \right), \quad (6.113)$$

where

$$B_{\phi_1} = \frac{a_c}{4(a_c^2 + \dot{\omega}_c^2)} + \frac{a_1}{4(a_1^2 + \dot{\omega}_1^2)},$$

$$C_{\phi_1} = \frac{\dot{\omega}_c}{4(a_c^2 + \dot{\omega}_c^2)} - \frac{\dot{\omega}_1}{4(a_1^2 + \dot{\omega}_1^2)},$$

$$B_{\phi_2} = \frac{a_c}{4(a_c^2 + \dot{\omega}_c^2)} + \frac{a_2}{4(a_2^2 + \dot{\omega}_2^2)},$$

$$C_{\phi_2} = \frac{\dot{\omega}_c}{4(a_c^2 + \dot{\omega}_c^2)} - \frac{\dot{\omega}_2}{4(a_2^2 + \dot{\omega}_2^2)},$$

Δh is the difference in frequency change rates;
 a_c is the coefficient characterizing the change rate of the input signal envelope;
 $\dot{\omega}_c$ is the change rate of the input signal frequency;
 a_1 and a_2 are coefficients characterizing the variation in signal envelope with passage through optimal filters of the first and second receiving channels;
 $\dot{\omega}_1$ and $\dot{\omega}_2$ are signal frequency change rates with passage through optimal filters of the first and second receiving channels.

§ 6.5. DESIGN METHODS OF DECREASING DIRECTION FINDING EQUIPMENT ERROR

Methods of decreasing equipment error are varied. They include technological methods connected with the perfection of the technology involved in making separate units and elements of equipment; operational methods connected with the preparation of equipment for work, its tuning, calibration, and operation; and design methods connected with working out schematic solutions which enable us to reduce substantially or completely exclude the effect of nonidentity in amplitude-phase characteristics of receiving channels.

Of greatest interest are the design methods covering various procedures for uniting the receiving channels of monopulse radars, stabilization of intermediate frequency, cross-switching of receiving channels, and a number of others.

Let us pause on the question of joining receiving channels. The essence of this lies in the fact that instead of two or three receiving channels necessary in accordance with the principle of a monopulse radar, one channel is used functionally replacing the two or three channels. Since, in this case, the extent of the separate channels is reduced to minimum, equipment errors caused by nonidentity of characteristics for these channels are also reduced. At the present time there are many methods enabling us to join functionally the receiving channels into a single channel. We should examine some of them.

6.5.1. A method of joining receiving channels on high frequency. The simplified system whose block diagram is presented in Fig. 6.11 relates to one of the first monopulse radars with amplitude direction finding, designed for determining coordinates in one plane [124].

The antenna system of this station consists of two parabolic reflectors mechanically connected to each other, one of which is receiving and the other transmitting. This design of antenna system makes it possible to avoid problems connected with the switching of high-frequency circuits to reception and transmission.

The distinguishing feature of this radar is the joining of receiving channels on high-frequency into one channel with the use of a time spread of signals received along different channels, accomplished by high-frequency delay of one of the signals for a time exceeding pulse width.

After the interconnection, high-frequency signals are converted into intermediate-frequency signals, amplified in a logarithmic amplifier, detected and separated by the proper gating. Separated signals are compared by the subtraction method. For this, an undelayed signal is delayed by the same amount of time the other signal is delayed with interconnection of channels.

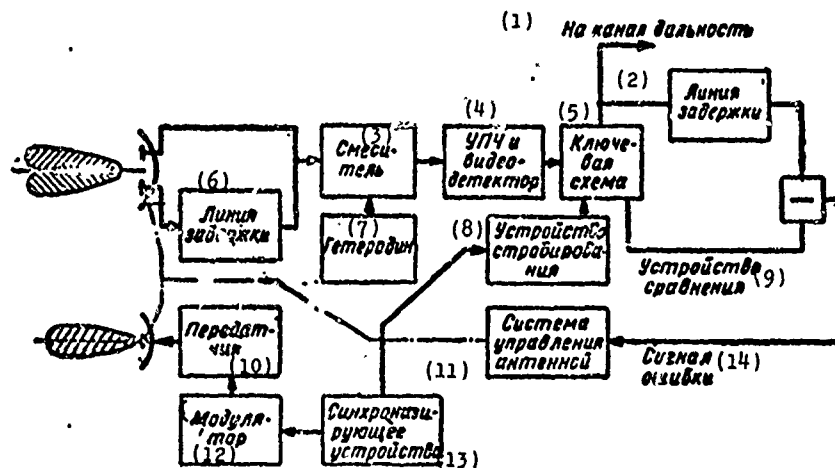


Fig. 6.11. Simplified block diagram of an amplitude-amplitude monopulse radar with interconnection of receiving channels on high frequency.

KEY: (1) To range channel; (2) Delay line; (3) Mixer; (4) I-f amplifier and video detector; (5) Key circuit; (6) Delay line; (7) Heterodyne; (8) Gating device; (9) Comparison device; (10) Transmitter; (11) Antenna control system; (12) Modulator; (13) Synchronizing device; (14) Error signal.

The disadvantage of this method of channel interconnection is a reduction in range resolution. Although a radar operating in normal

mode is capable of distinguishing targets radially spaced at a value corresponding to pulse width, this system is not capable of distinguishing targets whose radial spacing does not exceed two widths of the sounding pulse. In this case, signals reflected from a distant target and the delay signal from a near target will pass through the receiver simultaneously and not be separated.

Another disadvantage of this system is the fact that it is subject to the effect of interference in the form of paired pulses spaced at the value of delay, introduced into the system with the interconnection of receiving channels.

A design disadvantage of joining high-frequency receiving channels is the awkwardness of the delay line. Thus, in the Sommers radar [124] the delay line is a waveguide 3.5 m long rolled into a coil. A corresponding compensation for signal attenuation in the delay line is necessary. With this design there are difficulties in ensuring the identity of characteristics for the unjoined parts of the receiving channels.

6.5.2. A method of joining intermediate-frequency receiving channels. A simplified block diagram of the receiving part of a monopulse radar with amplitude direction finding and interconnection of intermediate-frequency receiving channels is presented in Fig. 6.12 [110].

Signals received by antennas 1 and 2 enter the mixers where, with the aid of the common heterodyne, they are transformed into i-f signals and then amplified in preliminary i-f amplifiers PIFA. After one of the PIFA the delay line is switched on, ensuring time delay for one of the signals received by a value exceeding the working pulse width. Spacing of signals with respect to time enables us to establish the amplification of both received signals in a common i-f amplifier.

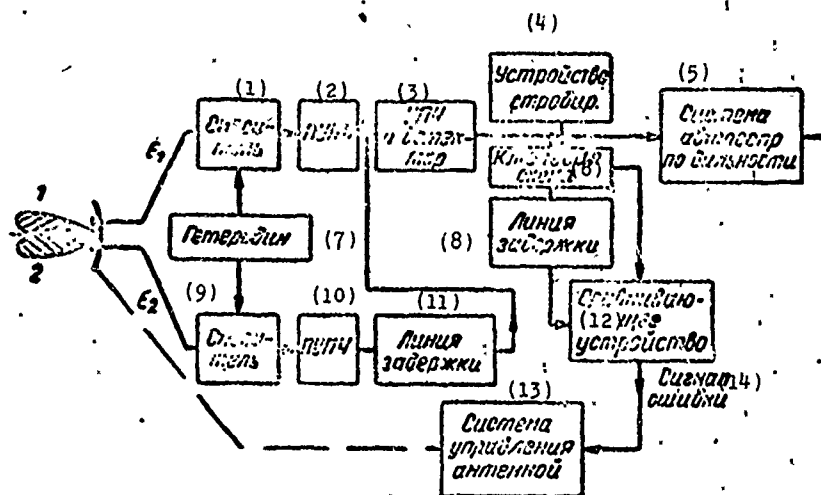


Fig. 6.12. Simplified block diagram of the receiving part of an amplitude-amplitude monopulse radar with interconnection of intermediate-frequency receiving channels.
 KEY: (1) Mixer; (2) PIFA; (3) I-f amplifier and detector; (4) Gating device; (5) System of automatic range tracking; (6) Key circuit; (7) Heterodyne; (8) Delay line; (9) Mixer; (10) PIFA; (11) Delay line; (12) Comparing device; (13) Antenna control system; (14) Error signal.

After amplification in this amplifier, the signals are detected, separated into two channels with the aid of the key circuit gating and fed to the comparing device.

The operation of the receiving system is explained by the diagrams in Fig. 6.13.

The receiving part of a monopulse radar with phase direction finding and interconnection of i-f receiving channels can be designed similarly.

Since it is considerably simpler to make a compact delay line on intermediate frequency than on high frequency, this diagram has an advantage over a diagram with the interconnection of high-frequency receiving channels presented in Fig. 6.11. Another advantage is the fact that with interconnection of intermediate-frequency receiving channels the direction finding system can be protected from the effect of interference in the form of paired pulses by the introduction

of gating for the preliminary i-f amplifiers, ensuring the passage of only one of the interfering pulses.

Also in the circuit with interconnection of i-f receiving channels, the effect of receiving channel nonidentity before their interconnection increases since their length is greater than that of the circuit in Fig. 6.11. As for the shortcoming of the circuit with interconnection of high-frequency receiving channels, which is the reduction in range resolution, this also exists in a circuit with intermediate-frequency interconnection.

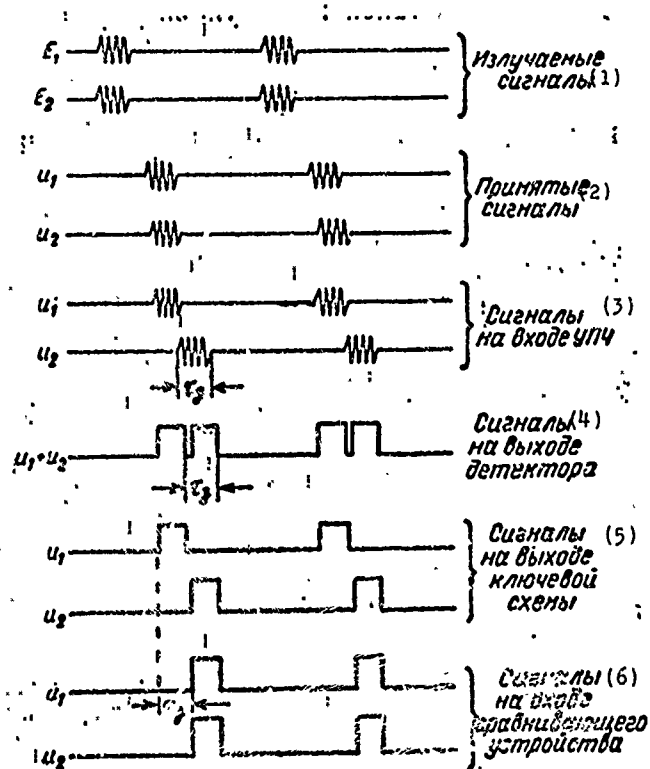


Fig. 6.13. Voltage diagrams describing the passage of signals in a receiver of an amplitude monopulse radar with interconnection of intermediate-frequency receiving channels.
 KEY: (1) Signals emitted; (2) Signals received; (3) Signals at i-f amplifier input; (4) Signals at detector output; (5) Signals at switching circuit output; (6) Signals at comparison input.

6.5.3. A method of joining i-f receiving channels with the use of phase shifts and time delay of signals. A simplified diagram of the receiving part of an amplitude sum-difference monopulse radar with the interconnection of range-measuring and angle-measuring channels by the method studied is presented in Fig. 6.14 [120].

Channels are joined at two stages. First the angle-measuring channels are joined. For this the difference signal of the azimuth channel $E_{p a}$ is shifted in phase 90° and is summed with the signal of the angle-measuring channel $E_{p y}$. After this the resulting angle-measuring signal is converted to an i-f signal, amplified in the preliminary i-f amplifier (PIFA), delayed in time equal approximately to the received signal width, and summed with the i-f sum signal which is simultaneously the range signal and the reference signal of the angle-measuring channels.

The output signal of the common i-f amplifier is branched into three directions: one is fed to the phase-sensitive detector of the angle-measuring channel, another with a phase shift of 90° to the phase-sensitive detector of the azimuth channel, and the third part of the signal, after additional amplification in the i-f amplifier stage and delay by a value equal to the delay of the angle-measuring signals before channel interconnection, is fed through the phase switcher to the range channel and to the phase-sensitive angle-measuring detectors as the reference signal.

Phase-sensitive elevation and azimuth detectors makes it possible to obtain elevation in azimuth signals. Upon obtaining an elevation signal, one signal from the common i-f amplifier is fed directly to the phase detector, and the other through the supplementary gated i-f amplifier stage, delay line, and phase switcher. Because of this the reference portion of the first signal appears in the detector simultaneously with the angular portion of the second signal (see voltage diagram in Fig. 6.15) and interacts with the latter, ensuring error signal proportional to the angle of target displacement with respect to elevation at the detector output.

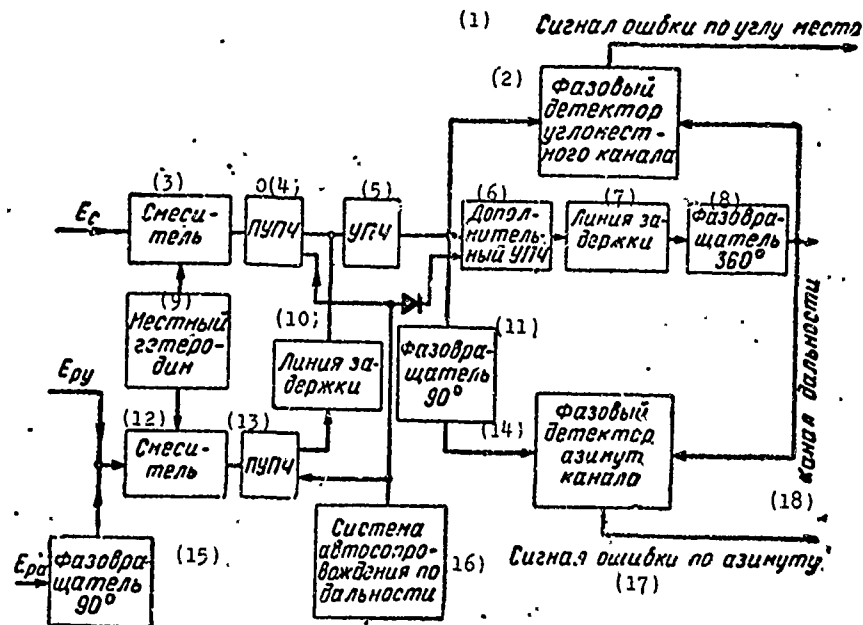


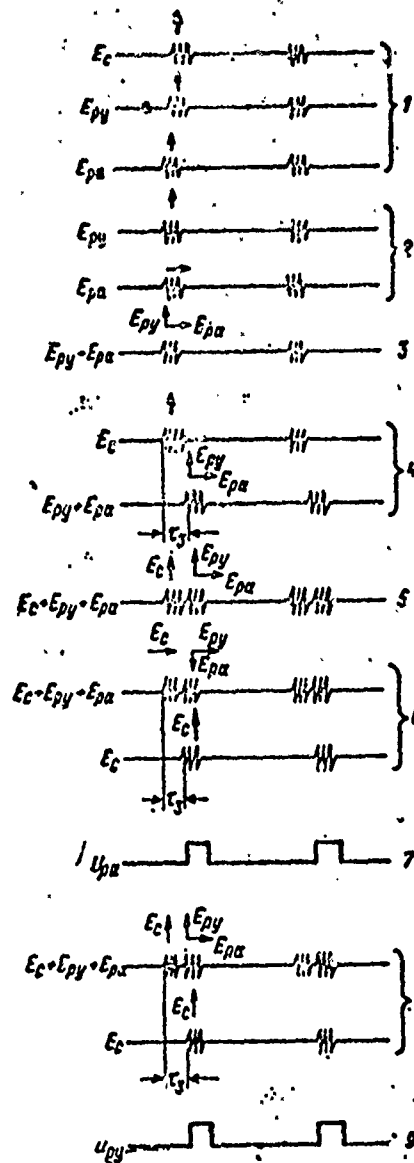
Fig. 6.14. Simplified block diagram of a receiver in an amplitude sum-difference monopulse radar with interconnection of range-measuring and angle-measuring channels on intermediate frequency with the use of phase shifts and time delay of signals. E_c sum signal; $E_p y$ difference signal of elevation channels; $E_p a$ difference signal of azimuth channel.

KEY: (1) Elevation error signal; (2) Phase detector of angle-measuring channel; (3) Mixer; (4) PIFA; (5) I-f amplifier; (6) Supplementary i-f amplifier; (7) Delay line; (8) Phase switcher 360°; (9) Local heterodyne; (10) Delay line; (11) Phase switcher; (12) Mixer; (13) PIFA; (14) Phase detector of azimuth channel; (15) Phase switcher; (16) Range autotracking system; (17) Azimuth error signal; (18) Range channel.

The part of the angle-measuring signal which corresponds to the angle of target displacement with respect to azimuth will not develop an error signal since it is in quadrature with the reference signal. Upon obtaining an azimuth error signal, one signal from the output of the i-f amplifier is fed to the phase detector through the phase switch, shifting it 90° in phase, while the other (reference) is fed through the supplementary gated i-f amplifier stage, the delay line, and the phase switcher. In this case the angular part of the first signal moves to the detector simultaneously with the reference

part of the second signal and develops at detector output an azimuth error signal. Part of the angle-measuring signal corresponding to the angle of target displacement with respect to elevation does not pass through the detector because of its quadrature with the reference signal.

Fig. 6.15. Signal voltage diagram, describing the work of the receiver of an amplitude sum-difference monopulse radar, illustrated in Fig. 6.14 (signal phase ratios are conditionally designated by errors). 1 - at output of waveguide bridges; 2 - at input of angle-measuring channel mixer; 3 - at output of angle-measuring channel mixer; 4 - at input of i-f amplifier; 5 - at output of i-f amplifier; 6 - at input of azimuth channel phase detector; 7 - at output of azimuth channel phase detector; 8 - at input of elevation channel phase detector; 9 - at output of elevation channel phase detector.



Since two delay lines are used in the circuit, this can cause a substantial misphasing of reference and angle-measuring signals. In order to compensate the parasitic phase shifts in the reference

signal channel, a phase switcher with wide phase control limits is provided.

In order that the signal/noise ratio not be impaired during signal passage through the receiving circuit, the PIFA is gated, thus ensuring the operation of the amplifier only during signal passage. A delay signal after the PIFA is essential since this improves the signal/noise ratio. Delay before the PIFA leads to signal attenuation at amplifier input and, consequently, a drop in the signal/noise ratio, which causes an impairment of the target tracking accuracy with respect to angular coordinates and range.

The disadvantage of this system is the relation of high sensitivity to phase difference for receiving channels. This deprives it of the main advantage of monopulse direction finders of the sum-difference type, in which a parasitic phase shift in receiving channels does not lead to a shift in equisignal direction. Sensitivity to phase nonidentity makes this system scarcely suitable for use in a radar with frequency tuning in a wide range.

In a number of cases the above relationship occurs only for difference channels and, in order to eliminate errors occurring with frequency tuning, automatic phase control is used for the channels [81, 93].

6.5.4. A method of receiving channel interconnection with the use of low-frequency modulation in one of the channels. A simplified block diagram of the receiving portion of a monopulse amplitude sum-difference radar with interconnection of channels by using low-frequency modulation of different signals is presented in Fig. 6.16 [125].

In this circuit the usual method of shaping sum and difference signals with a double waveguide bridge is used. The difference signal containing angular information on target position is modulated with respect to amplitude by a signal of sonic frequency Ω and is summed by a signal of the sum channel.

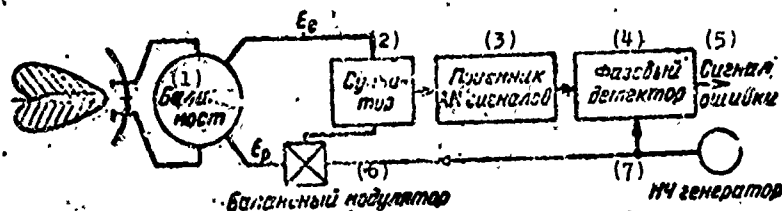


Fig. 6.16. Simplified block diagram of a receiver for an amplitude sum-difference radar with interconnection of receiving channels, using low-frequency modulation of the difference signal. KEY: (1) Balance bridge; (2) Summator; (3) AM signal receiver; (4) Phase detector; (5) Error signal; (6) Balance modulator; (7) L-f generator.

In accordance with this, the resulting signal, when approximating the sum diagram by function $\cos \theta$ and the difference diagram by function $\sin \theta$, can be represented by expression

$$\dot{E}(t, \theta) = E_m (\cos \theta + \sin \theta \sin \Omega t) \exp i \omega t. \quad (6.114)$$

With low values of angular error, expression (6.114) is changed to the form

$$\dot{E}(t, \theta) = E_m (1 + \theta \sin \Omega t) \exp i \omega t. \quad (6.115)$$

From expression (6.115) it is apparent that the modulation factor of the resulting signal is proportional to angular error. Therefore, signal amplitude detection at receiver output gives a signal of low frequency Ω , whose amplitude is proportional to the value of angular error, while phase indicates the direction of displacement. With passage of zero error, the phase of the low-frequency signal changes 180° .

The low-frequency signal from the output of the amplitude-modulated signal receiver is fed to the phase detector where

it is compared with respect to phase with the signal of the l-f oscillator and forms an error signal of constant voltage which acts on the servomechanism of the antenna position control.

In the receiving system we can use wide-band signal processing devices without reducing its sensitivity and because of this we can substantially reduce parasitic phase shifts. The narrow-band i-f amplifier, critical to tuning, ceases to be a source of errors since the sum and difference signals passing through it are shifted in phase by an identical quantity.

The system is simple enough to tune and stable under various operating conditions. However, the introduction of low-frequency modulation with the interconnection of receiving channels makes the direction finding system sensitive to amplitude fluctuation of the received signals and also vulnerable to the direction of limited amplitude-modulated noises. Obviously, in order to create such noises, it is enough to know the modulation frequency being used in the radar with an accuracy up to the band width of the servosystem. This is a serious disadvantage of this design of monopulse radar receiving system and limits its use.

6.5.5. A method of joining receiving channels with the use of signal spacing based on frequency. A simplified block diagram of a receiver for an amplitude sum-difference monopulse radar with interconnection of channels by spacing signals with respect to frequency is presented in Fig. 6.17 [42].

The principle of receiving channel interconnection consists in the fact that the sum and difference h-f signals are converted into i-f signals near in value, summed, and rigidly limited in a multistage wide-band amplifier - limiter. From the i-f amplifier output signals move to band-pass filters tuned to the corresponding frequencies of the joined signals and are separated by these filters into sum and difference signals. After separation the frequency of the sum signal is converted to the frequency of the difference signal. The signal obtained as a result of conversion is used as

the reference signal in the angle-measuring phase-sensitive detector during shaping of the error signal to be used later for the antenna control system.

This principle of channel interconnection can also be used in a system designed for direction finding in two planes. In this case, the signals to be joined (sum and two difference signals) are converted into signals of three closely located intermediate frequencies so that their spectra do not overlap and thus enable the sum signal to simultaneously shape both difference signals without using ordinary AGC systems based on the sum signal.

The use of this method of joining is not limited to systems of the sum-difference type; it can also be applied to other systems, for example, to amplitude systems with logarithmic receivers. The arrangement of the system, in this case, will differ from the arrangement illustrated in Fig. 6.17 only in the detector since, in order to obtain the value and sign of the angle of target deviation from equisignal direction, an amplitude detector is required instead of the phase detector used in the system illustrated.

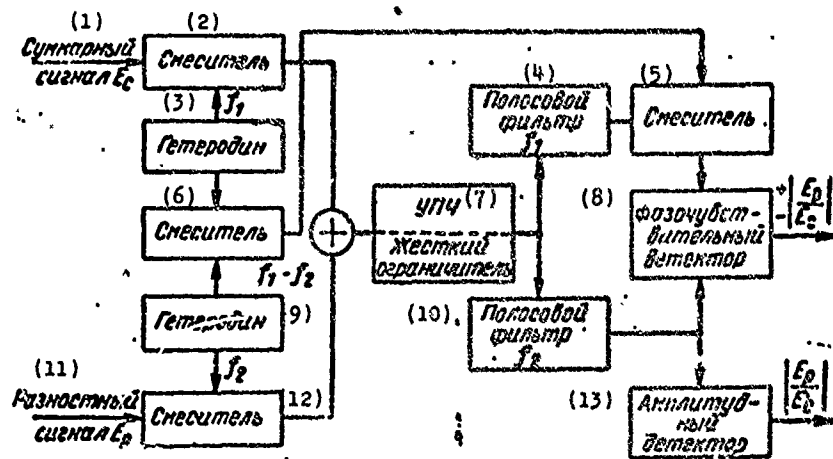


Fig. 6.17. Simplified block diagram of a receiver for an amplitude sum-difference pulse radar with the use of single-channel signal processing with frequency shift.

KEY: (1) From the signal; (2) Mixer; (3) Heterodyne; (4) Band-pass filter; (5) Mixer; (6) Mixer; (7) I-f amplifier limiter; (8) Phase-sensitive detector; (9) Heterodyne; (10) Band-pass filter. (11) Difference signal; (12) Mixer; (13) Amplitude detector.

Let us explain analytically the bases for the examined method of signal processing for the case of an ideal wide-band uneven limiter, by which we mean an installation consisting of the successive connection of an inertialess nonlinear element and a linear band-pass filter. For simplification, we shall perform our analysis in actual form.

Let the voltage of a signal at output of an ideal limiter be equal to the sum $S(t)$ of two narrow-band signals $S_1(t)$ and $S_2(t)$, where

$$S_1(t) = E_p \cos(\omega_1 t + \varphi_1), \quad (6.116)$$

$$\begin{aligned} S_2(t) &= E_c \cos(\omega_2 t + \varphi_2), \\ E_p &= E_p(t); \quad E_c = E_c(t); \\ \varphi_1 &= \varphi_1(t); \quad \varphi_2 = \varphi_2(t). \end{aligned} \quad (6.117)$$

With the aid of simple trigonometric transformation, $S(t)$ can be expressed by a single-narrow-band function with carrier frequency ω_1 in the following form

$$\begin{aligned} S(t) &= \{E_p^2 + E_c^2 + 2E_p E_c \cos[(\omega_2 - \omega_1)t + \\ &\quad + \varphi_2 - \varphi_1]\}^{1/2} \cos\left\{\omega_1 t + \arctg \frac{E_p \sin \varphi_1 + E_c \sin[(\omega_2 - \omega_1)t + \varphi_2]}{E_p \cos \varphi_1 + E_c \cos[(\omega_2 - \omega_1)t + \varphi_2]}\right\}. \end{aligned} \quad (6.118)$$

We know that when a narrow-band signal with amplitude and phase modulation is fed to input of an ideal band limiter, at output a signal is obtained with constant amplitude and the same phase modulation as the signal at input.

Taking this into account and the fact that after wide-band uneven limitation the signal assumes the form of a "meander," at limiter output we obtain

$$L(t) = \frac{4U_{\text{orp}}}{\pi} \cos \left\{ \omega_1 t + \arctg \frac{E_p \sin \varphi_1 + E_c \sin [(\omega_2 - \omega_1)t + \varphi_2]}{E_p \cos \varphi_1 + E_c \cos [(\omega_2 - \omega_1)t + \varphi_2]} \right\}, \quad (6.119)$$

where U_{orp} is limitation threshold.

If we use a trigonometric expansion in the form of

$$\begin{aligned} \cos(\omega_1 t + \arctg x) &= \cos \omega_1 t \cos(\arctg x) - \\ - \sin \omega_1 t \sin(\arctg x) &= \cos \omega_1 t \cos \left[\arccos \frac{1}{\sqrt{1+x^2}} \right] - \\ - \sin \omega_1 t \sin \left[\arcsin \frac{x}{\sqrt{1+x^2}} \right] &= \frac{1}{\sqrt{1+x^2}} \times \\ &\times (\cos \omega_1 t - x \sin \omega_1 t), \end{aligned}$$

we perform the following transformations of expression (6.119):

$$\begin{aligned} L(t) &= \\ &= \frac{4U_{\text{orp}}}{\pi} \frac{1}{\left\{ 1 + \left[\frac{E_p \sin \varphi_1 + E_c \sin [(\omega_2 - \omega_1)t + \varphi_2]}{E_p \cos \varphi_1 + E_c \cos [(\omega_2 - \omega_1)t + \varphi_2]} \right]^2 \right\}^{1/2}} \times \\ &\times \left(\cos \omega_1 t - \frac{E_p \sin \varphi_1 + E_c \sin [(\omega_2 - \omega_1)t + \varphi_2]}{E_p \cos \varphi_1 + E_c \cos [(\omega_2 - \omega_1)t + \varphi_2]} \sin \omega_1 t \right) = \\ &= \frac{4U_{\text{orp}}}{\pi} \frac{E_p \cos \varphi_1 + E_c \cos [(\omega_2 - \omega_1)t + \varphi_2]}{\{E_p^2 + E_c^2 + 2E_p E_c \cos [(\omega_2 - \omega_1)t + \varphi_2 - \varphi_1]\}^{1/2}} \times \\ &\times \frac{E_p \cos(\omega_1 t + \varphi_1) + E_c \cos(\omega_1 t + \varphi_2)}{E_p \cos \varphi_1 + E_c \cos [(\omega_2 - \omega_1)t + \varphi_2]} = \\ &= \frac{4U_{\text{orp}}}{\pi} \left[\frac{E_p \cos(\omega_1 t + \varphi_1) + E_c \cos(\omega_1 t + \varphi_2)}{\{E_p^2 + E_c^2 + 2E_p E_c \cos [(\omega_2 - \omega_1)t + \varphi_2 - \varphi_1]\}^{1/2}} \right] \end{aligned} \quad (6.120)$$

Dividing the numerator and denominator by E_c , we obtain

$$L(t) = \frac{4U_{\text{orp}}}{\pi} \left\{ 1 + \frac{E_p^2}{E_c^2} + \frac{2E_p}{E_c} \cos[(\omega_2 - \omega_1)t + \varphi_2 - \varphi_1] \right\}^{-1/2} \left\{ \frac{E_p}{E_c} \cos(\omega_1 t + \varphi_1) + \cos(\omega_2 t + \varphi_2) \right\}. \quad (6.21)$$

When $E_p < E_c$, which is virtually always fulfilled, the quantity under the square root sign can be represented in the form of power series (with the use of binomial expansion) in the following manner:

$$\begin{aligned} & \left[1 + \frac{E_p^2}{E_c^2} \right]^{-1/2} \left\{ 1 + \frac{2E_p E_c}{E_p^2 + E_c^2} \cos[(\omega_2 - \omega_1)t + \varphi_2 - \varphi_1] \right\}^{-1/2} = \left[1 + \frac{E_p^2}{E_c^2} \right]^{-1/2} \left\{ 1 + \left[\frac{E_p}{E_c} - \frac{E_p^3}{E_c^3} + \right. \right. \\ & \left. \left. + \frac{E_p^5}{E_c^5} - \dots \right] \cos[(\omega_2 - \omega_1)t + \varphi_2 - \varphi_1] \right\}^{-1/2} = \\ & = \left[1 - \frac{1}{2} \frac{E_p^2}{E_c^2} + \frac{3}{8} \frac{E_p^4}{E_c^4} - \dots \right] \times \\ & \times \left\{ 1 - \left(\frac{E_p}{E_c} - \frac{E_p^3}{E_c^3} + \frac{E_p^5}{E_c^5} - \dots \right) \cos[(\omega_2 - \omega_1)t + \varphi_2 - \varphi_1] + \frac{3}{2} \left(\frac{E_p}{E_c} - \frac{E_p^3}{E_c^3} + \frac{E_p^5}{E_c^5} - \dots \right) \cos^2[(\omega_2 - \right. \\ & \left. - \omega_1)t + \varphi_2 - \varphi_1] - \frac{15}{6} \left(\frac{E_p}{E_c} - \frac{E_p^3}{E_c^3} + \right. \right. \\ & \left. \left. + \frac{E_p^5}{E_c^5} - \dots \right)^2 \cos^3[(\omega_2 - \omega_1)t + \varphi_2 - \varphi_1] + \dots \right\}. \end{aligned} \quad (6.122)$$

Substituting (6.122) into (6.21), using trigonometric identities, and grouping terms, we obtain the following expressions for output voltages of the limiter:

$$L(t) = \frac{4U_{orp}}{\pi} \left\{ \left(\frac{E_p}{2E_c} + \frac{1}{16} \frac{E_p^3}{E_c^3} + \dots \right) \times \right. \\ \left. \times \cos(\omega_1 t + \varphi_1) + \left(1 - \frac{1}{4} \frac{E_p^2}{E_c^2} - \dots \right) \cos(\omega_2 t + \varphi_2) + \right. \\ \left. \text{[other terms on carrier frequencies } \omega_1 \pm n(\omega_2 - \omega_1)] \right\}, \quad (6.123)$$

where $n = 2, 3, 4, \dots$

At output of filters we obtain

$$\overline{S_1(t)} = \frac{4U_{orp}}{\pi} \left(\frac{E_p}{2E_c} + \frac{1}{16} \frac{E_p^3}{E_c^3} + \dots \right) \cos(\omega_1 t + \varphi_1), \quad (6.124)$$

$$\overline{S_2(t)} = \frac{4U_{orp}}{\pi} \left(1 - \frac{1}{4} \frac{E_p^2}{E_c^2} - \dots \right) \cos(\omega_2 t + \varphi_2). \quad (6.125)$$

Where $E_p/E_c \ll 1$

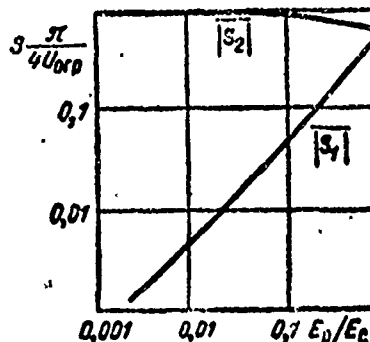
$$\overline{S_1(t)} \approx \frac{2U_{orp}}{\pi} \frac{E_p}{E_c} \cos(\omega_1 t + \varphi_1), \quad (6.126)$$

$$\overline{S_2(t)} \approx \frac{4U_{orp}}{\pi} (\cos \omega_2 t + \varphi_2). \quad (6.127)$$

The calculated dependences of amplitudes $\overline{S_1(t)}$ and $\overline{S_2(t)}$ on the ratio of instantaneous values of difference and sum signal amplitudes E_p/E_c are represented in Fig. 6.18. As seen from the figure, with low amplitude ratios for difference and sum signals, which usually occurs during automatic target tracking, output voltage $\overline{S_1(t)}$ is almost directly proportional to the instantaneous value of amplitude ratio E_p/E_c and, consequently, directly proportional to the amplitude ratio of signals received by the radar antenna. This circumstance makes it possible to measure direction to target by this method of signal processing with sufficient accuracy. The results obtained can be extended to both continuous and pulse signals.

This principle of single-channel receiving systems for monopulse radars with the use of signal frequency spacing is not unique. Other variations of it exist. As an example of such a variation, we can present the American phase monopulse system "Minitrack," designed for tracking artificial earth satellites.

Fig. 6.18. Standardized calculated dependence of signal amplitude at band-pass filter output on the amplitude ratio of difference and sum signals at input of an ideal limiter.



6.5.6. A method of joining receiving channels with the use of switching. Another method of compensating for nonidentity of amplitude-phase characteristics for receiving channels is alternate-period channel switching [18]. In this case, the receiving channels are switched with half pulse repetition rate, which provides the alternate connection of i-f amplifiers first to one antenna and then to the other. The phase shift because of nonidentity in amplitude-phase characteristics for receiving channels acquires first a positive then a negative value and in the averaged error signal the value of additional error from nonidentity of channels will be considerably reduced. Receiving channels can be switched also with an arbitrary rate not related to repetition rate.

We shall examine the values of channel switching analytically in an example of an amplitude-amplitude monopulse system with logarithmic receivers and error signal shaping according to law

$$S(\theta) = \ln |\dot{u}_1(t, \theta)| - \ln |\dot{u}_2(t, \theta)|. \quad (6.128)$$

As shown in § 6.3.1, in such systems when channel nonidentity is present, there occurs direction finding error determined by expression (6.34).

Let the receiving channel be identical in phase and switched directly at antenna output according to square law. Then signals at the i-f amplifier output of the channel can be represented in the form of the following expression:

$$\dot{u}_{11}(t, \theta) = \kappa_{01} \ln \kappa_1 E_0 (1 + \mu \theta) \exp i \omega_{np} t, \quad (6.129)$$

$$\dot{u}_{21}(t, \theta) = \kappa_{02} \ln \kappa_2 E_0 (1 - \mu \theta) \exp i \omega_{np} t, \quad (6.130)$$

$$\dot{u}_{12}(t, \theta) = \kappa_{01} \ln \kappa_1 E_0 (1 - \mu \theta) \exp i \omega_{np} t, \quad (6.131)$$

$$\dot{u}_{22}(t, \theta) = \kappa_{02} \ln \kappa_2 E_0 (1 + \mu \theta) \exp i \omega_{np} t, \quad (6.132)$$

where $\dot{u}_{11}(t, \theta)$, $\dot{u}_{21}(t, \theta)$ and $\dot{u}_{12}(t, \theta)$, $\dot{u}_{22}(t, \theta)$ are the expressions for signals at output of the first and second channels after the first and second half-period of switching, respectively.

In accordance with this, error signals for the first and second half-periods of switching are defined by expression

$$S_1(\theta) = |\dot{u}_{21}(t, \theta)| - |\dot{u}_{11}(t, \theta)| = \kappa_{01} \ln \kappa_1 E_0 (1 + \mu \theta) - \kappa_{02} \ln \kappa_2 E_0 (1 - \mu \theta), \quad (6.133)$$

$$S_2(\theta) = |\dot{u}_{12}(t, \theta)| - |\dot{u}_{22}(t, \theta)| = \kappa_{01} \ln \kappa_1 E_0 (1 - \mu \theta) - \kappa_{02} \ln \kappa_2 E_0 (1 + \mu \theta). \quad (6.134)$$

With the signal processing used the signs of error signals $S_1(\theta)$ and $S_2(\theta)$ are opposite; therefore, the resulting error signal is the half-difference of the error signals for the first and second half-period of switching, i.e.,

$$S(\theta) = \frac{1}{2} [S_1(\theta) - S_2(\theta)]. \quad (6.135)$$

Substituting expressions (6.133) and (6.134) and assuming direction finding errors are small, after elementary transformation we obtain

$$\begin{aligned} S(\theta) &= \frac{1}{2} \left[\kappa_{01} \ln \frac{1+\mu\theta}{1-\mu\theta} - \kappa_{02} \ln \frac{1-\mu\theta}{1+\mu\theta} \right] = \\ &= \frac{1}{2} [2\kappa_{01}\mu\theta + 2\kappa_{02}\mu\theta] = \kappa_{02} (g_0 + 1) \mu\theta. \end{aligned} \quad (6.136)$$

Obviously, the direction finding condition $S(\theta) = 0$ is fulfilled when $\theta = 0$ regardless of nonidentity of channels with respect to amplitude; however, direction finding system sensitivity drops by a factor of $2/(g_0 + 1)$. Thus, when using switching, the difference in amplification of receiving channels does not lead to systematic direction finding errors.

When the location of receiving channel switching is far from antenna output, the direction finding system becomes sensitive to nonidentity of amplitude characteristics for high-frequency channels even under the channel switching conditions. We shall show this analytically. Let switching be accomplished directly on input of channel i-f amplifiers. Then

$$\dot{u}_{11}(t, \theta) = \kappa_{01} \ln \kappa_1 E_0 (1 + \mu\theta) \exp i \omega_{np} t, \quad (6.137)$$

$$\dot{u}_{21}(t, \theta) = \kappa_{02} \ln \kappa_2 E_0 (1 - \mu\theta) \exp i \omega_{np} t, \quad (6.138)$$

$$\dot{u}_{12}(t, \theta) = \kappa_{01} \ln \kappa_2 E_0 (1 - \mu\theta) \exp i \omega_{np} t, \quad (6.139)$$

$$\dot{u}_{22}(t, \theta) = \kappa_{02} \ln \kappa_1 E_0 (1 + \mu\theta) \exp i \omega_{np} t, \quad (6.140)$$

$$\begin{aligned} S(\theta) &= \frac{1}{2} [S_1(\theta) - S_2(\theta)] = \\ &= \frac{1}{2} \left[\kappa_{01} \ln \left(\frac{\kappa_1}{\kappa_2} \frac{1+\mu\theta}{1-\mu\theta} \right) - \kappa_{02} \ln \left(\frac{\kappa_2}{\kappa_1} \frac{1-\mu\theta}{1+\mu\theta} \right) \right] = \\ &= \frac{1}{2} \kappa_{02} (g_0 + 1) (\ln g + 2\mu\theta). \end{aligned} \quad (6.141)$$

For the equation $S(\theta)$ relative to $\mu\theta$, we find

$$\mu\theta = \text{th} \left(-\frac{\ln g}{2} \right) \approx -\frac{\ln g}{2}. \quad (6.142)$$

The expression (6.142) is similar to expression (6.36), obtained in the examination of direction finding errors from nonidentities of amplitude characteristics for high-frequency receiver circuits without the use of channel switching.

There are also other methods for interconnection of receiving channels with the use of switching. One of these methods is based on high-frequency gating of the interconnected channels, which provides for turning them on alternately for a time period n times less than the operating pulse width (n is the number of interconnected channels). One of the components of the resulting signal in the receiving channel is used as the reference signal and the other two as angle-measuring signals [76]. Owing to the time separation of the received pulses being formed, the conversion and amplification of these signals can be accomplished with a single-channel receiver. The misphasing of signals which then occurs is compensated by specially selected delay lines and the corresponding signal separation at receiver output is accomplished by gating synchronized with the gating of the input channels.

A method is known for joining receiving channels by the alternate connection of antenna outputs without splitting the pulse [96].

The original circuit for channel interconnection with the use of switching is used in the monopulse system whose block diagram is illustrated in Fig. 6.19 [75]. The switching elements of this circuit are ferrite phase switchers connected to waveguide antenna channels and controlled from a special power source according to a specific program by feeding pulsed voltage.

In the absence of a magnetizing pulse on the ferrite phase switchers, all channels are in phase and the resulting radiation

pattern has a maximum which agrees with the orientation of the antenna axis.

When feeding a calibrated voltage pulse to any of the ferrite phase shifters in the corresponding channel there is created an additional phase shift which leads to a corresponding deviation of the axis of the resulting pattern from the axis of the antenna. Depending upon the channel in which a given ferrite phase switcher is connected, the radiation pattern deviates from the antenna axis downward, upward, to the right, or to the left.

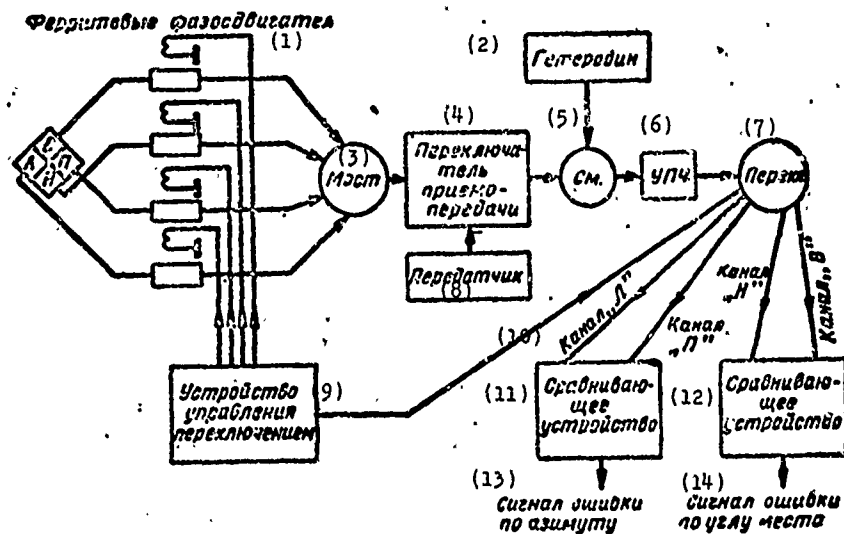


Fig. 6.19. Simplified block diagram of a monopulse radar with switching of the receiving-transmitting h-f channels.
KEY: (1) Ferrite phase shifters; (2) Heterodyne; (3) Bridge; (4) Send-receive switch; (5) Mixer; (6) I-f amplifier; (7) Switch; (8) Transmitter; (9) Switch control device; (10) Channel; (11) Comparing device; (12) Comparing device; (13) Azimuth error signal; (14) Elevation error signal.

Allowing for the sequence of axis positions for the resulting radiation pattern which are fed to receiver input, the signals will be spaced in time, thus making it possible for their subsequent conversion and amplification to be carried out in a single-channel

receiving device. At receiver output signals are separated with a switch controlled synchronously with the ferrite phase switcher and directed in pairs to the comparing devices which form azimuth and elevation error signals.

The antenna beam control rate can reach several kilohertz. In combination with coding, such a switching system is sufficiently noise-proof with respect to synchronous organized noises and low-frequency amplitude fluctuations inherent in reflected signals.

CHAPTER 7

INTERFERENCE IMMUNITY OF MONOPULSE RADARS

It is difficult to operate radar systems in combat situations without interference; therefore, in developing radars considerable attention is given to the problem of interference immunity. By the interference immunity of a radar system we usually mean its ability to reproduce with sufficient accuracy a useful signal and to perform the necessary operations with respect to target detection, coordinate measurement, and tracking, under noise conditions. If a radar cannot perform under these conditions, it cannot be designated noise-proof in spite of its high performance in the absence of interference.

With respect to automatic target tracking radars, interference immunity means the ability of the radar to track a target by its coordinates, with the necessary accuracy when radar countermeasures are being used.

Widely applied in this field before the introduction of the monopulse method, foreign single-channel angle-measuring systems of automatic tracking, based on the method of conical scanning and sequential beam switching, were vulnerable to organized interferences and could not perform their combat tasks in the presence of countermeasures. Thus, for example, these systems have low noise immunity from responding noises with amplitude modulation on beam scanning (switching) frequency. Therefore, one of the main reasons for developing the monopulse method and for the wide introduction of it into radar technology, which has been noted in the

last ten years, was the need to increase interference immunity in the angle-measuring channel, which is the main channel in radar systems for ground control of interception and automatic tracking.

In evaluating noise immunity in monopulse radars, with respect to contemporary forms of noise, it is necessary to take into account the fact that the monopulse method is used only for measuring angular coordinates. As for the method of determining range and speed, as well as methods of tracking by range and speed, they do not differ in principle from methods used in ordinary single-channel tracking radars. Therefore, there is a continuity in types of noises and methods of protection between single-channel and two-channel coordinates.

Before analyzing the interference immunity of monopulse radars and evaluating their advantages over single-channel angle-measuring coordinates, let us examine the present methods for creating radar interference.

§ 7.1. METHODS OF CREATING RADAR INTERFERENCE

By interference we mean any radio signal which upon reception impairs the quality of radar operation and destroys the reliability of its target information. Based on its character, interference can have both natural and artificial origins [10, 13, 30, 51, 61, 66, 67]. The first category includes noises occurring due to atmospheric storms, various types of precipitation (snow, hail, rain), the operation of poorly shielded electrical equipment, etc. The second category includes all noises intentionally created to disturb the operation of the radar equipment.

Artificial or intentional noises are usually created to camouflage or misinform. They also include noises from atomic explosions.

Camouflaging noises are used to prevent or substantially hinder detection or proper determination of target location. Jamming transmitters are the most widespread active means of creating such noises; metallic tape dipole reflectors are a passive means.

Misinforming noises are intended for the disorientation of the operator or the automatic radar equipment by creating false signals imitating the parameters of real targets and hindering the selection of true targets from false. The means of creating such noises can be either active (special transmitter) or passive (decoys).

The essential difference between misinforming noises and camouflaging noises is the degree to which their action can be concealed. A radar operator usually cannot determine that he is being misinformed, while he can easily recognize that camouflaging noises are being created from the image on the screen.

Noises from high-altitude nuclear explosion covers an entire complex of phenomena which occur during these explosions, leading to a disturbance of conditions for radio propagation and affecting electronic equipment.

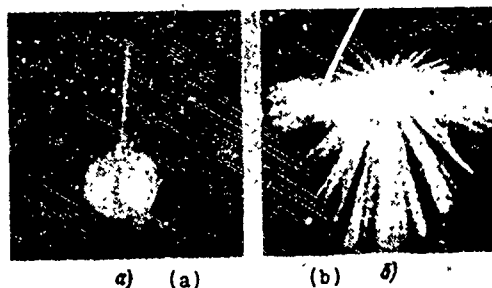
Let us examine in greater detail the main characteristics of intentional noises.

7.1.1. Active camouflaging interference. The most widespread means known today of active camouflaging interference is jamming. When the power is sufficient, this causes the screen to fully or partially light up with interference, due to which the blips of the actual targets are camouflaged (Fig. 7.1).

The classical method of jamming is to radiate a continuous high-frequency signal modulated in amplitude, frequency, or phase by noises. Selective jamming and barrage jamming differ. Selective jamming is characterized by a narrow noise spectrum commensurate with the passband of the radar being suppressed and, in this respect, has power advantages over barrage jamming. However, selective jamming suppresses only one chosen radar and, with its insufficient mobility, it can be tuned out by changing the working frequency of the radar. Barrage jamming is characterized by a wide spectrum of modulating noises and, in principle, can act simultaneously on

several radars, including radars with limited frequency tuning. But this is done at the cost of power loss. In order to create the same effect, a barrage jamming transmitter must have considerably high power than a selective jamming transmitter.

Fig. 7.1. View of PPI screen under the effect of mid-power (a) and high-power (b) jamming.



The advantage of barrage jamming lies in the fact that a radar under its effect, as a rule, cannot be tuned from it by frequency retuning. Barrage jamming can be achieved by the direct amplification of noise of a corresponding source (for example, a directly heated noise diode) with a uniform noise spectrum.

An intermediate position between selective and barrage jamming is occupied by noise with frequency wobbling. Such noise makes it possible for a specific period of time to concentrate a high density of noise power in all the working channels being covered. With the proper selection of frequency wobble rate for the noise transmitter, the radar receiver will not be able to reestablish full sensitivity in the period between effects, as a result of which the camouflaging effect of this noise will be sufficiently effective. In order to create noise with frequency wobbling, a carcinotron, modulated with respect to noise frequency, can be used for providing random variation in noise frequency.

The effect of noise with random frequency variation differs somewhat from the effect of noise with amplitude noise modulation. With a deviation in carrier frequency significantly exceeding the receiver passband and a sufficiently narrow spectrum of modulating noises as compared with the carrier frequency, the effect of such noise will cause at receiver output pulses of almost constant amplitude

whose shape is similar to the frequency characteristic of the receiver. Such pulses will be obtained during each pass of the carrier frequency through the receiver passband, and the interval between them will vary according to random law.

Camouflaging noises can also include nonsynchronous pulsed noises with low and high repetition rates. Such noises create coarse or fine-grained indicator lighting with a bright spot for a group of pulsed spots moving on the amplitude indicators, making detection and tracking of the actual target difficult.

These active camouflaging noises belong to the category of "power" means of countermeasures since they suppress radars at the cost of rather high noise power. Active misinforming noises, as we shall show later, require less power losses.

Power suppression noises should also include noise in the form of an unmodulated carrier. This noise is capable, with the proper power, of reducing radar receiver sensitivity so much that an illusion of station failure is created.

Recently foreign countries have been widely studying new means of creating active camouflaging noises with the use of ejectable miniature radiators. These radiators usually are made on solid-state circuits and generate noises at a certain frequency for a short period of time sufficient, it is assumed, to get ballistic missiles through an antimissile defense system [113].

7.1.2. Passive camouflaging noises. One of the first means for creating passive camouflaging noises, which has found practical application, is the use of dipole reflectors which are ordinary metal tapes half the length of the working wavelength of the radar. Ejected from aircraft, packages of dipole reflectors are spread by the wind and form an extended reflecting cloud, as a result of which on the screen of unprotected radars there is formed an intense cloud of light corresponding to the dipole cloud camouflaging the target.

Since radars, as a rule, operate at spaced frequencies, dipole reflectors are made with various dimensions in accordance with the known or probable working frequencies of the radars which they are intended to suppress.

An effective method of combating this type of passive noise is the use of frequency selection based on the frequency difference between signals reflected from the actual target and those reflected from the dipole reflectors, which is caused by the difference in speeds. The speed of dipole reflectors is determined by their weight, aerodynamic characteristics, and wind speed; as compared with an aircraft, dipole reflectors are slowly moving targets which makes their elimination possible based on speed.

Dipole reflectors can be ejected with the aid of special instruments in any direction from the aircraft they are protecting. Reflectors ejected forward can disrupt, for a certain period of time, the operation of the speed and range tracking system and even cause a radar to reaim on the dipoles [44].

With the aim of improving dipole noise effectiveness, dipole illumination is sometimes resorted to with the aid of high-frequency signals created by special transmitters installed on the object being protected [105]. The illuminating signal is emitted either with a frequency shift relative to the frequency of the radar beam illuminated in order to imitate false dipole speed or with a time shift imitating the range displacement of the dipole. This ensures that the characteristics of these signals received from the dipole cloud are similar to the characteristics of the actual targets and substantially hinder their selection.

Since the length of a dipole must correspond to the wave length of a radar and increases with an increase in the latter, a conversion of the radars in foreign antiaircraft and antimissile defense systems in the upper region of decimeter and meter ranges of waves is considered one of the possible means of weakening the interfering effect of dipole noises [113].

7.1.3. Active misinforming noises. Unlike jamming noises, misinforming noises mainly distort the information about the target by forming interference signals with false parameters, which differ little from the parameters of actual reflected signals. Therefore, the result of such noises is not to camouflage signals reflected from a target but to introduce error for the operator and the automatic instruments of the radar station. Creating such noises requires a more complex apparatus and a greater quantity of information on the operating principles of the radar being suppressed.

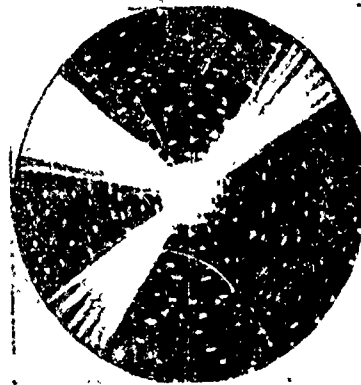
Misinforming noises created from one point in space include:

- multiple responding noises;
- range diversion noises;
- speed diversion noises;
- angular coordinate diversion noises.

The principle involved in creating multiple responding noises consists in the fact that the noise transmitter in response to a radar pulse received emits on the same frequency a series of similarly shaped moving pulses, spread in range and angle and imitating a group of targets [87]. Such noise hinders the operator's selection of the true target and reduces the operational effectiveness of the detection and target-indicating system. Because of this, instead of the actual target, interception may be undertaken for many false targets. This leads to a scattering of forces and means of aerial defense, which has a favorable effect on the probability of the aircraft reaching their objectives. Multiple noise along with the imitation of aerial targets can be used also for imitating naval targets.

The effectiveness of multiple responding noises increases when the multiple responding noise is combined with jamming (Fig. 7.2) and thus the targets covered by the noise producer are imitated, and also when false target blips are created not along the main lobe of the radiation pattern but along the side lobes, which is ensured by the proper synchronization of the responding pulse emission with the scanning period of the radar [128].

Fig. 7.2. View of multiple responding noise combined with jamming on the PPI screen of a radar.



It is possible to create false targets also with the aid of miniature radiators ejected from the protected object - repeaters whose development has recently been given considerable attention in foreign countries [113]. These miniature repeaters are designed on integral circuits with the use of tunnel diodes intended for "trapping" radar signals and reradiating them with a certain time delay. In the foreign press it is noted that this method of creating misinforming noises is considered promising for use by the antimissile defense system [113].

Unlike multiple responding noises, diverting noises are created by automatic target tracking systems. The main task of such noises is to create conditions where a radar will switch from tracking the reflected signal to tracking the noise. When creating range diversion noises, noise transmitters will emit pulsed signals similar in parameters to the reflected signals but with a smoothly changing time delay which imitates the motion of the target with a speed unlike the speed of the actual target, thus creating noise.

If the power of the noise exceeds the power of the reflected signal, the range strobe of the automatic tracking system will be distracted by the noise pulse and leave the blip of the actual target. Thus false target range is given, substantially hampering the determination of target location. Delay in noise signal can be reduced or increased until sufficient range error is provided. Switching off the noise after the range strobe is led away from the blip of the real target leads to loss of target by the automatic tracking system and transition of the radar to search mode.

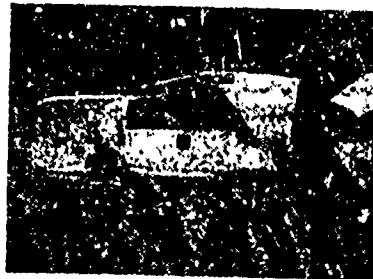
Similarly speed diversion noise is created for a radar with continuous and quasicontinuous radiation mode, the only difference being that, in this case, a smooth variation in noise signal frequency relative to radar signal frequency occurs. This leads to a smooth variation in doppler frequency and the imitation of target speed variation. With a sufficient surplus of noise power the speed tracking strobe moves according to the noise frequency shift and the servosystem gives out erroneous target speed information. Switching off noise after signal frequency is shifted by a value exceeding the width of the speed strobe leads to loss of target and transition of radar to search mode just as when switching off range diversion noise.

The principle involved in creating angular coordinate diversion noises consists of providing noises with such properties as to ensure error signal in the autotracking system when there is no antenna disagreement with target direction.

It should be noted that active misinforming noises are more advantageous with respect to power than active camouflaging noises since virtually the maximum power which can be provided by the noise receiver is concentrated in the radar receiver band. However, from the technical point of view, such noises are more complicated since they require special complex equipment.

7.1.4. Passive misinforming noises. Passive misinforming equipment creating radar noise includes various decoys capable of imitating the actual target. If the radar does not distinguish the decoy from the target, the operator or automatic device can take it for a dangerous target and direct interception against it, which reduces the probability of interception for the actual target.

Fig. 7.3. The Quail missile.



The simplest decoys are angular reflectors, with comparatively small geometric dimensions, capable of giving reflected signals corresponding in level to large targets. Being ejected at the moment of an attack, in many cases, these reflectors can divert the means of interception from the object being protected and cause them to track the decoy. The more modern decoys can have their own motors with which to imitate the target not only in reflecting properties but in speed. The typical size of such decoys used by the Capitalist Armed Forces is the small aircraft missile slung under the wings of a bomber and launched into free flight at the proper moment (Fig. 7.3) [30]. In order to increase the density of signals reflected from small objects, sometimes active responders are located on them.

Decoys have been given considerable attention overseas in the protection of warheads for overcoming antimissile defense systems [46]. Taking into account the specifics of warhead motion, in the middle portions of the flight trajectory, the use of light decoys is provided (inflated spheres, balloons), and in the final section of the trajectory upon reentry, heavier decoys capable of motion in the atmosphere without burning up.

As passive misinforming noises, bundles of dipole reflectors can also be used, ejected from the protected object in order to realign the radar on the decoy.

7.1.5. Noises from atomic explosions. Atomic explosions create substantial noises in the operation of radar stations [68]. These explosions are accompanied by electromagnetic effects of two main types. One of these is the radiation of short-duration electromagnetic pulses as a result of the appearance of a certain asymmetry in the distribution of the electrical charge in the regions surrounding the explosion and because of the rapid expansion of rather conductive plasma which forms with the explosion in earth's magnetic field. The second effect is connected with the considerable disturbances of the electromagnetic waves used in the radio and radar ranges,

which occur under the effect of the ionizing radiation of the nuclear blast or are caused by fission products or water vapor introduced into the atmosphere as a result of the explosion.

Ionization, i.e., the formation of ion pairs consisting of separated electrons and positive ions, is the main cause of the disruption of radar operation in a wide range of waves. Ionization can occur either directly or indirectly under the effect of gamma rays and neutrons of the initial nuclear radiation, beta particles and gamma rays of the residual nuclear radiation, and also under the effect of X-rays and even ultraviolet rays present in the primary thermal radiation. Consequently, after an atomic explosion electron density in the atmosphere in the region of a blast increases strongly. These electrons can affect radars in at least two ways. First, under the proper conditions, they can reduce wave energy and thus weaken the signal; second, a wave front propagating from one region to another (with differing electron density) will be twisted, i.e., the direction of radiowave propagation will be changed. This phenomenon is called refraction. Consequently, the ionized region occurring in the atmosphere under the effect of a high-altitude nuclear blast will affect radars whose propagation trajectory passes through this region.

The effect of atmospheric ionization on radars depends upon the altitude and power of the explosion, the type and working frequency of the station. In the foreign press it has been noted that explosions at altitudes below 16 km do not bring about significant or prolonged ionization and, consequently, do not affect radars seriously. With blasts at altitudes above 16 km and particularly at altitudes above 70 km, where the air density is less, significant ionization occurs and exerts a strong effect on the operation of radars.

In many cases, the refraction of a radar beam, as a result of electron density changes with a nuclear explosion, can play as important a role as its attenuation. The amount of beam deflection with this is directly proportional to the change in electron density

and inversely proportional to the square of the signal frequency. With large angles of beam incidence signal reflection will occur and a radar signal will be turned back without passing through the attenuating layer.

On the basis of an analysis of a large amount of experimental data, American experts assume that high-altitude nuclear explosions can disrupt the operation of radar stations for a period from several seconds to several hours depending upon the power and altitude of the explosion, as well as the type and working frequency of the radar station.

§ 7.2. NOISES BY MONOPULSE RADAR SYSTEMS

It has been mentioned earlier that in monopulse radars only the angle-measuring channels have high noise immunity, while the speed and range-measuring channels with respect to noise immunity have no advantages over the speed and range-measuring channels in single-channel radars. Such noises as speed and range diversion noises will affect rather effectively monopulse radars also if no special protection measures are provided them. Speed and range noises, to a certain extent, impair the noise immunity of the angle-measuring channel. A disruption of range or speed tracking forces the radar to search mode on corresponding parameters. If there are several targets in the radar's coverage zone, it is possible to pick up a new target located in a different direction from that of the one being tracked earlier. This leads to a resighting of the radar's antenna and an increase in angular errors. Furthermore, range and speed, as we know, in foreign rocket complexes are used in calculating the anticipated firing angle (rocket launch). If these parameters are fed into a computer with significant errors, the anticipated point of encounter will also be determined with error, which in turn, affects firing accuracy. When the rocket is launched, an error in calculating the anticipated point can lead to an increase in G forces on the rocket during its motion and a reduction in the probability of striking the target.

Because of this, the protection of target selection channel must also be given rather serious consideration, although it is not fundamental, since in radar systems for tracking and guidance the main channel is the angle-measuring channel.

The high noise immunity of the angle-measuring channel in a monopulse system is due to its operating principle. As we know, in monopulse systems one pulse is sufficient, in principle, for the accurate determination of target direction. Since during the time of this pulse the effective reflecting surface of the target is virtually unchanged, a monopulse system has little sensitivity to amplitude fluctuations in the reflected signals. Hence it follows that the angle-measuring channel has little sensitivity also to noises with amplitude modulation. On the contrary, amplitude-modulated noise, possessing a certain power excess over a reflected signal, eases the operation of a monopulse angle-measuring channel since it increases the equivalent reflecting surface of the target and thus broadens the range of ranges in which normal target tracking is possible.

This is valid not only for amplitude-modulated noises but also for noises with other types of modulation emitted from one point in space, for example, frequency modulated and phase modulated noises, if only the receiving channels are identical in amplitude-phase characteristics.

However, in practice it is difficult to create ideal monopulse receivers and defects can occur in design and circuitry. These defects can reduce noise immunity with respect to active noises, including noises emitted from one point.

Defects which reduce noise immunity in monopulse radars, in addition to nonidentity of amplitude-phase characteristics, usually include nonlinearity of amplitude characteristics for receiving channels, time lag of the AGC system, a difference in transmission factors for antenna channels, etc.

With nonlinearity of the amplitude characteristics strong noise can overload receiving channels and thus disrupt normal operating conditions since with saturation in the circuit element of the autotracking system, the transmission of amplitude signal variations is hindered, which, with the amplitude method of direction finding, leads to partial or full breakdown of error signal shaping. The latter is equivalent to servosystem disconnection and inevitably increases direction finding error.

Errors obviously increase if overload is created periodically by manipulation (turning on and off) of noises since, in this case, to eliminate errors in a radar, identity of static characteristics is insufficient; identity of dynamic characteristics for the receiving channels is also required. In a number of cases, the effect of powerful noise, manipulated with a specific frequency, can cause an angular swing of the antenna because of the resonance properties and the time lag of the servosystem. However, the possibility of manipulated noises is substantially reduced with the use of receivers with logarithmic characteristics and high-speed amplification control systems.

In the presence of an inertial AGC system, the switching off of powerful noise can lead to the disconnection of the servosystem circuit for the period of time necessary to restore sensitivity of the receiver to a level sufficient for the reception of reflected signal. Without control signals at its input, the antenna system in this period will either remain still or move from inertia, which, in both cases, increases angular tracking errors. In the case of a logarithmic receiver or a receiver with a high-speed AGC system, motion from inertia or a constant antenna state will be reduced to a minimum since after switching off the powerful noise the servosystem almost instantaneously will go to tracking on the signal reflected from the target.

Occupying a somewhat isolated position with respect to noise immunity are monopulse systems which use receiving channel switching to reduce the requirements for identity of amplitude-phase char-

acteristics. The introduction of switching makes such systems, under certain conditions, vulnerable to amplitude-modulated noises emitted from one point [75]. We shall illustrate this in the example of an amplitude-amplitude system with signal processing according to the principle

$$S(\theta) = \ln |\dot{u}_1(t, \theta)| - \ln |\dot{u}_2(t, \theta)|. \quad (7.1)$$

7.2.1. Noises of a monopulse radar on receiving channel switching frequency. When switching receiving channels in an amplitude-amplitude monopulse radar with logarithmic amplifiers, as shown in in Chapter 6 (section 6.4.6), error signal is determined by expression

$$S(\theta) = \kappa_{02} (g_0 + 1) \mu \theta. \quad (7.2)$$

According to this expression, the equilibrium of the system corresponding to the condition for target finding occurs at $\theta = 0$ regardless of the inequality of receiving channel transmission factors.

Let us consider the effect of amplitude-modulated noise on direction finding accuracy for this system. For simplicity we shall disregard the reflected signal and assume that the noise is modulated by a signal of meander form with switching frequency of the radar receiving channels in phase with the switching signal. Then signals at output of the i-f amplifier channels for the first and second cycles of the switch in designations used for Chapter 6 can be represented in the form of the following expressions:

$$\dot{u}_{11}(t, \theta) = \kappa_{01} \ln \kappa_1 E_0 (1 + m_n) (1 + \mu \theta) \exp i \omega_{np} t, \quad (7.3)$$

$$\dot{u}_{21}(t, \theta) = \kappa_{02} \ln \kappa_2 E_0 (1 + m_n) (1 - \mu \theta) \exp i \omega_{np} t, \quad (7.4)$$

$$\dot{u}_{12}(t, \theta) = \kappa_{01} \ln \kappa_1 E_0 (1 - m_n) (1 - \mu \theta) \exp i \omega_{np} t, \quad (7.5)$$

$$\dot{u}_{22}(t, \theta) = \kappa_{02} \ln \kappa_2 E_0 (1 - m_n)(1 + \mu) \exp i \omega_{np} t, \quad (7.6)$$

where m_n is the modulation index of the noise.

Hence we obtain the resulting error signal at output of the comparing device:

$$\begin{aligned} S(\theta) &= \frac{1}{2} [S_1(\theta) - S_2(\theta)] = \frac{1}{2} [|\dot{u}_{11}(t, \theta)| - \\ & - |\dot{u}_{21}(t, \theta)| - |\dot{u}_{12}(t, \theta)| + |\dot{u}_{22}(t, \theta)|] = \\ &= \frac{1}{2} \left[\kappa_{01} \ln \frac{(1 + m_n)(1 + \mu\theta)}{(1 - m_n)(1 - \mu\theta)} - \right. \\ & \left. - \kappa_{02} \ln \frac{(1 + m_n)(1 - \mu\theta)}{(1 - m_n)(1 + \mu\theta)} \right] = \\ &= \frac{1}{2} \kappa_{02} \left[(g_0 - 1) \ln \left(\frac{1 + m_n}{1 - m_n} \right) + \right. \\ & \left. + (g_0 + 1) \ln \left(\frac{1 + \mu\theta}{1 - \mu\theta} \right) \right] \approx \frac{1}{2} \kappa_{02} \left[(g_0 - 1) \times \right. \\ & \left. \times \ln \left(\frac{1 + m_n}{1 - m_n} \right) + 2(g_0 + 1) \mu\theta \right]. \end{aligned} \quad (7.7)$$

Equating $S(\theta)$ to zero and solving the equation relative to $\mu\theta$, we find

$$\mu\theta = \frac{g_0 - 1}{2(g_0 + 1)} \ln \left(\frac{1 - m_n}{1 + m_n} \right) = \ln \left(\frac{1 - m_n}{1 + m_n} \right)^{\kappa}, \quad (7.8)$$

where $\kappa = \frac{g_0 - 1}{2(g_0 + 1)}$.

The quantity under the logarithm sign is positive and small with the assumptions made. This makes it possible to use the

familiar expansion of a logarithmic function in series [8] and to limit ourselves to taking the first term of the series. As a result, we obtain the following calculation formula

$$\mu\theta \approx \left[2 \frac{\left(\frac{1-m_n}{1+m_n} \right)^2 - 1}{\left(\frac{1-m_n}{1+m_n} \right) + 1} \right] \quad (7.9)$$

Expression (7.9) indicates that the modulation of the noise with channel switching frequency leads to systematic direction finding errors. The value of these errors is determined by the noise modulation index and the value of nonidentity of i-f amplifier channels with respect to transmission factor.

Figure 7.4 presents the dependence of generalized direction finding error on the value of amplitude nonidentity for receiving channels, calculated according to formula (7.9) for the case $m_n = 0.5$ and 0.9 . As is apparent from the figure, with identical channels ($g_0 = 1$) direction finding error is zero and noise with amplitude modulation on the switching frequency of the receiving channels has no harmful effect.

Using the calculated dependences, we can, based on known direction finding sensitivity, determine the absolute value of direction finding error. Thus, when $m_n = 0.9$ and $g_0 = 1.3$, systematic angular error is 0.8° with $\mu = 0.25$ 1/deg; 0.33° with $\mu = 0.6$ 1/deg and 0.27° with $\mu = 0.75$ 1/deg.

The direction finding error which occurs under the effect of noise with synchronous amplitude modulation on switching frequency is near in value to the errors in a similar direction finding system without switching (Fig. 6.6), occurring because of the nonidentity of amplitude characteristics for receiving channels. Consequently, synchronous amplitude modulated noise on switching frequency is capable of substantially disturbing the effectiveness of introducing channel switching.

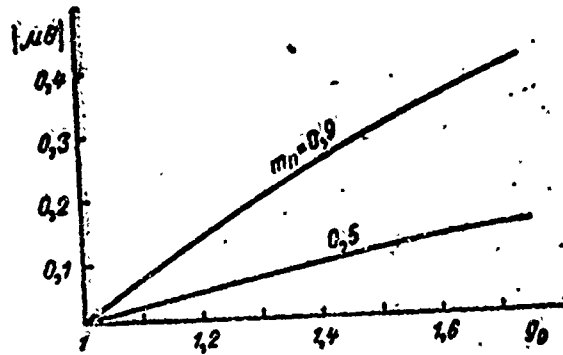


Fig. 7.4. Dependence of generalized systematic direction finding error on the value of nonidentity of transmission factors for receiving channels under the effect of amplitude-modulated noise on switching frequency.

This case corresponds to ideal conditions when noise modulation in amplitude is accomplished in phase with switching frequency for receiving channels. Under actual conditions, such a case does not exist since we can calculate only to an approximate value the switching frequency of the receiving channels. In this case, the effectiveness of noise will depend not only upon its modulation index but also upon modulation frequency and phase ratios of the modulation and switching signals.

Since the servosystem of the radar is narrow-band, one of the conditions for creating noise on switching frequency is

$$|\Omega_n - \Omega_p| \leq 2\pi \Delta F_{cc} \dots \quad (7.10)$$

where ΔF_{cc} is the passband width of the radar's servosystem, Ω_n is the noise modulation frequency, and Ω_p is the switching frequency of the receiving channels.

Condition (7.10) means that amplitude-modulated noise can have an effect on a monopulse radar using the switching of receiving

channels only if its modulation frequency is equal to the switching frequency of the channels with accuracy up to the passband of the servosystem.

When the switching frequency is accurately known but it is not possible to synchronize the amplitude modulation of the noise with respect to phase, the phase ratios can be changed from $-\pi$ to π and the effectiveness of the noise will also change from zero to its maximum value determined by formula (7.9). The need to change phase ratio is also brought about by instability of switching frequency for receiving channels and modulation frequency of the noise.

On the assumption of the equally probable law of phase shift distribution in the process of a noise effect, the value of errors in this case, can be characterized by standard error

$$\sigma = \frac{\theta_{\max}}{\sqrt{3}}. \quad (7.11)$$

Taking into account the secret nature of switching frequency, the possibility of creating synchronous noise on the switching frequency is unlikely. This is even more valid if switching based on a special coded program is used.

7.2.2. Coherent noises created from two points in space. The principle involved in creating coherent noises is found in the creation of phase nonuniformity in the aperture of the receiving antenna by irradiating it with coherent signals from two separated points in space [10, 78].

The physical bases for this method of creating noise is discussed in Chapter 5 in sufficient detail in the discussion of a phase wave front of a signal from a two point target. It has been established that if the target has two signal sources, then, with certain amplitude and phase ratios for the signals, the phase

front of the wave is distorted as compared with the case of a single-point target, due to which conditions are created which impair direction finding accuracy for several types of radars including those working on the monopulse method.

For further clarification of phenomena connected with the reception of signals from a two-point target and encompassing the possibility of countermeasures by radar direction finding systems with the aid of organized noises, let us examine the reception and processing of signals from two point coherent sources in amplitude and phase monopulse systems.

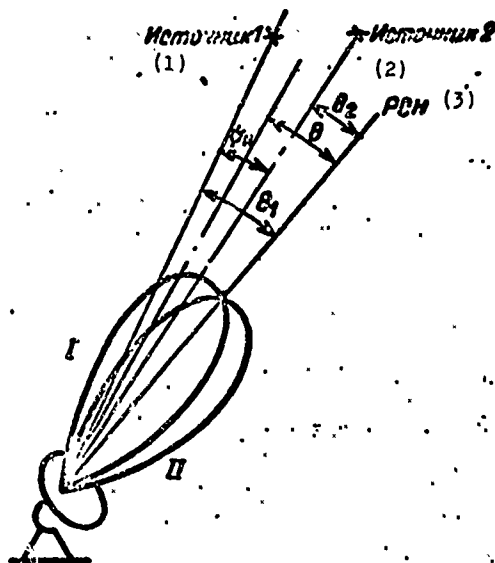


Fig. 7.5. Diagram of amplitude direction finding on a two-point target.

KEY: (1) Source 1; (2) Source 2; (3) ESD.

1. *Direction finding of a two-point source of coherent signals by an amplitude sum-difference monopulse radar.* Let us assume that point sources of coherent signals (Fig. 7.5) are located within the linear section of the direction finding characteristic and a linear approximation of radiation patterns is valid

$$F(\theta_0 \pm \theta) = F(\theta_0)(1 \mp \mu\theta). \quad (7.12)$$

In analyzing the direction finding of a two-point source of coherent signals by an amplitude sum-difference monopulse system, we use expression (4.23). Taking into account (7.12), we obtain

$$\begin{aligned} W_1 &= 4\mu\theta_1 F^2(\theta_0), \\ W_2 &= (1 + \mu\theta_1)(1 + \mu\theta_2) F^2(\theta_0) \cos \alpha, \\ W_3 &= (1 - \mu\theta_1)(1 - \mu\theta_2) F^2(\theta_0) \cos \alpha, \\ W_4 &= 4\mu\theta_2 F^2(\theta_0), \\ W_5 &= 4F^2(\theta_0), \\ W_6 &= 4F^2(\theta_0) \cos \alpha, \\ W_7 &= 4F^2(\theta_0). \end{aligned}$$

Substituting these values into (4.23), after elementary conversions we obtain

$$S(\theta) = \frac{\mu[\theta_1(1+a \cos \alpha) + \theta_2(a^2 + a \cos \alpha)]}{1 + 2a \cos \alpha + a^2}. \quad (7.13)$$

Equating (7.13) to zero, we find the condition determining the position of equisignal direction during direction finding on a two-point target:

$$\theta_1(1 + a \cos \alpha) + \theta_2(a^2 + a \cos \alpha) = 0. \quad (7.14)$$

For convenience, let us estimate the direction finding error being formed relative to the middle of the base (distance between sources). In this case,

$$\theta_1 = \theta + \frac{\psi_B}{2}; \quad \theta_2 = \theta - \frac{\psi_B}{2}.$$

Substituting the values of θ_1 and θ_2 into (7.14) and taking into account the fact that $a < 1$, as a result of solving equation (7.14) relative to θ , we obtain the familiar expression first deduced by Meed [33]

$$\frac{\theta}{\psi_n} = \frac{1-a^2}{2(1+a^2+2a \cos \alpha)} \quad (7.15)$$

Expression (7.15) is analogous to expression (5.14) determining the change in the slope of the phase front of a wave from a two-point source as compared with the phase front formed by a point signal source.

The correspondence obtained attests to the fact that during direction finding on point sources with small errors a radar system, in the final analysis, seeks the direction of the normal to the phase front of waves reflected from target, and distortions of the phase front from interference phenomena of a multipoint source of target signals or from intended parameter control by radiated noise signals must inevitably lead to an increase in direction finding errors. The value of direction finding error, as can be seen from expression (7.15), depends upon the distance between radiating sources, the phase shift of signals emitted by them, and their amplitude ratios at input of the direction finding system.

Figure 7.6 presents the calculated dependences of angular direction finding error in relative values of base dimension (distance between sources) on amplitude and phase ratios of noise signals. The calculated curves show that the value of direction finding errors does not depend upon the direction of the deviation relative to the sources.

Examining the dependence when $a = 1.25$, we can see that with signals in phase the value of angular error is approximately 0.6 the value of angular distance between sources. Therefore, even with proper aiming of the radar to one of the sources, equisignal direction moves to a point located approximately in the middle between the targets. With an increase in noise signal phase difference the value of angular error increases and reaches maximum value with a signal phase shift of 180° . Theoretically, direction finding error, at this moment, can reach very high values. In practice,

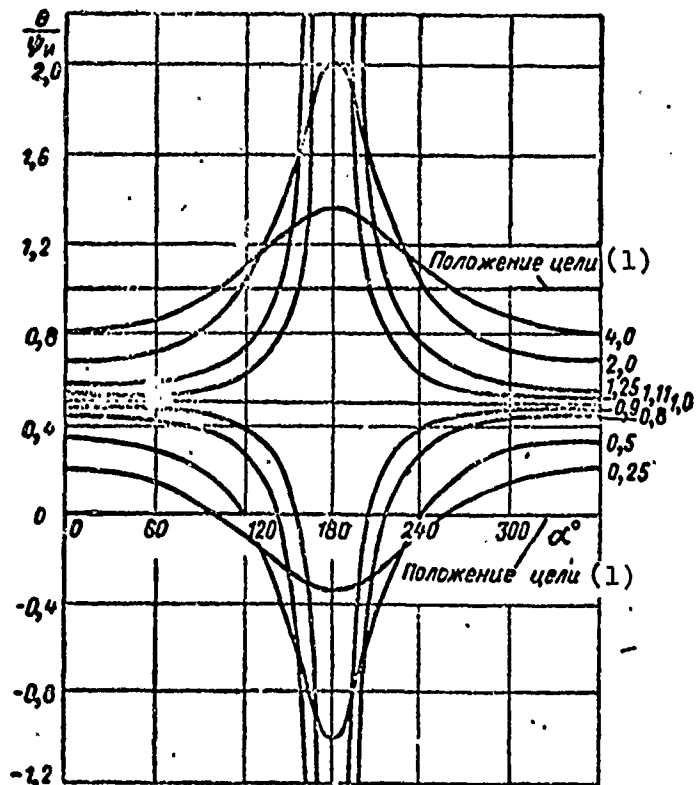
however, these errors are limited by the radiation pattern and cannot exceed in value the width of the radiation pattern of the suppressed radar's receiving antenna.

With receiving signals in phase ($\alpha = 0$) direction finding error decreases to a value of $(1 - a)/2(1 + a)$, which corresponds to the power "center of gravity" of the two sources. If signal amplitudes are equal, the power "center" agrees with geometric center, passing through the middle of the base of coherent signal sources.

The direction of radar antenna deflection upon reception of signals from two coherent sources is determined by amplitude ratio a and when passing through a point corresponding to equality of signals, changes to the inverse (Fig. 7.7). We should keep in mind that the graphs presented in Figs. 7.6 and 7.7 are valid only up to values of errors lying within the linear part of the antenna radiation pattern.

Fig. 7.6. Calculated dependence of angular direction finding errors for a two-point target on amplitude and phase ratios of coherent signals radiated by the target.

KEY: (1) Target position.



2. Direction finding of a two-point source of coherent signals by a phase sum-difference monopulse system. The direction finding condition for a two-point target by a phase sum-difference monopulse system (Fig. 7.8) can be found from equation $S(\theta) = 0$. Using expression (4.42), in accordance with this, we obtain

$$F^2(\theta_1) \sin \varphi_1 + a^2 F^2(\theta_2) \sin \varphi_2 - a F(\theta_1) F(\theta_2) \times \\ \times [\sin(\alpha - \varphi_1) - \sin(\alpha + \varphi_2)], \quad (7.16)$$

where α is the initial phase shift for signals from a two-point target;

$$\varphi_1 = \kappa l \sin \theta_1; \quad \varphi_2 = \kappa l \sin \theta_2.$$

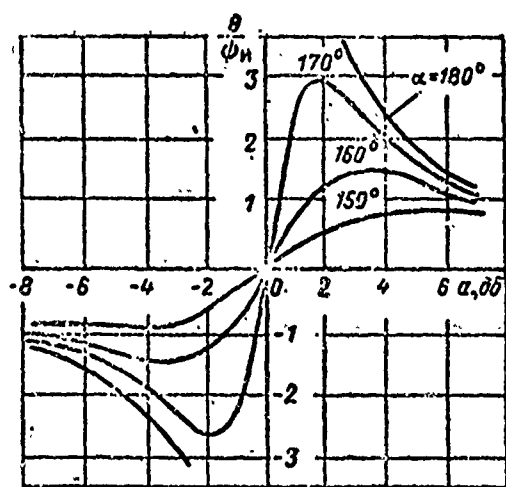


Fig. 7.7. Dependence of relative angular direction finding error for a two-point target on signal ratios for selected values of phase shift.

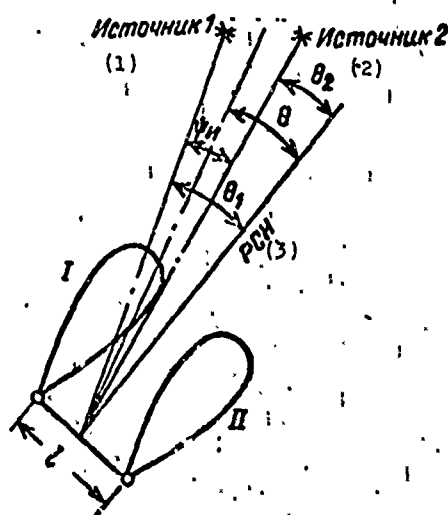


Fig. 7.8. Diagram of phase direction finding for a two-point target. KEY: (1) Source 1; (2) Source 2; (3) ESD.

Assuming the radiation pattern of the receiving antenna is wide enough and angles θ_1 and θ_2 are small, we can take $F(\theta_1) = F(\theta_2)$ and then equation (7.16) is simplified to

$$\sin \varphi_1 + a^2 \sin \varphi_2 - a [\sin(\alpha - \varphi_1) - \sin(\alpha + \varphi_2)] = 0. \quad (7.17)$$

Substituting into equation (7.17) the values of ϕ_1 and ϕ_2 , we obtain:

$$\sin \kappa l \theta_1 + a^2 \sin \kappa l \theta_2 - a [\sin(\alpha - \kappa l \theta_1) - \sin(\alpha + \kappa l \theta_2)] = 0. \quad (7.18)$$

Introducing angular coordinate θ , read from the middle of the base of sources and the angular value of the base ψ_n , connected with the relationships $\theta_1 = \theta + \frac{\psi_n}{2}$, $\theta_2 = \theta - \frac{\psi_n}{2}$, and performing elementary trigonometric transformations, equation (7.18) can be presented in the form

$$\begin{aligned} & \sin \kappa l \theta \cos \kappa l \frac{\psi_n}{2} + \cos \kappa l \theta \sin \kappa l \frac{\psi_n}{2} + \\ & + a^2 \left[\sin \kappa l \theta \cos \kappa l \frac{\psi_n}{2} - \cos \kappa l \theta \sin \kappa l \frac{\psi_n}{2} \right] + \\ & + 2a \cos \left(\alpha - \kappa l \frac{\psi_n}{2} \right) \sin \kappa l \theta = 0, \\ & \kappa l \theta = \frac{2\pi l}{\lambda} \theta = 2\pi \frac{\theta}{\theta_{0.5}}; \\ & \kappa l \frac{\psi_n}{2} = \pi \frac{\psi_n}{\theta_{0.5}}. \end{aligned} \quad (7.19)$$

With small direction finding errors the values of $\kappa l \theta$ and $\kappa l \frac{\psi_n}{2}$ are rather low; therefore,

$$\begin{aligned} \sin 2\pi \frac{\theta}{\theta_{0.5}} & \approx 2\pi \frac{\theta}{\theta_{0.5}}; \quad \cos 2\pi \frac{\theta}{\theta_{0.5}} \approx 1; \\ \sin \pi \frac{\psi_n}{\theta_{0.5}} & \approx \pi \frac{\psi_n}{\theta_{0.5}}; \quad \cos \pi \frac{\psi_n}{\theta_{0.5}} \approx 1. \end{aligned}$$

In accordance with this, expression (7.19) is simplified to:

$$2\theta + \psi_n + a^2(2\theta - \psi_n) + 4a \cos\left(\alpha - \pi \frac{\psi_n}{\theta_{0.5}}\right)\theta = 0 \quad (7.20)$$

or

$$2\theta \left[1 + 2a \cos\left(\alpha - \pi \frac{\psi_n}{\theta_{0.5}}\right) + a^2 \right] = \psi_n (a^2 - 1). \quad (7.21)$$

Disregarding the quantity $\pi\psi_n/\theta_{0.5}$ as compared with the value of α , since the region of highest errors. (of interest to us) lies near $\alpha = \pi$, we obtain with $a < 1$

$$\frac{\theta}{\psi_n} = \frac{1 - a^2}{2(1 + 2a \cos \alpha + a^2)}. \quad (7.22)$$

The expression obtained is analogous to that derived for the case of an amplitude sum-difference monopulse system. We can show that for simple amplitude and phase monopulse systems expressions determining direction finding error for a two-point signal source are obtained in the same manner.

Thus, with respect to angular errors during the direction finding of a two-point source of coherent signals, monopulse systems with amplitude and phase direction finding are identical and all conclusions made with respect to an amplitude monopulse system pertain, to the same extent, to a phase monopulse system.

The correspondence of formulas (7.22) and (5.14) attests to the fact that phase systems, as well as amplitude, during direction finding of points target with low errors, determine the position of the normal to the phase front of the signals received and the different distortions of the phase front inevitably lead to a reduction in direction finding accuracy.

The phenomena described above, observed during direction finding of two-point sources of coherent signals, are basic to the creation of coherent noises by a monopulse radar. Because of this, in the creation of coherent noise radiation is carried out through two antennas and the parameters of the noise signals (amplitude and phase ratios) are adjusted so as to ensure the conditions for obtaining maximum direction finding errors by the suppressed radar. The effect of coherent noise is manifest in the deflection of the equisignal direction of the suppressed radar from the direction to noise producer-target.

A limitation of this method of creating noise is the fact that it requires rapid information processing with optimization of noise signal parameters and also that it is suitable only for use at short distances [78]. The latter is a consequence of the operating characteristics of coherent noises, the fact that direction finding errors are proportional to the value of the distance between noise sources and at great distances, when the angle of sight for sources arranged within the geometric dimensions of the noise producer is of low value, they are insignificant. Therefore, the expected effectiveness of coherent noises at great distances to the noise producer is low. To arrange these sources with the purpose of increasing the base for various aircraft obviously is not advisable since difficulties are involved with ensuring the coherence of noise signals.

Coherent noise also has power limitations since in creating it high power levels are required. This is due to the fact that its maximum effect is noted with signals out of phase, when, in essence, noise signals emitted through the spaced antennas significantly compensate each other. Therefore, in order to create the necessary excess of resulting noise over reflected signals, comparatively high power levels for the noise signals are required. These levels, in practice, must exceed the levels of known noises emitted from one point in space.

With an increase in the distance between coherent noise sources, the requirements for noise power, as for guidance accuracy of noise signals in amplitude and phase, are somewhat reduced.

In spite of the existing limitations, coherent noise is usually considered one of the possible types of active noises in a countermeasure system and the character of its action is taken into account. We should keep in mind the fact that coherent noise acts both on single-channel and two-channel angle-measuring coordinators to the same extent; therefore, monopulse direction finding systems with respect to coherent noise immunity have no special advantages over ordinary single-channel systems of direction finding.

7.2.3. Flickering noises created from two points in space.

In the creation of flickering noise from two points in space foreign engineers have installed on their noise carriers autonomous transmitters with programmed emission. In the simplest version this is merely the alternate switching of transmitters on and off. The effect of this noise is based on the limited resolution of angle-measuring coordinators and can be explained in the following manner.

Let several signal sources be located in the unresolvable space of an angle-measuring coordinator. Without assuming the possibility of resolution for each of the sources with respect to direction, the radar will track the position of the equivalent power center. In the case of an amplitude sum-difference monopulse radar, as shown in § 4.2, the position of the power center M of the sources can be determined from equation

$$\sum_{m=1}^M P_m(t) [F^2(\theta_0 - \theta_m) - F^2(\theta_0 + \theta_m)] = 0, \quad (7.23)$$

where P_m is the power radiated by the m -th source;

θ_m is the angular coordinate of the m -th source relative to equisignal direction.

In the presence of two noise producers with angular positions θ_1 and θ_2 , equation (7.23) assumes the form

$$[P_{n1}(t) + P_{c1}(t)] [F^2(\theta_0 - \theta_1) - F^2(\theta_0 + \theta_1)] + [P_{n2}(t) + P_{c2}(t)] [F^2(\theta_0 - \theta_2) - F^2(\theta_0 + \theta_2)] = 0, \quad (7.24)$$

where P_{c1} and P_{c2} are the powers of signals reflected from targets; P_{n1} and P_{n2} are the powers of noises radiated by the targets.

Approximating the radiation pattern by the proper functions, we can find the direction finding condition at any value of target spacing and power ratios for signals being emitted from the target.

With small angular target spread, when the antenna radiation pattern can be approximated by linear function

$$F(\theta_0 \pm \theta) = F(\theta_0)(1 \mp \mu\theta), \quad (7.25)$$

we obtain

$$[P_{n1}(t) + P_{c1}(t)] \theta_1 + [P_{n2}(t) + P_{c2}(t)] \theta_2 = 0. \quad (7.26)$$

Assuming $P_{c1} = P_{c2} = P_c$, which is sufficiently valid with single-type targets and reading direction finding error $\Delta\theta$ relative to the position of the geometric center of the targets, when

$$\theta_1 = \Delta\theta - \frac{\psi_n}{2} \text{ и } \theta_2 = \Delta\theta + \frac{\psi_n}{2},$$

[и = and]

where ψ_n is the angular base of the sources, equation (7.26) can be represented in the form

$$[P_{n1}(t) + P_{n2}(t) + 2P_c(t)] \Delta\theta - [P_{n1}(t) - P_{n2}(t)] \frac{\psi_n}{2} = 0.$$

Hence it follows that

$$\frac{2\Delta\theta}{\psi_n} = \frac{P_{n1}(t) - P_{n2}(t)}{P_{n1}(t) + P_{n2}(t) + 2P_s(t)} \quad (7.27)$$

The equation obtained defines the provision of the power center of the radiation relative to the geometric center of the signal sources.

For simplification let us assume that the power of the reflected signal is substantially less than the power of the noise sources. Then we can write

$$\frac{2\Delta\theta}{\psi_n} = \frac{P_{n1}(t) - P_{n2}(t)}{P_{n1}(t) + P_{n2}(t)} \quad (7.28)$$

From expression (7.28) it follows that position of the power center of the radiation is determined by the power ratios of the noise sources and the character of the noise variation with time.

Let the noise transmitter power be equal and transmitter emission be alternate. Then when $P_{n1} = 0$ $\frac{2\Delta\theta}{\psi_n} = -1$, when $P_{n2} = 0$ $\frac{2\Delta\theta}{\psi_n} = 1$. We obtain a trival result establishing the movement of the power center within the source arrangement in a cycle with the switching of noise transmitters.

A radar tracking the noise producers, in this case, will attempt to track first one then another target, due to which the radar antenna will swing in cycle with the switching of the noise. This substantially complicates determining angular coordinates of targets and their resolution with respect to direction. The angle between targets, at which their resolution under flickering noise begins, increases.

In guiding a missile to a paired target, an increase in critical target resolution angle inevitably leads to an increase in the extent of the miss, since a miss and critical target resolution

angle are connected by relationship [10]

$$\Delta l = \frac{l_0}{2} - \frac{1 \cdot n g l_0^2}{2 \cdot V_{OTH}^2 \theta_{HP}^2}, \quad (7.29)$$

where Δl is the value of the miss in linear units;

l_0 is the projection of the linear value of the base (distance between target) to a plane perpendicular to the line of view;

ng is the maximum possible G forces;

V_{OTH} is the rate of convergence of rocket and target;

θ_{HP} is the critical target resolution angle.

Because of this, foreign experts consider flickering noise an effective type of noise for missile guidance systems [103].

Obviously, in order that the direction finding system track the power center moving in space under the effect of flickering noises, transmitter switching frequency must be in agreement with the pass-band of the servosystem of the angle-measuring coordinator ΔF_{cc} .

If we assume the minimum duration of radiation for each of the transmitters as equal to the time constant of the servosystem, then with a high-speed AGC system for the radar receiver the permissible switching frequency for noise transmitters on square law can be determined from the following inequality:

$$\frac{T_x}{2} \geq \frac{1}{\Delta F_{cc}}, \quad (7.30)$$

where T_x is the transmitter switching period.

Hence

$$F_x \leq \frac{\Delta F_{cc}}{2}. \quad (7.31)$$

Since the effect of flickering noises reduces to the repeated realignment of the suppressed angle-measuring coordinator from one target to another by irradiating it with a more powerful signal from another direction, another no less important noise parameter than switching frequency is its power or, more accurately, the excess of noise over the signal. With the linearization of direction finding characteristic assumed, the excess of noise power over signals necessary for causing radar realignment can be determined from expression (7.27).

Let us assume that at the initial moment target 2 is being tracked. When the radar is realigned on target 1, noise emission from target 2 ceases ($P_{n2} = 0$) and noise emission by target 1 is turned on. Expression (7.27) in this situation assumes the form

$$\frac{2\Delta\theta}{\psi_n} = \frac{P_{n1}}{P_{n1} + 2P_s} \quad (7.32)$$

Solving equation (7.32) relative to $a = \frac{P_{n1}}{P_s}$, we obtain

$$a = \frac{2y}{1-y}, \quad (7.33)$$

where $y = \frac{2\Delta\theta}{\psi_n}$.

The quantity $y = 1.0$ corresponds to the case of accurate direction finding when the radar antenna swings in a sector equal to the angular separation of the noise producers ψ_n .

Calculations with formula (7.33) show that in order to provide antenna swing in sector $0.8\psi_n$, noise excess over signals must be 9 dB. If the dimension of the angular target base exceeds the limits of the linear section of the direction finding characteristic, calculations must be performed taking into account the actual radiation pattern and expression (7.24), using this method. We should mention that noise transmitter switching can be carried out only according to random law.

As with coherent noise emitted from two points, flickering noise is universal in the sense that under certain conditions it can affect direction finding systems of various types. This is explained by the fact that its effect, in the final analysis is also connected with the change in the slope of the phase front of radio waves received by a radar antenna.

7.2.4. Noises with frequency wobble created from two or more points. It was shown earlier that transmitters with continuous rapid retuning (wobbling) of frequency can be used as a source of camouflaging noises. As in the case of flickering noises, a radar in this case, as it were, sees various targets appearing in a rapid sequence as the frequency of the noise transmitters successfully hits in the passband of the radar receiver. The interfering effect from the angle-measuring channel, in this case, will be somewhat similar to the effect of an ordinary group target with the only difference being that range resolution will be impossible since the noise transmitters operate in continuous mode [103].

If the transmitter frequency wobble rate decreases in accordance with the requirements of action on an angle-measuring channel, and the aircraft flying in a dispersed formation are supplied with such transmitters, frequency-retunable noises, in principle, can create the effect of flickering noise and can be a means of suppressing an angle-measuring channel, including one operating on the monopulse method.

The effect of flickering noises with frequency wobble, in this case, is explained by the fact that a radar at the moment noise frequency agrees with the tuning frequency of its receiver will go to autotracking on the corresponding noise producer. With noise frequency output beyond the passband of the receiver, radars will continue to track the same target but always on the reflected signal.

At the moment the frequency of noise emitted from another aircraft coincides with receiver tuning, the range-measuring channel of a radar is jammed by the noise, due to which target selection

with respect to range is hampered and the radar goes to autotracking on a new target based on the noise. Since an aircraft emitting noise, in the latter case, will be in another direction the antenna system turns to this new direction. A similar reaiming occurs with a second arrival of noise from the first target or another new target. As a result of the repeated action of noises emitted from spaced sources of frequency-retunable noises, the antenna system will go from tracking one target to tracking another target and, consequently, will experience rocking in accordance with the programmed operation of noise transmitters.

In order that a radar be able to find the source of noise, the duration of the period the frequency-retunable noise is in the receiver passband, obviously, must be equal to the time constant of the angle measuring servosystem or be greater than it. If the receiver passband is Δf , noise frequency retuning rate is V_f , and angle-measuring servosystem passband is $\Delta F_{c c}$, the indicated condition for creating noise with frequency wobble can be expressed mathematically in the form:

$$\frac{\Delta f}{V_f} \geq \frac{1}{\Delta F_{c c}} \quad (7.34)$$

Hence we can determine the anticipated frequency retuning rate for noise from formula

$$V_f \leq \Delta f \Delta F_{c c} \quad (7.35)$$

When $\Delta f = 3 \text{ MHz}$, $\Delta F_{c c} = 1.5 \text{ Hz}$, $V_f \leq 4.5 \text{ MHz/s}$.

The permissible noise frequency retuning rate is rather low, which is its limitation since with retuning in a wide frequency range the interval between noise action will be large, substantially reducing the expected flickering effect for the target being tracked.

With significantly higher retuning rate when the time between effects becomes commensurate with the time constant of the receiver,

the expected effect in the angle-measuring channel is similar to the effect of a group target regardless of the difference of distances from the radar to the separate targets of the group, since range resolution, in this case, is hampered by the effect of the noise.

The effect of noise with frequency wobble on many radars whose operating frequencies cover the range of transmitter frequency tuning and the comparative simplicity of the noise equipment are advantages of this type of noise.

7.2.5. Noises on crosspolarization. Unlike the types of noises examined in paragraphs 7.2.2.-7.2.4, noise on crosspolarization is created from one point and therefore, is considered suitable for the individual protection of objects. The principle of its creation lies in the irradiation of radar receiving antennas by high frequency signals which agree in frequency but have polarization which agrees with the crosspolarization of the antenna [78].

Earlier (Chapter 2) it was shown that antenna systems, in addition to radiation on a main (working) polarization, radiate part of their power in crosspolarization, orthogonal to working polarization. Because of this, an antenna, in addition to a radiation pattern on working polarization, has a radiation pattern on crosspolarization which differs in its structure. Thus, in parabolic antennas the radiation pattern on crosspolarization usually has four lobes symmetrically ranged with respect to the equisignal direction of the antenna, with maxima which do not coincide with the maximum of the main diagram.

Since the level of the pattern on crosspolarization differs from the level of the pattern on main polarization by approximately two orders, under normal operating conditions, the effect is scarcely noticeable. When an antenna is irradiated by powerful signals with a polarization which agrees with its crosspolarization, the role of the radiation pattern on crosspolarization can be amplified and thus distort the radiation pattern of the direction finding antenna.

In the extreme case, when the power of the noise exceeds by several orders the power of the reflected signal, the resulting pattern of the receiving antenna will be determined by the pattern on crosspolarization. Since the radiation pattern on crosspolarization substantially differs in structure from the main radiation pattern, this leads to a distortion of the direction finding characteristic of the system and, as a consequence, to the substantial impairment of direction finding accuracy.

During countermeasures on a radar with linear polarization the effective noise is noise with a polarization orthogonal to the working polarization of the radar. In this case [78], noise on crosspolarization generates a strong interconnection of azimuth and elevation channels, i.e., leads to a misphasing of the coordinate system. With the creation of such noise, guidance based on polarization is accomplished automatically based on radar signals received on board the aircraft with the aid of a system which analyzes the polarization of the radar signals and automatically establishes a polarization of the emitted noise signals orthogonal to the polarization of the suppressed radar [78].

Since noise on crosspolarization leads to a distortion of the working radiation pattern for the radar antenna, it must act both on monopulse and on the ordinary single-channel angle-measuring coordinators. In this sense, noise on crosspolarization is universal.

§ 7.3. METHODS OF PROTECTING MONOPULSE RADARS FROM CERTAIN TYPES OF RADIO NOISES

Table 7.1 lists several types of noises which can be applied to monopulse radars and the possible method of protection from them [68, 74].

The listed type of noises generally affect either the visual channel of the radar or the target tracking channel with respect to range and speed. Let us pause for more detail on the protection of an angle-measuring channel from certain noises.

Types of radio noises	Protection methods
Nonsynchronous pulsed noise with low repetition frequency	Pulse delay for repetition period, its comparison with next pulse and blanking.
Wide-band noise. Nonsynchronous pulsed noise with very high repetition frequency	Increase of observation time and integration. Suppression of side lobes of antenna radiation pattern. Transmitter frequency retuning.
Noise in the form of unmodulated carrier	Elimination of receiver saturation (instantaneous automatic gain control, use of logarithmic amplifiers, etc.).
Multiple responding pulsed noise	Repetition frequency wobble in combination with protection measures against nonsynchronous pulsed noise.
Noise with low-frequency wobble	As in the case of nonsynchronous pulsed noise.
Noise with high-frequency wobble	As in the case of wide-band noise.
Decoys	Selection based on reflecting properties, mass and dimensions, with respect to trajectory parameters, degree of deceleration in the atmosphere, and ionization of the air.
Dipole reflectors	Selection based on speed and acceleration.
Diversion of range strobe from true target	Use of Doppler shift of frequency, narrow range strobe, gating based on acceleration.
Noises from high-altitude nuclear explosions	Territorial spacing of radars of one group, operation on different frequencies of single-type stations, duplication of objects for the antiaircraft and antimissile defense systems.

7.3.1. Methods of protection from flickering noises created from two or more points in space. Since flickering noises, as has been shown, pursue the target, impairing target resolution, one of the possible methods of radar protection from such noises is the increase of radar resolution undergroup-target operating conditions. Therefore, the version of a monopulse system with increased resolution, discussed in Chapter 4 (Fig. 4.12), also has increased immunity from flickering noises. With the creation of flickering noises,

transmitters installed on targets flying in a group are turned on and off periodically or randomly and substantially complicate the tracking of a specific target for the time necessary for an accurate determination of its location and the proper defense measures. Under these conditions the monopulse system discussed above makes it possible to track either a left or right target according to the choice made by the operator.

If tracking is carried out, for example, on a left target and the signal from this target suddenly disappears and instead of it there appears another signal emitted by a target located to the right, the resulting negative error signal for the target selection channel will block the gating device for a certain period of time and the servosystem will not go to tracking the new powerful signal source [103]. Thus the main target pursued by the flickering noises and lying in the area of autotracking breakdown or resolution impairment will not be reached.

The effect of noises with frequency wobble, created from several targets of a group, is similar to the effect of flickering noises. Therefore, the described method of protection from flickering noises is also a protection from noises with frequency wobble.

Restricting the radiation pattern and reducing its side lobes is also a means of increasing the noise immunity of monopulse radars from flickering noises and noises with frequency wobble since this procedure leads to an increase in the required noise power and an increase in the resolution of a radar with respect to angular coordinates.

7.3.2. Protection from noises on crosspolarization. Since noise on crosspolarization differs substantially in polarization from the working polarization of a radar, the obvious method of protection from it is the polarization selection of signals. A familiar means of such selection is the polarization grids installed in antenna apertures [28, 77].

As described in Chapter 6, such grids ensure the transmission of the working signals with low attenuation and strongly attenuate signals with a polarization orthogonal to the working polarization. Thus noise on cross polarization during passage through the polarization grid is strongly attenuated and its effectiveness considerably reduced.

Sometimes as a polarization filter the antenna reflector itself is used, for which it is made in the form of a system of parallel metal plates (wires) [62, 63, 112]. In this case, the crosspolarization components of the excitation field pass through the reflector and are not reflected from it, which also substantially weakens the cross polarization components of the emitted and received signals.

Measures directed toward reducing antenna crosspolarization, partially discussed in Chapters 2 and 5, can also be considered protection from noises on crosspolarization.

Presently in foreign countries serious attention is being given to the development of radar systems with a polarization spread [130]. Such systems are built on the multichannel principle and can operate on a receiving channel whose polarization most nearly agrees with the polarization of the signals received. This makes it possible to substantially compensate the effect of the depolarization of signals reflected from the target and also increase the immunity of a radar from noises on crosspolarization.

CHAPTER 8

THE USE OF MODELING IN A STUDY OF COORDINATE DETERMINATION ERRORS FOR MONOPULSE RADARS

§ 8.1. COMMON PROBLEMS AND TRENDS IN SIMULATION

In the development of monopulse radars a wide circle of problems must be solved, such as:

- the evaluation of the basic characteristics of a station and their laws of distribution;
- the establishment of the dependence of main characteristics on various factors and the clarification of the most substantial and least important factors;
- the processing and evaluation of algorithms used in handling radar information;
- the development of assumptions with respect to the perfection of specific characteristics.

In order to solve these problems, in recent years, along with full-scale tests and physical simulation, mathematical modeling has been widely used. Since any monopulse radar can be characterized by a series of characteristics, in practice, we can follow two directions for modeling:

- the development of a common model which makes it possible to obtain the evaluation of all characteristics;
- the development of specific models each of which enable us to evaluate one or several characteristics.

The development of a mathematical model enabling the evaluation of all characteristics is a very difficult task and, in addition, such a model cannot always be accomplished in a computer. Therefore, it is expedient to use models following the second direction. If, however, in studies with a model we find that it is necessary to obtain certain other characteristics, we must refine the old model further or develop a new one. The composition of new models which differ from those already developed is not particularly difficult because of the presence of a number of separate model units and the experience acquired by the developer.

To study the main characteristics of monopulse radar, numerical probability (statistical) models, also called Monte Carlo models, have been the most widely used.

Below we shall discuss such models for the evaluation of coordinate determination accuracy by amplitude sum-difference monopulse autotracking radars and monopulse scanning radars with amplitude direction finding, using a wide-band signal.

§ 8.2. A MODEL OF AN AMPLITUDE SUM-DIFFERENCE MONOPULSE TRACKING RADAR

A simplified block diagram of an amplitude sum-difference monopulse radar designed for the automatic tracking and determining of angular target coordinates in one plane is presented in Fig. 1.9.

The greatest complexity in modeling is the mathematical description of the angular discriminator. This description can be made by several methods. We shall examine the method connected with calculating signals and noises in elements of the angular discriminator. This method most fully describes the processes taking place in an actual discriminator, and, in addition, makes it possible to calculate the effect of phase nonidentity in channels.

In this monopulse radar, to form the radiation pattern a parabolic antenna with diameter d is used. With uniform field distribution in

the antenna aperture each of the four partial radiation patterns is described by expression

$$F(\theta) = \frac{J_1(2.62\theta)}{1.31\theta}, \quad (8.1)$$

where $J_1(x)$ is the Bessel function of the first type;

$\theta = \frac{\theta_\alpha}{\theta_{0.5}}$ is the angular coordinate in relative units;

$\theta_{0.5}$ is the width of the partial beam in minutes;

θ_α is the angular coordinate in minutes, read from the center of the radiation pattern.

Coefficient 2.62 is selected from the condition of obtaining the width of the square of the sum radiation pattern with respect to voltage equal to one at level 0.7 from maximum value. Standardization of the radiation pattern with respect to the square is due to the use of the same antenna for transmission and reception. The cross-section of the sum radiation pattern in one plane (from the four horns), passing through equisignal direction, is described by expression

$$F_c(\theta) = \frac{F(\theta-0.625) + F(\theta+0.625) + 2F(\sqrt{\theta^2+0.625^2})}{2}. \quad (8.2)$$

The difference diagram has the form

$$F_p(\theta) = \frac{F(\theta-0.625) - F(\theta+0.625)}{\sqrt{2}}. \quad (8.3)$$

Coefficients $1/2$ and $1/\sqrt{2}$ are due to the summation (subtraction) of signals received by each beam of the antenna, in the waveguide bridges. The reflected signal at antenna input can be written in the form

$$u_{\text{ax}} = f(u_R, u_\phi). \quad (8.4)$$

where u_R is the component of the reflected signal depending on potential and range to target;

u_ϕ is the component of reflected signal depending on the fluctuations of the effective scattering area of the target.

For further studies the reflected signal is conveniently represented in relative units reduced to the receiver noise power of the sum channel.

The signal/noise ratio with respect to power, converted to antenna input, can be written in the form

$$q_{\Sigma}^2 = \frac{\Pi \sigma(\theta_n)}{R^4}, \quad (8.5)$$

where Π is the potential of the station determined by transmitter power, receiver sensitivity, and losses in the circuits;

$\sigma(\theta_n)$ is the effective scattering area of the target;
 R is range to target.

In amplitude sum-difference monopulse radars the value of phase nonidentity for the high-frequency circuit is usually 10-40°. Such phase nonidentity has a substantial effect on angular coordinate determination accuracy and is only slightly expressed in a decrease in the value of the sum signal. Therefore, we shall disregard the effect of the phase nonidentity of the high-frequency circuit in calculating the amplitude signal and the sum/noise ratio in the sum channel.

Under these conditions, the expressions for sum signal and signal/noise ratio with respect to power at waveguide bridge output have the form

$$u_\Sigma = u_{\Sigma x} F_\Sigma^2(\theta), \quad (8.6)$$

$$q_\Sigma^2 = \frac{\Pi \sigma(\theta_n)}{R^4} F_\Sigma^4(\theta). \quad (8.7)$$

The sum signal received passes through the linear part of the receiver, where it is added with noises, and the envelope demodulator. The sum signal at output of the linear part of the receiver can be represented as:

$$\vec{u}_{\text{свмх}} = \vec{u}_{\text{с}} + \vec{u}_{\text{шс}}, \quad (8.8)$$

where $u_{\text{шс}}$ is the noise voltage at output of the linear part of the receiver.

Expressions for modulus and phase of sum signal at output of the linear part of the receiver can be written in the form

$$|u_{\text{свмх}}| = \sqrt{U_{\text{с}}^2 + U_{\text{шс}}^2 + 2U_{\text{с}}U_{\text{шс}}\cos(\varphi_{\text{свмх}} - \varphi_{\text{шс}})}, \quad (8.9)$$

where $\varphi_{\text{шс}}$ is the phase of the noise signal at output of the linear part of the receiver;

$\varphi_{\text{свмх}}$ is the phase of the sum signal at output of the linear part of the receiver, equal to

$$\varphi_{\text{свмх}} = \text{arctg} \frac{|U_{\text{с}}| \sin \varphi_{\text{с}} + |U_{\text{шс}}| \sin \varphi_{\text{шс}}}{|U_{\text{с}}| \cos \varphi_{\text{с}} + |U_{\text{шс}}| \cos \varphi_{\text{шс}}}, \quad (8.10)$$

where $\varphi_{\text{с}}$ is the phase of the sum signal at output of the waveguide bridge, equal to

$$\varphi_{\text{с}} = \text{arctg} \frac{u(\theta_1) \sin \varphi_1 + u(\theta_2) \sin \varphi_{11}}{u(\theta_1) \cos \varphi_1 + u(\theta_2) \cos \varphi_{11}}, \quad (8.11)$$

where $u(\theta_1)$ and $u(\theta_2)$ are the values of the moduli of the sum signals in the first and second planes accordingly;

$$u(\theta_1) = U_{\text{BX}} \sqrt{F_1^2(\theta_1) + F_2^2(\theta_1) + 2F_1(\theta_1)F_2(\theta_1)\cos\varphi_1},$$

$$u(\theta_2) = U_{\text{BX}} \sqrt{F_3^2(\theta_2) + F_4^2(\theta_2) + 2F_3(\theta_2)F_4(\theta_2)\cos\varphi_{II}}.$$

φ_I and φ_{II} are the phases of sum signals in the first and second planes,

$$\varphi_I = \text{arctg} \frac{F_1(\theta_1)\sin\varphi_1 + F_2(\theta_1)\sin\varphi_2}{F_1(\theta_1)\cos\varphi_1 + F_2(\theta_1)\cos\varphi_2},$$

$$\varphi_{II} = \text{arctg} \frac{F_3(\theta_2)\sin\varphi_3 + F_4(\theta_2)\sin\varphi_4}{F_3(\theta_2)\cos\varphi_3 + F_4(\theta_2)\cos\varphi_4}.$$

$\varphi_1, \varphi_2, \varphi_3$ and φ_4 are the initial phases of the signals received along each partial radiation pattern, taking into account phase non-identity.

The law of phase distribution for noise oscillations can be assumed uniform in the range 0 to 2π .

For further studies, the modulus of the sum signal at detector input is conveniently represented in relative units reduced to the noise power of the receiver of the sum channels. Then

$$\left| \frac{u_{\text{c BX}}}{2\sigma_{\text{ш c}}^2} \right| = \sqrt{\frac{U_c^2}{2\sigma_{\text{ш c}}^2} + \frac{U_{\text{ш c}}^2}{2\sigma_{\text{ш c}}^2} + \frac{U_c U_{\text{ш c}}}{\sigma_{\text{ш c}}^2} \left| \cos(\varphi_{\text{c BX}} - \varphi_{\text{ш c}}) \right|}. \quad (8.12)$$

The signal/noise ratio at output of the linear part of the sum channel receiver can be written in the form

$$q_{\text{c BX}}^2 = \frac{\Pi\sigma(\theta_{II})F_c^4(\theta)}{2\sigma_{\text{ш c}}^2 R^4} + U_{\text{ш c OTH}}^2 +$$

$$+ 2 \sqrt{\frac{\Pi\sigma(\theta_{II})F_c^4(\theta)}{2\sigma_{\text{ш c}}^2 R^4}} U_{\text{ш c OTH}} \cos(\varphi_{\text{c BX}} - \varphi_{\text{ш c}}), \quad (8.13)$$

where $U_{\text{ш c OTH}} = \frac{U_{\text{ш c}}}{\sqrt{2}\sigma_{\text{ш c}}}$ is the relative value of the amplitude of sum channel receiver noise.

If an actual amplitude detector is approximated by an inertialless linear detector, the voltage and the signal/noise ratio at its output will be determined, accordingly, by equations (8.9) and (8.13) multiplied by the transmission factor of the detector.

The expression for the signal/noise ratio at sum channel receiver output, taking into account the operation of the AGC system, will be obtained later after a description of the AGC system operation.

The difference signal at input of the receiver will be written as

$$u_p = U_p \sin(\omega t + \varphi_p), \quad (8.14)$$

where

$$U_p = U_c \sqrt{F_1^2(\theta_1) + F_2^2(\theta_2) - 2F_1(\theta_1)F_2(\theta_2)\cos\varphi_p} = U_c \Delta F(\theta); \quad \varphi_p = \varphi_1 - \varphi_2. \quad (8.15)$$

The phase of the difference signal at output of the waveguide bridge φ_p can have a series of values and be determined from the following relationships:

$$\varphi_p = \arctg \begin{cases} \frac{F_2(\theta_2) \sin \varphi_p}{F_1(\theta_1) - F_2(\theta_2) \cos \varphi_p} \\ \text{при } F_1(\theta_1) > F_2(\theta_2) \cos \varphi_p; \\ \frac{F_2(\theta_2) \sin \varphi_p}{F_1(\theta_1) - F_2(\theta_2) \cos \varphi_p} + \pi \\ \text{при } \begin{cases} \varphi_p = 0 \\ F_1(\theta_1) < F_2(\theta_2) \cos \varphi_p; \end{cases} \\ \frac{F_2(\theta_2) \sin \varphi_p}{F_1(\theta_1) - F_2(\theta_2) \cos \varphi_p} - \pi \\ \text{при } \begin{cases} \varphi_p > 0 \\ F_1(\theta_1) < F_2(\theta_2) \cos \varphi_p. \end{cases} \end{cases} \quad (8.16)$$

при = when

The difference signal received in the linear part of the receiver is added with the noise signal. Consequently, at input of the phase detector the difference signal can be written in the form

$$\vec{u}_{p \text{ вых}} = \vec{u}_p + \vec{u}_{ш p}. \quad (8.17)$$

The modulus of the difference signal is

$$|u_{p \text{ вых}}| = \sqrt{U_p^2 + U_{ш p}^2 + 2U_p U_{ш p} \cos(\varphi_{ш p} - \varphi_{p \text{ вых}})}, \quad (8.18)$$

where $\varphi_{ш p}$ is the initial phase of the noise signal at output of the linear part of the difference channel receiver.

The phase $\varphi_{p \text{ вых}}$ of the difference signal at output of the linear part of the receiver can have a number of values and be determined by the following relationships:

$$\varphi_{p \text{ вых}} = \varphi_{p \text{ в}} + \left\{ \begin{array}{l} \arcsin \frac{|U_{ш p}|}{|U_p|} \sin(\varphi_{ш p} - \varphi_{p \text{ в}}) \text{ при } |U_p| > |U_{ш p}|; \\ \arcsin \frac{|U_{ш p}|}{|U_p|} \sin(\varphi_{ш p} - \varphi_{p \text{ в}}) \\ \quad |U_p| < |U_{ш p}|; \\ \text{при } \left\{ \begin{array}{l} \varphi_{ш p} - \varphi_{p \text{ в}} = 0 + \frac{\pi}{2}; \\ \varphi_{ш p} - \varphi_{p \text{ в}} = \frac{3}{2}\pi + 2\pi; \end{array} \right. \\ \arcsin \frac{|U_{ш p}|}{|U_p|} \sin(\varphi_{ш p} - \varphi_{p \text{ в}}) + \frac{\pi}{2} \\ \text{при } \left\{ \begin{array}{l} |U_p| < |U_{ш p}|; \\ \varphi_{ш p} - \varphi_{p \text{ в}} = \frac{\pi}{2} + \pi; \end{array} \right. \\ \arcsin \frac{|U_{ш p}|}{|U_p|} \sin(\varphi_{ш p} - \varphi_{p \text{ в}}) - \frac{\pi}{2} \\ \text{при } \left\{ \begin{array}{l} |U_p| < |U_{ш p}|; \\ \varphi_{ш p} - \varphi_{p \text{ в}} = \pi + \frac{3}{2}\pi \end{array} \right. \end{array} \right. \quad (8.19)$$

[при = when]

We shall assume that the amplitudes of the sum and difference signals relative to the sum signal amplitude are standardized with the aid of the AGC system described in § 3.3; a block diagram of such an AGC is presented in Fig. 3.18.

Then, taking into account the work of the AGC system, the modulus of the difference signal at detector input has the form

$$|u'_{p \text{ Вых}}| = \left| \frac{u'_{p \text{ Вых}}}{U_{p \text{ Вых}}} \right| = \sqrt{\frac{U_p^2}{U_{p \text{ Вых}}^2} + \frac{U_{ш \text{ п}}^2}{U_{p \text{ Вых}}^2} + 2 \frac{|U_p| |U_{ш \text{ п}}|}{U_{p \text{ Вых}}^2} \cos(\varphi_{ш \text{ п}} - \varphi_{p \text{ Вых}})} \quad (8.20)$$

where $U_{p \text{ Вых}}$ is the voltage of the monitoring signal at output of the linear part of the receiver, in accordance with which standardization is carried out for the amplification factor and the difference channel receiver.

For further studies the standardized modulus of the difference signal can be represented in relative units reduced to the noise power of the difference channel receiver

$$|u'_{p \text{ п}}| = \sqrt{\frac{\Delta F^2(\theta) q_c^2}{q_{p \text{ Вых}}^2} + \frac{U_{ш \text{ п отн}}^2}{q_{p \text{ Вых}}^2} + 2 \frac{\Delta F(\theta) U_{ш \text{ п отн}} q_c}{q_{p \text{ Вых}}^2} \cos(\varphi_{ш \text{ п}} - \varphi_{p \text{ Вых}})} \quad (8.21)$$

where $q_{p \text{ Вых}}^2$ is the signal/noise ratio of the monitoring signal with respect to power at the output of the linear part of the receiver of the difference signal;

$U_{ш \text{ п отн}}$ is the relative value of noise amplitude at output of the difference channel receiver.

The sign of the error signal is determined by the phase difference of difference and sum signals. Phases of sum and difference signals at phase detector input are determined by expressions (8.10) and (8.19).

Voltage at output of the linear phase detector, in accordance with (3.52), is determined by expression

$$u_p(\theta) = 2\kappa_{\Phi \Delta} |u'_{p \text{ Вых}}| \cos(\varphi_{p \text{ Гых}} - \varphi_{c \text{ Вых}}). \quad (8.22)$$

Then error signal in the angle channel can be written

$$u_p(\theta) = 2\kappa_{\Phi \Delta} \times \left[\sqrt{\frac{\Delta F^2(\theta) q_c^2}{q_{pк \text{ Вых}}^2} + \frac{U_{mp \text{ Гых}}}{q_{pк \text{ Вых}}^2} + 2 \frac{\Delta F(\theta) U_{mp \text{ Гых}} q_c}{q_{pк \text{ Вых}}^2} \cos(\varphi_{mp} - \varphi_{c \text{ Вых}})} \right] \times \cos(\varphi_{p \text{ Вых}} - \varphi_{c \text{ Вых}}). \quad (8.23)$$

Error signal $u_p(\theta)$ from receiver output of the difference channel enters antenna drive.

Here we determine the mathematical expression of the signal/noise ratio of the monitoring signal $q_{pк \text{ Вых}}^2$ in the receiver, taking into account the work of the AGC system. With modeling, in the case of small variations in signal amplitude $\Delta U_{\text{Вых}}$ at receiver input from the time lag of the AGC, exponential approximation of the AGC control characteristics gives good results. The requirement for small variations in signal amplitude $\Delta U_{\text{Вых}}$ at receiver output corresponds to the actual requirements for the operation of monopulse radar receivers performing automatic target tracking.

With such an approximation of the control characteristics we have

$$\kappa_{\text{пер}} = \kappa_m \exp - (b_A U_{\text{пер}}). \quad (8.24)$$

The amplitude of the monitoring signal at output of the linear part of the difference channel receiver with an operating AGC system is equal to

$$U_{pк \text{ Гых}} = \kappa_{mp} U_{pк \text{ Гх}} \exp - [b_{Ap} (U_{pк \text{ Гх}} - U_{p \text{ зад}}) F_{Ap}(p)] \text{ при } \kappa_{mp} U_{pк \text{ Гх}} > U_{p \text{ зад}} \quad (8.25)$$

$$U_{pк \text{ Вых}} = \kappa_{mp} U_{pк \text{ Гх}} \text{ при } \kappa_{mp} U_{pк \text{ Гх}} \leq U_{p \text{ зад}}$$

[при = when]

where $U'_{\text{рк вых}}$ is the amplitude of the monitoring signal voltage at input of the difference channel receiver.

The values of k_m , b_A , $U_{\text{зад}}$, $F_A(p)$ were determined in § 3.3.

$$U_{\text{рх их}} = U_c \exp - [b_{Ac}(U'_{c \text{ ых}} - U_{c \text{ зад}})F_{Ac}(p)] \text{ при } U_c < U_{c \text{ зад}},$$

$$U_{\text{рх их}} = U_c \text{ при } U_c \leq U_{c \text{ зад}}, \quad (8.26)$$

[при = when]

where $U'_{c \text{ вых}}$ is the amplitude of the sum signal voltage at output of the linear part of the sum channel receiver, taking into account the operation of the AGC system.

After dividing the right and left sides of equations (8.25) by $\sqrt{2}\sigma_{\text{шр}} = \sqrt{2}\sigma_{\text{шр вых}} \cdot k_{\text{мр}}$, we obtain

$$q_{\text{рк ых}} = q_{\text{рк их}} \exp - [b'_{Ap}(q_{\text{рк ых}} - q_{\text{р зад}})F_{Ap}(p)]$$

$$\text{при } q_{\text{рк ых}} > q_{\text{р зад}},$$

$$q_{\text{рк ых}} = q_{\text{рк их}} \text{ при } q_{\text{рк ых}} \leq q_{\text{р зад}}. \quad b'_{Ap} = b'_{Ap} \sqrt{2} \sigma_{\text{шр}} \quad (8.27)$$

[при = when]

Analogously, for (8.26) we write

$$q_{\text{рх их}} = q_c \exp - [b'_{Ac}(q'_{c \text{ ых}} - q_{c \text{ зад}})F_{Ac}(p)]$$

$$\text{при } q'_{c \text{ ых}} > q_{c \text{ зад}},$$

$$q_{\text{рх их}} = q_c \text{ при } q'_{c \text{ ых}} \leq q_{c \text{ зад}}. \quad (8.28)$$

[при = when]

Accordingly, taking into account the work of the AGC system, at output of the linear part of the sum channel receiver we can write

$$q'_{c \text{ вых}} = q_c \exp - [b'_{Ac}(q'_{c \text{ ых}} - q_{c \text{ зад}})F_{Ac}(p)]$$

$$\text{при } q'_{c \text{ ых}} > q_{c \text{ зад}},$$

$$q'_{c \text{ вых}} = q_c \text{ при } q'_{c \text{ ых}} \leq q_{c \text{ зад}}. \quad (8.29)$$

[при = when]

In order to take into account the effect of reflected signal fluctuations on angular coordinate determination accuracy, it is necessary to describe mathematically and well the reflected signal fluctuation in the reflected signal shaping unit. The selection of the type of approximation will depend upon the type of target, (aircraft, rocket, satellite) and upon the convenience of its use for modeling. The method of imitating reflected signal fluctuations will not be discussed.

The above analysis makes it possible to conclude that a model (Fig. 8.1) for studying the accuracy of angular coordinate determination in one plane by an amplitude sum-difference monopulse-tracking radar must consist of the following basic units: reflected signal shaping taking into account the fluctuation of the effective scattering area of the target; antenna and sum-difference waveguide bridges; sum signal receiver with AGC; amplitude detector; difference signal receiver with AGC; phase detector; noise generators (transmitters of random numbers); antenna drives; target trajectory shaping; statistical processing of angular coordinate measurement error.

Algorithms simulating the antenna radiation pattern and signal at outputs of the sum-difference waveguide bridge are made up on the basis of expressions (8.2), (8.3), (8.4), (8.5), (8.6), (8.7), (8.14), (8.15) and (8.16). The sum signal at output of the linear part of the receiver is described by expressions (8.9), (8.10) and (8.13). The sum signal at output of the amplitude detector is determined by expressions (8.9), (8.13), (8.29), multiplied by the detection factor.

To describe the difference channel receiver unit equalities (8.18)-(8.21) are used.

The work of the phase detector is approximated by expression (8.23).

The amplification factor standardization circuit with the aid of the AGC in the difference and sum signal receiver is modeled in accordance with expressions (8.25) and (8.29).

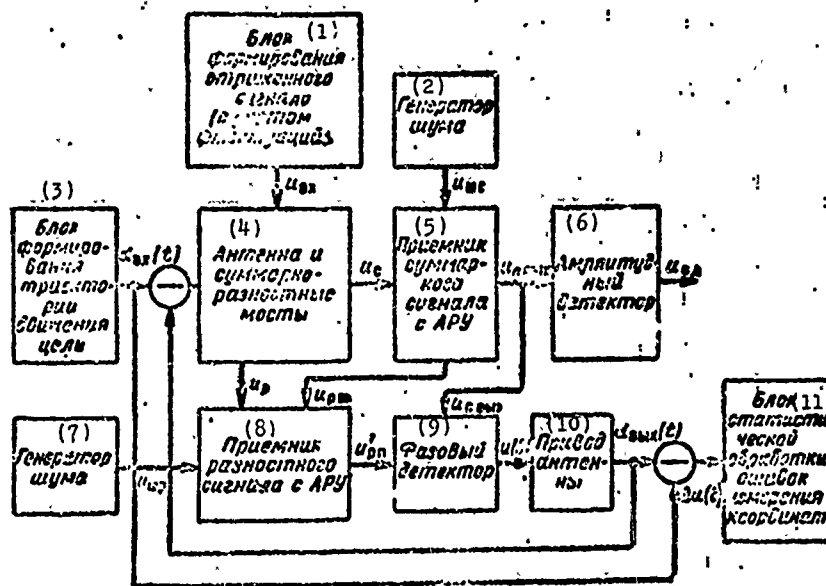


Fig. 8.1. Block diagram of a model of an amplitude sum-difference monopulse tracking radar.

KEY: (1) Unit for reflected signal shaping (taking fluctuations into account); (2) Noise generator; (3) Unit for target trajectory shaping; (4) Antenna and sum-difference bridges; (5) Sum signal receiver with AGC; (6) Amplitude detectors; (7) Noise generator; (8) Difference signal receiver with AGC; (9) Phase detector; (10) Antenna drive; (11) Unit for statistical processing of coordinate measurement errors.

The noise generator (random number transmitter) must generate a random sequence of numbers with a normal law of distribution. Noise dispersion is calculated for maximum radar range based on a single sounding signal width. Methods of shaping such random sequences in a computer are discussed in [9].

Modeling the antenna drive is not difficult and we will not discuss it here.

As an input effect on the input of the model in the target trajectory shaping unit we can assign the equivalent sinusoid

$$a_{вх}(t) = A_0 \sin \omega_0 t, \quad (8.30)$$

where $A_{\omega} = \frac{\dot{x}}{\omega_{\omega}}$ is amplitude and $\omega_{\omega} = \frac{\ddot{x}}{x}$ is frequency;

\dot{x} and \ddot{x} are the first and second derivative of the polynomial approximating target trajectory.

Reference data for determining dynamic and fluctuation errors in angular coordinate measurement are the models of error signal for processing of input effect by antenna drives in the presence of receiver noises and reflected signal fluctuations. Statistical processing is carried out on a group of models for the selected mean values of the signal/noise ratio.

The task of statistical processing is to distinguish the dynamic and fluctuation component from the total tracking error

$$\Delta\alpha(t) = \alpha_{\text{BYX}}(t) - \alpha_{\text{BYN}}(t) = \delta_D \sin(\omega_D t + \varphi_D) + \Delta\varepsilon(t), \quad (8.31)$$

where $\alpha_{\text{BYX}}(t)$ is the measured value of an angular coordinate;

δ_D and φ_D are amplitude and phase of dynamic errors;

$\Delta\varepsilon(t)$ is the value of fluctuation error.

Amplitude and phase of dynamic error when writing in discrete form can be determined from expression

$$\delta_{Dt} = \frac{2}{n} \left[\sin \varphi_{Dt} \sum_{i=1}^n \Delta\alpha^*(\Delta t \cdot i) \cos(\omega_D \Delta t \cdot i) + \cos \varphi_{Dt} \sum_{i=1}^n \Delta\alpha^*(\Delta t \cdot i) \sin(\omega_D \Delta t \cdot i) \right], \quad (8.32)$$

$$\varphi_{Dt} = \text{arctg} \frac{\sum_{i=1}^n \Delta\alpha^*(\Delta t \cdot i) \cos(\omega_D \Delta t \cdot i)}{\sum_{i=1}^n \Delta\alpha^*(\Delta t \cdot i) \sin(\omega_D \Delta t \cdot i)}, \quad (8.33)$$

where $\Delta t \cdot i = t$;

$i = 1, 2, 3, \dots, n$;

$$\Delta\alpha^*(\Delta t \cdot i) = \Delta\alpha(\Delta t \cdot i) - \overline{\Delta\alpha(\Delta t \cdot i)}; \quad \overline{\Delta\alpha(\Delta t \cdot i)} = \frac{\sum_{i=1}^n \Delta\alpha(\Delta t \cdot i)}{n}.$$

The average value of dynamic error will be equal to

$$\bar{\delta}_R = \frac{\sum_{i=1}^{k_0} \delta_{Ri}}{k_0}, \quad (8.34)$$

where k_0 is the number of error signal models;

δ_{Ri} is the dynamic error for fixed values of the mean signal/noise ratio in each of the models.

After subtracting in each model sum $\Delta\alpha^*(\Delta t \cdot i)$ the determined component $\delta_{Ri} \sin [\omega_0 (\Delta t \cdot i) + \phi_{Ri}]$, we obtain the model of fluctuation error

$$\Delta\epsilon^*(\Delta t \cdot i) = \Delta\alpha^*(\Delta t \cdot i) - \delta_{Ri} \sin [\omega_0 (\Delta t \cdot i) + \phi_{Ri}]. \quad (8.35)$$

The average value of the correlation function of fluctuation error will have the form

$$R(\Delta t \cdot i) = \frac{\sum_{i=1}^{k_0} R_i(\Delta t \cdot i)}{k_0}, \quad (8.36)$$

where

$$R_i(\Delta t \cdot i) = \frac{1}{N-m} \sum_{i=1}^{N-m} \Delta\epsilon^*(\Delta t \cdot i) \Delta\epsilon^*[\Delta t(i+1)],$$

N is the total number of points in the calculation of the correlation functions;

$m = 1, 2, 3, \dots, \frac{N}{5}$ are the points in which the correlation function is calculated;

$\Delta t = \frac{T}{N}$ is the time range of discreteness.

T is the total length of model (averaging interval).

Mean value of spectral density of fluctuation error is determined by formula

$$G(\Delta f, \bar{t}) = 4\Delta t \sum_0^{N-m} \overline{R(\Delta t \cdot i) \cos[\omega_0(\Delta t \cdot i)]} \quad (8.37)$$

where Δf is the frequency interval of discreteness.

The average value of fluctuation error variance will be

$$D_{\phi_0} = \frac{\sum_{i=1}^{k_0} \sum_{k_0=1}^n [\Delta \epsilon^*(\Delta t \cdot i)]^2}{n \cdot k_0} \quad (8.38)$$

Parameters N , m , Δt , Δf and k_0 are selected based on the necessary accuracy involved in obtaining estimates of dynamic and fluctuation errors.

§ 8.3. OVERALL BLOCK DIAGRAM OF A MODEL OF A SCANNING MONOPULSE RADAR WITH FREQUENCY-MODULATED SIGNALS AND AMPLITUDE DIRECTION FINDING

The task of determining coordinate measurement accuracy with a model will be examined for an arbitrary signal/noise ratio and the case when at model output are formed single evaluations of measured parameters of the signal and the evaluations obtained are not leveled.

In models of scanning monopulse radars whose block diagrams are presented in Figs. 1.12 and 1.13, the main difficulty lies in describing the signal and the angular discriminator.

In the model at input of each channel is shaped a pulse whose amplitude depends upon the angle of target deviation from equisignal direction in accordance with the antenna radiation patterns, while the envelope and instantaneous pulse phase are determined by the type of sounding signal selected in the radar. Then amplitude phase distortions required for studying the form (random or regular) are introduced into the pulse. The distorted pulse is mixed with normal white noise whose spectral density can be varied for the assignment of a necessary signal/noise ratio. Then linear filtration of the signal and noise mixture is modeled by a filter with a weight

function in agreement with the undistorted signal or containing distortions of the required form. Detection in the model can be represented as a determination of the process envelope at output of the linear filter. After detection, evaluations of amplitude and pulse time delay can be formed with respect to algorithms selected for processing radar information, which were examined in Chapter 1.

Let us consider models of an amplitude-amplitude and an amplitude sum-difference scanning radar for determining coordinates in one plane. In connection with this it is necessary to represent in the model two different measuring channels in which the amplitude of input pulses, distortion, and noise must be assigned independently. If the volume of computer memory in which modeling is produced is sufficient, we can model both channels in parallel; in the opposite case, first one of the channels is modeled and the output results are stored and then the second channel is modeled and an evaluation of the angle of target deviation from equisignal direction is formed. This gives an overall representation of one cycle of modeling work. The model will be described in more detail below.

In order to determine the statistical characteristics of evaluating measured parameters, the computing cycles on the model are repeated. In each cycle a new model of noise and random distortions is used. When necessary, we can change the amplitude of input signals and their temporary position, from cycle to cycle, for modeling the fluctuation of reflected signals and the displacement of the target with respect to angular coordinates and range. In this case, the given models will be used later for studying smoothing algorithms for output coordinates and characteristics of trajectory determination accuracy.

8.3.1. Representation of signal and noise. In modeling with a computer the signal $s(t)$ can be represented only by a set of several numbers, knowing which, we can calculate any of the current values of the signal, using prescribed operations.

There is an infinite set of variants for selecting the necessary set of numbers. Common problems of signal representation are studied in reference [108] where a generalized representation in the form of a double series is assumed:

$$s(t) = \sum_{m=1}^{M_c} \sum_{n=1}^{N_c} a_{mn} V_{mn}(t), \quad (8.39)$$

where $V_{mn}(t)$ are known functions.

In [57, 108] it is shown that for representing a signal with width τ_c whose spectrum occupies the frequency band W_c , $M_c N_c = \tau_c W_c$ is required, as well as coefficient a_{mn} . Consequently, the selection of any system of function $V_{mn}(t)$ is determined only by the convenience of solving a specific problem. For the studies being conducted an expansion of the signal in Kotel'nikov's series has indisputable advantages:

$$s(t) = \sum_{i=-N/2}^{N/2} s(i\Delta_t) \frac{\sin \frac{\pi}{\Delta_t} (t - i\Delta_t)}{\frac{\pi}{\Delta_t} (t - i\Delta_t)}, \quad (8.40)$$

when the expansion factors are values of signal $s(i\Delta_t)$ with sample step $\Delta_t = \frac{\tau_c}{N}$.

In the representation (8.40) instead of continuous signal $s(t)$ we obtain discrete signal $s(i\Delta_t)$, which enables us to use in the calculation an extended mathematical apparatus of discrete systems [14, 58]. For a wide-band signal with intrapulse linear frequency modulation, we can write

$$s(t) = S(t) \exp \left\{ i \left(\omega_0 t + \frac{\Omega}{2\tau_c} t^2 \right) \right\}, \quad |t| = \frac{\tau_c}{2}, \quad (8.41)$$

where $S(t)$ is the signal envelope;

$\frac{\Omega}{2\pi}$ is frequency deviation;

ω_0 is average signal frequency which later will be called carrier frequency.

There is a simple relationship between the expansion factors of the signal and the expansion factors of its spectrum since, in accordance with the method of stationary phase [80], the signal spectrum (8.41) is described by function

$$\begin{aligned} \tilde{s}(i\omega) = & \sqrt{\frac{2\pi\tau_c}{\Omega}} S\left[(\omega - \omega_0)\frac{\tau_c}{\Omega}\right] \times \\ & \times \exp\left\{-i\left[(\omega - \omega_0)^2 \frac{\tau_c}{2\Omega} - \frac{\pi}{4}\right]\right\}, \end{aligned} \quad (8.42)$$

where $S\left[(\omega - \omega_0)\frac{\tau_c}{\Omega}\right]$ is the signal envelope.

Let us go to the question of choosing the sample step Δ_t . We shall designate the discrete signal in terms of $s\left[\frac{t}{\Delta_t}\right]$ so that $s[i] = s(i\Delta_t)$ when $i = -\frac{N}{2}, -\frac{N}{2} + 1, \dots, \frac{N}{2}$ and $s[i] = 0$ when i is not a whole number, where $i = \frac{t}{\Delta_t}$.

Let us determine the spectrum $S^*(i\omega)$ of discrete signal $\left[\frac{t}{\Delta_t}\right]$. The expression connecting discrete and continuous signals is written in the following form [14]:

$$s\left[\frac{t}{\Delta_t}\right] = \sum_{l=-\infty}^{\infty} \int_{-\infty}^{\infty} s(t) \delta(t - i\Delta_t) dt, \quad |t| \leq \frac{\tau_c}{2}. \quad (8.43)$$

We shall use the known equality [14]:

$$\sum_{l=-\infty}^{\infty} \delta(t - i\Delta_t) = \frac{1}{\Delta_t} \sum_{l=-\infty}^{\infty} e^{i\frac{2\pi l t}{\Delta_t}}. \quad (8.44)$$

Multiplying both sides of equality (8.44) by $s(t)e^{-i\omega t}$ and integrating with respect to time from $-\infty$ to $+\infty$, we obtain

$$S^*(i\omega) = \frac{1}{\Delta_t} \sum_{i=-\infty}^{\infty} \tilde{s}\left[i\left(\omega + \frac{2\pi i}{\Delta_t}\right)\right], \quad (8.45)$$

i.e., the spectrum of the discrete signal is a periodic function with period $2\pi/\Delta_t$. Then let the continuous signal have limited spectrum

$$|\tilde{s}(i\omega)| = 0 \text{ при } |\omega| > \frac{\Omega}{2} = \pi W_c. \quad (8.46)$$

[при = when]

For the possibility of representing continuous signal $s(t)$ by discrete $s[i]$ agreement is required with accuracy up to the unessential factors (in this case, $\frac{1}{\Delta_t}$) of the spectrum of the continuous signal $\tilde{s}(i\omega)$ and one of the periods of the spectrum of discrete signal $S^*(i\omega)$ [58]. This agreement occurs if, in accordance with (8.45) and (8.46), inequality $\frac{2\pi}{\Delta_t} > \Omega$ is fulfilled, from which it follows that the sample step is limited at the top by quantity

$$\Delta_t < \frac{2\pi}{\Omega} = \frac{1}{W_c}. \quad (8.47)$$

Accordingly, the sample volume $N + 1$ must satisfy inequality

$$N > W_c T_c. \quad (8.48)$$

Let us note another peculiarity of representing continuous signals by discrete. The periodic character of the spectrum of a discrete signal leads to the fact that continuous signals with carrier frequencies spaced according to (8.45) by magnitude $\frac{2\pi i}{\Delta_t}$, have identical discrete representations. In other words, we can represent continuous signals in discrete form only with a carrier frequency of ω_0 , less than $2\pi/\Delta_t$. Thus, for representation in the model we must use an undistorted input, also with a carrier frequency equal to zero. Possible variations in the model of the carrier up to a magnitude of $2\pi/\Delta_t$

are sufficient for studying the effect of displacement of carrier with phase distortions of input signal on the shape of the output signal and the accuracy of measuring its parameters.

We know that radar signals always have $\omega_0 \gg \Omega$. More detail will be presented in paragraph 8.3.2. on the permissibility of using in modeling signals with a zero carrier frequency in order to study the processing of radar signals whose carrier frequency considerably exceeds the band limited by their spectra.

Let us examine what sample volume is required for representing a square pulse with linear modulation frequency

$$s(t) = \exp \left\{ i \left(\omega_0 t + \frac{\Omega}{2\tau_c} t^2 \right) \right\}, \quad |t| \leq \frac{\tau_c}{2}. \quad (8.49)$$

Calculating a Fourier transformation from (8.49), we find the input pulse spectrum [23]

$$\begin{aligned} \tilde{s}(i\omega) = & \sqrt{\frac{\tau_c}{2W_c}} \exp \left[-i \frac{\tau_c}{2\Omega} (\omega - \omega_0)^2 \right] \times \\ & \times \left\{ Z \left[\frac{1}{\pi} \sqrt{\frac{\tau_c}{2W_c}} (\omega - \omega_0) + \sqrt{\frac{W_c \tau_c}{2}} \right] - \right. \\ & \left. - Z \left[\frac{1}{\pi} \sqrt{\frac{\tau_c}{2W_c}} (\omega - \omega_0) - \sqrt{\frac{W_c \tau_c}{2}} \right] \right\}. \end{aligned} \quad (8.50)$$

where $Z(u) = \int_0^u \exp(i \frac{\pi x^2}{2}) dx$ is the Fresnel integral in complex form.

An analysis of equation (8.50) shows that with an increase in the compression $D_r = W_c \tau_c = \frac{\Omega}{2\pi} \tau_c$ the amplitude spectrum $|\tilde{s}(i\omega)|$ is similar to rectangular with the total frequency band tending toward Ω . With a decrease in coefficient D_r the number of components goes all the more beyond the frequency band Ω . Thus, for example, when $D_r = 50$, studies have shown that for a representation of such a signal with virtually unsubstantial error, a sample volume of 90 numbers is required.

Linear filtration does not lead to an expansion of the signal spectrum. Let us examine, therefore, the expansion of signal spectrum during detection. In the case of the large compression factors from (8.50) we obtain [35]

$$|\tilde{s}(i\omega)| \approx \sqrt{\frac{\tau_c}{W_0}} \operatorname{rect} \frac{\omega - \omega_0}{\Omega} \quad (8.51)$$

The signal at output of the matched filter is

$$s_\phi(t) = \frac{1}{2\pi} \int_{-\infty}^{\infty} |\tilde{s}(i\omega)|^2 \exp(i\omega t) d\omega = \tau_c \frac{\sin \frac{\Omega t}{2}}{\frac{\Omega t}{2}} \exp(i\omega_0 t), \quad (8.52)$$

and the signal after square-law detection is determined by expression

$$L^2 \{s_\phi(t)\} = \tau_c^2 \left(\frac{\sin \frac{\Omega \tau_c}{2}}{\frac{\Omega \tau_c}{2}} \right)^2 \quad (8.53)$$

A Fourier transform from (8.53) can be written as

$$\tau_c^2 \int_{-\infty}^{\infty} \frac{\sin^2 \frac{\Omega t}{2}}{\frac{\Omega^2 t^2}{2}} \exp(-i\omega t) dt = \frac{\tau_c^2}{W_0} \left(1 - \left| \frac{\omega}{\Omega} \right| \right), \quad \left| \frac{\omega}{\Omega} \right| \leq 1 \quad (8.54)$$

Comparison of formulas (8.51) and (8.54) shows that a square-law detector expands the spectrum by a factor of 2. Taking into account the fact that the spectrum of the input signals with distortions can be somewhat expanded as compared with the spectrum of an undistorted signal and keeping in mind the convenience of using output data, we finally obtain a sample volume equal to 201, i.e., $N = 4D_r = 200$, and a sample step of $\Delta_t = \frac{\pi}{\Omega}$. Thus, the signal in actual form with a zero carrier frequency and compression factor $D_r = 50$ will be

$$s(t) = \cos \frac{\Omega}{2\tau_c} t^2, \quad |t| \leq \frac{\tau_c}{2}, \quad \frac{\Omega \tau_c}{2\pi} = 50 \quad (8.55)$$

and is represented in the model by discrete signal

$$s[i] = \cos \left[\frac{\Omega}{2\tau_0} \left(i - \frac{\tau_0}{N} \right)^2 \right] = \cos \varphi_{20} \cdot i^2, \quad (8.56)$$

where $i = -\frac{N}{2}, -\frac{N-1}{2}, \dots, \frac{N}{2}$;

$$\varphi_{20} = \frac{\Omega \tau_0}{2N^2} = \frac{\pi D_r}{N^2}.$$

For the selected numerical values $N = 200$ and $D_r = 50$, we obtain $\varphi_{20} = 0.00393$.

At the beginning of this section it was shown that in the model the amplitude of the input pulse serves for the assignment of target deviation from equisignal direction and modeling of reflected signal fluctuations, while the additional components characterize the distortions of the envelope and instantaneous phase. Consequently, input pulse can be represented by a discrete signal in the form

$$s_{LW}[i] = A_c (1 + \Delta S[i]) \cos \Phi[i] \operatorname{rect} \frac{i}{N}. \quad (8.57)$$

where

$$\Phi[i] = \varphi_\phi + \varphi_{\phi 1} \cdot i + \varphi_{\phi 2} \cdot i^2 + \varphi_{\phi 3} \cdot i^3 + \Delta \varphi_\phi [i].$$

The quantities A_c and $\Delta S[i]$ serve to change pulse amplitude and to assign the distortions of the pulse envelope. Coefficient $\varphi_{\phi 2}$ determines the steepness of linear frequency modulation. Coefficients φ_ϕ , $\varphi_{\phi 1}$, $\varphi_{\phi 3}$ and the quantity $\Delta \varphi_\phi [i]$ serve to assign various laws of variation for instantaneous pulse phase. The quantities $\Delta S[i]$ and $\Delta \varphi_\phi [i]$ can be random.

In examining the question of representing white noise in a model, normal noise $n(t)$ with mathematical expectation $\overline{n(t)} = 0$ and correlation function

$$\overline{n(t_1)n(t_2)} = N_{\text{ш}}\delta(t_1 - t_2), \quad (8.58)$$

where $2N_{\text{ш}}$ is the spectral density of the noise,

$\delta(t_1 - t_2)$ is the delta function, is replaced with noise in a limited frequency band which is several times wider than the signal frequency band. Under these conditions, the noise used in the model we can assume to be white with respect to a given signal. Then when representing a continuous noise by discrete and using (8.40), for noise $n_n(t)$ limited in band we write

$$n_n(t) = \sum_{i=-\infty}^{\infty} n(i\Delta_t) \frac{\sin \frac{\pi}{\Delta_t} (t - i\Delta_t)}{\frac{\pi}{\Delta_t} (t - i\Delta_t)}, \quad (8.59)$$

i.e., continuous noise $n_n(t)$ is represented by discrete noise $n[i] \equiv n(i\Delta_t)$, and i varies from $-\infty$ to $+\infty$. Mathematical expectation of continuous noise $n_n(t)$, represented in the form (8.59), is

$$\overline{n_n(t)} = \sum_{i=-\infty}^{\infty} \overline{n(i\Delta_t)} \sin \frac{\frac{\pi}{\Delta_t} (t - i\Delta_t)}{\frac{\pi}{\Delta_t} (t - i\Delta_t)} = 0,$$

and the correlation function is

$$\begin{aligned} R_n(t_1, t_2) &= \sum_{i=-\infty}^{\infty} \sum_{k=-\infty}^{\infty} \overline{n(i\Delta_t)n(k\Delta_t)} \frac{\sin \frac{\pi}{\Delta_t} (t_1 - i\Delta_t)}{\frac{\pi}{\Delta_t} (t_1 - i\Delta_t)} \times \\ &\times \frac{\sin \frac{\pi}{\Delta_t} (t_2 - k\Delta_t)}{\frac{\pi}{\Delta_t} (t_2 - k\Delta_t)} = N_{\text{ш}} \sum_{i=-\infty}^{\infty} \frac{\sin \frac{\pi}{\Delta_t} (t_1 - i\Delta_t)}{\frac{\pi}{\Delta_t} (t_1 - i\Delta_t)} \times \\ &\times \frac{\sin \frac{\pi}{\Delta_t} (t_2 - i\Delta_t)}{\frac{\pi}{\Delta_t} (t_2 - i\Delta_t)} = N_{\text{ш}} \frac{\sin \frac{\pi}{\Delta_t} (t_1 - t_2)}{\frac{\pi}{\Delta_t} (t_1 - t_2)}. \end{aligned} \quad (8.60)$$

The power spectrum of the noise $n_n(t)$

$$\tilde{R}_n(\omega) = 2 \int_{-\infty}^{\infty} R_n(t) \exp(i\omega t) dt \quad (8.61)$$

is calculated by substituting (8.60) into (8.61):

$$\tilde{R}_n(\omega) = 2N_w \int_{-\infty}^{\infty} \frac{\sin \frac{\pi}{\Delta_t} t}{\frac{\pi}{\Delta_t}} \exp(i\omega t) dt. \quad (8.62)$$

An integral in the form of (8.62) is studied in work [57]; it agrees in mean-square and is

$$\tilde{R}_n(\omega) = 2N_w \Delta_t \operatorname{rect} \frac{\omega \Delta_t}{2\pi}. \quad (8.63)$$

Thus, the power spectrum of the noise, represented in the form (8.59), is uniform in frequency band $\frac{2\pi}{\Delta_t}$. In modeling, it is convenient to choose the same sample step Δ_t for representing signal and noise, i.e., $\Delta_t = \frac{\pi}{2\Omega}$.

Then noise frequency band is 4Ω and, consequently, noise $n_n(t)$ represents white noise well with respect to a signal whose basic energy is concentrated in frequency band Ω .

Discrete noise $n[i]$, in accordance with the above, is a sequence of independent random numbers with zero average and variance $\sigma_w^2 = N_w$, distributed according to normal law. Methods for obtaining such sequences on a computer are described in [9]. Determining the necessary sample volume for noise will be carried out in paragraph 8.3.2.

The required signal/noise ratio q_c^2 in the model is assigned by the amplitude of the input signal A_c and the variance of noise σ_w^2 . The power of the undistorted input signal is

$$s_{1x_0}(t) = A_c \cos\left(\frac{\Omega}{2\tau_0} t^2\right), \quad |t| \leq \frac{\tau_0}{2},$$

represented in the form (8.4C), equal to

$$\begin{aligned} A_c^2 \sum_{i=-N/2}^{N/2} \int_{-\infty}^{\infty} \frac{\sin^2 \frac{\pi}{\Delta t} (t - i\Delta t)}{\left[\frac{\pi}{\Delta t} (t - i\Delta t)\right]^2} \cos^2\left(\frac{\Omega}{2\tau_0} i^2 \Delta t^2\right) dt = \\ = A_c^2 \Delta t \sum_{i=-N/2}^{N/2} \cos^2\left(\frac{\Omega}{2\tau_0} \Delta t^2 i^2\right). \end{aligned} \quad (8.64)$$

Spectral density of the noise, according to (8.63), is equal to $2\sigma_w^2 \Delta t$; consequently, the ratio of signal energy to spectral density of noise will be determined by formula

$$q_0^2 = \frac{\sum_{i=-N/2}^{N/2} s_{1x_0}^2(i)}{2\sigma_w^2}. \quad (8.65)$$

Substituting into (8.65) the selected values $N = 200$ and $D_r = 40$, we obtain

$$q_0^2 = A_c^2 \frac{100}{2\sigma_w^2}.$$

8.3.2. Modeling the processing of a signal in the receiving channel. Signal processing in the receiving channel includes the linear filtration of input pulse and noise, as well as the distinguishing of the envelope obtained after the filtration of the additive mixture of signal and noise. We shall write the input pulse in the form

$$s_{LX}(t) = S_{BX}(t) \exp\{i[\omega_0 t + \varphi_{LX}(t)]\}, \quad |t| \leq \frac{\tau_0}{2}, \quad (8.66)$$

its envelope $S_{BX}(t)$ and phase modulation $\phi_{BX}(t)$ contain distortions relative to undistorted $S_{BX0}(t) = A_c$ and $\phi_{BX0}(t)$. In the model all distortions are introduced more conveniently into the signal only; therefore, the weight function of the filter is assumed matched with the undistorted pulse and is equal to

$$h(t) = \exp \left\{ -i \left[-\omega_0 \left(t - \frac{\tau_0}{2} \right) + \varphi_{BX0} \left(\frac{\tau_0}{2} - t \right) \right] \right\}, \quad |t| \leq \frac{\tau_0}{2}. \quad (8.67)$$

As a result of filtration, at filter output we have the signal

$$s_i(t) = \int_{-\infty}^{\infty} s_{iX}(\tau) h(t-\tau) d\tau = \exp \left[i\omega_0 \left(t - \frac{\tau_0}{2} \right) \right] \times [s_{ic}(t) + i s_{is}(t)], \quad (8.68)$$

where

$$s_{ic}(t) = \frac{1}{2} \int_{t-\tau_0}^t S_{iX}(\tau) \cos \left[\varphi_{iX}(\tau) - \varphi_{BX0} \left(\tau - t + \frac{\tau_0}{2} \right) \right] \times \text{rect} \frac{\tau}{\tau_0} d\tau, \\ s_{is}(t) = \frac{1}{2} \int_{t-\tau_0}^t S_{iX}(\tau) \sin \left[\varphi_{iX}(\tau) - \varphi_{BX0} \left(\tau - t + \frac{\tau_0}{2} \right) \right] \times \text{rect} \frac{\tau}{\tau_0} d\tau. \quad (8.69)$$

The signal envelope at filter output is

$$L \{s_i(t)\} = [s_{ic}^2(t) + s_{is}^2(t)]^{1/2}, \quad (8.70)$$

and instantaneous phase

$$\arg \{s_1(t)\} = \omega_0 \left(t - \frac{\tau_c}{2} \right) + \operatorname{arctg} \frac{s_{1s}(t)}{s_{1c}(t)}. \quad (8.71)$$

The formulas presented show that carrier frequency ω_0 is present only in the linear phase term $\omega_0(t - \frac{\tau_c}{2})$ known a priori, and is not of interest in the study. Thus, for modeling linear signal filtration it is necessary to represent in the model operations (8.69), while the carrier frequency of the input pulse can be given as zero.

Input white noise gives at output of the linear filter with weight function (8.67) the noise process

$$n_1(t) = \int_{-\infty}^{\infty} n(\tau) f(t-\tau) d\tau = [n_{1c}(t) + i n_{1s}(t) \exp[i\omega_0(t - \frac{\tau_c}{2})]], \quad (8.72)$$

where

$$\begin{aligned} n_{1c}(t) &= \int_{t-\tau_c}^t n(\tau) \cos \left[\omega_0 \tau + \varphi_{\text{BX } 0} \left(\tau - t + \frac{\tau_c}{2} \right) \right] d\tau; \\ n_{1s}(t) &= - \int_{t-\tau_c}^t n(\tau) \sin \left[\omega_0 \tau + \varphi_{\text{BX } 0} \left(\tau - t + \frac{\tau_c}{2} \right) \right] d\tau. \end{aligned} \quad (8.73)$$

The sum process at output of linear filter is an additive mixture of signal $s_1(t)$ and noise $n_1(t)$:

$$y_1(t) = [y_{1c}(t) + i y_{1s}(t)] \exp \left[i \omega_0 \left(t - \frac{\tau_c}{2} \right) \right], \quad (8.74)$$

where

$$y_{1c}(t) = s_{1c}(t) + n_{1c}(t), \quad y_{1s}(t) = s_{1s}(t) + n_{1s}(t). \quad (8.75)$$

The envelope of the input process is

$$L\{y_1(t)\} = [y_{1,c}^2(t) + y_{1,s}^2(t)]^{1/2}, \quad (8.76)$$

and its instantaneous phase is

$$\arg\{y_1(t)\} = \omega_0 \left(t - \frac{\tau_0}{2} \right) + \arctg \frac{y_{1,s}(t)}{y_{1,c}(t)}. \quad (8.77)$$

Since in the model we assign carrier frequency as zero, in order to model linear noise filtration, it is necessary to perform operations

$$\begin{aligned} n_{1c}(t) &= \int_{t-\tau_0}^t n(\tau) \cos \left[\varphi_{\text{max}} \left(\tau - t + \frac{\tau_0}{2} \right) \right] d\tau, \\ n_{1s}(t) &= - \int_{t-\tau_0}^t n(\tau) \sin \left[\varphi_{\text{max}} \left(\tau - t + \frac{\tau_0}{2} \right) \right] d\tau. \end{aligned} \quad (8.78)$$

In analogy with (8.40), the weight function of the linear filter is written in the form

$$h(t) = \sum_{i=-N/2}^{N/2} h(i\Delta_t) \frac{\sin \frac{\pi}{\Delta_t} (t - i\Delta_t)}{\frac{\pi}{\Delta_t} (t - i\Delta_t)}, \quad \Delta_t = \frac{\tau_0}{N}, \quad (8.79)$$

so that the continuous weight function $h(t)$ is represented by discrete function $h[i] \equiv h(i\Delta_t)$. Then for the operation of linear signal filtration

$$s_1(t) = \int_{-\infty}^{\infty} s_{\text{max}}(\tau) h(t - \tau) d\tau$$

we have discrete output signal

$$s_1(i\Delta_t) = \sum_{l=-N/2}^{N/2} \sum_{k=-N/2}^{N/2} s_{\text{max}}(l\Delta_t) h(k\Delta_t) \int \frac{\sin \frac{\pi}{\Delta_t} (\tau - l\Delta_t)}{\frac{\pi}{\Delta_t} (\tau - l\Delta_t)} \times$$

$$\begin{aligned} & \times \frac{\sin \frac{\pi}{\Delta t} [\tau - (i + \kappa) \Delta t]}{\frac{\pi}{\Delta t} [\tau - (i + \kappa) \Delta t]} d\tau = \Delta t \sum_{\kappa=-N/2+1}^{N/2} S_{\text{BX}}(\kappa \Delta t) h(i \Delta t - \kappa \Delta t) \equiv \\ & \equiv \Delta t \sum_{\kappa=-N/2+1}^{N/2} S_{\text{BX}}[\kappa] h[i - \kappa], \end{aligned} \quad (8.80)$$

representing in the model the continuous output signal

$$s_1(t) = \sum_{i=-N_1}^{N_2} s_1(i \Delta t) \frac{\sin \frac{\pi}{\Delta t} (t - i \Delta t)}{\frac{\pi}{\Delta t} (t - i \Delta t)}. \quad (8.81)$$

Let us determine the necessary calculation limits for the values of the output discrete signal N_1 and N_2 . As shown above, the weight function of a linear filter (8.67) is in agreement with the undistorted input signal with a zero carrier frequency

$$s_{\text{BX}_0}(t) = A_c \exp \{i \varphi_{\text{BX}_0}(t)\}, \quad |t| \leq \frac{\tau_c}{2} \quad (8.82)$$

and, consequently, is equal to

$$h(t) = \exp \left\{ -\varphi_{\text{BX}_0} \left(\frac{\tau_c}{2} - t \right) \right\}, \quad 0 \leq t \leq \tau_c. \quad (8.83)$$

For the studied signal with linear frequency modulation $\varphi_{\text{BX}_0}(t) = \frac{\Omega}{2\tau_c} t^2$ the undistorted output signal is described by expression

$$\begin{aligned} s_{10}(t) &= \int_{-\infty}^{\infty} s_{\text{BX}_0}(\tau) h(t - \tau) d\tau = A_c \int_{t-\tau_c}^t \exp \left\{ i \frac{\Omega}{2\tau_c} \times \right. \\ & \times \left. \left[\tau^2 - \left(\frac{\tau_c}{2} - t + \tau \right)^2 \right] \right\} \text{rect} \frac{\tau}{\tau_c} d\tau = \frac{A_c \tau_c}{2} \times \end{aligned} \quad (8.84)$$

$$\times \frac{\sin \frac{\Omega}{2} \left(t - \frac{\tau_c}{2} \right) \left[1 - \frac{\left(t - \frac{\tau_c}{2} \right)}{\tau_c} \right]}{\frac{\Omega}{2} \left(t - \frac{\tau_c}{2} \right)},$$

$$-\frac{\tau_c}{2} \leq t \leq \frac{3\tau_c}{2}.$$

For studies it is completely sufficient to reproduce the output signal (8.84) within the four side lobes nearest to the main lobe, i.e., for $|t - \frac{\tau_c}{2}| \leq \frac{10\pi}{\Omega}$. Hence we obtain the computation limits for discrete signal $s_1[i]$:

$$N_1 = \frac{1}{\Delta t} \left(\frac{\tau_c}{2} - \frac{10\pi}{\Omega} \right),$$

$$N_2 = \frac{1}{\Delta t} \left(\frac{\tau_c}{2} + \frac{10\pi}{\Omega} \right), \quad (8.85)$$

Substituting into (8.85) the selected value $\Delta t = \frac{\pi}{2\Omega}$, we obtain $N_1 = 80$, $N_2 = 120$.

This makes it possible to write the algorithm of linear signal filtration in the model, representing operations (8.69) for the input signal (8.57), in the following form:

$$s_{1s}[i] = \sum_{\kappa=i-N}^i \frac{1}{2} A_c \Delta t (1 + \Delta S[\kappa]) \cos \left[\Phi[\kappa] - \right.$$

$$\left. - \varphi_{20} \left(\kappa - i + \frac{N}{2} \right)^2 \right] \text{rect} \frac{\kappa}{N},$$

$$s_{1s}[i] = \sum_{\kappa=i-N}^i \frac{1}{2} A_c \Delta t (1 + \Delta S[\kappa]) \sin \left[\Phi[\kappa] - \right.$$

$$\left. - \varphi_{20} \left(\kappa - i + \frac{N}{2} \right)^2 \right] \text{rect} \frac{\kappa}{N}, \quad N_1 \leq i \leq N_2.$$

(8.86)

Just as accurately, for representing linear noise filtration (8.78), we obtain

$$\begin{aligned}
 n_{1c}[i] &= \Delta_t \sum_{\kappa=i-N}^i n[\kappa] \cos \left[\varphi_{20} \left(\kappa - i + \frac{N}{2} \right)^2 \right], \\
 n_{1s}[i] &= \Delta_t \sum_{\kappa=i-N}^i n[\kappa] \sin \left[\varphi_{20} \left(\kappa - i + \frac{N}{2} \right)^2 \right].
 \end{aligned} \tag{8.87}$$

Let us determine the necessary sample volume of discrete noise $n[k]$ after calculating the statistical characteristics of one of the processes (8.87) when $n[k] = 0$ at $k > N_3$ and $k < -N_4$; $N_4, N_3 > N/2$. The values of N_3 and N_4 will be lower. For a thus limited input noise sequence, from (8.87) we shall have

$$\begin{aligned}
 & \frac{1}{\Delta_t} n_{1c}[i] = \\
 & = \begin{cases} \sum_{\kappa=-N_4}^i n[\kappa] \cos \left[\varphi_{20} \left(\kappa - i + \frac{N}{2} \right)^2 \right], & i < N - N_4, \\ \sum_{\kappa=i-N}^i n[\kappa] \cos \left[\varphi_{20} \left(\kappa - i + \frac{N}{2} \right)^2 \right], & N - N_4 \leq i \leq N_3, \\ \sum_{\kappa=i-N}^{N_3} n[\kappa] \cos \left[\varphi_{20} \left(\kappa - i + \frac{N}{2} \right)^2 \right], & i > N_3. \end{cases}
 \end{aligned} \tag{8.88}$$

Since in $\overline{n[k]} = 0$, and $\overline{n[k]n[i]} = \sigma_w^2 \delta_{k-i}$, from (8.88) we obtained the average value of noise $\overline{n_{1c}[i]} = 0$ and the noise variance $n_{1c}[i]$, related to $\sigma_w^2 \Delta_t^2$, equal to

$$\frac{\overline{n_{1c}^2}[i]}{\Delta_t^2 \sigma_w^2} = \begin{cases} \sum_{\kappa=-N/2}^{i-N/2+N_4} \cos^2(\varphi_{20} \kappa^2), & i < N - N_4, \\ \sum_{\kappa=-N/2}^{N/2} \cos^2(\varphi_{20} \kappa^2), & N - N_4 \leq i \leq N_3, \\ \sum_{\kappa=-N/2}^{-i+N_3+N/2} \cos^2(\varphi_{20} \kappa^2), & i > N_3. \end{cases} \tag{8.89}$$

The noise variance established according to (8.89) occurs when $N - N_4 \leq i \leq N_3$. Being given the natural requirement of stationary output additive noise for all calculated points of the signal $N_1 \leq i \leq N_2$, we obtain $N_4 = N - N_1$, $N_3 = N_2$. With the selected values $N = 200$, $N_1 = 80$ and $N_2 = 120$, the sequence of discrete input noise $n[k]$ must fall within $-120 \leq k \leq 120$.

The sum discrete output processes, in accordance with (8.75), are equal to

$$\begin{aligned} y_{1c}[i] &= s_{1c}[i] + n_{1c}[i], \\ y_{1s}[i] &= s_{1s}[i] + n_{1s}[i]. \end{aligned} \quad (8.90)$$

To reduce the volume of computation, it is advisable to add signal and noise before the summation operations (8.86) and (8.87). Discarding the same standardizing factor Δ_t , we finally obtain

$$\begin{aligned} y_{1c}[i] &= \sum_{\kappa=i-N}^i \left\{ \frac{1}{2} A_c (1 + \Delta S[\kappa]) \cos \left[\Phi[\kappa] - \varphi_{20} \left(\kappa - i + \frac{N}{2} \right)^2 \right] \times \right. \\ &\quad \left. \times \text{rect} \frac{\kappa}{N} + n[\kappa] \cos \left[\varphi_{20} \left(\kappa - i + \frac{N}{2} \right)^2 \right] \right\}, \\ y_{1s}[i] &= \sum_{\kappa=i-N}^i \left\{ \frac{1}{2} A_c (1 + \Delta S[\kappa]) \sin \left[\Phi[\kappa] - \varphi_{20} \left(\kappa - i + \frac{N}{2} \right)^2 \right] \times \right. \\ &\quad \left. \times \text{rect} \frac{\kappa}{N} + n[\kappa] \sin \left[\varphi_{20} \left(\kappa - i + \frac{N}{2} \right)^2 \right] \right\}, \\ &\quad N_1 \leq i \leq N_2, \end{aligned} \quad (8.91)$$

$$\Phi[\kappa] = \varphi_0 + \varphi_{\phi_1} \cdot \kappa + \varphi_{\phi_2} \cdot \kappa^2 + \varphi_{\phi_3} \cdot \kappa^3 + \Delta \varphi_0[\kappa].$$

If the compression factor of the undistorted signal is taken as 50, the calculated values of the constants are $N = 200$, $N_1 = 80$, $N_2 = 120$, $\varphi_{20} = 3.93 \cdot 10^{-3}$.

Usually in a radar the process from output of the matched filter is subjected to additional linear filtration with the aim of suppressing the side lobes of the output pulse. When using weighted treatment for suppressing lateral lobes, the weight function of the second linear filter has the form

$$h_2(t) = \delta(t) + p_\Phi \left[\delta\left(t - \frac{2\pi}{\Omega}\right) + \delta\left(t + \frac{2\pi}{\Omega}\right) \right],$$

$$p_\Phi = 0,425. \quad (8.92)$$

The discrete rate function $h_2[i] \equiv h_2(i\Delta_t)$, when the quantity $\Delta_t = \frac{\pi}{2\Omega}$, is then equal to

$$h_2[i] = \delta[i] + p_\Phi \{ \delta[i-4] + \delta[i+4] \}, \quad (8.93)$$

and the discrete processes at output of the second linear filter are described by expressions

$$y_{2c}[i] = \sum_{\kappa=N_1}^i y_{1c}[\kappa] h_2[i-\kappa] =$$

$$= y_{1c}[i] + p_\Phi \{ y_{1c}[i-4] + y_{1c}[i+4] \},$$

$$y_{2s}[i] = y_{1s}[i] + p_\Phi \{ y_{1s}[i-4] + y_{1s}[i+4] \},$$

$$N_1 + 4 \leq i \leq N_2 - 4. \quad (8.94)$$

In accordance with (8.76) and (8.77), in order to determine the discrete envelope and discrete phase modulation of the process at output, we must calculate

$$L\{y_2[i]\} = \sqrt{y_{2c}^2[i] + y_{2s}^2[i]} \quad (8.95)$$

and

$$\arg\{y_2[i]\} = \arctg \frac{y_{2s}[i]}{y_{2c}[i]}.$$

Let us note that in order to exclude the operation of suppressing side lobes of a signal, it is sufficient to assume $p_\phi = 0$.

All discrete signals in the model represent actual continuous signals and are connected with them by a Kotel'nikov series (8.40); therefore, when it is necessary to obtain intermediate values of signals at points $i + \eta_M$, $|\eta_M| < 1$, we should perform interpolation

$$F(i + \eta_M) = \sum_k F[k] \frac{\sin \pi(i + \eta_M - k)}{\pi(i + \eta_M - k)}, \quad (8.96)$$

where $F[k]$ is the interpolated signal.

Figure 8.2 presents a simplified block diagram of the part of the model described, for one receiving channel. In the signal unit (БС) the following quantities are calculated:

$$A_c(1 + \Delta S[k]) \cdot \Phi[k] = \varphi_\phi + \varphi_{\phi_1} \cdot k + \varphi_{\phi_2} \cdot k^2 + \varphi_{\phi_3} \cdot k^3 + \Delta \varphi_\phi[k]$$

[$n = \text{and}$]

for $-\frac{N}{2} \leq k \leq \frac{N}{2}$. Quantities A_c , $\Delta S[k]$, $\Delta \varphi_\phi[k]$ are given by table or are calculated in other units of the model, depending upon the purposes of the study. Units of the matched filters (БСФ-1 and БСФ-2) perform the operation (8.91) and the weighted processing unit (БВУ) the operations in (8.94). Two square-law function generators and the add circuit represent the amplitude quadratic detector. If, however, it is necessary to model a linear amplitude detector, at output of the add circuit the unit which extracts the square root is connected.

Later, when we study the block diagram of a model of a specific scanning monopulse radar, the БСФ and БВУ units will be designated БВУ (optimal processing unit); the two square-law function generators, the add circuit, and the square-root extraction unit will be called the amplitude detector unit (БАД).

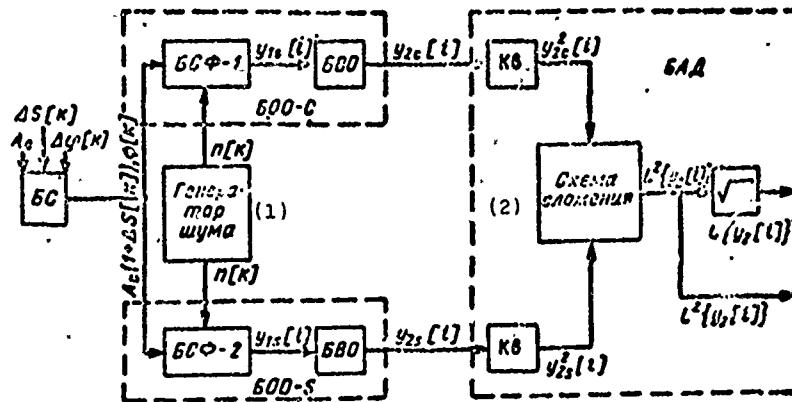


Fig. 8.2. Block diagram of a model of one receiving channel in a scanning monopulse radar.
KEY: (1) Noise generator; (2) Add circuit.

§ 8.4. MODELS OF AMPLITUDE-AMPLITUDE AND AMPLITUDE SUM-DIFFERENCE SCANNING RADARS

The block diagram of an amplitude-amplitude scanning radar is presented in Fig. 1.12 and the block diagram of the model of this station is presented in Fig. 8.3 in order to evaluate the accuracy of angular coordinate determination when direction finding in one plane.

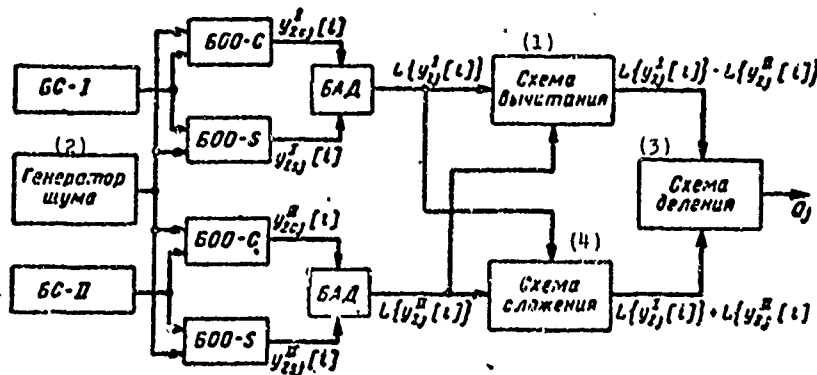


Fig. 8.3. Block diagram of a model of an amplitude-amplitude scanning monopulse radar for determining coordinates in one plane.
KEY: (1) Subtraction circuit; (2) Noise generator; (3) Division circuit; (4) Add circuit.

In accordance with formula (1.39), in order to form an evaluation of the angle of target deviation from equisignal direction, in the model the following ratio is used

$$Q_j = \frac{L \left\{ y_2^I \left[\frac{N}{2} \right] \right\} - L \left\{ y_2^{II} \left[\frac{N}{2} \right] \right\}}{L \left\{ y_2^I \left[\frac{N}{2} \right] \right\} + L \left\{ y_2^{II} \left[\frac{N}{2} \right] \right\}}, \quad (8.97)$$

where $L \left\{ y_2^I \left[\frac{N}{2} \right] \right\}$ and $L \left\{ y_2^{II} \left[\frac{N}{2} \right] \right\}$ are the values of signal envelopes at outputs of the amplitude detector units for the first and second channels when $i = \frac{N}{2}$, which, with undistorted input signal, corresponds to the maximum value of the output signal envelope. In formula (1.36) they are designated as $u_1(\theta)$ and $u_2(\theta)$, respectively. At model input in each of these cycles with respect to j , input signals are given:

$$\begin{aligned} s_{s,j}^I[k] &= A_{s,j}^I (1 + \Delta S_j^I[k]) \cos \Phi_j^I[k], \\ s_{s,j}^{II}[k] &= A_{s,j}^{II} (1 + \Delta S_j^{II}[k]) \cos \Phi_j^{II}[k], \end{aligned} \quad (8.98)$$

where

$$\begin{aligned} \Phi_j^{I(III)}[k] &= \varphi_{\phi,j}^{I(III)} + \varphi_{\phi,j}^{I(III)} \cdot k + \\ &+ \varphi_{\phi,j}^{I(III)} \cdot k^2 + \varphi_{\phi,j}^{I(III)} \cdot k^3 + \Delta \varphi_{\phi,j}^{I(III)}[k], \\ A_{s,j}^I &= a_{q,j} F_1(\theta); \quad A_{s,j}^{II} = a_{q,j} F_2(\theta). \end{aligned}$$

$a_{q,j}$ is the coefficient assigning the value of the signal/noise ratio in accordance with (8.65).

Radiation patterns $F_1(\theta)$ and $F_2(\theta)$ can be given by table or by corresponding formulas.

The quantities $\Delta S_j[k]$, $\varphi_{\phi,j}$, $\varphi_{\phi,1j}$, $\varphi_{\phi,2j}$, $\varphi_{\phi,3j}$, $\Delta \varphi_{\phi,j}[k]$, which determine amplitude and phase distortions of input signals can be given independently in both channels or in only one channel. In the latter case, they will represent the relative distortions of the characteristics of one channel with respect to the other.

envelopes $L\{y_{2j}^I[1]\}$ and $L\{y_{2j}^{II}[1]\}$ of processes at outputs of the first and second channels are obtained in the model according to the algorithms described in paragraph 8.3.2.

The angle of target deviation from equisignal direction θ_j is determined according to the value obtained for \check{Q}_j (8.97) from the direction finding characteristic, equal to

$$Q_j = S(\check{\theta}) = \frac{F_1(\check{\theta}) - F_2(\check{\theta})}{F_1(\check{\theta}) + F_2(\check{\theta})}. \quad (8.99)$$

A block diagram of an amplitude sum-difference scanning monopulse radar is presented in Fig. 1.13 and the block diagram of the model in Fig. 8.4.

In reference [55] it is shown that antenna radiation patterns for the sum and difference channels are determined according to the diagrams of the first and second channels with the aid of a matrix equation

$$\begin{pmatrix} f_c(\theta) \\ f_p(\theta) \end{pmatrix} = \begin{pmatrix} \dot{\eta}_{11} & \dot{\eta}_{12} \\ \dot{\eta}_{21} & \dot{\eta}_{22} \end{pmatrix} \begin{pmatrix} F_1(\theta) \\ F_2(\theta) \end{pmatrix}, \quad (8.100)$$

where complex quantity η_{ij} , ($ij = 1, 2$) gives the amplitude and phase nonidentity of the difference waveguide bridge. If we designate

$$\eta_{ij} = \eta_{ij} \exp i\varphi_{ij},$$

then from (8.100) we obtain

$$\begin{aligned} f_c(\theta) &= F_c(\theta) \exp [i\varphi_c(\theta)], \\ f_p(\theta) &= F_p(\theta) \exp [i\varphi_p(\theta)], \end{aligned} \quad (8.101)$$

where

$$\begin{aligned} F_c^2(\theta) &= [\eta_{11} \cos \varphi_{11} F_1(\theta) + \eta_{12} \cos \varphi_{12} F_2(\theta)]^2 + \\ &+ [\eta_{11} \sin \varphi_{11} F_1(\theta) + \eta_{12} \sin \varphi_{12} F_2(\theta)]^2, \\ \varphi_c(\theta) &= \text{arctg} \frac{\eta_{11} \sin \varphi_{11} F_1(\theta) + \eta_{12} \sin \varphi_{12} F_2(\theta)}{\eta_{11} \cos \varphi_{11} F_1(\theta) + \eta_{12} \cos \varphi_{12} F_2(\theta)}, \end{aligned} \quad (8.102)$$

$$F_p^2(\theta) = [\eta_{21} \cos \varphi_{21} F_1(\theta) - \eta_{22} \cos \varphi_{22} F_2(\theta)]^2 + [\eta_{21} \sin \varphi_{21} F_1(\theta) - \eta_{22} \sin \varphi_{22} F_2(\theta)]^2, \quad (8.103)$$

$$\varphi_p(\theta) = \text{arctg} \frac{\eta_{21} \sin \varphi_{21} F_1(\theta) - \eta_{22} \sin \varphi_{22} F_2(\theta)}{\eta_{21} \cos \varphi_{21} F_1(\theta) - \eta_{22} \cos \varphi_{22} F_2(\theta)}$$

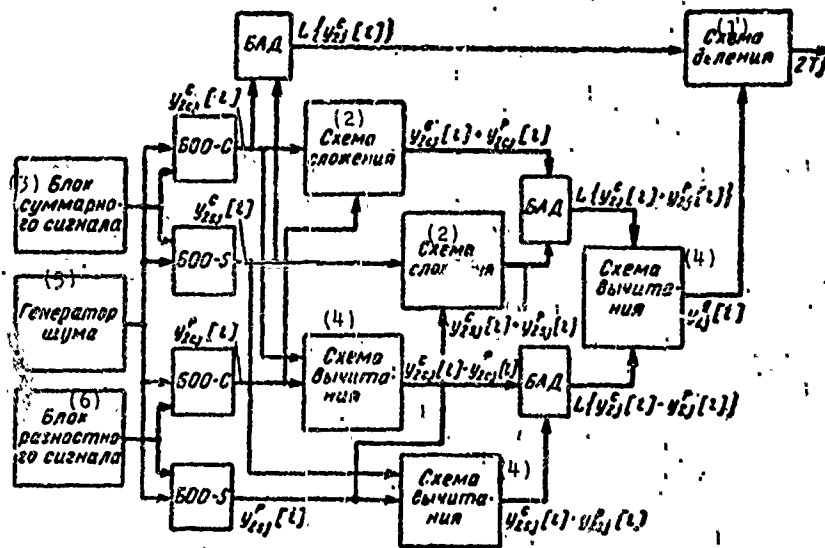


Fig. 8.4. Block diagram of a model of an amplitude sum-difference scanning monopulse radar for determining coordinates in one plane. KEY: (1) Division circuit; (2) Add circuit; (3) Sum signal unit; (4) Subtraction circuit; (5) Noise generator; (6) Difference signal unit.

The waveguide bridge is strictly balanced if $\eta_{1j} = 1$, $\phi_{1j} = 0$.

In accordance with equalities (8.101), (8.102) and (8.103), when modeling, in each cycle the two input signals should be given:

$$S_{\text{вх } c j}[\kappa] = A_{0j}^c (1 + \Delta S_j^c[\kappa]) \cos \psi_j^c[\kappa],$$

$$S_{\text{вх } p j}[\kappa] = A_{0j}^p (1 + \Delta S_j^p[\kappa]) \cos \psi_j^p[\kappa], \quad (8.104)$$

where

$$\begin{aligned}
 A_{c,j}^c &= a_{q,j} F_c(\theta), \quad A_{c,j}^p = a_{q,j} F_p(\theta); \\
 \Phi_j^c[\kappa] &= \varphi_{\phi,j}^c + \varphi_{\phi,j}^c \cdot \kappa + \varphi_{\phi,j}^c \cdot \kappa^2 + \varphi_{\phi,j}^c \cdot \kappa^3 + \\
 &\quad + \Delta\varphi_{\phi,j}^c[\kappa] + \varphi_c(\theta); \\
 \Phi_j^p[\kappa] &= \varphi_{\phi,j}^p + \varphi_{\phi,j}^p \cdot \kappa + \varphi_{\phi,j}^p \cdot \kappa^2 + \varphi_{\phi,j}^p \cdot \kappa^3 + \\
 &\quad + \Delta\varphi_{\phi,j}^p[\kappa] + \varphi_p(\theta).
 \end{aligned}$$

Signals (8.104) mixed with noises give, at output of the linear part of the model, processes $y_{2j}^c[i]$ and $y_{2t}^p[i]$, represented by two orthogonal components (8.94), each in accordance with algorithms examined in paragraph 8.3.2.

In order to evaluate target deviation from equisignal direction, processes are used, as indicated in Chapter 1, at phase detector output and at sum channel output. To model the process at quadratic phase detector output, it is necessary to calculate

$$\begin{aligned}
 y_{2j}^x[i] &= \frac{1}{4} L^2 \{y_{2j}^c[i] + y_{2j}^p[i]\} - \\
 &\quad - \frac{1}{4} L^2 \{y_{2j}^c[i] - y_{2j}^p[i]\}.
 \end{aligned} \tag{8.105}$$

At linear detector output we must determine

$$\begin{aligned}
 y_{2j}^x[i] &= \frac{1}{2} L \{y_{2j}^c[i] + y_{2j}^p[i]\} - \\
 &\quad - \frac{1}{2} L \{y_{2j}^c[i] - y_{2j}^p[i]\}.
 \end{aligned} \tag{8.106}$$

After this, in accordance with formula (1.43), to determine the target deviation angle from equisignal direction, the following ratio is computed:

$$T_j = \frac{y_{2j}^x \left[\frac{N}{2} \right]}{L^2 \left\{ y_{2j}^c \left[\frac{N}{2} \right] \right\}}$$

or

$$T_j = \frac{y_{2j}^A \left[\frac{N}{2} \right]}{L \left\{ y_{2j}^C \left[\frac{N}{2} \right] \right\}} \quad (8.107)$$

where $L\{y_{2j}^C[\frac{N}{2}]\}$ is the value of the sum signal envelope at output of the amplitude detector unit.

Target deviation angle from equisignal direction $\check{\theta}_j$ is determined based on the value obtained for T_j from the direction finding characteristic

$$T_j = S(\check{\theta}) = \frac{F_1(\check{\theta}) - F_2(\check{\theta})}{F_1(\check{\theta}) + F_2(\check{\theta})} \quad (8.108)$$

Methods of assigning various types of amplitude and phase distortions for input signals and methods of processing results are determined by the specific purpose of the study, as well as the purpose and characteristics of the radar, and we shall not discuss them here.

CHAPTER 9

AREAS OF APPLICATION AND CERTAIN CHARACTERISTICS OF FOREIGN MONOPULSE RADARS

Monopulse systems, as indicated above, have high accuracy, noise immunity, and rapid action. Because of these advantages they have found wide application in guidance and control systems of rocket weapons, ballistic and space target interception systems and satellite tracking systems.

In this chapter we shall examine monopulse radars for these systems, about which we have information from foreign and domestic literature.

§ 9.1. RADARS FOR TRACKING BOTH BALLISTIC AND SPACE TARGETS

The first monopulse radar used in the USA for tracking ballistic rockets and artificial satellites is the AN/FPS-16 [73, 89]. The antenna system of this set consists of a parabolic reflector and a four-horn feed (Fig. 9.1). Tracking is carried out in two planes.

In double waveguide bridges the sum and two difference signals are processed, then amplified and multiplied in the phase detector. The error signals obtained are used for bringing into motion the antenna drive, i.e., the AN/FPS-16 is an amplitude sum-difference monopulse target tracking radar.

The characteristics of many AN/FPS-16 radars presently in operation have been considerably improved as a result of a whole

series of modifications. In the antenna between the feed and the reflector a polarization device has been installed for transforming the linear polarization of the signal into circular polarization; in the receiving device an improved crystal mixer has been used and a parametric amplifier which reduces the noise factor to 5 dB. The main tactical and technical characteristics of the AN/FPS-16, for both versions, are presented in Table 9.1.

Based on the perfected AN/FPS-16, the AN/FPQ-6 has been developed (Fig. 9.2); the main tactical and technical characteristics of this set are also presented in Table 9.1.

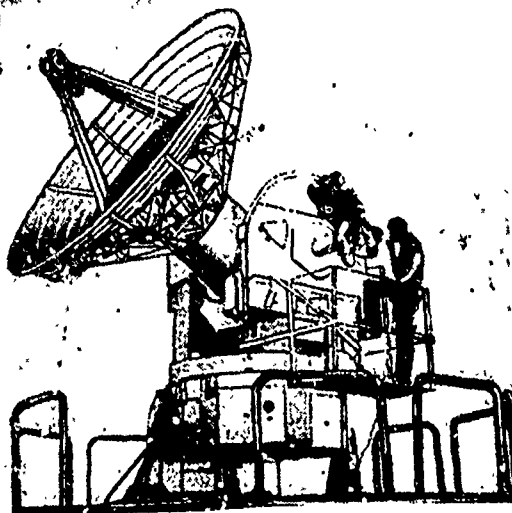


Fig. 9.1. The AN/FPS-16 radar antenna.

The parameters of the AN/FPQ-6 are being improved with the aim of increasing target tracking range by using a cooled parametric amplifier, doubling the transmitter power, and using the method of pulse compression. It is to be expected that these improvements will lead to an effective target range from $\sigma_{\text{эфф}} = 1 \text{ m}^2$ to 3400 km.

Table 9.1.

(2) Основные характеристики	(1) Индексы для различных типов РЛС			
	(3) N/FRS-16		N/FRS-17	N/FRS-18
	(3) исходный вариант	(4) модифицированный вариант		
(5) Дальность действия по цели с $\sigma_{эфф} = 1 \text{ м}^2$, км	335	500	900	4800
(6) Рабочая частота, МГц	5500—5900	5400—5900	5400—5900	(7) длинноволновый (438 МГц) и коротковолновый участки дециметрового диапазона
(8) Импульсная мощность, Мвт	1	3	3	(9) несколько мегаватт
(10) Частота следования импульсов, гц	142—1707	142—1707	160—1707	—
(11) Длительность импульса, мкс	0,25; 0,5; 1,0	0,25; 0,5; 1,0	0,25; 0,5; 1,0; 2; 3	—
(12) Коэффициент шума приемника, дБ	10	5	8	—
(13) Ошибка по дальности, м	4,6	4,6	4,6	—
(14) Ошибка по углу, угл. мин	0,7	0,35	0,4	—
(15) Диаметр антенны, м	3,60	5	8,8	25
(16) Ширина диаграммы направленности, град	1,1	0,7	0,4	2
(17) Коэффициент усиления антенны, дБ	44,5	43	51	—
(18) Облучатель антенны	(19) четырехрурный	(19) четырехрурный	(20) пятирурный	(19) четырехрурный

KEY: (1) Indices for various types of radar; (2) Main characteristics (3) First version; (4) Modified version; (5) Effective target range with $\sigma_{эфф} = 1 \text{ м}^2$, km; (6) Operating frequency, MHz; (7) Long wave (438 MHz) and short wave sections of decimeter range; (8) Pulse power, Mw; (9) Several megawatts; (10) Pulse repetition frequency, Hz; (11) Pulse width μs ; (12) Receiver noise factor, dB; (13) Range error, m; (14) Angular coordinate error, angle·min.; (15) Antenna diameter, m; (16) Radiation pattern width, deg; (17) Antenna amplification factor, dB; (18) Antenna feed; (19) four-horn; (20) five-horn.

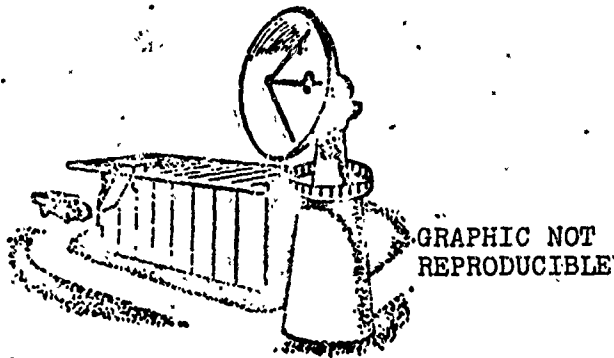


Fig. 9.2. Overall view of AN/FPQ-6 radar.

The monopulse AN/FPS-49 radar in the early warning BMEWS system is designed for detecting and tracking long-range and medium-range rockets as well as artificial earth satellites. It is a pulse-doppler radar operating on two frequencies in the long wave region of the detinator range and in the short wave region of this same range.

In target search spiral scanning is used. The set detects targets from $\sigma_{\text{RCS}} = 1 \text{ m}^2$ at a range of 4800 km and after detecting them changes to tracking mode, during which time it calculates speed, direction of flight, and impact point if the target is a rocket [36].

The antenna has a parabolic reflector 25 m in diameter (Fig. 9.3) mounted on a dome 45 m in diameter. The frameless spherical dome (Fig. 9.4) of honeycomb design has very small losses. It is made up of 1646 hexagonal elements 15 cm thick. The overall weight of the dome is approximately 100 t. It can withstand windspeed up to 200 km/h. Antenna rotation is accomplished with a hydroelectric drive. Space scan in azimuth is 360° and in elevation is 90° . The basic tactical and technical data are presented in Table 9.1.

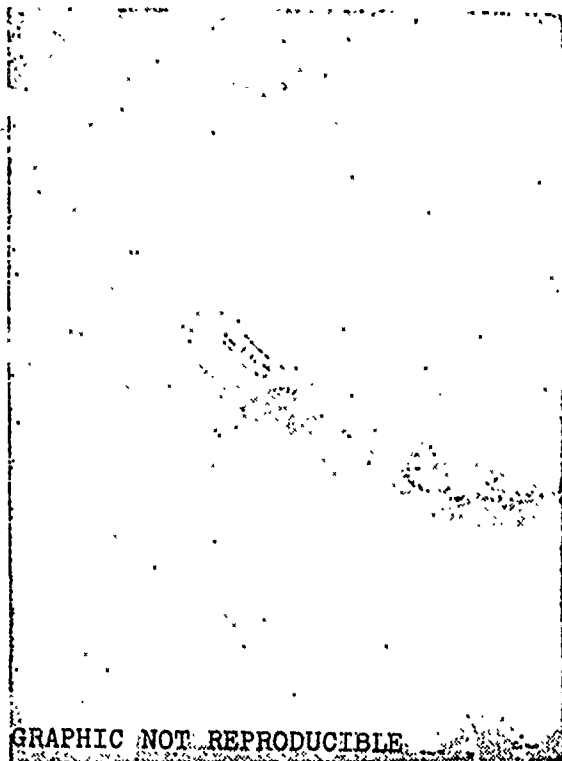


Fig. 9.3. The AN/FPS-49 radar antenna.

In the detection mode signals reflected from a target and received by the AN/FPS-49, from receiver output are fed to a system of information logging and preliminary processing. Information on range, angular coordinates, and doppler rate is fed into a preliminary data processing computer which, by correlation of signals, shifts signals reflected from nonballistic targets and preliminarily distinguishes potentially dangerous targets with a ballistic trajectory. Data on these targets are fed into an IBM 7090 computer which performs the final solution concerning the presence of a target. In this computer intercontinental ballistic missiles are separated from artificial satellites based on the rate of azimuth and range variation and also a comparison of dynamic characteristics of targets described in the memory. The IBM 7090 can simultaneously compute the trajectories of several hundred targets and distinguish potentially dangerous

targets on a background of false ones. On the basis of data obtained, antenna control signals are processed for the AN/FPS-49 radars designed to track targets.

Based on the AN/FPS-49 radar, a more advanced radar, the AN/FPS-92, designed for tracking ballistic missiles and satellites, was developed for the BMEWS system in 1966. This radar is more reliable and noise-immune than the AN/FPS-49. Semiconductor circuits are widely used in its design. The radar is equipped with a device which ensures normal operation in periods of the aurora polaris [90].

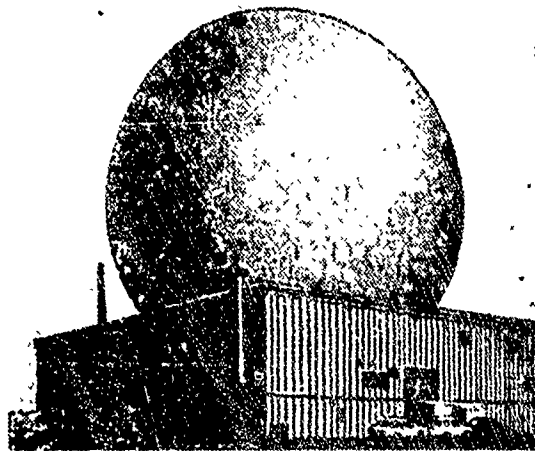


Fig. 9.4. Antenna dome for AN/FPS-49 radar.

§ 9.2. RADAR SYSTEMS FOR REMOTE TRACKING AND COMMUNICATION WITH SATELLITES AND SPACE SHIPS

The system of space communication and tracking TRAC(E) (Tracking and Communication, Extraterrestrial) [7], which provides for tracking and maintaining communication with earth satellites, the moon, and other space objectives, has a monopulse amplitude sum-difference tracking radar with a mirror-parabolic antenna 25.5 m in diameter (Fig. 9.5). The antenna feed is in the form of four turniquet radiators and four coaxial couplers connected with respect to the bridge circuit. Signals received by these feeds are added in the bridge circuit so that a sum and two difference radiation

patterns are obtained. The width of the sum pattern at the half-power level is on the order of 1° . To detect moving targets the station is provided with spiral space scanning in a $\pm 3^\circ$ sector with controllable scanning rate.

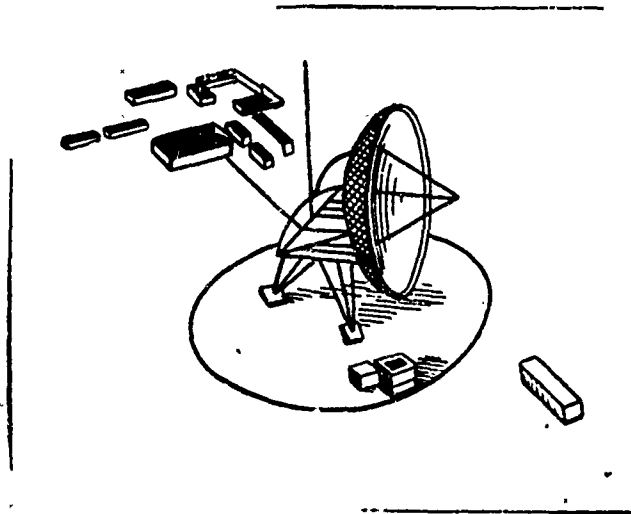


Fig. 9.5. Overall view of receiving set for TRAC(E) system.

The TRAC(E) system is one-sided, enabling it to measure angular coordinates, doppler frequency, and receive telemetric information. The ground station of the system operates on signals from a transmitter on board. The tracking range for the space rocket Pioneer IV, on board which there is installed a responder with a power of 0.2 W operating at a frequency of 960 Mhz, is 690,000 km.

The monopulse method of determining angular coordinates is used in ground stations of the detection and automatic tracking system for the communications satellite Telstar [39]. The system accomplishes multiple transmission of various coded information along 118 channels. Transmission of a full cycle of information requires 1 min.

Telstar has the following characteristics:

apogee	5600 km
perigee	1100 km
orbital inclination	45°
tangential velocity	560 km/min.

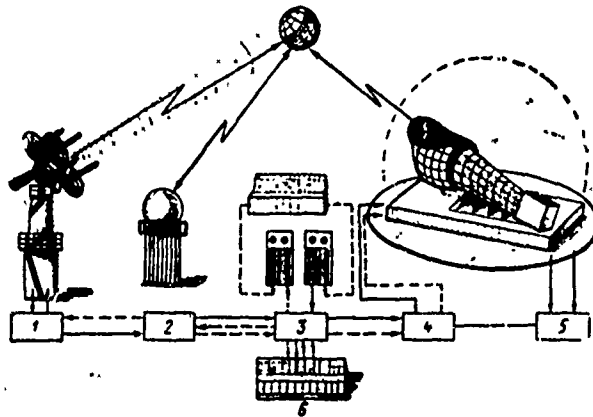


Fig. 9.6. Functional diagram of ground equipment. 1 - coarse guidance station; 2 - precise guidance station; 3 - computer; 4 - antenna of automatic tracking station; 5 - autotracking system; 6 - control panel.

Two beacons operating on frequencies of 136 MHz and 4080 MHz, as well as telemetric and communications equipment, are installed on the satellite. Signals communicated from earth to the satellite are transmitted on a frequency of 6390 MHz and from the satellite to earth on a frequency of 4170 MHz. Telemetric data from the satellite is transmitted on 136 MHz; the satellite beacon signal will be modulated at this frequency by telemetric data.

The ground post of the system consists of stations for coarse guidance, precise guidance, and automatic tracking (Fig. 9.6), which operate on signals from the two satellite beacons [39].

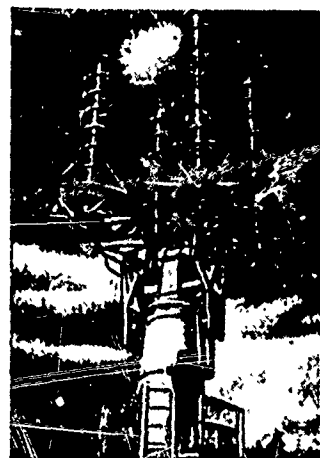


Fig. 9.7. Antenna of coarse guidance station.

Satellite detection and tracking is accomplished in the following manner. According to data obtained after launching the satellite, operators from the control panel of the ground post direct the antenna device of the command line (Fig. 9.7), used in the coarse guidance station, to a point where the satellite is expected to appear. After the reception of signals from the beacon on board the satellite at a frequency of 136 MHz, the coarse guidance system changes to automatic tracking mode. After this, the operators send a series of commands which bring into action the main systems of the satellite.

On the satellite the beacon begins to operate on a frequency of 4080 MHz; its signals are received by the precise guidance station and lock-on occurs. After lock-on by the precise guidance station, its automatic tracking begins and the antennas of the precise guidance and automatic tracking stations operate synchronously.

The coarse guidance station is a phase sum-difference station. In addition to a rough determination of satellite position, this station receives microwave telemetric signals from it and the antenna system is also used for transmitting coded signals to the satellite. The transmitter with a power of 200 W operates in continuous mode. A block diagram of the station is presented in Fig. 9.8.

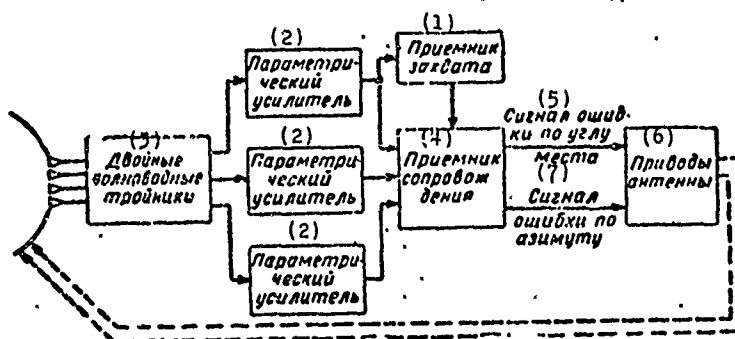


Fig. 9.9. Block diagram of precise guidance station.
 KEY: (1) Lock-on receiver; (2) Parametric amplifier; (3) Double waveguide T-joints; (4) Tracking receiver; (5) Elevation error signal; (6) Antenna drive; (7) Azimuth error-signal.

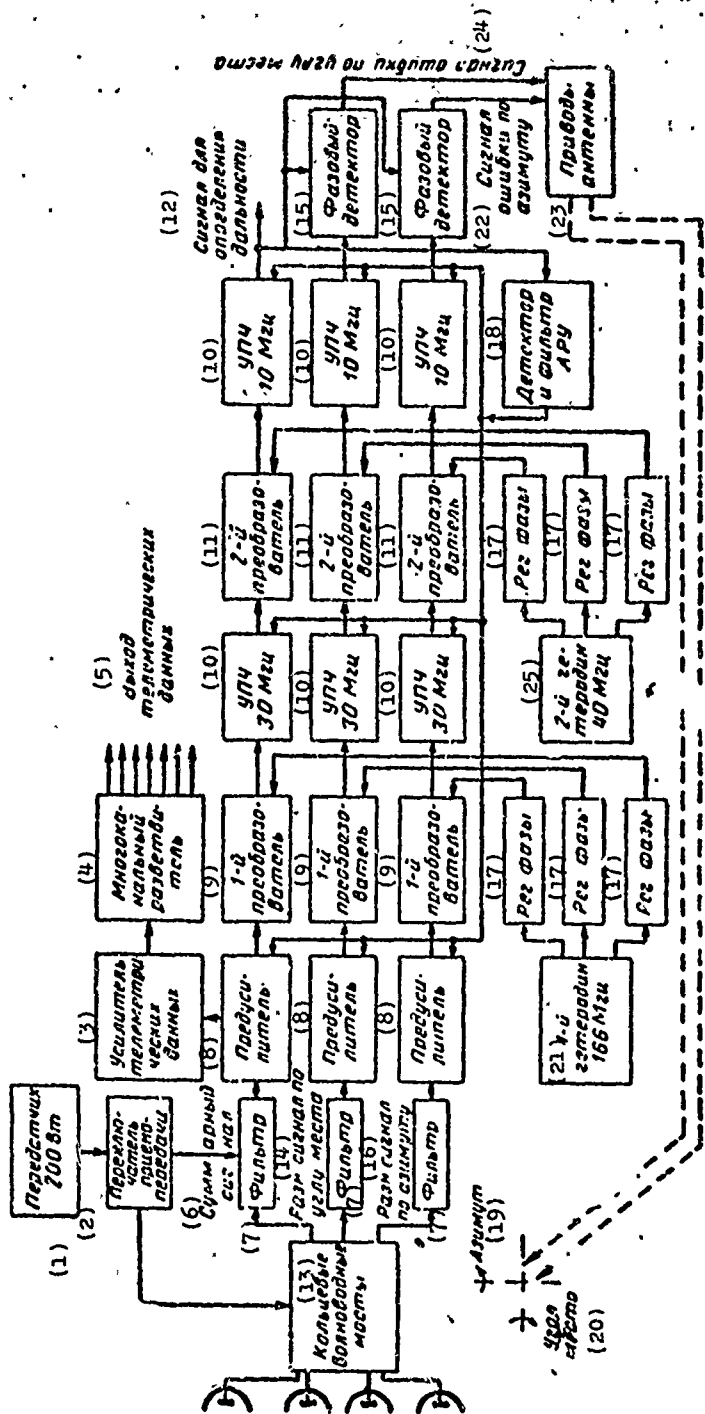
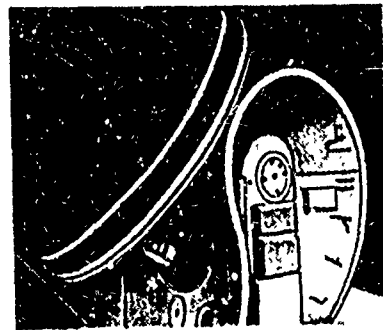


Fig. 9-8. Block diagram of a coarse guidance station.
 KEY: (1) Transmitter 200 W; (2) Send-receive switch; (3) Amplifier of telemetric data; (4) Multichannel coupler; (5) Output of telemetric data; (6) Sum signal; (7) Filter; (8) Preamplifier; (9) First converter; (10) I-f amplifier MHz; (11) Second converter; (12) Signal for range determination; (13) Annular waveguide bridges; (14) Elevation difference signal; (15) Phase detector; (16) Azimuth difference signal; (17) Phase reg.; (18) AGC filter and detector; (19) Antenna drive; (20) Elevation error signal; (21) 1st heterodyne, 166 MHz; (22) Azimuth error signal; (23) Antenna drive; (24) Elevation error signal; (25) 2nd heterodyne, 40 MHz.

The antenna system of this station consists of four spiral antennas (Fig. 9.7). The width of the antenna radiation pattern with respect to half-power level is 20° . The high-frequency signals received by the spiral antennas are fed to four angular waveguide bridges with the aid of which the elevation and azimuth sum and difference signals are formed. Sum and difference signals are fed through high-pass filters to a three-channel phase-sensitive receiver. The total receiver noise factor is 3.5 dB. Conversion to the first intermediate frequency 30 MHz is accomplished with a thermostatic heterodyne with quartz stabilization, whose stability is 0.001%. In each of the three independent outputs of the first heterodyne, phase is adjusted by more than $\pm 60^\circ$. In order to preserve phase coherence between the sum and difference signals in all three receiving channels, identical amplifiers, converters, generators, and AGC circuits, developed for the sum channel are used. Secondary converters in all three receiving channels convert the frequency 30 MHz to 10 MHz. Azimuth and elevation error signals are fed to antenna drive.

The precise guidance station is an amplitude sum-difference station whose block diagram is presented in Fig. 9.9. The antenna of the station (Fig. 9.10) consists of a parabolic reflector 2.4 m in diameter, a hyperbolic primary radiator 0.9 m in diameter, and four horn feeds. The width of the radiation pattern is 2.1° .

Fig. 9.10. Overall view of antenna of precise guidance station.



Signals from antenna output are fed to four double waveguide T-joints, with whose aid the azimuth and elevation sum and difference signals are formed. Sum and difference signals are fed to three parametric amplifiers and then to the tracking receiver in which azimuth and elevation error signal separation occurs. Error signals then move to the azimuth and elevation antenna drives. At the same time, part of the sum signal energy moves to the lock-on receiver which accelerates the tracking receiver's entrance into normal operating mode.

In the three-channel tracking receiver, two stages of frequency conversion are used (60 and 5 MHz). The voltage for the AGC system is developed in the sum channel and applied to all channels. The sign of the azimuth and elevation error signal is determined by comparing the phases of the sum and corresponding difference signals in the phase detector.

The automatic tracking station is also an amplitude sum-difference monopulse station operating on a frequency of 4070 MHz on the signal of the beacon on board the satellite. The block diagram of this station is presented in Fig. 9.11.

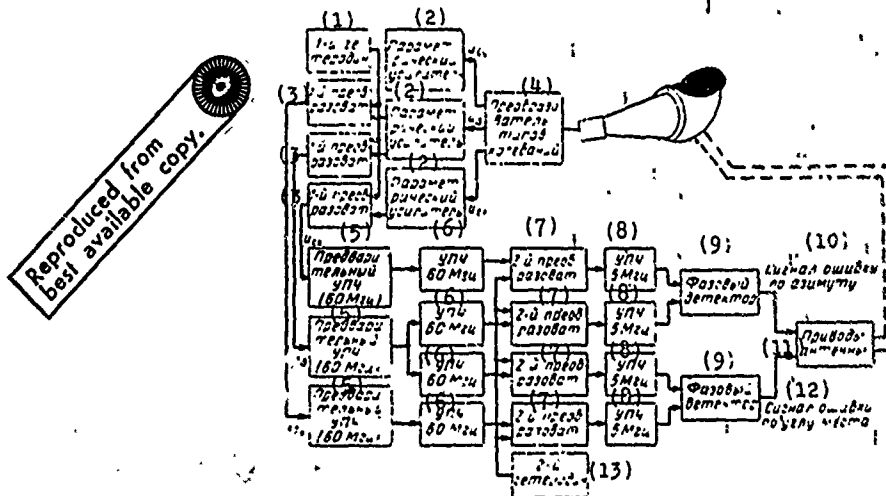


Fig. 9.11. Block diagram of an automatic tracking station.
 KEY: (1) 1st heterodyne; (2) Parametric amplifier; (3) 1st converter; (4) Converter of types of oscillations; (5) Preliminary i-f amplifier (60 MHz); (6) I-f amplifier 60 MHz; (7) 2nd converter; (8) I-f amplifier 5 MHz; (9) Phase detector; (10) Azimuth error signal; (11) Antenna drive; (12) Elevation error signal; (13) 2nd heterodyne.

A horn-parabolic antenna, whose overall view is presented in Fig. 9.12, is used in the station. The antenna consists of a parabolic reflector irradiated by a conical horn. The tip of the horn agrees with the focus of the paraboloid; the axis of the horn is perpendicular to the axis of the paraboloid. The antenna has the following basic characteristics:

aperture angle of conical horn	-	31.5°
focal distance	-	18.2 m
aperture diameter	-	20.6 m
aperture area	-	334 m
beam width (at frequency 4080 MHz)	-	0.24°.

The antenna is covered by an inflated dome 65 m in diameter.

Two types of waves, H_{11} and E_{01} , are propagated in the horn on beacon frequency. For waves H_{11} there are both vertically polarized and horizontally polarized components (i.e., vertically polarized and horizontally polarized waves of this type are propagated). In [39] it is shown that the radiation patterns of a circular aperture excited by H_{11} and E_{01} waves are very similar in form to the sum and difference patterns of a monopulse system. The sum pattern is formed by the H_{11} wave and the difference by the E_{01} wave. The H_{11} and E_{01} wave are separated in the station with a converter of oscillation types. Since the components of the H_{11} wave are geometrically orthogonal, with the aid of two hybrid junctions, they are separated into vertical and horizontal components.

Fig. 9.12. Antenna of automatic tracking station. 1 - upper equipment; 2 - bearing of elevation rotation device; 3 - wheel of elevation device; 4 - parabolic mirror; 5 - azimuth drive gear; 6 - door; 7 - compressors of dome inflation system.



Reproduced from
best available copy.

Then horizontal and vertical components are modulated and amplified separately. Two of these sum signals u_{cx} , u_{cy} , along with the modulated difference signal u_{Δ} , form three automatic tracking signals obtained from the component of the elliptically polarized incident wave. These three signals u_{cx} , u_{cy} and u_{Δ} are amplified and converted with respect to frequency in independent channels. Each channel consists of a varactor parametric amplifier, a balance mixer, and a preliminary mixer on 60 MHz. Then these signals on intermediate frequencies 60 MHz are fed to the i-f amplifier in which the difference signals are standardized. Then a second conversion of intermediate frequency occurs (to 5 MHz). The angular error in each plane is separated by the phase detector to which the sum and difference signals are fed. Error signals move to the elevation and azimuth antenna drives, respectively.

The radar complex Haystack, developed in the USA, is a monopulse radar of very high power, designed both for tracking space vehicles and for operating in the fields of communication and radio astronomy, including obtaining information on such distant planets as Mars, Mercury, and Jupiter [36].

The antenna of the station (Fig. 9.13) consists of a parabolic reflector 37 m in diameter with a primary radiator 2.85 m in diameter and horn feeds. The reflector consists of separate aluminum panels of honeycomb design. The antenna amplification factor is 69 dB and radiation pattern width is approximately 3 angular minutes. The antenna is protected from winter winds and frost by a spherical dome 45 m in diameter made from glass fibre 0.76 mm thick reinforced with aluminum.

In order to ensure antenna orientation accuracy no less than ± 0.3 angular minutes with a radiation pattern width on the order of 3 angular minutes, the use of a special hydrostatic bearing weighing approximately 24 t is necessary. The antenna position is controlled by a UNIVAC-490 computer.

The transmitter operates in continuous radiation mode or by pulses of long duration and has an average output power of 100 kW and working frequency of 7750 MHz.

Weak signals are received with the aid of several paramagnetic amplifiers (masers) and parametric amplifiers which can be cooled to the temperature of liquid helium.

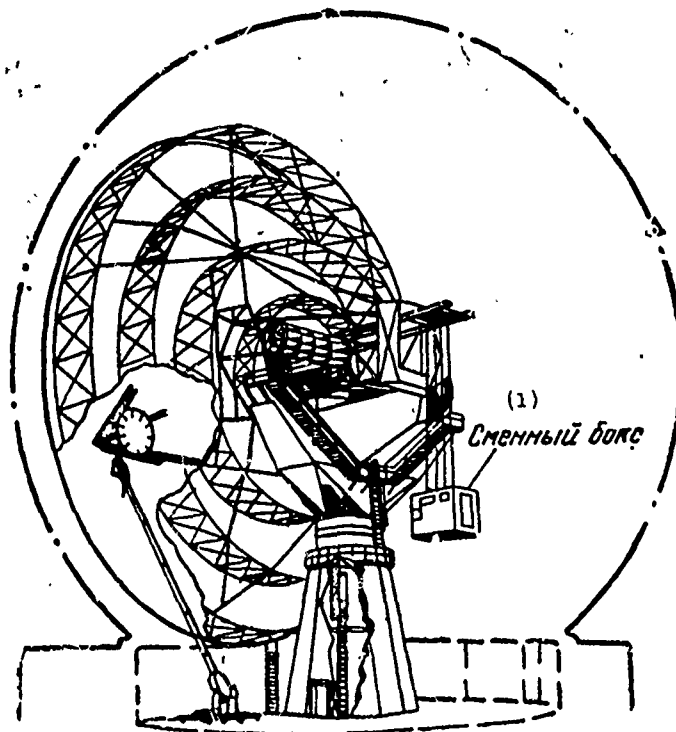


Fig. 9.13. Haystack antenna complex.
KEY: (1) Detachable box.

§ 9.3. RADARS OF THE ANTIMISSILE DEFENSE SYSTEM

At the present time the USA has developed and is using in their antimissile defense system the Nike-X, designed for the defense of large cities, industrial centers and concealed rocket bases where the Atlas, Titan, and Minuteman rockets are located.

The basic elements of the Nike-X system are the MAR, TASMAR, PAR, MSR radars, the Spartan and Sprint antimissiles, a computer for processing data obtained during target tracking and used for guiding the antimissile missile [36, 69, 79]. These elements are assumed to be in the antimissile defense system Nike-X, designed for protecting the territory of the USA from massive rocket and nuclear attack. This system will be deployed in the second stage of the antimissile defense system creation. In the first stage the Department of Defense made the decision to deploy the "limited" safeguard system with the introduction period in 1972-1973.

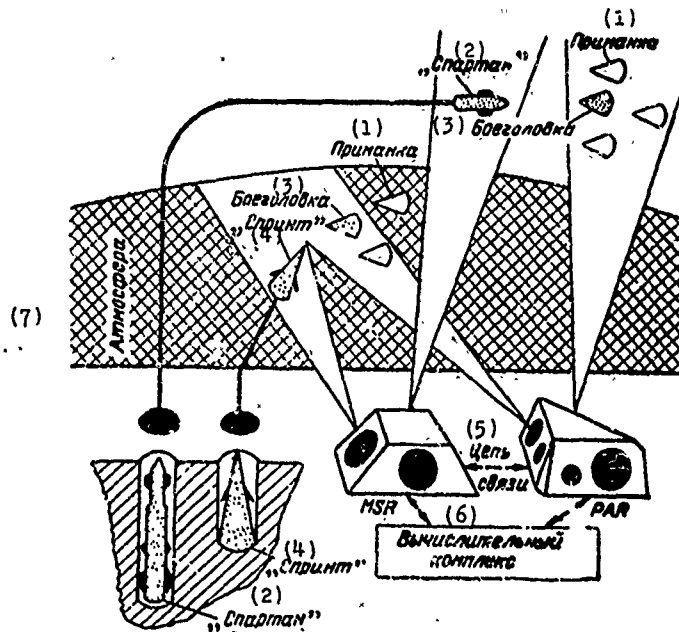


Fig. 9.14. Elements of the "limited" ABM system, the Safeguard.

KEY: (1) Decoy; (2) Spartan; (3) Warhead; (4) Sprint; (5) Communications link; (6) Computer complex; (7) Atmosphere.

The Safeguard ABM system will have the PAR and MSR radars, a computer complex consisting of several computers, 15-20 launch positions for the Spartan antimissile missile (to intercept warheads beyond the dense layers of atmosphere) and for the Sprint (to intercept warheads at low altitudes), and a communications line (Fig. 9.14).

The MAR multioperational radar, in the case of a massive enemy missile attack using advanced means of ABM system penetration, solves the following problems: performs search and detection of targets at a range of approximately 3000 km, target tracking and identification of warheads from decoys, and guidance of antimissile missiles. The MAR radar has to serve several launch positions for the antimissile missiles and is located 25 km from them.

The MAR equipment is mounted in an underground reinforced concrete site with a useful area of 6000 m² and under three protective domes (Fig. 9.15). Under the large dome is the receiving equipment and under the two smaller ones the transmitting equipment. In the walls of the large and one of the two small domes are "windows" in which antennas made in the form of phased arrays are mounted.



GRAPHIC NOT REPRODUCIBLE

Fig. 9.15. Overall view of MAR station. 1 - large dome; 2 - small domes.

The TASMAR radar, which is a somewhat simplified version of the MAR, solves the above listed problem during a less than massive missile attack using less advanced means of ABM system penetration. The radar is located in one building 30 m high and occupies one area of 75 × 75 m.

The PAR radar serves for very remote target detection and also for guiding the Spartan antimissile missile, designed to intercept

targets on distance approaches to the defended objective (at a range of up to 960 km). The PAR has separate receiving and transmitting phased arrays and will probably operate on frequencies in the upper part of the meter range (Fig. 9.16). Antenna arrays are located on two faces to provide scanning in azimuth 180°. The larger array is the receiving array.

The MSR radar also has a phased antenna array and makes possible the simultaneous guidance of a large number of Sprint and Spartan antimissile missiles (Fig. 9.17). This station is unique in the system, in which a common phased array operating on transmission and reception is used. The radar is located directly at launch position. Probably four MSR radars would fit on one MAR. In case of necessity, the MSR can be replaced by the TASMAR.

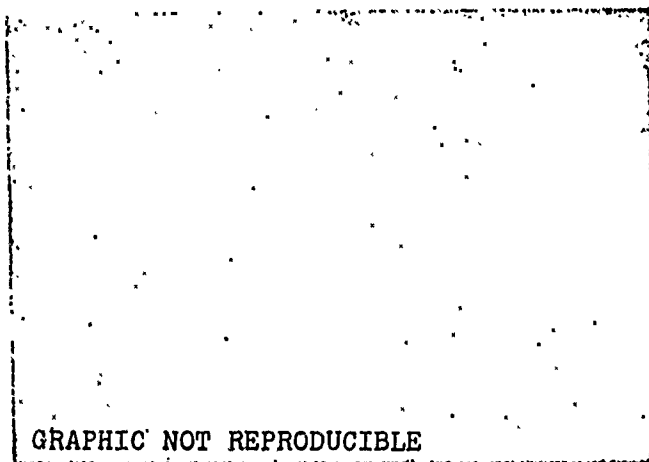


Fig. 9.16. Overall view of PAR.

In the initial period of deployment of an ABM system, each of its radars will have two transmitting and two receiving arrays, providing azimuth scan of 180°.

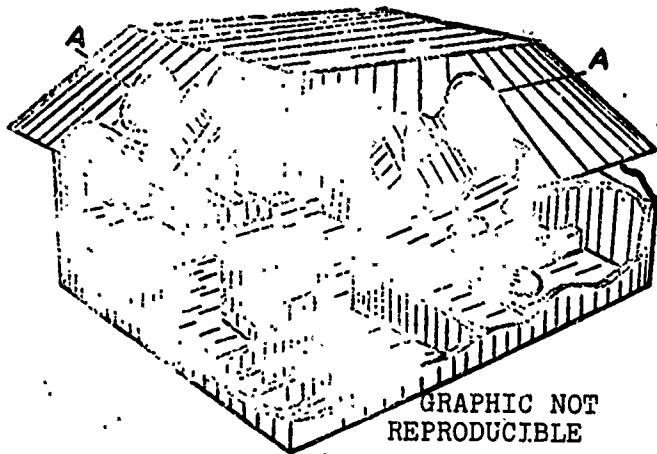


Fig. 9.17. Overall view and arrangement of equipment in the building housing the MSR. A - antenna array.



Fig. 9.18. Antenna of the Rampart radar.

Since the problem of distinguishing the head of the missile on a background of decoys is one of the most important in the creation of an ABM system, a great deal of attention has been given in the USA to building radars for target identification.

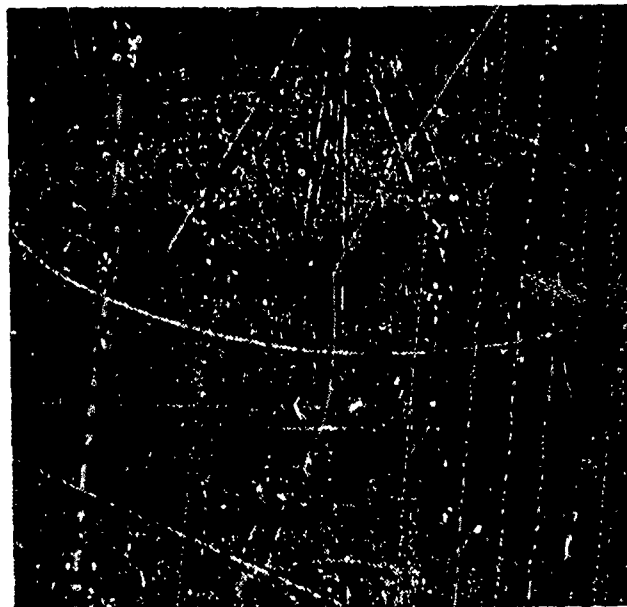
Thus, the Rampart monopulse radar has two transmitters with a total power of 24 MW which operate on one antenna 18 m in diameter (Fig. 9.18). Radiation is on a frequency of 3032 MHz. The antenna has an amplification of 52 dB [36].

The emitted pulse consists of ten separate pulses, each 1 μ s in duration, spaced 1 MHz in frequency. The front of each pulse coincides with the drop of the preceding pulse so that the signal emitted appears as one pulse 10 μ s in duration. Signals reflected from a target and received by the radar receiver are fed from its output to visual indicators and are recorded on tape or paper tape, and, in digital form, on magnetic tape.

A more modern experimental radar for identification than the Rampart is the Tradex, designed for studying complex targets and identifying warheads at ranges to 3200 km [36].

The overall view of the antenna for this radar is presented in Fig. 9.19. A two-frequency method of operation is used, with which two transmitters operate simultaneously. The first transmitter with a pulse power of 4 MW operates on a frequency of 425 MHz. The second transmitter operates on 1320 MHz and has a pulse power of 1.25 MW. Pulse repetition frequency is 1500 Hz.

Fig. 9.19. Antenna of Tradex radar.



Reproduced from
best available copy.

Search and detection of target are carried out at 1320 MHz. At this frequency pulses broaden during radiation and contract during reception. With a pulse expansion factor of 50, a 50-fold increase in the energy of the emitted pulse is achieved with the same pulse power of the transmitter. After reception the pulse is compressed by a factor of 50.

Target tracking is accomplished by the monopulse method at 425 MHz. Data obtained during target tracking are stored and converted to digital and analog form for use by computers and operators.

To analyze a complex target containing a large number of separate parts, data on all elements of the complex target are stored in the i-f channel. Upon target lock-on 30 successive range strobe pulses are generated; the signals in each strobe are stored from pulse to pulse on a magnetic disk in accordance with the sequential position of each strobe. Information is given in the form of a continuous sequence of signals corresponding to the doppler frequencies of the targets in each strobe. The simultaneous use of frequency and time methods of analysis, i.e., range strobing and narrow-band filtration in the i-f channel provides high resolution.

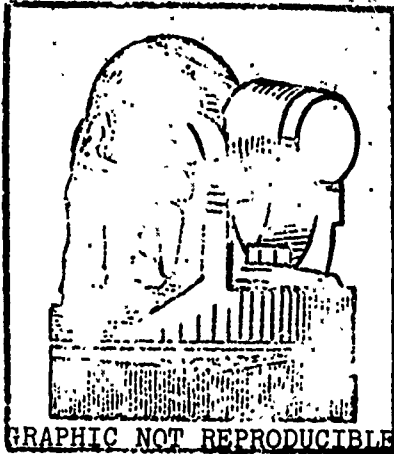
Because of this high resolution, the wide-band range tracking, and the narrow-band tracking based on doppler frequency, data on dimensions, target shape, forward speed, rotational velocity, and acceleration can be obtained from the statements of the developers.

§ 9.4. RADARS FOR GUIDING ANTI-AIRCRAFT ROCKETS

Monopulse radars are widely used in American and British systems for guiding ground-to-air rockets (Nike-Ajax, Nike-Hercules, Bloodhound) and in ship systems for controlling the fire of anti-aircraft rockets (Tartar, Talos, Terrier).

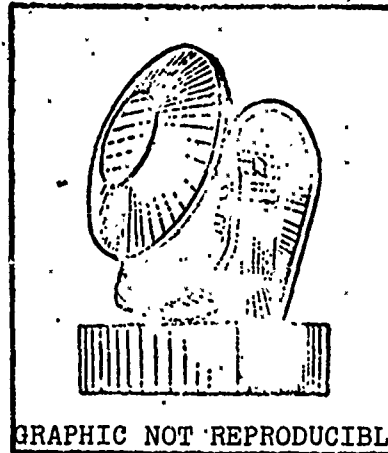
The Nike-Ajax system includes a circular scan section, a target tracking section, and an anti-aircraft rocket guidance section (ZUR),

the last two of which are monopulse stations MPA-4 [98]. These sets operate on 9100 MHz ($\lambda = 3.3$ cm) and have lens antennas 1.9 m in diameter and a beam width of 1.2° . The external view of the antenna is presented in Fig. 9.20. Pulse power of the transmitter is 200 kW. Pulse width is 0.25 μ s and repetition frequency is 2000 Hz.



GRAPHIC NOT REPRODUCIBLE

Fig. 9.20. Antenna for Nike-Ajax tracking system.



GRAPHIC NOT REPRODUCIBLE

Fig. 9.21. Antenna for Nike-Hercules guidance system.

The Nike-Hercules [91, 114] has a target detection radar and a monopulse ZUR guidance station. A spherical antenna system with a double lens (Fig. 9.21), enclosed in a dome of silicone resin is used in the guidance station.

In the modified ZUR guidance radar the transmitter power has been increased and the antenna dimensions almost doubled (i.e., its aperture is 8 m). The modified Nike-Hercules system is capable of acting not only against aircraft but also against rockets; rockets are detected at a range of 300-1000 km.

In the English Bloodhound system a two-channel radar station is used for illuminating and guiding ZUR (Fig. 9.22) while accomplishing, at the same time, target tracking and rocket guidance. In this

station there is a channel in the 10-cm range with horizontal polarization and with a wide beam for lock-on and initial tracking (from 2 to 6°) and a channel in the 3-cm range with circular polarization and a narrower beam (1°) for precise tracking and target illumination. An antenna with a parabolic reflector 2.15 m in diameter and a four-horn feed is used in the radar. Repetition frequency and working frequency can be changed; three frequency types and six repetition frequencies are available.

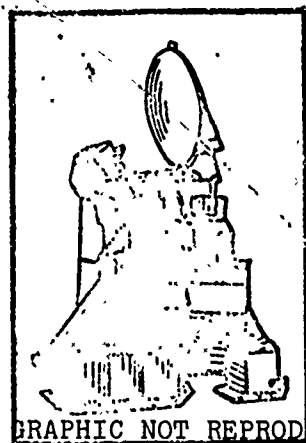


Fig. 9.22. Bloodhound guidance system radar.

GRAPHIC NOT REPRODUCIBLE

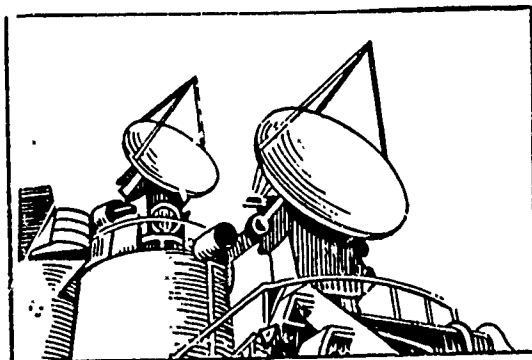


Fig. 9.23. The AN/SPG-51 fire control radar.

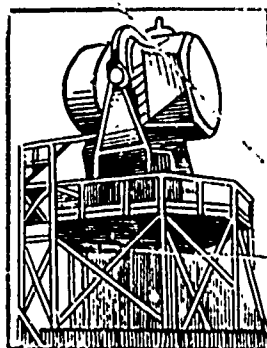


Fig. 9.24. The AN/SPG-49 tracking radar.

After target detection the radar goes into precise tracking mode. Its data are fed to the computer, which works out the commands for rocket launch and control in the initial stage. In the final stage

of flight the rocket is brought to a semiactive self-guidance mode on signals reflected from the target.

Monopulse radars with lens antennas have found wide application in ship systems for controlling the firing of antiaircraft rockets.

In the Tartor system the AN/SPG-51 monopulse radar is used to control firing (Fig. 9.23), which ensures automatic lock-on and target tracking [92]. Several seconds before launch the intensifying beam is turned on and the rocket is guided by signals reflected from the target. For tracking and intensification, one parabolic reflector antenna 2.4 m in diameter is used.

In the Talos system, to detect the targets and guide the ZUR, the monopulse AN/SPG-49 (Fig. 9.24) is used [70, 115]. In 1958 a new AN/SPG-56 was developed for this system. Lens antennas are used in the stations, forming simultaneously both the lock-on and target tracking beam and the tracking beam used during the flight of the ZUR; therefore, they can simultaneously guide to a target two or more ZUR.

In the AN/SPG-49 a magnetron with a power of 4 MW is used, and in the AN/SPG-56 a klystron with an average power of several kilowatts.

In the Terrier system [99] for guiding antiaircraft rockets an AN/SPG-5 (Fig. 9.25) is used and since 1957 an AN/SPG-55 with lens antennas. Powerful klystrons with an average power of several kilowatts are used in the transmitters. These radars have long range, altitude, high accuracy, and stability in guiding rockets launched in groups or singly.

§ 9.5. A RADAR FOR DETECTING GROUND TARGETS ON THE LOCAL BACKGROUND

In 1958 the USA developed a phase sum-difference experimental monopulse radar for detecting and determining the distance to ground targets on a background of interfering reflections from vegetation

[59]. The block diagram of this station is illustrated in Fig. 9.26 and its basic characteristics are presented in Table 9.2.

Fig. 9.25. The AN/SPQ-5 anti-aircraft rocket guidance radar.

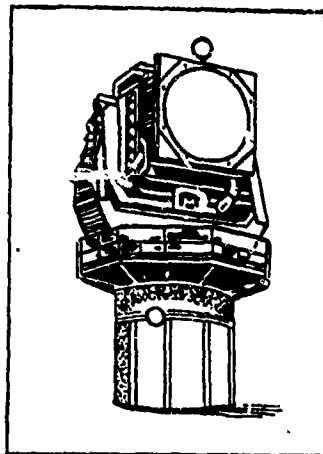


Table 9.2.

Basic characteristics	Indices
Working frequency	35000 MHz
Pulse power	35 kW
Pulse width	0.06 μ s
Repetition rate	4000 pulse/s
Intermediate frequency	60 MHz
I-f amplifier bandwidth	20 MHz
Receiver noise factor in each channel	18 dB
Diameter of each parabolic antenna reflector	61 cm
Antenna amplification	44 dB
Radiation pattern width	
in azimuth	3°
in elevation	1°

The antenna system is a double parabolic reflector with two horn feeds whose centers are spaced 61.4 cm in the horizontal plane for signal phase comparison.

Signals reflected from the target move from the antenna system output to the double waveguide T-joints in which summation and subtraction of high-frequency signals is performed; then, the converted signals are fed to the two-channel receiver at whose output sum

and difference video signals are obtained. The electronic switch at receiver output ensures the simultaneous indication of sum and difference video signals on the indicator.

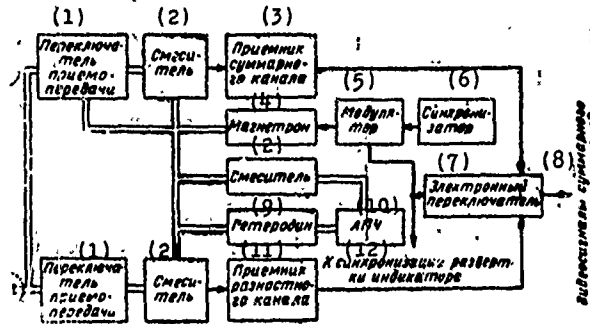


Fig. 9.26. Block diagram of a ground target detection radar.
KEY: (1) Send-receive switch; (2) Mixer; (3) Sum channel receiver; (4) Magnetron; (5) Modulator; (6) Synchronizer; (7) Electronic switch; (8) Video signals of sum and difference channels; (9) Heterodyne; (10) ASC; (11) Difference channel receiver; (12) Two indicator sweep synchronization.

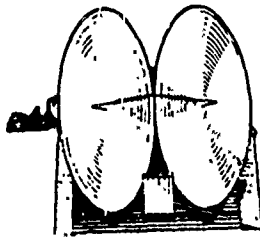


Fig. 9.27. Antenna of ground target detection radar.

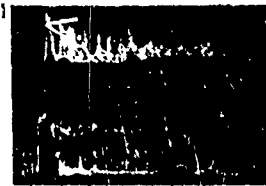


Fig. 9.28. Oscillograms of video signals at radar output. a) with conical scanning; b) sum channel, in monopulse radar; c) difference channel.

Figure 9.28 illustrates data on the simultaneous variation of video signals in sum (b) and difference (c) channels during reflection from a truck on a background of thick bushes and woods. The observation results were compared with data obtained with a T-47 radar with conical scanning, located beside the monopulse radar. The video pulses at receiver output for the radar with conical scanning are shown

in Fig. 9.28a. The distance between the truck and the radars was 750 m.

As seen from Fig. 9.28a the detection of a truck on a background of bushes with a radar having conical beam scanning is practically impossible due to the very high level of interfering reflections. A monopulse station correctly detects such a target based on the maximum value of the sum signal (d) and the absence of a difference signal. The signal (e) following the signal from the truck is caused by a reflection from the side of the road behind the truck.

Bibliography

1. Айзенберг Г. З. Антенны ультракоротких волн. Связьиздат, 1957.
2. Аренберг А. Г., Распространение дециметровых и сантиметровых волн. Изд-во «Советское радио», 1957.
3. Бакут П. А., Большаков И. А. и др. Вопросы статистической теории радиолокации. Т. 1, 2. Изд-во «Советское радио», 1964.
4. Бартон Д. К., Радиолокационные системы. Пер. с англ. под ред. К. Н. Трофимова. Воениздат, 1967.
5. Брокнер Ч. Угловые ошибки радиолокационных станций, автоматически сопровождающих цель. «Вопросы радиолокационной техники», 1951, № 6.
6. Бреннан Л. Е. Точность измерения угловых координат радиолокатором с антенной в виде фазированной решетки, «Зарубежная радиоэлектроника», 1962, № 1.
7. Брокман М. Х., Буханан Х. Р., Чоут Р. А. и Мэллинг Л. Р. Система TRAC (E) для связи и сопровождения космических объектов. «Зарубежная радиоэлектроника», 1960, № 12.
8. Брошштейн И. Н. и Семендяев К. А. Справочник по математике. Гостехиздат, 1953.
9. Бусленко Н. П., Шрейдер Ю. А. Метод статистических испытаний (Монте-Карло) и его реализация на вычислительных машинах. Физматгиз, 1961.
10. Вакин С. А., Шустов Л. Н. Основы радиопротиводействия и радиотехнической разведки. Изд-во «Советское радио», 1968.
11. Васильев В. В., Влахов О. В., Дудник П. И., Степанов Б. М. Авиационная радиолокация. Изд-во ВВИА им. проф. Н. Е. Жуковского, 1964.
12. Волков В. М. Логарифмические усилители. Гостехиздат, Киев, 1952.
13. Волгин А. Н., Янович В. А. Противорадиолокация. Воениздат, 1960.
14. Волгин Л. Н. Элементы теории управляющих машин. Изд-во «Советское радио», 1962.
15. Вудворд Ф. М. и Лаусон Д. Д. Теоретическая точность получения произвольной диаграммы излучения источника конечных размеров. ПЭЭ (Лондон), 1948, sept., pt. III.

16. Гинзбург В. М., Белова И. И. Расчет параболических антенн. Изд-во «Советское радио», 1959.
17. Градштейн И. С., Рыжик И. М. Таблицы интегралов, сумм, рядов и произведений. Физматгиз, 1963.
18. Дулевич В. Е., Коростелев А. А. и др. Теоретические основы радиолокации. Изд-во «Советское радио», 1964.
19. Дани, Ховард, Кинг. Влияние флуктуаций эхо-сигнала на работу радиолокационных станций сопровождения цели. «Радиотехника и электроника за рубежом», 1959, № 6.
20. Дани, Ховард. Влияние автоматической регулировки усиления на точность сопровождения целей моноимпульсными радиолокационными системами. «Радиотехника и электроника за рубежом», 1959, № 5.
21. Делаис Р. Теория мерцания цели и угловые ошибки при радиолокационном сопровождении. «Вопросы радиолокационной техники», 1954, № 1.
22. Жук М. С., Молочков Ю. Б. Проектирование антенно-фидерных устройств. Изд-во «Энергия», 1966.
23. Клаудер Н. Р. и др. Теория и расчет импульсных радиолокационных станций с частотной модуляцией. «Зарубежная радиоэлектроника», 1961, № 1.
24. Корф М., Брайндли С. М., Лоу М. Н. Одновременное измерение угловых координат многих целей с помощью моноимпульсной РЛС сопровождения. «Зарубежная радиоэлектроника», 1963, № 6.
25. Крылов Н. Н. Электрические процессы в нелинейных цепях радиоприемников. Связьиздат, 1949.
26. Кривицкий Б. X. Автоматические системы радиотехнических устройств. Госэнергиздат, 1962.
27. Киркпатрик Г. М. Фазовый детектор с расширением углового диапазона. Патент США № 2751555 выдан 19.6.1956 с приоритетом от 3.10.1951.
28. Кандрейкин Д. Б., Павлов Н. Ф., Потехин В. А. Поляризация радиолокационных сигналов. Изд-во «Советское радио», 1966.
29. Карпентье М. Современная теория радиолокации. Пер. с англ. Изд-во «Советское радио», 1965.
30. Кинт, Холахан, Дэкс, Симпсон, Ламберт, Хэтчер. Методы и техника радиопротиводействия и борьбы с ним. «Зарубежная радиоэлектроника», 1960, № 11.
31. Кук. Повышение эффективности радиолокационных устройств за счет сжатия импульса. «Зарубежная радиоэлектроника», 1960, № 9.
32. Лукошкин А. П. Радиолокационные усилители с большим диапазоном входных сигналов. Изд-во «Советское радио», 1964.
33. Локк А. С. Управление снарядами. Пер. с англ. Гостехиздат, 1957.
34. Левин Б. Р. Теория случайных процессов и ее применение в радиотехнике. Изд-во «Советское радио», 1960.
35. Лезин Ю. С. Оптимальные фильтры и накопители импульсных сигналов. Изд-во «Советское радио», 1963.
36. Леонов А. И. Радиолокация в противоракетной обороне. Восстандиздат, 1967.
37. Островитянов Р. В. К вопросу об угловом шуме. «Радиотехника и электроника», 1966, № 4...
38. Петерс, Веймер. Радиолокационное сопровождение сложных целей. «Зарубежная радиоэлектроника», 1964, № 7.
39. Покрас А. М. Антенные устройства зарубежных линий связи через искусственные спутники Земли. Изд-во «Связь», 1965.

40. Рузе Д. Влияние ошибок раскрыва на диаграммы направленности антенн. «Вопросы радиолокационной техники», 1956, № 2.
41. Родс Д. Р. Введение в моноимпульсную радиолокацию. Пер. с англ. Изд-во «Советское радио», 1960.
42. Рубин, Камен. Новый метод построения схем сравнения в моноимпульсной радиолокации. «Зарубежная радиоэлектроника», 1965, № 8.
43. Сергиевский Б. Д. Определение угловых координат совокупности излучателей. «Радиотехника», 1967, № 4.
44. Скольник М. Введение в технику радиолокационных систем. Пер. с англ. под ред. К. Н. Трофимова. Изд-во «Мир», 1965.
45. Свиридов Э. Ф. Сравнительная эффективность моноимпульсных радиолокационных систем пеленгации. Изд-во «Судостроение», 1964.
46. Сергиевский Б. Д. Методы и средства противодействия противоракетной обороне. «Зарубежная радиоэлектроника», 1966, № 1.
47. Сиверс А. П. Радиолокационные приемники. Расчет и проектирование. Изд. 3. Изд-во «Советское радио», 1959.
48. Соловьев Н. П. Отражающие свойства земных покровов. Труды Рижского института инженеров ГВФ», 1963, вып. 27.
49. Смит. Широкополосная антенна круговой поляризации диапазона «С» для одноимпульсного локатора. В сб. переводов «Антенны эллиптической поляризации». Изд-во иностранной литературы, 1961.
50. Тартаковский Г. П. Динамика систем автоматической регулировки. Госэнергоиздат, 1957.
51. Трофимов К. Н. Помехи радиолокационным станциям. Изд-во ДОСААФ, 1962.
52. Фельд Я. Н., Бененсон Л. С. Антенны сантиметровых и дециметровых волн, ч. 1. Изд-во ВВИА им. проф. Н. Е. Жуковского, 1955.
53. Фьеллбрант. Сравнение чувствительности моноимпульсных систем и РЛС с коническим сканированием. «Зарубежная радиоэлектроника», 1964, № 8.
54. Фалькович С. Е. Прием радиолокационных сигналов на фоне флюктуационных помех. Изд-во «Советское радио», 1961.
55. Хеллгрен Г. Вопросы теории моноимпульсной радиолокации. «Зарубежная радиоэлектроника», 1962, № 12; 1963, № 1.
56. Ханнан П. Двухзеркальные антенны, построенные на принципе телескопа Кассегрена. «Зарубежная радиоэлектроника», 1961, № 12.
57. Хургин Я. Н., Яковлев В. Методы теории целых функций в радиофизике, теории связи и оптике. Физматгиз, 1962.
58. Цыпкин Я. З. Теория импульсных систем. Физматгиз, 1958.
59. Ченг, Стабилито. Экспериментальное исследование возможности применения моноимпульсной РЛС для выделения сигналов от наземных целей на фоне местности. «Зарубежная радиоэлектроника», 1961, № 11.
60. Шифрин Я. С. Статистика поля линейной антенны. Изд-во АРТА им. Говорова, 1962.
61. Шлезингер Р. Радиоэлектронная война. Воениздат, 1963.
62. «Антенны сантиметровых волн». Пер. с англ. под ред. Я. Н. Фельда: Изд-во «Советское радио», 1950.
63. Сканирующие антенные системы СВЧ. Пер. с англ. под ред. Г. Т. Маркова и А. Ф. Чаплина. Изд-во «Советское радио», 1966.
64. Справочник по основам радиолокационной техники. Под ред. В. В. Дружинина. Воениздат, 1967.
65. «Исследования точности и помехоустойчивости фазовых радиопеленгаторов». Сборник статей Московского авиационного института. Изд-во «Судпромгиз», 1959.

66. «Радиолокационная война». Пер. с англ. Изд-во «Советское радио», 1946.
67. Борьба с вражеской радиолокацией. Пер. с англ. Изд-во «Советское радио», 1946.
68. Действие ядерного оружия. Пер. с англ. Воениздат, 1963.
69. Aviation Week, 1967, 25/IX; 23/X.
70. Aviation Week, 1968, 3/II.
71. Bates R. H. Random errors in aperture distributions. IRE Trans., 1960, v. AP-7, p. 263—275.
72. Baur. Der Wellenanalysator. Frequenz, 1960, Bd. 14, № 2.
73. Barton D. K. The future of pulse radar for missile and space range instrumentation. IRE Trans., 1961, v. MIL-5, X, № 4.
74. Barton D. K. Accuracy of a monopulse radar. Proc. 3 Conf. Nat. Conv. Military Electronics, 1959, p. 179—186.
75. Blasberg L. A., Hughes W. A., Lader L. J. Sequential lobing system with ferrite phase shifters. Патент США № 2929058 or 4/IV—1955.
76. Blasberg L. A., Hughes W. A., Lader L. J. Single channel monopulse radar system. Патент США № 3175215 or 8.9.1954.
77. Bock M. J., Rosen H. A., Polarization grating for scanning antennas. Патент США № 3188642 or 26.8.1959.
78. Butler J. L. Radar countermeasures antenna system. Патент США № 3171125 or 5.10.1961.
79. Bulletin of Atomic Scientists, 1967, v. 23, VI, p. 21—24.
80. Bernfeld M., Cook C., Paolillo J., Palmieri C. Matched filtering pulse compression and waveform design. Microwave J., 1964, Part I, № 10; Part II, № 11; Part III, № 12.
81. Chadwick G. G. and Shelton J. P. Two-channel monopulse techniques. Theory and practice. IEEE Military Electronics Conference Record, 1965, Washington, p. 177—181.
82. Cohen W., Steinmetz C. M. Amplitude and phase—sensing monopulse system parameters. Part I. Microwave J., 1959, v. 2, № 10, p. 21—23. Part II, № 11, p. 33—38.
83. Copeland J. R. Radar target classification by polarization properties. Proc. IRE, 1960, v. 48, VII, № 7.
84. Chu T. S., Konyoumian R. G. An analysis of polarization variation and its application to circularly—polarized radiators. IRE Trans., 1962, v. AP-10, № 2.
85. Develci J. A. Thermal—noise errors in simultaneous—lobing and conical—scan angle—tracking systems. IRE Trans., 1961, v. SET-7, VI, p. 42—51.
86. Dunn J. H., Howard D. D. Precision tracking with monopulse radar. Electronics, 1950, v. 33, № 17, p. 51—56.
87. Deloraine E. M., Busignils H. G. Pulse radar countermeasure. Патент США № 2943318 or 5.8.1942.
88. Elliot R. S. Mechanical and electrical tolerances for two—dimensional scanning antenna arrays. IRE Trans., 1968, v. AP-6, p. 114—120.
89. Electronics, 1962, 13/VII.
90. Electronics, 1963, 25/VII.
91. Electronics, 1961, 3/XI.
92. Electronics, 1959, 30/X.
93. Franklin S. B., Hilbers C. L. and Kosydar W. E. A wideband two channel monopulse technique. IEEE Military Electronics Conference Record, 1965, Washington, p. 174—176.
94. Hausz N., Zachary R. A. Phase-amplitude monopulse system. IRE Trans., 1962, v. MIL-6, № 2.
95. Hannan P. W. and Loth P. A. A monopulse antenna independent optimization of the sum and difference modes. IRE Intern. Conv. Record, 1961, Part I.

96. Hoyda R. E. Monopulse receiving apparatus. Patent CIAA № 3229287 or 1.7.1963.
97. Howard D. Radar target angular scintillation in tracking and guidance system based on echo signal phase front distortion. Proc. Nat. Electr. Conf., 1959, v. 15, p. 12—14.
98. Hamman P. L. The radar of Nike-Ajax. Bell Labs. Rec., 1959, v. 39, № 9.
99. Interavia Air Letter, 1960, 20/11.
100. Jones. Low side lobes in pencil beam antennas. Convention Record of the IRE, 1953, Pt 2.
101. John F., Ramsay J. F. Polarization characteristics of antennas. IRE Intern. Conv. Record, 1952, Pt 1.
102. George S. F., Zamanakos A. S. Multiple target resolution of monopulse versus scanning radars. Proc. of the National Electronics Conference, 1959, v. XV, p. 814—822.
103. Kuck J. H. Means for tracking multiple target formations by radar. Patent CIAA № 3130402 or 12.2.1957.
104. Kellecher K. S., Scott W. C. Cross-polarization effect on antenna radiation patterns. Conventions Record IEE, 1966, v. 4, Pt. 1.
105. Kownacki S. Simulation of radar range and doppler effect by means of stationary target. IEEE Trans. of Aerospace and Electronics Systems, 1967, p. 148—149.
106. Krishen K., Koepsel W. W., Durrani S. H. Cross-polarization measurements and their relation to target surface properties. IEEE Transactions on Antennas and Propagation, 1966, № 5, p. 629—635.
107. Leichter M. Beam pointing errors of long line sources. IRE Trans., 1960, v. AP-8, p. 268—275.
108. Lerner R. M. Представление сигналов. IRE Trans. Circuit Theory, 1959, v. 5, V.
109. Mathis H. F., Zurcher L. A., Cunderman R. J. Cut radar hardware needs and costs with a special multi—mode antenna feed that requires only two hybrids to measure azimuth and elevation. Electron. Design, 1966, № 8.
110. McClellan C. Monopulse radar system. Patent CIAA № 2980906 or 18.04.1961.
111. McCann J. G., Stegen R. J., Falstrom W. Split parabolic radar antenna utilizing means to discriminate against cross-polarized energy. Patent CIAA № 3092834 or 23.12.1958.
112. Miller P. S., Peeler G. D. M. Polarization filter antenna utilizing reflector consisting of parallel separated metal strips mounted on low loss dish. Patent CIAA № 3119109 or 31.12.1958.
113. Miller B. US penetration capability erodes. Aviation Week and Space Technology, 1977, № 17, p. 99, 95, 98, 99, 105, 108, 109.
114. Missiles and Rockets, 1961, № 20, 15/V.
115. Missiles and Rockets, 1959, 21/IX.
116. Nester N. H. A study of tracking accuracy in monopulse phased arrays. IRE Trans., 1952, v. AP-10, № 3.
117. Page P. M. Monopulse radar. IRE Conv. Record, 1955, Pt. 8.
118. Ricardi L., Niro L. Design of a twelvehorn monopulse feed. IRE Intern. Conv. Record, 1961, Pt. I, III.
119. Rondinelli L. A. Effects of random errors on the performance of antenna arrays of many elements. IRE Natl. Conv. Record, 1959, v. 7, Pt. 1, p. 173—187.
120. Raboy B. Radar system. Patent CIAA № 3129425 or 27.9.1957.
121. Rusch W. V. T. Phase error and associated cross-polarization effects in Cassegrainian—fed microwave antennas. IRE Trans., 1966, v. AP-14, № 3, p. 266—275.
122. Schwarzkopf D. A high precision monopulse receiver. Microwave J., 1967, v. 10, № 9, p. 92—101.
123. Sonner G. E. Three beam monopulse radar system and apparatus. Patent CIAA № 3129425 or 27.9.1957.

124. Sommers H. S. Signal comparison system. Патент США № 2721320.
125. Storke F. P. A monopulse instrumentation system. Proc. IRE, 1951, v. 49, № 8, p. 1328—1329.
126. Sharensen S. Angle estimation with a monopulse radar in the search mode. IRE Trans., 1962, v. ANE-9, № 3.
127. Watson R. B., Horton G. W. Simultaneous lobe comparison for radar direction finding. Патент США № 3025517 от 31.01.1952.
128. White S. B. Radar countermeasure. Патент США № 3019433 от 27.3.1959.
129. Zachary R. Automatic gain control for monopulse radar. Патент США № 2943317.
130. Taylor R. E. Satellite tracking simultaneous — lobing monopulse receiving system with polarization diversity capability. IRE Trans., 1957, v. AES-3, № 4.
131. Thourel L. Theorie des circuits hyperfréquence á comparaison de phase ou d'amplitude. Annales de Radioelectricité, 1958, № 52, p. 130—139.
132. Thompson A. S. Boresight shift in phase sensing monopulse antennas due to reflected signals. Microwave J., 1966, v. 9, № 5, p. 47—48.
133. Като Сюсукэ и др. Устройство для устранения перекрестной поляризации в антенне. Японский патент № 22327 от 27.02.63.
134. Като Сюсукэ, Нака хара Сигэо. Устройство для устранения перекрестной поляризации. Японский патент № 17205 от 4.04.63.